Development of a $5N$-moment Multi-Fluid Plasma Model for D-T Fusion in an Axisymmetric Z Pinch

Yu Takagaki

A dissertation
submitted in partial fulfillment of the
requirements for the degree of

Doctor of Philosophy

University of Washington

2023

Reading Committee:

Uri Shumlak, Chair

Eric T. Meier

Justin Little

Program Authorized to Offer Degree:
Aeronautics & Astronautics

University of Washington

Abstract

Development of a $5N$-moment Multi-Fluid Plasma Model
for D-T Fusion in an Axisymmetric Z Pinch

Yu Takagaki

Chair of the Supervisory Committee:
Uri Shumlak
Department of Aeronautics & Astronautics

The thermonuclear fusion process in a D-T Z pinch is investigated by developing the multi-component, deuterium-tritium-helium-electron, model including fusion reactions and inter-species collisions via the WARPXM simulation framework. The geometric source terms are implemented into WARPXM to solve axisymmetric problems in cylindrical coordinates without changing the code's infrastructure. The $5N$-moment growth rates peak at the expected wavenumber and further stabilize at large wavenumbers in a manner that agrees with previously published studies using higher fidelity kinetic models. The radially-sheared axial flow, $\partial_r v_z \neq 0$, stabilizes the sausage instabilities significantly as observed in the Fusion Z-pinch Experiment (FuZE) at the University of Washington. Braginskii viscosity and thermal conductivity also indicates the stronger stabilizing effects with decreasing plasma collisionality. The energetic alphas produced in the core of the Z-pinch plasma expand radially and interact with the azimuthal magnetic field, which drives an axial current of alpha particles. The primary energy cascade initiates from energetic alphas to electrons, and eventually the electron energy transfers to the ions. The increase in fusion gain becomes significant when the plasma pinch current exceeds 1.35 MA, which corresponds to a pinch radius equal to the gyroradius of a D-T fusion alpha. While never reaching ignition, the fusion gain increases from 8.14 to 151.8 with the increasing pinch current and 7% of the alpha heating fraction.

TABLE OF CONTENTS

LIST OF FIGURES

GLOSSARY

n: number density

ρ: mass density

ρ_c: charge density

v: particle velocity

u: fluid bulk velocity

V_A: Alfvén velocity

v_{th}: thermal velocity

J: current density

P: pressure

T: temperature

E: electric fields

B: magnetic fields

ϵ_0: permittivity of free space

μ_0: permeability of free space

c: speed of light

k_B: Boltzmann constant

k_Z: axial wave number

r_L: Larmor radius

r_p: pinch radius of a Z-pinch, which is the radial position of the peak azimuthal magnetic fields

ω_c: cyclotron frequency

ω_p: plasma frequency

$\nu_{\alpha\beta}$: collision frequency

δ_p: skin depth

τ_A: Alfvén transit time

$\tau_{\alpha\beta}$: collision period

Π: viscosity

h: heat flux

$R_{\alpha\beta}$: frictional force

$Q_{\alpha\beta}$: heat generation

σ_{fus}: fusion crosssection area

V_{rel}: relative velocity

$\mathcal{S}$: reactive source term

ACKNOWLEDGMENTS

I would like to express my sincere gratitude to many people who have supported my research. Prof. Uri Shumlak has been incredibly supportive, always inspired me to achieve the educational goals, and extremely patient with my research progress and English. Dr. Eric Meier in Zap Energy provided me a lot of opportunities and support to understand kinetics and Braginskii transport. Dr. Iman Datta in Zap Energy, and Dr. Andrew Ho in LLNL gave me their immense help and guidance for the programming in the WARPXM framework. Dr. Daniel Crews, Dr. Sina Taheri, and Dr. Whitney Thomas supported me to get through the graduate school with a lot of proficient discussions. All members in Computational Plasma Dynamics Lab, Jack Coughlin, Aria Johansen, Howard Cheng, and Evan Bluhm gave me constructive feedback and conductive environment for my research. Thanks to my committee members, Prof. Justin Little for instructing the physics of fusion, Prof. Marco Salviato for teaching FEM, and Prof. Bernard Deconinck for assisting to understand nonlinear dynamics. I also thank all of the staff in William E. Boeing Department of Aeronautics and Astronautics for supporting me with multiple teaching assistant appointment. Lastly, I would like to thank all of my family and friends for their encouragement to pursue this degree.

This research has been supported by the Air Force Office of Scientific Research under Award No. FA9550-15-1-0271.

DEDICATION

to my parents and sister

Chapter 1

INTRODUCTION

Fusion energy holds significant promise as a clean and limitless energy source. Unlike fossil fuels, fusion uses isotopes of hydrogen (e.g., deuterium and tritium) that are abundant in nature or can be bred through a blanket[3]. Also, fusion has the potential to satisfy the increasing global demand for energy and to achieve the long-term sustainability by producing tremendous amounts of energy without emitting greenhouse gases and high-level radioactive waste. While recent renewable energy sources (e.g., solar power, wind power, hydroelectric power, and geothermal power) can also deliver a clean energy, fusion can work as a stable baseload power supply anywhere on earth without being affected by weather or other environmental conditions. Moreover, well-controlled fusion is inherently safer than fission reactions since fusion does not involve possible runaway chain reactions or meltdown. Unfortunately, it is still challenging to sustain fusion reactions for long durations due to the existence of various plasma instabilities that occur on multiple temporal and spatial scales; however, decades of dedicated research and international collaborations has made progress and is delivering critical breakthroughs.

1.1 Motivation for Fusion Propulsion

The required electrical power and payload mass for spacecrafts are increased for modern missions.[4] For an interplanetary space explanation within the solar system, a spacecraft should change its velocity on the order of 10^4 m/s. From the rocket equation with assumptions of the constant exhaust velocity and gravity-free space, increasing the enthalpy of propellant or decreasing the payload mass fraction can produce high acceleration of a spacecraft and reduce trip time

$$\Delta v_{sc} = v_{ex} \ln \frac{m_0}{m_f} \tag{1.1}$$

where v_{sc} and v_{ex} are the spacecraft and exhaust velocities, respectively, and m_0 and m_f are initial and dry masses of the spacecraft. The shorter trip time is not only economically beneficial for robotic missions but can reduce the risk of lethal radiational exposures for astronauts. However, larger enthalpy of the exhaust flow usually requires more external power source which reduces the payload mass fraction. There exists a tradeoff between the payload mass fraction and trip time to achieve an optimum thrust.

The methods to increase enthalpy of propellant classify the types of the propulsion systems such as chemical propulsion through combustion, electric propulsion using electrothermal or Lorentz forces, and nuclear propulsion converting fission or fusion energy directly. While chemical propulsion is the oldest and most conventional method, the increase of enthalpy is limited by the chemical binding energy of propellant. Electric propulsion requires a sufficiently large external power source to ionize and accelerate propellant gas. The solar cell is a popular external power source for current electric propulsion, but solar power (electromagnetic field energy) drops as $1/r^2$ where r is the distance from the sun and restricts possible missions beyond Earth orbit. The available energy through nuclear reactions is also limited by nuclear binding force but the corresponding energies are 10^6 or 10^7 higher than those of chemical reactions.[5] However, there are some difficulties to withstand thermal stresses and control radiative flux on a spacecraft. Until today, there does not exist an adequate propulsion system for deep space explorations. Plasma physics can describe the naturally existing charged gas in space environments (e.g., the solar wind, the Van Allen radiation belts) and control thermonuclear fusion. Electric propulsion is one example of the practical applications of plasma physics over the past half century. Nuclear fusion can be applied either to directly accelerate a propellant or to produce electrical power to drive an electric propulsion system. Both approaches offer promising solutions for future space exploration.

1.2 Why Z-pinch Fusion Thruster

The major fusion reactor concepts can be classified by the four methods of confining the plasma: Inertial Electrostatic Confinement (IEC), Magnetic Confinement Fusion (MCF), Inertial Confinement Fusion (ICF), MagnetoInertial Fusion (MIF). IEC uses a spherical grid to produce radial electric field for confining plasma and its simple device known as Farnsworth-Hirsch fusor has been built by some hobbyists.[6] Although it has a simple and low cost assembly, it is difficult to confine hot and dense plasma and achieve the fusion energy breakeven $Q = 1$ due to kinetic instabilities leading to high energy and particle losses. MCF (e.g., equilibrium Z pinches, tokamaks, spheromaks, stellarators, field-reversed configuration (FRC) and magnetic mirrors) uses strong magnetic fields to confine relatively low-density plasma for a long steady-state operation and attracts a lot of plasma physicists and engineers trying to realize a fusion reactor. However, the typical MCF reactor size is too large to mount on a spacecraft. ICF applies spherically distributed high-energy laser pulses onto the pellets to be heated and compressed by implosions and ignites fusion reactions.[7] While ICF can produce highly energized and dense plasma, it is difficult to secure the power source for the laser pulses in space environment. MIF, for example fast Z pinch that quickly implodes a cylindrical plasma, combines the aspects of MCF and ICF. A Shear-Flow-Stabilized (SFS) Z pinch[8], which is equilibrium Z pinch and MCF approach, has self-generated magnetic fields confining and compressing plasma due to the interactions between the azimuthal magnetic fields and the axial current. The advantage of a Z-pinch is that it does not require external magnetic field coils and thereby has reduced cost and complexity. Increasing axial current produces higher plasma parameters and achieves smaller pinch radius. The Z-pinch fusion thruster is described as the viable option for future space explorations by Shumlak et al. in 2006.[9] As plasma flows towards an open end of the Z pinch, its thermal energy heated by fusion products expands and converts to directed kinetic energy and produces thrust.

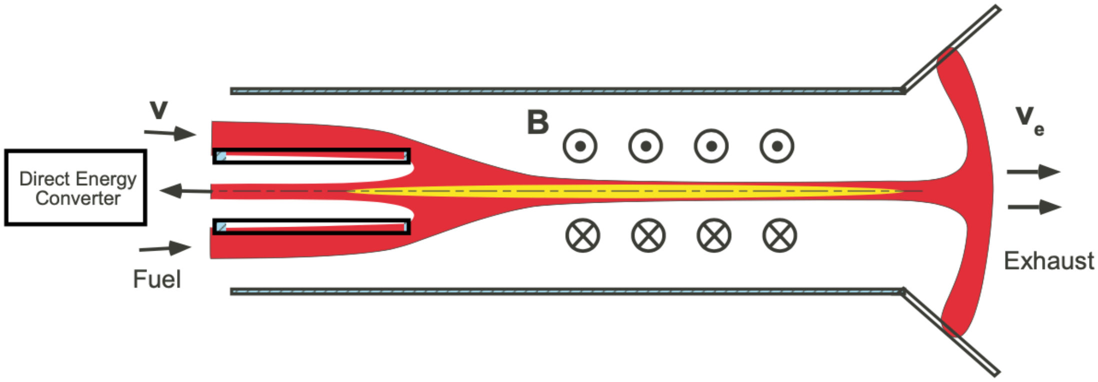

Figure 1.1: Schematic illustration for the Z-pinch fusion thruster

1.3 Importance of Alpha Heating

Deuterium-tritium (D-T) fusion is one of the most promising terrestrial fusion reaction since it has the highest reactivity with the currently feasible temperature of the confined plasma.

$$ {}^2_1\mathrm{D} + {}^3_1\mathrm{T} \longrightarrow \; = {}^4_2\mathrm{He}(3.5\ \mathrm{MeV}) + {}^1_0n(14.1\ \mathrm{MeV}) \tag{1.2} $$

With sufficiently high magnetic fields, the high-temperature alphas can be magnetically confined and heat D-T fuel. This alpha heating effect can significantly increase the fusion gain, Q, which is defined as the ratio of fusion power to input power. Magnetic nozzles, which are produced by external coils, have the potential to improve conversion of the thermal energy of confined alphas into kinetic energy to obtain higher specific impulse and larger thrust. Therefore, it is important to understand the dynamics of energetic alpha particles and their interactions with the bulk Z-pinch plasma.

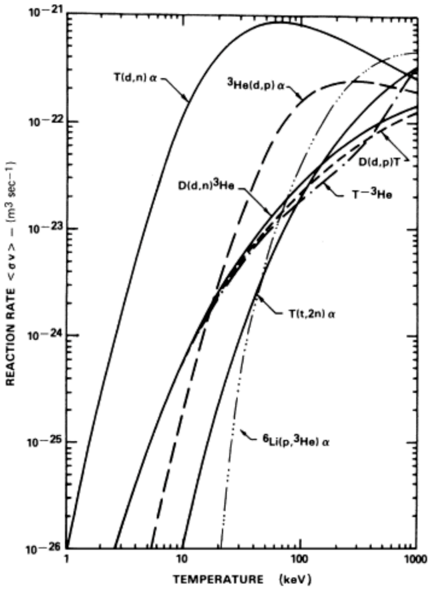

Figure 1.2: Comparison of reaction rates for various fusion fuel temperature[1]

1.4 Outline for the Dissertation

The main components of this research are (1) implementing cylindrical coordinates to simulate axisymmetric plasmas, (2) including a model for thermonuclear fusion reactions in a multi-species plasma, and (3) numerically investigating the dynamics of energetic alphas and the effect of alpha heating in the D-T Z-pinch fusion. The all of numerical results are obtained by using WARPXM version 1.5.9. The dissertation is organized as follows. Chapter 2 describes the numerical methods and develops the WARPXM code with the geometric source terms needed to simulations in the cylindrical geometry, which is useful to describe the physics of the plasma pinch. Chapter 3 presents the results of several benchmark tests for the geometric source terms. The comparisons between the simple analytical results and the numerical results validate the correct implementations of the geometric source terms in WARPXM. Chapter 4 discusses the stability and dynamics of a shear-free and shear-flow-stabilized Z-pinch that includes Braginskii transport, which accounts for non-

Maxwellian or non-ideal distribution functions[10]. Chapter 5 develops the multi-component (e.g., deuterium-tritium-helium-electron) $5N$-moment plasma model for Z-pinch fusion reactions and presents the numerical results of the 1D D-T Z-pinch dynamics as a result of self-consistent fusion reactions and interspecies collisional interactions. This chapter includes the study reactions such that some confined fusion alphas contribute to collisional heating of the fusion fuel. Chapter 6 presents the conclusions and proposes future directions to extend the research.

Chapter 2

NUMERICAL METHODS

Washington Approximate Riemann Plasma eXtended modeling platform - Multi-core (WARPXM)[11] solves the following partial differential equations (PDEs) in conservative form by using the Discontinuous Galerkin (DG) Finite Element Method (FEM)

$$\frac{\partial \vec{Q}}{\partial t} + \nabla \cdot \overset{\leftrightarrow}{F} = \vec{S} \tag{2.1}$$

where $\vec{Q}$ is the vector of conservative variables, $\overset{\leftrightarrow}{F}$ is the flux tensor, $\vec{S}$ is the vector of source terms. Section 2.1 explains the fundamentals and advantages of using DG-FEM. Section 2.2 introduces the general expression of the geometric source terms and gives analytical examples in multiple different plasma fluid models. WARPXM has been developed for meshes and equations described in Cartesian coordinates; however, cylindrical coordinates are useful to describe the geometry of many MCF plasmas, such as the Z pinch. The geometric source terms which were introduced by Srinivasan[12] for WARPX can also be implemented into WARPXM to simulate axisymmetric problems in cylindrical coordinates. Section 2.3 describes the spatial gradients for the conservative variables in DG-FEM. The gradients are used to apply L'Hôpital's rule into the geometric source terms at $r = 0$ in cylindrical coordinates and are used to implement the Braginskii viscosity tensor. The gradients can also be used in Hall and resistive MHD models. Section 2.4 and Section 2.5 shows the boundary conditions and the Runge-Kutta method used for time integration, respectively. Section 2.6 indicates the maximum possible CFL numbers in DG-FEM with the geometric source terms to ensure stable numerical results.

2.1 Discontinuous Galerkin Method

In the Finite Difference Method (FDM), which is the simplest and oldest numerical approach introduced by Euler in 1768[13], the approximate numerical solutions $\vec{Q}_n$, flux $\overleftrightarrow{F}_n$ and source terms $\vec{S}_n$ satisfy

$$\frac{d\vec{Q}_n(\vec{x}^k,t)}{dt} + \nabla \cdot \overleftrightarrow{F}_n(\vec{x}^k,t) - \vec{S}_n(\vec{x}^k,t) = \vec{\mathscr{R}}(\vec{x}^k,t) \tag{2.2}$$

where $\vec{x}^k$ is the local node position and $\vec{\mathscr{R}}$ is the residuals between the exact solution and numerical solution. The flux and source terms are described in terms of $\vec{Q}_n$ and the derivatives are approximated by applying Taylor expansions. Calculations can yield converged numerical solutions and simulations with sufficiently small residuals. However, it is difficult to apply the FDM for a problem with complex geometries and an unstructured mesh.

The Finite Volume Method (FVM) is introduced in the field of Computational Fluid Dynamics (CFD) by Mc-Donald in 1971 and Mac-Cormack and Paullay in 1972[14] based on the FDM, but includes the geometric flexibility. In general, the physical domain is discretized into the finite volumes (cells) V^k, and the integral form of the PDEs within each volume is numerically solved.

$$\frac{d}{dt}\int_{V^k} \vec{Q}_n dV^k + \oint_{\Omega^k} \overleftrightarrow{F}_n \cdot d\vec{\Omega}^k - \int_{V^k} \vec{S}_n dV^k = \vec{\mathscr{R}} \tag{2.3}$$

The integrated numerical solutions, flux and source terms are evaluated as the cell-averaged properties, and the choice of the numerical flux at the finite volume cell interface $\vec{\Omega}^k$ identifies the types of the numerical scheme. While the FVM has the advantageous property of satisfying local conservation, increasing the order of accuracy in space in a high-dimensional problem requires a numerical stencil that expands over many cells and becomes nonlocal. To increase the order of the local approximated solutions on the interface, which are obtained by using the cell-averaged solutions, the FVM requires a particular number of cells that restricts the grid structure and the geometric flexibility.

On the other hand, the FEM does not use cell averages to find the local approximated solutions. The FEM was originally developed in the structural engineering fields by Hrennikoff in 1941[15] and McHenry in 1943[16]. In the FEM, the local approximated solutions $\vec{Q}^k_n$ in the element D^k are expressed as

$$\vec{Q}^k_n(\vec{x},t) = \sum_{l=1}^{N_p} \bar{Q}^k_l(t)\psi^k_l(\vec{x}) = \sum_{l=1}^{N_p} \vec{Q}^k_l(\vec{x}^k_l,t)\ell^k_l(\vec{x}) \tag{2.4}$$

where $\bar{Q}^k_l$ are the coefficients, $\psi^k_l(\vec{x})$ are the basis functions, N_p is the total number of the local nodes in each element D^k and $\ell^k_l(\vec{x})$ are the Lagrange basis polynomials. The first expression using a polynomial basis function $\psi^k_l(\vec{x})$ is known as the modal form and the latter one using the Lagrange basis polynomial $\ell^k_l(\vec{x})$ is known as the nodal form. It is important to mention that the node location $\vec{y}^k_l \in D^k$ associates with the Lagrange basis polynomial $\ell^k_l(\vec{x})$ by using the shifted delta-function $\delta(\vec{x}-\vec{y}^k_l)$; however, $\vec{y}^k_l$ is independent of $\vec{x}^k_l \in D^k$ used to describe the coefficient $\vec{Q}^k_l(\vec{x}^k_l,t)$. The global approximated solutions $\vec{Q}_n$ are obtained by using the piecewise local solutions $\vec{Q}^k_n$,

$$\vec{Q}_n(\vec{x},t) = \bigoplus_{k=1}^{K} \vec{Q}^k_n(\vec{x},t) \tag{2.5}$$

Similarly, the global flux and source terms are

$$\overleftrightarrow{F}_n(\vec{x},t) = \bigoplus_{k=1}^{K} \overleftrightarrow{F}^k_n(\vec{x},t) = \bigoplus_{k=1}^{K}\sum_{l=1}^{N_p} \bar{\overleftrightarrow{F}}^k_l(t)\psi^k_l(\vec{x}) = \bigoplus_{k=1}^{K}\sum_{l=1}^{N_p} \overleftrightarrow{F}^k_l(\vec{x}^k_l,t)\ell^k_l(\vec{x}) \tag{2.6}$$

$$\vec{S}_n(\vec{x},t) = \bigoplus_{k=1}^{K} \vec{S}^k_n(\vec{x},t) = \bigoplus_{k=1}^{K}\sum_{l=1}^{N_p} \bar{S}^k_l(t)\psi^k_l(\vec{x}) = \bigoplus_{k=1}^{K}\sum_{l=1}^{N_p} \vec{S}^k_l(\vec{x}^k_l,t)\ell^k_l(\vec{x}) \tag{2.7}$$

WARPXM adopts the nodal form and the governing equations are

$$\bigoplus_{k=1}^{K}\sum_{l=1}^{N_p}\left[\frac{d}{dt}\vec{Q}^k_l(\vec{x}^k_l,t)\ell^k_l(\vec{x}) + \nabla\cdot\left(\overleftrightarrow{F}^k_l(\vec{x}^k_l,t)\ell^k_l(\vec{x})\right) - \vec{S}^k_l(\vec{x}^k_l,t)\ell^k_l(\vec{x})\right] = \bigoplus_{k=1}^{K}\sum_{l=1}^{N_p}\vec{\mathscr{R}}^k_l(\vec{x},t) \tag{2.8}$$

Einstein notation simplifies the representation as

$$\vec{Q}^k_n(\vec{x},t) = \sum_{l=1}^{N_p} \vec{Q}^k_l(\vec{x}^k_l,t)\ell^k_l(\vec{x}) = \vec{Q}^k_l(\vec{x}^k_l,t)\ell^k_l(\vec{x}) \tag{2.9}$$

Applying the weighted residual method, the governing equations in a local frame become

$$\begin{aligned}\int_{D^k}\left[\frac{d}{dt}\vec{Q}^k_l(\vec{x}^k_l,t)\ell^k_l(\vec{x})w^k_m(\vec{x})+w^k_m(\vec{x})\nabla\cdot\left(\overset{\leftrightarrow}{F}{}^k_l(\vec{x}^k_l,t)\ell^k_l(\vec{x})\right)-\vec{S}^k_l(\vec{x}^k_l,t)\ell^k_l(\vec{x})w^k_m(\vec{x})\right]dV^k&\\ =\int_{D^k}\vec{\mathcal{R}}^k_l(\vec{x},t)w^k_m(\vec{x})dV^k&\end{aligned}\tag{2.10}$$

where $w^k_m(\vec{x})$ is the weight function (test function) and the choice of $w^k_m(\vec{x})$ determines a method of FEMs. The weighted residual methods is adapted by B. A. Szabo and G. C. Lee in 1969.[17] If the weight function is chosen as the same to the basis function, $w^k_m(\vec{x})=\ell^k_l(\vec{x})$, the method is known as the Galerkin method. Using the product rule and the divergence theorem for the flux terms,

$$\begin{aligned}&\int_{D^k}w^k_m(\vec{x})\nabla\cdot\left(\overset{\leftrightarrow}{F}{}^k_l(\vec{x}^k_l,t)\ell^k_l(\vec{x})\right)dV^k\\ &\qquad=\int_{D^k}\nabla\cdot\left(\overset{\leftrightarrow}{F}{}^k_l(\vec{x}^k_l,t)\ell^k_l(\vec{x})w^k_m(\vec{x})\right)dV^k-\int_{D^k}\nabla w^k_m(\vec{x})\cdot\overset{\leftrightarrow}{F}{}^k_l(\vec{x}^k_l,t)\ell^k_l(\vec{x})dV^k\\ &\qquad=\int_{\Omega^k}\overset{\leftrightarrow}{F}{}^k_l(\vec{x}^k_l,t)\ell^k_l(\vec{x})w^k_m(\vec{x})\cdot d\vec{\Omega}^k-\int_{D^k}\nabla w^k_m(\vec{x})\cdot\overset{\leftrightarrow}{F}{}^k_l(\vec{x}^k_l,t)\ell^k_l(\vec{x})dV^k\end{aligned}\tag{2.11}$$

which leads

$$\begin{aligned}\int_{D^k}\left[\frac{d}{dt}\vec{Q}^k_l(\vec{x}^k_l,t)\ell^k_l(\vec{x})w^k_m(\vec{x})-\nabla w^k_m(\vec{x})\cdot\overset{\leftrightarrow}{F}{}^k_l(\vec{x}^k_l,t)\ell^k_l(\vec{x})-\vec{S}^k_l(\vec{x}^k_l,t)\ell^k_l(\vec{x})w^k_m(\vec{x})\right]dV^k&\\ =-\int_{\Omega^k}\overset{\leftrightarrow}{F}{}^k_l(\vec{x}^k_l,t)\ell^k_l(\vec{x})w^k_m(\vec{x})\cdot d\vec{\Omega}^k+\int_{D^k}\vec{\mathcal{R}}^k_l(\vec{x},t)w^k_m(\vec{x})dV^k&\end{aligned}\tag{2.12}$$

This equation can be simplified as

$$\begin{aligned}&\mathcal{M}_{lm}\frac{d}{dt}\vec{Q}^k_l(\vec{x}^k_l,t)-\mathcal{A}_{ilm}\cdot\overset{\leftrightarrow}{F}{}^k_l(\vec{x}^k_l,t)-\mathcal{M}_{lm}\vec{S}^k_l(\vec{x}^k_l,t)\\ &\qquad=-\int_{\Omega^k}\overset{\leftrightarrow}{F}{}^k_l(\vec{x}^k_l,t)\ell^k_l(\vec{x})w^k_m(\vec{x})\cdot d\vec{\Omega}^k+\int_{D^k}\vec{\mathcal{R}}^k_l(\vec{x},t)w^k_m(\vec{x})dV^k\end{aligned}\tag{2.13}$$

where $\mathcal{M}_{lm}$ is the mass matrix and $\mathcal{A}_{lm}$ is the stiffness matrix such that

$$\mathcal{M}_{lm}\equiv\int_{D^k}\ell^k_l(\vec{x})w^k_m(\vec{x})dV^k\tag{2.14}$$

$$\mathcal{A}_{ilm} = \int_{D^k} \ell_l^k(\vec{x}) \nabla_i w_m^k(\vec{x}) dV^k \tag{2.15}$$

Note that the number of subscripts indicates the order of a tensor and those subscripts do not describe the dimensions. In the FEM, the higher order of accuracy in space can be easily achieved by choosing an appropriate order of the basis function without losing the geometric flexibility. However, since the basis function is defined globally, inverting the global mass matrix for time-dependent dynamics becomes quite computationally expensive and the continuous FEM has difficulty at solving problems with discontinuities or problems described by hyperbolic equations. To deal with those problems, the DG method was introduced by Reed and Hill in 1973[18, 19].

In the DG method, the local approximated solutions $\vec{Q}_n^k$ are discontinuous but the interface flux, which is known as the numerical flux and shared by the adjacent elements, is continuous. Thus Eq. (2.12) becomes

$$\begin{aligned}\int_{D^k} \left[\frac{d}{dt} \vec{Q}_l^k(\vec{x}_l^k, t) \ell_l^k(\vec{x}) w_m^k(\vec{x}) - \nabla w_m^k(\vec{x}) \cdot \overset{\leftrightarrow}{F}{}_l^k(\vec{x}_l^k, t) \ell_l^k(\vec{x}) - \vec{S}_l^k(\vec{x}_l^k, t) \ell_l^k(\vec{x}) w_m^k(\vec{x}) \right] dV^k \\ = - \int_{\Omega^k} \overset{\leftrightarrow}{F}{}_l^*(\vec{x}_l^k, t) \ell_l^k(\vec{x}) w_m^k(\vec{x}) \cdot d\vec{\Omega}^k + \int_{D^k} \vec{\mathcal{R}}_l^k(\vec{x}, t) w_m^k(\vec{x}) dV^k\end{aligned} \tag{2.16}$$

where $\overset{\leftrightarrow}{F}{}_l^*(\vec{x}_l^k, t)$ is the numerical flux and $\overset{\leftrightarrow}{F}{}_l^k(\vec{x}_l^k, t)$ is called the internal flux. Similar to the FVM, the choice of numerical flux identifies the type of numerical scheme, and limiter are applied to improve numerical stability.

2.2 Geometric Source Terms

The governing equation Eq. (2.1) in Cartesian coordinates is

$$
\begin{aligned}
\frac{\partial \vec{Q}}{\partial t} + \nabla \cdot \overset{\leftrightarrow}{F} &= \frac{\partial \vec{Q}}{\partial t} + \begin{bmatrix} \frac{\partial F_{xx}}{\partial x} + \frac{\partial F_{yx}}{\partial y} + \frac{\partial F_{zx}}{\partial z} \\ \frac{\partial F_{xy}}{\partial x} + \frac{\partial F_{yy}}{\partial y} + \frac{\partial F_{zy}}{\partial z} \\ \frac{\partial F_{xz}}{\partial x} + \frac{\partial F_{yz}}{\partial y} + \frac{\partial F_{zz}}{\partial z} \end{bmatrix} \\
&= \frac{\partial \vec{Q}}{\partial t} + \frac{\partial F_{ij}}{\partial q^k} g^{ik} \vec{b}^j = \vec{S} \qquad (2.17) \\
&= \frac{\partial \vec{Q}}{\partial t} + \frac{\partial}{\partial q^k} \left(\frac{\bar{F}_{ij}}{\sqrt{g^{ii} g^{jj}}} \right) g^{ik} \sqrt{g^{jj}} \bar{b}^j = \vec{S} \\
&= \frac{\partial \vec{Q}}{\partial t} + \frac{\partial \bar{F}_{ij}}{\partial q^k} g^{ik} \bar{b}^j = \vec{S}
\end{aligned}
$$

where q^i is the generalized coordinates $(q^1, q^2, q^3) = (x, y, z)$, $[g^{ij}]$ is the contravariant metric tensor, $\vec{b}$ is the basis vector and $\bar{b}^j$ is the normalized contravariant basis vector

$$
\bar{b}^j = \frac{\vec{b}^j}{\sqrt{g^{jj}}} \qquad (2.18)
$$

The indices follow the Einstein notation and the summations for a first-order tensor (vector) can be simplified as

$$
\vec{Q} = \sum_{j=1} Q_j \vec{b}^j = Q_j \vec{b}^j \qquad (2.19)
$$

where Q_j are covariant components of $\vec{Q}$. Using contravariant components Q^j and physical components $\bar{Q}_j$,

$$
\vec{Q} = Q_j \vec{b}^j = Q^j \vec{b}_j = \bar{Q}_j \bar{b}^j \qquad (2.20)
$$

In general curvilinear coordinates (e.g., cylindrical coordinates and spherical coordinates), $Q_j \neq Q^j \neq \bar{Q}_j$. Similarly, a second-order tensor (matrix) can be expressed as

$$
\overset{\leftrightarrow}{F} = F^{ij} \vec{b}_i \otimes \vec{b}_j = F_{ij} \vec{b}^i \otimes \vec{b}^j = \bar{F}_{ij} \bar{b}^i \otimes \bar{b}^j \qquad (2.21)
$$

where the physical components $\bar{F}_{ij}$ are

$$\bar{F}_{ij} = F_{ij}\sqrt{g^{ii}g^{jj}} \tag{2.22}$$

While none of those differences show up in Cartesian coordinates on a Euclidian space, the covariance, the contravariance and the metric tensor are important to consider for spatial derivatives in curvilinear coordinates. The brief summary of those notations in the Riemannian geometry, particularly the tensor analysis in curvilinear coordinates[20, 21, 22, 23, 24], is provided in Appendix A. In curvilinear coordinates, the divergence of a first-order flux tensor (vector) is

$$\begin{aligned}\nabla \cdot \overset{\leftrightarrow}{F} &= \frac{\partial F^i}{\partial q^i} - \Gamma^i_{li}F^l = \left[\frac{\partial F_i}{\partial q^k} - \Gamma^l_{ki}F_l\right] g^{ik} \\ &= \left[\frac{1}{\sqrt{g^{ii}}}\frac{\partial \bar{F}_i}{\partial q^k} + \bar{F}_i\frac{\partial}{\partial q^k}\left(\frac{1}{\sqrt{g^{ii}}}\right) - \Gamma^l_{ki}\frac{\bar{F}_l}{\sqrt{g^{ll}}}\right] g^{ik}\end{aligned} \tag{2.23}$$

where Γ^i_{jk} is the Christoffel symbol defined as

$$\Gamma^t_{ij} \equiv \frac{1}{2}g^{tk}\left(\frac{\partial g_{jk}}{\partial q^i} + \frac{\partial g_{ki}}{\partial q^j} - \frac{\partial g_{ij}}{\partial q^k}\right) \tag{2.24}$$

Using Eq. (2.21), the divergence of a second-flux tensor becomes

$$\begin{aligned}\nabla \cdot \overset{\leftrightarrow}{F} &= \left[\frac{\partial F^{ij}}{\partial q^i} + \Gamma^i_{il}F^{lj} + \Gamma^j_{il}F^{il}\right]\vec{b}_j = \left[\frac{\partial F_{ij}}{\partial q^k} - \Gamma^l_{ki}F_{lj} - \Gamma^l_{kj}F_{il}\right] g^{ik}\vec{b}^j \\ &= \left[\frac{1}{\sqrt{g^{ii}g^{jj}}}\frac{\partial \bar{F}_{ij}}{\partial q^k} + \bar{F}_{ij}\frac{\partial}{\partial q^k}\left(\frac{1}{\sqrt{g^{ii}g^{jj}}}\right) - \Gamma^l_{ki}\frac{\bar{F}_{lj}}{\sqrt{g^{ll}g^{jj}}} - \Gamma^l_{kj}\frac{\bar{F}_{il}}{\sqrt{g^{ii}g^{ll}}}\right] g^{ik}\sqrt{g^{jj}}\bar{b}^j\end{aligned} \tag{2.25}$$

when implemented transforms the governing equation to

$$\begin{aligned}&\frac{\partial \vec{Q}}{\partial t} + \nabla \cdot \overset{\leftrightarrow}{F} \\ &\quad = \frac{\partial \vec{Q}}{\partial t} + \left[\frac{1}{\sqrt{g^{ii}g^{jj}}}\frac{\partial \bar{F}_{ij}}{\partial q^k} + \bar{F}_{ij}\frac{\partial}{\partial q^k}\left(\frac{1}{\sqrt{g^{ii}g^{jj}}}\right) - \Gamma^l_{ki}\frac{\bar{F}_{lj}}{\sqrt{g^{ll}g^{jj}}} - \Gamma^l_{kj}\frac{\bar{F}_{il}}{\sqrt{g^{ii}g^{ll}}}\right] g^{ik}\sqrt{g^{jj}}\bar{b}^j \\ &\quad = \vec{S}\end{aligned} \tag{2.26}$$

The divergence of a higher-order tensor can be derived in the similar manner. In Euclidean space with an orthonormal basis (e.g., Cartesian coordinates), the metric tensor becomes identical to the Kronecker delta δ_{ij} (or the identity matrix $\overleftrightarrow{I}$)

$$\left[g^{ij}\right]_{Cart} = \delta^{ij} = \begin{bmatrix} 1 & 0 & 0 \\ 0 & 1 & 0 \\ 0 & 0 & 1 \end{bmatrix} \tag{2.27}$$

which yields $\frac{\partial}{\partial q^k}\left(\frac{1}{\sqrt{g^{ii}g^{jj}}}\right)$ and the Christoffel symbols are zero in Eq. (2.26). In curvilinear coordinates, those terms are not necessarily zero and can be treated as geometric source terms $\vec{\mathcal{S}}$ such that

$$\vec{\mathcal{S}} = \left[-\bar{F}_{ij}\frac{\partial}{\partial q^k}\left(\frac{1}{\sqrt{g^{ii}g^{jj}}}\right) + \Gamma^l_{ki}\frac{\bar{F}_{lj}}{\sqrt{g^{ll}g^{jj}}} + \Gamma^l_{kj}\frac{\bar{F}_{il}}{\sqrt{g^{ii}g^{ll}}}\right] g^{ik}\sqrt{g^{jj}}\bar{b}^j \tag{2.28}$$

Therefore, the governing equations in curvilinear coordinates can be expressed as

$$\frac{\partial \vec{Q}}{\partial t} + \frac{1}{\sqrt{g^{ii}g^{jj}}}\frac{\partial \bar{F}_{ij}}{\partial q^k} g^{ik}\bar{b}^j = \vec{S} + \vec{\mathcal{S}} \tag{2.29}$$

Note that the spatial derivatives $\frac{1}{\sqrt{g^{ii}g^{jj}}}\frac{\partial \bar{F}_{ij}}{\partial q^k} g^{ik}\bar{b}^j$ in cylindrical (curvilinear) coordinates are different from the ones in Cartesian coordinates due to the different metric tensors. In three-dimensional cylindrical coordinates where $(q^1, q^2, q^3) = (r, \theta, z)$,

$$\left[g^{ij}\right]_{Cyl} = \begin{bmatrix} 1 & 0 & 0 \\ 0 & \frac{1}{r^2} & 0 \\ 0 & 0 & 1 \end{bmatrix} \tag{2.30}$$

Comparing with Eq(2.27), the difference shows up in the $i = k = 2$ component of the spatial derivatives $\frac{1}{\sqrt{g^{ii}g^{jj}}}\frac{\partial \bar{F}_{ij}}{\partial q^k} g^{ik}\bar{b}^j$; however, the axisymmetric assumption $\frac{\partial}{\partial q^2} = \frac{\partial}{\partial \theta} = 0$ causes portions of the metric tensor to vanish. Thus, adding geometric source terms allows simulating axisymmetric problems in cylindrical coordinates without changing the infrastructure significantly in WARPXM.

2.2.1 Maxwell's Equations

The governing equations for plasma physics include Maxwell's quations, specifically Ampère's law and Faraday's law. Gauss' laws for Electromagnetic (EM) fields should be satisfied by initial conditions and boundary conditions. The typical expressions for Ampère's law and Faraday's law are not in the conservative form. Ampère's law and Faraday's law are

$$-\epsilon_0 \mu_0 \frac{\partial \vec{E}}{\partial t} + \nabla \times \vec{B} = \mu_0 \vec{J} \tag{2.31}$$

$$\frac{\partial \vec{B}}{\partial t} + \nabla \times \vec{E} = 0 \tag{2.32}$$

respectively and Gauss' laws for EM fields are

$$\epsilon_0 \nabla \cdot \vec{E} = \rho_c \tag{2.33}$$

$$\nabla \cdot \vec{B} = 0 \tag{2.34}$$

where $\vec{E}$ is the electric field, $\vec{B}$ is the magnetic field, $\vec{J}$ is the current density, ρ_c is the charge density, μ_0 is the permeability in vacuum and ϵ_0 is the permittivity in vacuum. Considering the curl of a first-order tensor $\overset{\leftrightarrow}{F}$,

$$\nabla \times \overset{\leftrightarrow}{F} = \epsilon^{ijk} \left[\frac{\partial F_j}{\partial q^i} - \Gamma^l_{ji} F_l \right] \vec{b}_k \tag{2.35}$$

where

$$\epsilon_{ijk} = \frac{1}{\sqrt{|\det[g_{ij}]|}} \varepsilon_{ijk} \tag{2.36}$$

$$\epsilon^{ijk} = \sqrt{|\det[g_{ij}]|} \varepsilon^{ijk} \tag{2.37}$$

$$\varepsilon_{ijk} = \varepsilon^{ijk} = \begin{cases} +1 & \text{if } (i,j,k) \text{ is an even permutation of } (1,2,3) \\ -1 & \text{if } (i,j,k) \text{ is an odd permutation of } (1,2,3) \\ 0 & \text{otherwise} \end{cases} \tag{2.38}$$

ϵ_{ijk} and ϵ^{ijk} are covariant and contravariant permutation symbols, respectively and $\varepsilon_{ijk} = \varepsilon^{ijk}$ are permutation symbols known as the Levi-Civita symbols. Since the l-th Christoffel symbols are symmetric

$$\Gamma^l_{ij} = \Gamma^l_{ji} \tag{2.39}$$

the covariant derivatives multiplied by the permutation symbols can be simplified as

$$\epsilon^{ijk}\left[\frac{\partial F_j}{\partial q^i} - \Gamma^l_{ji}F_l\right]\vec{b}_k = \epsilon^{ijk}\frac{\partial F_j}{\partial q^i}\vec{b}_k \tag{2.40}$$

which leads

$$\begin{aligned}\nabla \times \overset{\leftrightarrow}{F} =&\epsilon^{ijk}\left[\frac{\partial F_j}{\partial q^i} - \Gamma^l_{ji}F_l\right]\vec{b}_k = \epsilon^{ijk}\frac{\partial F_j}{\partial q^i}g_{kk}\vec{b}^k \\ =&\ \epsilon^{ijk}\left[\frac{1}{\sqrt{g^{jj}}}\frac{\partial \bar{F}_j}{\partial q^i} + \bar{F}_j\frac{\partial}{\partial q^i}\left(\frac{1}{\sqrt{g^{jj}}}\right)\right]g_{kk}\sqrt{g^{kk}}\bar{b}^k\end{aligned} \tag{2.41}$$

Eq. (2.41) obviously indicates different tensor form compared with Eqs. (2.23) and (2.25). However, the first term in Eq. (2.41) can be manipulated such that the spatial derivatives in the divergence of a tensor in the conservative form and the second term can be treated as geometric source terms. Maxwell's equations can then be expressed as

$$\frac{\partial \vec{Q}}{\partial t} + \epsilon^{ijk}\frac{1}{\sqrt{g^{jj}}}\frac{\partial \bar{F}_j}{\partial q^i}g_{kk}\sqrt{g^{kk}}\bar{b}^k = \vec{S} + \vec{\mathcal{S}} \tag{2.42}$$

where

$$\vec{\mathcal{S}} = \epsilon^{ijk}\bar{F}_j\frac{\partial}{\partial q^i}\left(\frac{1}{\sqrt{g^{jj}}}\right)g_{kk}\sqrt{g^{kk}}\bar{b}^k \tag{2.43}$$

Again, while the spatial derivatives $\epsilon^{ijk}\frac{1}{\sqrt{g^{jj}}}\frac{\partial \bar{F}_j}{\partial q^i}g_{kk}\sqrt{g^{kk}}\bar{b}^k$ in Cartesian coordinates are different from the ones in cylindrical coordinates due to the different metric tensors, they can be treated by applying axisymmetric assumptions in cylindrical coordinates and adding appropriate source terms to the Cartesian form of the governing equations. Therefore, the Maxwell's equations in cylindrical coordinates with the axisymmetric assumptions in WARPXM can be manipulated to satisfy the conservative form of the governing equations, Eq. (2.1), by using the following physical components

$$\vec{Q} = \begin{bmatrix} E_r \\ E_\theta \\ E_z \\ B_r \\ B_\theta \\ B_z \end{bmatrix} \tag{2.44}$$

$$\overset{\leftrightarrow}{F} = \begin{bmatrix} 0 & -c^2B_z & c^2B_\theta \\ c^2B_z & 0 & -c^2B_r \\ -c^2B_\theta & c^2B_r & 0 \\ 0 & E_z & -E_\theta \\ -E_z & 0 & E_r \\ E_\theta & -E_r & 0 \end{bmatrix} \tag{2.45}$$

$$\vec{S} = \begin{bmatrix} -c^2\mu_0 J_r \\ -c^2\mu_0 J_\theta \\ -c^2\mu_0 J_z \\ 0 \\ 0 \\ 0 \end{bmatrix} \tag{2.46}$$

$$\vec{\mathcal{S}} = \begin{bmatrix} 0 \\ 0 \\ c^2\frac{B_\theta}{r} \\ 0 \\ 0 \\ -\frac{E_\theta}{r} \end{bmatrix} \tag{2.47}$$

Note that at $r = 0$, the geometric source terms become singular. In three-dimensional cylindrical coordinates, Eq. (2.43) can be expressed as

$$\vec{\mathcal{S}} = \epsilon^{ijk}\bar{F}_j\frac{\partial}{\partial q^i}\left(\frac{1}{\sqrt{g^{jj}}}\right)g_{kk}\sqrt{g^{kk}}\bar{b}^k = -\begin{bmatrix}0\\0\\\frac{\bar{F}_\theta}{r}\end{bmatrix} \tag{2.48}$$

If the numerators of Eq. (2.48) satisfy the following conditions

$$\lim_{r\to 0}\bar{F}_\theta = 0 \tag{2.49}$$

and $\lim_{r\to 0}\frac{\partial\bar{F}_\theta}{\partial r}$ exists, L'Hôpital's rule can be applied to resolve the singular case such that

$$\lim_{r\to 0}\frac{\bar{F}_\theta}{r} = \lim_{r\to 0}\frac{\partial\bar{F}_\theta}{\partial r} \tag{2.50}$$

In general, Eqs. (2.49) and the existence of the derivative can be satisfied by choosing appropriate assumptions and boundary conditions at $r = 0$.

2.2.2 5N-moment Multi-Fluid Plasma Model

The governing equations for a fluid model for a multi-species plasma are derived by taking moments of the Vlasov-Boltzmann equation (see Appendix B.1). The $5N$-moment fluid model consists of a continuity equation, a momentum equation, and an energy equation for each of the N plasma species. In particular, the scalar energy equation in the $5N$-moment fluid model is obtained by using a tensor contraction of the dyadic products of the second velocity moment. Thus, the continuity equation and the energy equation have the divergence of a first-order flux tensor $\vec{F}$, but the momentum equation contains the divergence of a second-order flux tensor $\overleftrightarrow{F}$. In general, a higher-moment fluid model is described by using a higher-order tensor. From Eq. (2.23), the divergence of a first-order tensor in cylindrical coordinates with axisymmetric assumptions is

$$\begin{aligned}\nabla\cdot\overleftrightarrow{F} &= \left[\frac{1}{\sqrt{g^{ii}}}\frac{\partial\bar{F}_i}{\partial q^k} + \bar{F}_i\frac{\partial}{\partial q^k}\left(\frac{1}{\sqrt{g^{ii}}}\right) - \Gamma^l_{ki}\frac{\bar{F}_l}{\sqrt{g^{ll}}}\right]g^{ik}\\ &= \frac{\partial\bar{F}_r}{\partial r} + \cancel{\frac{1}{r}\frac{\partial\bar{F}_\theta}{\partial\theta}} + \frac{\bar{F}_r}{r} + \frac{\partial\bar{F}_z}{\partial z}\end{aligned} \tag{2.51}$$

which yields the following geometric source terms

$$\mathcal{S} = \left[-\bar{F}_i \frac{\partial}{\partial q^k} \left(\frac{1}{\sqrt{g^{ii}}} \right) + \Gamma^l_{ki} \frac{\bar{F}_l}{\sqrt{g^{ll}}} \right] g^{ik} = -\frac{\bar{F}_r}{r} \tag{2.52}$$

Also, Eq. (2.25) indicates the divergence of a second-order tensor in cylindrical coordinates with the axisymmetric assumptions as

$$\begin{aligned} \nabla \cdot \overset{\leftrightarrow}{F} &= \left[\frac{1}{\sqrt{g^{ii} g^{jj}}} \frac{\partial \bar{F}_{ij}}{\partial q^k} + \bar{F}_{ij} \frac{\partial}{\partial q^k} \left(\frac{1}{\sqrt{g^{ii} g^{jj}}} \right) - \Gamma^l_{ki} \frac{\bar{F}_{lj}}{\sqrt{g^{ll} g^{jj}}} - \Gamma^l_{kj} \frac{\bar{F}_{il}}{\sqrt{g^{ii} g^{ll}}} \right] g^{ik} \sqrt{g^{jj}} \bar{b}^j \\ &= \begin{bmatrix} \frac{\partial \bar{F}_{rr}}{\partial r} + \cancel{\frac{1}{r} \frac{\partial \bar{F}_{r\theta}}{\partial \theta}} + \frac{\bar{F}_{rr}}{r} - \frac{\bar{F}_{\theta\theta}}{r} + \frac{\partial \bar{F}_{zr}}{\partial z} \\ \frac{\partial \bar{F}_{r\theta}}{\partial r} + \cancel{\frac{1}{r} \frac{\partial \bar{F}_{\theta\theta}}{\partial \theta}} + \frac{\bar{F}_{r\theta}}{r} + \frac{\bar{F}_{\theta r}}{r} + \frac{\partial \bar{F}_{z\theta}}{\partial z} \\ \frac{\partial \bar{F}_{rz}}{\partial r} + \cancel{\frac{1}{r} \frac{\partial \bar{F}_{\theta z}}{\partial \theta}} + \frac{\bar{F}_{rz}}{r} + \frac{\partial \bar{F}_{zz}}{\partial z} \end{bmatrix} \end{aligned} \tag{2.53}$$

where

$$\begin{aligned} \vec{\mathcal{S}} &= \left[-\bar{F}_{ij} \frac{\partial}{\partial q^k} \left(\frac{1}{\sqrt{g^{ii} g^{jj}}} \right) + \Gamma^l_{ki} \frac{\bar{F}_{lj}}{\sqrt{g^{ll} g^{jj}}} + \Gamma^l_{kj} \frac{\bar{F}_{il}}{\sqrt{g^{ii} g^{ll}}} \right] g^{ik} \sqrt{g^{jj}} \bar{b}^j \\ &= - \begin{bmatrix} \frac{\bar{F}_{rr} - \bar{F}_{\theta\theta}}{r} \\ \frac{\bar{F}_{r\theta} + \bar{F}_{\theta r}}{r} \\ \frac{\bar{F}_{rz}}{r} \end{bmatrix} \end{aligned} \tag{2.54}$$

Similar to Maxwell's equations in axisymmetric cylindrical coordinates, the $5N$-moment fluid model can become undefined at $r = 0$ since the geometric source terms become singular. If the numerators of Eqs. (2.52) and (2.54) satisfy the following conditions

$$\lim_{r \to 0} \begin{bmatrix} \bar{F}_r \\ \bar{F}_{rr} - \bar{F}_{\theta\theta} \\ \bar{F}_{r\theta} + \bar{F}_{\theta r} \\ \bar{F}_{rz} \end{bmatrix} = 0 \tag{2.55}$$

and the derivatives of Eq. (2.55) exist, L'Hôpital's rule can be applied to resolve the evaluations at the geometric axis such that

$$\lim_{r\to 0}\begin{bmatrix} \frac{\bar{F}_r}{r} \\ \frac{\bar{F}_{rr}-\bar{F}_{\theta\theta}}{r} \\ \frac{\bar{F}_{r\theta}+\bar{F}_{\theta r}}{r} \\ \frac{\bar{F}_{rz}}{r} \end{bmatrix} = \lim_{r\to 0}\begin{bmatrix} \frac{\partial \bar{F}_r}{\partial r} \\ \frac{\partial}{\partial r}(\bar{F}_{rr}-\bar{F}_{\theta\theta}) \\ \frac{\partial}{\partial r}(\bar{F}_{r\theta}+\bar{F}_{\theta r}) \\ \frac{\partial \bar{F}_{rz}}{\partial r} \end{bmatrix} \tag{2.56}$$

Therefore, in the $5N$-moment multi-fluid plasma model, the conservative variables $\vec{Q}_\alpha$, the flux $\overset{\leftrightarrow}{F}_\alpha$, the source terms $\vec{S}_\alpha$ and geometric source terms $\vec{\mathcal{S}}_\alpha$ for each species α in axisymmetric cylindrical coordinates are

$$\vec{Q}_\alpha = \begin{bmatrix} \rho_\alpha \\ \rho_\alpha u_{\alpha r} \\ \rho_\alpha u_{\alpha\theta} \\ \rho_\alpha u_{\alpha z} \\ \epsilon_\alpha \\ E_r \\ E_\theta \\ E_z \\ B_r \\ B_\theta \\ B_z \end{bmatrix} \tag{2.57}$$

$$\overleftrightarrow{F}_\alpha = \begin{bmatrix} \rho_\alpha u_{\alpha r} & \rho_\alpha u_{\alpha\theta} & \rho_\alpha u_{\alpha z} \\ \rho_\alpha u_{\alpha r} u_{\alpha r} + P_{\alpha rr} & \rho_\alpha u_{\alpha\theta} u_{\alpha r} + P_{\alpha\theta r} & \rho_\alpha u_{\alpha z} u_{\alpha r} + P_{\alpha zr} \\ \rho_\alpha u_{\alpha r} u_{\alpha\theta} + P_{\alpha r\theta} & \rho_\alpha u_{\alpha\theta} u_{\alpha\theta} + P_{\alpha\theta\theta} & \rho_\alpha u_{\alpha z} u_{\alpha\theta} + P_{\alpha z\theta} \\ \rho_\alpha u_{\alpha r} u_{\alpha z} + P_{\alpha rz} & \rho_\alpha u_{\alpha\theta} u_{\alpha z} + P_{\alpha\theta z} & \rho_\alpha u_{\alpha z} u_{\alpha z} + P_{\alpha zz} \\ \epsilon_\alpha u_{\alpha r} + \left(\vec{u}_\alpha \cdot \overleftrightarrow{P}_\alpha\right) \cdot \hat{r} + h_{\alpha r} & \epsilon_\alpha u_{\alpha\theta} + \left(\vec{u}_\alpha \cdot \overleftrightarrow{P}_\alpha\right) \cdot \hat{\theta} + h_{\alpha\theta} & \epsilon_\alpha u_{\alpha z} + \left(\vec{u}_\alpha \cdot \overleftrightarrow{P}_\alpha\right) \cdot \hat{z} + h_{\alpha z} \\ 0 & -c^2 B_z & c^2 B_\theta \\ c^2 B_z & 0 & -c^2 B_r \\ -c^2 B_\theta & c^2 B_r & 0 \\ 0 & E_z & -E_\theta \\ -E_z & 0 & E_r \\ E_\theta & -E_r & 0 \end{bmatrix} \tag{2.58}$$

$$\vec{S}_\alpha = \begin{bmatrix} 0 \\ \rho_{c\alpha}\left(E_r + u_{\alpha\theta} B_z - u_{\alpha z} B_\theta\right) + \sum_{\beta\neq\alpha} R_{\alpha\beta r} \\ \rho_{c\alpha}\left(E_\theta + u_{\alpha z} B_r - u_{\alpha r} B_z\right) + \sum_{\beta\neq\alpha} R_{\alpha\beta\theta} \\ \rho_{c\alpha}\left(E_z + u_{\alpha r} B_\theta - u_{\alpha\theta} B_r\right) + \sum_{\beta\neq\alpha} R_{\alpha\beta z} \\ \rho_{c\alpha}\vec{u}_\alpha \cdot \vec{E} + \sum_{\beta\neq\alpha}\left(\vec{u}_\alpha \cdot \vec{R}_{\alpha\beta} + \mathcal{Q}_{\alpha\beta}\right) \\ -c^2 \mu_0 J_r \\ -c^2 \mu_0 J_\theta \\ -c^2 \mu_0 J_z \\ 0 \\ 0 \\ 0 \end{bmatrix} \tag{2.59}$$

$$\vec{\mathcal{S}}_\alpha = -\frac{1}{r}\begin{bmatrix} \rho_\alpha u_{\alpha r} \\ (\rho_\alpha u_{\alpha r} u_{\alpha r} + P_{\alpha rr}) - (\rho_\alpha u_{\alpha\theta} u_{\alpha\theta} + P_{\alpha\theta\theta}) \\ 2\rho_\alpha u_{\alpha\theta} u_{\alpha r} + P_{\alpha\theta r} + P_{\alpha r\theta} \\ \rho_\alpha u_{\alpha z} u_{\alpha r} + P_{\alpha zr} \\ \epsilon_\alpha u_{\alpha r} + \left(\vec{u}_\alpha \cdot \overset{\leftrightarrow}{P}_\alpha\right) \cdot \hat{r} + h_{\alpha r} \\ 0 \\ 0 \\ -c^2 B_\theta \\ 0 \\ 0 \\ E_\theta \end{bmatrix} \tag{2.60}$$

where ρ_α and $\rho_{c\alpha}$ are the mass density and the charge density, respectively

$$\rho_\alpha = n_\alpha m_\alpha \tag{2.61}$$

$$\rho_{c\alpha} = n_\alpha q_\alpha \tag{2.62}$$

n_α is the number density, m_α is the mass and q_α is the charge. $\vec{u}_\alpha$ is the fluid bulk velocity and $\vec{J}$ is the net current density

$$\vec{J} = \sum_\alpha \vec{J}_\alpha = \sum_\alpha \rho_{c\alpha} \vec{u}_\alpha \tag{2.63}$$

ϵ_α is the total energy

$$\epsilon_\alpha = \frac{1}{\gamma - 1} P_\alpha + \frac{1}{2}\rho_\alpha u_\alpha^2 \tag{2.64}$$

where γ is the heat capacity ratio and P_α is the isotropic pressure satisfying

$$\overset{\leftrightarrow}{P}_\alpha = P_\alpha \overset{\leftrightarrow}{I} + \overset{\leftrightarrow}{\Pi}_\alpha \tag{2.65}$$

where $\overset{\leftrightarrow}{I}$ is the identity matrix and $\overset{\leftrightarrow}{\Pi}_\alpha$ is the anisotropic pressure (Braginskii stress) tensor.[10] $\left(\hat{r}, \hat{\theta}, \hat{z}\right)$ are the physical unit vectors. $\vec{h}_\alpha$ is the heat flux, $\vec{R}_{\alpha\beta}$ is the frictional force due to the random collisions between species α and β and $\mathcal{Q}_{\alpha\beta}$ is the frictional heat generation due to the random collisions. Applying the following assumptions,

$$\overleftrightarrow{\Pi}_\alpha = \overleftrightarrow{0} \tag{2.66}$$

$$\vec{h}_\alpha = \vec{0} \tag{2.67}$$

$$\vec{R}_{\alpha\beta} = \vec{0} \tag{2.68}$$

$$\mathcal{Q}_{\alpha\beta} = 0 \tag{2.69}$$

the generalized $5N$-moment fluid model can be simplified as the ideal $5N$-moment fluid model such that

$$\vec{Q}_\alpha = \begin{bmatrix} \rho_\alpha \\ \rho_\alpha u_{\alpha r} \\ \rho_\alpha u_{\alpha\theta} \\ \rho_\alpha u_{\alpha z} \\ \epsilon_\alpha \\ E_r \\ E_\theta \\ E_z \\ B_r \\ B_\theta \\ B_z \end{bmatrix} \tag{2.70}$$

$$\overset{\leftrightarrow}{F}_\alpha = \begin{bmatrix} \rho_\alpha u_{\alpha r} & \rho_\alpha u_{\alpha\theta} & \rho_\alpha u_{\alpha z} \\ \rho_\alpha u_{\alpha r} u_{\alpha r} + P_\alpha & \rho_\alpha u_{\alpha\theta} u_{\alpha r} & \rho_\alpha u_{\alpha z} u_{\alpha r} \\ \rho_\alpha u_{\alpha r} u_{\alpha\theta} & \rho_\alpha u_{\alpha\theta} u_{\alpha\theta} + P_\alpha & \rho_\alpha u_{\alpha z} u_{\alpha\theta} \\ \rho_\alpha u_{\alpha r} u_{\alpha z} & \rho_\alpha u_{\alpha\theta} u_{\alpha z} & \rho_\alpha u_{\alpha z} u_{\alpha z} + P_\alpha \\ \left(\epsilon_\alpha + P_\alpha\right) u_{\alpha r} & \left(\epsilon_\alpha + P_\alpha\right) u_{\alpha\theta} & \left(\epsilon_\alpha + P_\alpha\right) u_{\alpha z} \\ 0 & -c^2 B_z & c^2 B_\theta \\ c^2 B_z & 0 & -c^2 B_r \\ -c^2 B_\theta & c^2 B_r & 0 \\ 0 & E_z & -E_\theta \\ -E_z & 0 & E_r \\ E_\theta & -E_r & 0 \end{bmatrix} \tag{2.71}$$

$$\vec{S}_\alpha = \begin{bmatrix} 0 \\ \rho_{c\alpha}\left(E_r + u_{\alpha\theta} B_z - u_{\alpha z} B_\theta\right) \\ \rho_{c\alpha}\left(E_\theta + u_{\alpha z} B_r - u_{\alpha r} B_z\right) \\ \rho_{c\alpha}\left(E_z + u_{\alpha r} B_\theta - u_{\alpha\theta} B_r\right) \\ \rho_{c\alpha} \vec{u}_\alpha \cdot \vec{E} \\ -c^2 \mu_0 J_r \\ -c^2 \mu_0 J_\theta \\ -c^2 \mu_0 J_z \\ 0 \\ 0 \\ 0 \end{bmatrix} \tag{2.72}$$

$$\vec{\mathcal{S}}_\alpha = -\frac{1}{r}\begin{bmatrix} \rho_\alpha u_{\alpha r} \\ \rho_\alpha \left(u_{\alpha r} u_{\alpha r} - u_{\alpha\theta} u_{\alpha\theta}\right) \\ 2\rho_\alpha u_{\alpha\theta} u_{\alpha r} \\ \rho_\alpha u_{\alpha z} u_{\alpha r} \\ \left(\epsilon_\alpha + P_\alpha\right) u_{\alpha r} \\ 0 \\ 0 \\ -c^2 B_\theta \\ 0 \\ 0 \\ E_\theta \end{bmatrix} \tag{2.73}$$

2.2.3 Ideal MHD Model

While this dissertation mainly focuses on the physics in the multi-fluid model, the geometric source terms can also be implemented in various MagnetoHydroDynamic (MHD) models. The following subsections provide the analytical forms of the geometric source terms for the ideal, Hall and resistive MHD models. The typical and general MHD model is derived by applying the following asymptotic approximations for a center-of-mass single-fluid model extended from a $5N$-moment two-fluid model.

1. Infinite speed of light

$$\epsilon_0 \to 0$$

2. Negligible electron inertia

$$m_e \to 0$$

where the speed of light c is

$$c = \frac{1}{\sqrt{\epsilon_0 \mu_0}} \tag{2.74}$$

In the generalized MHD model, the continuity equation is

$$\frac{\partial \rho}{\partial t} + \nabla \cdot (\rho \vec{u}) = 0 \tag{2.75}$$

where ρ is the mass density and $\vec{u}$ is the fluid velocity. The momentum equation is

$$\frac{\partial \left(\rho \vec{u}\right)}{\partial t} + \nabla \cdot \left(\rho \vec{u}\vec{u} + P\overleftrightarrow{I} + \overleftrightarrow{\Pi}\right) = \vec{J} \times \vec{B} \tag{2.76}$$

where P is the isotropic pressure and $\overleftrightarrow{\Pi}$ is the anisotropic pressure tensor. The right hand side of Eq. (2.76) can be expressed in terms of the divergence by using Ampére's law, Eq. (2.31), and Gauss' law for magnetic fields, Eq. (2.34), such that

$$\begin{aligned} \vec{J} \times \vec{B} &= \frac{1}{\mu_0}\left(\nabla \times \vec{B}\right) \times \vec{B} \\ &= \frac{1}{\mu_0}\left[\left(\vec{B} \cdot \nabla\right)\vec{B} - \frac{1}{2}\nabla(\vec{B} \cdot \vec{B})\right] \\ &= \frac{1}{\mu_0}\left[\nabla \cdot \left(\vec{B}\vec{B}\right) - \left(\nabla \cdot \vec{B}\right)\vec{B} - \nabla \cdot \left(\frac{1}{2}|\vec{B}|^2 \overleftrightarrow{I}\right)\right] \\ &= \nabla \cdot \left(\frac{1}{\mu_0}\vec{B}\vec{B} - \frac{|\vec{B}|^2}{2\mu_0}\overleftrightarrow{I}\right) \end{aligned} \tag{2.77}$$

where $|\vec{B}|$ is the magnitude of $\vec{B}$. Thus, Eq. (2.76) becomes

$$\frac{\partial \left(\rho \vec{u}\right)}{\partial t} + \nabla \cdot \left(\rho \vec{u}\vec{u} + P\overleftrightarrow{I} + \overleftrightarrow{\Pi} - \left(\frac{1}{\mu_0}\vec{B}\vec{B} - \frac{|\vec{B}|^2}{2\mu_0}\overleftrightarrow{I}\right)\right) = 0 \tag{2.78}$$

The generalized Ohm's law is derived by applying the asymptotic approximations for the momentum equation of electrons such that

$$\vec{E} + \vec{u} \times \vec{B} = \eta \vec{J} - \frac{1}{n_e q_e}\left(\vec{J} \times \vec{B} - \nabla P_e - \nabla \cdot \overleftrightarrow{\Pi}_e\right) \tag{2.79}$$

where the frictional force $\vec{R}_{ei}$ is simply assumed to be

$$\vec{R}_{ei} = n_e m_e \left(\vec{u}_i - \vec{u}_e\right)\nu_{ei} = -n_e q_e \eta \vec{J} \tag{2.80}$$

ν_{ei} is the collision frequency between electrons and ions and η is the Spitzer resistivity[25, 26, 27]

$$\eta = \frac{m_e \nu_{ei}}{n_e q^2} \tag{2.81}$$

Note that η and $\vec{R}_{ei}$ do not vanish with $m_e \to 0$ asymptotic assumption since $\nu_{ei} \propto \frac{1}{m_e}$. The energy equation is

$$\begin{aligned}\frac{\partial e_t}{\partial t} &+ \nabla \cdot \left(\left(e_t + P + \frac{|\vec{B}|^2}{2\mu_0} \right) \vec{u} + \vec{u} \cdot \overset{\leftrightarrow}{\Pi} + \vec{h} - \frac{1}{\mu_0} \left(\vec{B} \cdot \vec{u} \right) \vec{B} \right) \\ &= \frac{1}{\mu_0} \nabla \cdot \left(\left(e_{te} + P_e + \frac{|\vec{B}|^2}{2\mu_0} \right) \frac{\nabla \times \vec{B}}{n_e q} + \frac{\nabla \times \vec{B}}{n_e q} \cdot \overset{\leftrightarrow}{\Pi}_e - \frac{1}{\mu_0} \left(\vec{B} \cdot \frac{\nabla \times \vec{B}}{n_e q} \right) \vec{B} \right. \\ &\qquad \left. - \eta \vec{J} \times \vec{B} + \frac{1}{n_e q} \nabla P_e \times \vec{B} + \frac{1}{n_e q} \left(\nabla \cdot \overset{\leftrightarrow}{\Pi}_e \right) \times \vec{B} \right)\end{aligned} \tag{2.82}$$

where $e_{t\alpha}$ is the total $5N$-moment fluid energy with the magnetic field energy

$$e_{t\alpha} \equiv \epsilon_\alpha + \frac{|\vec{B}|^2}{2\mu_0} \tag{2.83}$$

and e_t is the total energy in MHD model

$$e_t = \sum_\alpha e_{t\alpha} = \sum_\alpha \epsilon_\alpha + \frac{|\vec{B}|^2}{2\mu_0} \tag{2.84}$$

Faraday's law is

$$\frac{\partial \vec{B}}{\partial t} + \nabla \cdot \left(\vec{u}\vec{B} - \vec{B}\vec{u} \right) = -\nabla \times \left(\eta \vec{J} - \frac{1}{n_e q_e} \left(\vec{J} \times \vec{B} - \nabla P_e - \nabla \cdot \overset{\leftrightarrow}{\Pi}_e \right) \right) \tag{2.85}$$

In the energy equation and Faraday's law, the electric field is replaced by using the generalized Ohm's law. Thus, the time-evolution of the electric field (Ampére's law) is not diretly solved, which enables the governing equations in MHD model to consist of the continuity equation, the momentum equations, the energy equation and Faraday's law. In FEM, reducing the size of the matrix is important to decrease the computational costs.

Applying the following assumptions

1. High collisionality

$$\frac{\tau_{ii}}{\tau} \ll 1$$

2. Small Larmor radius (high magnetization)

$$\frac{r_{Li}}{L} \ll 1$$

3. Low resistivity

$$\left(\frac{m_e}{m_i}\right)^{\frac{1}{2}} \left(\frac{r_{Li}}{L}\right)^2 \frac{\tau}{\tau_{ii}} \ll 1$$

4. Thermal equilibrium

$$T_i \simeq T_e$$

where τ_{ii} is the ion-ion collision period, τ is the characteristic period, r_{Li} is the ion Larmor radius and L is the characteristic plasma length, the generalized MHD model is simplified to the ideal MHD model

$$\frac{\partial \rho}{\partial t} + \nabla \cdot (\rho \vec{u}) = 0 \tag{2.86}$$

$$\frac{\partial (\rho \vec{u})}{\partial t} + \nabla \cdot \left(\rho \vec{u}\vec{u} + P\overset{\leftrightarrow}{I} - \left(\frac{1}{\mu_0}\vec{B}\vec{B} - \frac{|\vec{B}|^2}{2\mu_0}\overset{\leftrightarrow}{I} \right) \right) = 0 \tag{2.87}$$

$$\frac{\partial e_t}{\partial t} + \nabla \cdot \left(\left(e_t + P + \frac{|\vec{B}|^2}{2\mu_0} \right) \vec{u} - \frac{1}{\mu_0} \left(\vec{B} \cdot \vec{u} \right) \vec{B} \right) = 0 \tag{2.88}$$

$$\frac{\partial \vec{B}}{\partial t} + \nabla \cdot \left(\vec{u}\vec{B} - \vec{B}\vec{u} \right) = 0 \tag{2.89}$$

$$\vec{E} + \vec{u} \times \vec{B} = 0 \tag{2.90}$$

If the Maxwellian (or Maxwell-Boltzmann) distribution function is used to eventually derive the generalized MHD model, the thermal equilibrium conditions is already included and unnecessary to derive the ideal MHD model. Therefore, the governing equations in the conservative form consist of the following variables

$$\vec{Q}_I = \begin{bmatrix} \rho \\ \rho u_r \\ \rho u_\theta \\ \rho u_z \\ e_t \\ B_r \\ B_\theta \\ B_z \end{bmatrix} \tag{2.91}$$

$$\overset{\leftrightarrow}{F}_I = \begin{bmatrix} \rho u_r & \rho u_\theta & \rho u_z \\ \rho u_r u_r + P - \frac{1}{\mu_0}\left(B_r B_r - \frac{|\vec{B}|^2}{2}\right) & \rho u_\theta u_r - \frac{1}{\mu_0} B_\theta B_r & \rho u_z u_r - \frac{1}{\mu_0} B_z B_r \\ \rho u_r u_\theta - \frac{1}{\mu_0} B_r B_\theta & \rho u_\theta u_\theta + P - \frac{1}{\mu_0}\left(B_\theta B_\theta - \frac{|\vec{B}|^2}{2}\right) & \rho u_z u_\theta - \frac{1}{\mu_0} B_z B_\theta \\ \rho u_r u_z - \frac{1}{\mu_0} B_r B_z & \rho u_\theta u_z - \frac{1}{\mu_0} B_\theta B_z & \rho u_z u_z + P - \frac{1}{\mu_0}\left(B_z B_z - \frac{|\vec{B}|^2}{2}\right) \\ \left(e_t + P + \frac{|\vec{B}|^2}{2\mu_0}\right) u_r - \frac{1}{\mu_0}\left(\vec{B}\cdot\vec{u}\right) B_r & \left(e_t + P + \frac{|\vec{B}|^2}{2\mu_0}\right) u_\theta - \frac{1}{\mu_0}\left(\vec{B}\cdot\vec{u}\right) B_\theta & \left(\epsilon + P + \frac{|\vec{B}|^2}{2\mu_0}\right) u_z - \frac{1}{\mu_0}\left(\vec{B}\cdot\vec{u}\right) B_z \\ 0 & u_\theta B_r - B_\theta u_r & u_z B_r - B_z u_r \\ u_r B_\theta - B_r u_\theta & 0 & u_z B_\theta - B_z u_\theta \\ u_r B_z - B_r u_z & u_\theta B_z - B_\theta u_z & 0 \end{bmatrix} \tag{2.92}$$

$$\vec{S}_I = \begin{bmatrix} 0 \\ 0 \\ 0 \\ 0 \\ 0 \\ 0 \\ 0 \\ 0 \end{bmatrix} \tag{2.93}$$

$$\vec{\mathcal{S}}_I = -\frac{1}{r} \begin{bmatrix} \rho u_r \\ \rho\left(u_r u_r - u_\theta u_\theta\right) - \frac{1}{\mu_0}\left(B_r B_r - B_\theta B_\theta\right) \\ 2\left(\rho u_r u_\theta - \frac{1}{\mu_0} B_r B_\theta\right) \\ \rho u_z u_r \\ \rho u_r u_z - \frac{1}{\mu_0} B_r B_z \\ 0 \\ 0 \\ u_r B_z - B_r u_z \end{bmatrix} \tag{2.94}$$

2.2.4 Hall MHD Model

Hall MHD model is derived by applying the high collisionality, the low resistivity and the thermal equilibrium approximations but the Larmor radius is not assumed small (low magnetization). Thus, the governing equations are

$$\frac{\partial \rho}{\partial t} + \nabla \cdot \left(\rho \vec{u}\right) = 0 \tag{2.95}$$

$$\frac{\partial\left(\rho\vec{u}\right)}{\partial t}+\nabla\cdot\left(\rho\vec{u}\vec{u}+P\overleftrightarrow{I}-\left(\frac{1}{\mu_0}\vec{B}\vec{B}-\frac{|\vec{B}|^2}{2\mu_0}\overleftrightarrow{I}\right)\right)=0 \tag{2.96}$$

$$\begin{aligned}\frac{\partial e_t}{\partial t}&+\nabla\cdot\left(\left(e_t+P+\frac{|\vec{B}|^2}{2\mu_0}\right)\vec{u}-\frac{1}{\mu_0}\left(\vec{B}\cdot\vec{u}\right)\vec{B}\right)\\&=\frac{1}{\mu_0}\nabla\cdot\left(\left(e_{te}+P_e+\frac{|\vec{B}|^2}{2\mu_0}\right)\frac{\nabla\times\vec{B}}{n_eq}-\frac{1}{\mu_0}\left(\vec{B}\cdot\frac{\nabla\times\vec{B}}{n_eq}\right)\vec{B}+\frac{1}{n_eq}\nabla P_e\times\vec{B}\right)\end{aligned} \tag{2.97}$$

$$\frac{\partial\vec{B}}{\partial t}+\nabla\cdot\left(\vec{u}\vec{B}-\vec{B}\vec{u}\right)=-\nabla\times\left(\frac{1}{n_eq}\vec{J}\times\vec{B}-\frac{1}{n_eq}\nabla P_e\right) \tag{2.98}$$

$$\vec{E}+\vec{u}\times\vec{B}=\frac{1}{n_eq}\left(\vec{J}\times\vec{B}-\nabla P_e\right) \tag{2.99}$$

While the typical Hall MHD model does not typically include the diamagnetic drift term $\propto\nabla P_e$ in the Ohm's law, Eq. (2.99), the Hall MHD model in WARPXM includes the term. Introducing

$$\vec{e}_H\equiv-\frac{1}{\mu_0}\left(\left(e_{te}+P_e+\frac{|\vec{B}|^2}{2\mu_0}\right)\frac{\nabla\times\vec{B}}{n_eq}-\frac{1}{\mu_0}\left(\vec{B}\cdot\frac{\nabla\times\vec{B}}{n_eq}\right)\vec{B}+\frac{1}{n_eq}\nabla P_e\times\vec{B}\right) \tag{2.100}$$

$$\vec{E}_H\equiv\frac{1}{n_eq}\left(\vec{J}\times\vec{B}-\nabla P_e\right) \tag{2.101}$$

Eqs. (2.97) and (2.98) can be simplified as

$$\frac{\partial e_t}{\partial t}+\nabla\cdot\left(\left(e_t+P+\frac{|\vec{B}|^2}{2\mu_0}\right)\vec{u}-\frac{1}{\mu_0}\left(\vec{B}\cdot\vec{u}\right)\vec{B}\right)+\nabla\cdot\vec{e}_H=0 \tag{2.102}$$

$$\frac{\partial\vec{B}}{\partial t}+\nabla\cdot\left(\vec{u}\vec{B}-\vec{B}\vec{u}\right)+\nabla\times\vec{E}_H=0 \tag{2.103}$$

Therefore, the variables in the Hall MHD model are

$$\vec{Q}_H=\vec{Q}_I \tag{2.104}$$

$$\overleftrightarrow{F}_H = \overleftrightarrow{F}_I + \begin{bmatrix} 0 & 0 & 0 \\ 0 & 0 & 0 \\ 0 & 0 & 0 \\ 0 & 0 & 0 \\ e_{Hr} & e_{H\theta} & e_{Hz} \\ 0 & E_{Hz} & -E_{H\theta} \\ -E_{Hz} & 0 & E_{Hr} \\ E_{H\theta} & -E_{Hr} & 0 \end{bmatrix} \tag{2.105}$$

$$\vec{S}_H = \vec{S}_I \tag{2.106}$$

$$\vec{\mathcal{S}}_H = \vec{\mathcal{S}}_I - \frac{1}{r}\begin{bmatrix} 0 \\ 0 \\ 0 \\ 0 \\ e_{Hr} \\ 0 \\ 0 \\ E_{H\theta} \end{bmatrix} \tag{2.107}$$

2.2.5 Resistive MHD Model

The resistive MHD model is derived by applying the high collisionality, the small Larmor radius (high magnetization) and the thermal equilibrium approximations but the low resistivity approximation is not applied. Thus, the governing equations are

$$\frac{\partial \rho}{\partial t} + \nabla \cdot (\rho \vec{u}) = 0 \tag{2.108}$$

$$\frac{\partial (\rho \vec{u})}{\partial t} + \nabla \cdot \left(\rho \vec{u}\vec{u} + P\overleftrightarrow{I} - \left(\frac{1}{\mu_0}\vec{B}\vec{B} - \frac{|\vec{B}|^2}{2\mu_0}\overleftrightarrow{I} \right) \right) = 0 \tag{2.109}$$

$$\frac{\partial e_t}{\partial t} + \nabla \cdot \left(\left(e_t + P + \frac{|\vec{B}|^2}{2\mu_0} \right) \vec{u} - \frac{1}{\mu_0}\left(\vec{B} \cdot \vec{u} \right) \vec{B} \right) = -\frac{1}{\mu_0}\nabla \cdot \left(\eta \vec{J} \times \vec{B} \right) \tag{2.110}$$

$$\frac{\partial \vec{B}}{\partial t} + \nabla \cdot \left(\vec{u}\vec{B} - \vec{B}\vec{u} \right) = -\nabla \times \left(\eta \vec{J} \right) \tag{2.111}$$

$$\vec{E} + \vec{u} \times \vec{B} = \eta \vec{J} \tag{2.112}$$

Similar to the Hall MHD case, introducing

$$\vec{e}_R \equiv \frac{1}{\mu_0} \eta \vec{J} \times \vec{B} \tag{2.113}$$

$$\vec{E}_R \equiv \eta \vec{J} \tag{2.114}$$

Eqs. (2.110) and (2.111) can be simplified as

$$\frac{\partial e_t}{\partial t} + \nabla \cdot \left(\left(e_t + P + \frac{|\vec{B}|^2}{2\mu_0} \right) \vec{u} - \frac{1}{\mu_0} \left(\vec{B} \cdot \vec{u} \right) \vec{B} \right) + \nabla \cdot \vec{e}_R = 0 \tag{2.115}$$

$$\frac{\partial \vec{B}}{\partial t} + \nabla \cdot \left(\vec{u}\vec{B} - \vec{B}\vec{u} \right) + \nabla \times \vec{E}_R = 0 \tag{2.116}$$

Therefore, the variables in the resistive MHD model are

$$\vec{Q}_R = \vec{Q}_I \tag{2.117}$$

$$\overset{\leftrightarrow}{F}_R = \overset{\leftrightarrow}{F}_I + \begin{bmatrix} 0 & 0 & 0 \\ 0 & 0 & 0 \\ 0 & 0 & 0 \\ 0 & 0 & 0 \\ e_{Rr} & e_{R\theta} & e_{Rz} \\ 0 & E_{Rz} & -E_{R\theta} \\ -E_{Rz} & 0 & E_{Rr} \\ E_{R\theta} & -E_{Rr} & 0 \end{bmatrix} \tag{2.118}$$

$$\vec{S}_R = \vec{S}_I \tag{2.119}$$

$$\vec{\mathcal{S}}_R = \vec{\mathcal{S}}_I - \frac{1}{r}\begin{bmatrix} 0 \\ 0 \\ 0 \\ 0 \\ e_{Rr} \\ 0 \\ 0 \\ E_{R\theta} \end{bmatrix} \tag{2.120}$$

2.3 Gradients of Conservative Variables

The Hall MHD and the resistive MHD models expressing $\vec{J}$ in terms of the curl of $\vec{B}$ include spatial derivatives of conservative variables in the flux tensor and the geometric source terms, particularly in $\vec{e}_H$, $\vec{E}_H$, $\vec{e}_R$ and $\vec{E}_R$, which means $\overleftrightarrow{F}_I = \overleftrightarrow{F}_I\left(\vec{Q}\right)$ but $\overleftrightarrow{F}_H = \overleftrightarrow{F}_H\left(\vec{Q}, \nabla\vec{Q}\right)$. While $\vec{J}$ can be treated as the additional conservative variable by considering Kirchhoff's law (continuity equation), it is replaced by the curl of $\vec{B}$ in WARPXM to reduce the computational costs. The current WARPXM adopts the Local Discontinuous Galerkin(LDG) method[28, 18] and Interior Penalty (IP) method[29, 30, 18] to evaluate flux terms and gradients. In the LDG method, the gradient of a conservative variable is defined as

$$\overleftrightarrow{\sigma}^k_n(\vec{x}, t) \equiv \nabla\vec{Q}^k_n(\vec{x}, t) = \nabla\left(\vec{Q}^k_l(\vec{x}^k_l, t)\ell^k_l(\vec{x})\right) \tag{2.121}$$

Applying the weighted method in a local frame and the product rule,

$$\begin{aligned}
\int_{D^k} \overleftrightarrow{\sigma}^k_n w^k_m(\vec{x}) dV^k &= \int_{D^k} \nabla\left(\vec{Q}^k_l(\vec{x}^k_l, t)\ell^k_l(\vec{x})\right) w^k_m(\vec{x}) dV^k \\
&= \int_{D^k} \nabla\left(\vec{Q}^k_l(\vec{x}^k_l, t)\ell^k_l(\vec{x}) w^k_m(\vec{x})\right) dV^k - \int_{D^k} \vec{Q}^k_l(\vec{x}^k_l, t)\ell^k_l(\vec{x})\nabla w^k_m(\vec{x}) dV^k \\
&= \int_{\Omega^k} \vec{Q}^*_l(\vec{x}^k_l, t)\ell^k_l(\vec{x}) w^k_m(\vec{x}) d\vec{\Omega}^k - \int_{D^k} \vec{Q}^k_l(\vec{x}^k_l, t)\ell^k_l(\vec{x})\nabla w^k_m(\vec{x}) dV^k
\end{aligned} \tag{2.122}$$

where $\vec{Q}^*_l(\vec{x}^k_l, t)$ is the interface conservative variable that is continuous and shared by the adjacent element. In the IP method, the following alternative gradient is used

$$\overset{\leftrightarrow}{\sigma}{}^k_n(\vec{x}^k_i, t) \equiv \vec{Q}^k_l(\vec{x}^k_l, t)\nabla \ell^k_l|_{\vec{y}^k_i} \tag{2.123}$$

where the gradient of a basis function is assumed to satisfy the local approximations such that

$$\nabla \ell^k_l(\vec{x}) = \sum_{i=1}^{N_p} \left(\nabla \ell^k_l|_{\vec{y}^k_i}\right) \ell^k_i(\vec{x}) \tag{2.124}$$

2.4 Boundary Conditions

The Dirichlet boundary conditions $\vec{Q}^*$ in the DG method are applied as the averaged values of the interior and exterior information[18] such that

$$\vec{Q}^* = \frac{1}{2}\left(\vec{Q}^+ + \vec{Q}^-\right) \tag{2.125}$$

where ”$-$” notation indicates the interior information of the element and ”$+$” notation indicates the exterior information in the ghost cells. WARPXM implements a homogeneous Neumann (zero-gradient) boundary conditions if the interior and outer information are continuous at the interface such that $\vec{Q}^* = \vec{Q}^- = \vec{Q}^+$. Boundary conditions are initially set for the primary variables. Then, those primary variables on the boundaries are converted into the conservative variables in WARPXM.

2.4.1 Axis Boundary Conditions

As the axis boundary conditions, the radial and azimuthal vector components are set to zero, and the scalar variables and axial vector components are set to homogeneous Neumann boundary conditions on the z-axis in cylindrical coordinates. For example, in the $5N$-moment multi-fluid model, the axis boundary conditions are applied for the primary variables and the converted conservative, respectively, as follows

$$\vec{U}_\alpha^+ = \begin{bmatrix} \rho_\alpha^- \\ -u_{\alpha r}^- \\ -u_{\alpha\theta}^- \\ u_{\alpha z}^- \\ P_\alpha^- \\ -E_r^- \\ -E_\theta^- \\ E_z^- \\ -B_r^- \\ -B_\theta^- \\ B_z^- \end{bmatrix} \tag{2.126}$$

$$\vec{Q}_\alpha^+ = \begin{bmatrix} \rho_\alpha^- \\ -\rho_\alpha^- u_{\alpha r}^- \\ -\rho_\alpha^- u_{\alpha\theta}^- \\ \rho_\alpha^- u_{\alpha z}^- \\ \epsilon_\alpha^- \\ -E_r^- \\ -E_\theta^- \\ E_z^- \\ -B_r^- \\ -B_\theta^- \\ B_z^- \end{bmatrix} \tag{2.127}$$

2.4.2 Conducting Wall Boundary Conditions

The conducting wall boundary conditions have continuous tangential components of $\vec{E}$ and a normal component of $\vec{B}$.[31]

$$\hat{n} \times \vec{E} = 0 \tag{2.128}$$

$$\hat{n} \cdot \vec{B} = 0 \tag{2.129}$$

where $\hat{n}$ is normal to the boundary surfaces. The boundary conditions can be simplified as

$$\vec{E}_{\parallel} = 0 \tag{2.130}$$

$$\vec{B}_{\perp} = 0 \tag{2.131}$$

Surface charges and currents on the interface allows the presence of a normal component of $\vec{E}$ and tangential components of $\vec{B}$.

2.4.3 No-slip and Free-slip Wall Boundary Conditions

Either no-slip or free-slip wall boundary conditions can be applied. While the fluid velocities are the same to the wall velocity in no-slip wall boundary conditions[32], the free-slip wall sets tangential velocities as homogeneous Neumann boundary conditions. Both conditions set the normal velocity to the wall velocity. Thus, the no-slip and free-slip boundary conditions respectively can be expressed as

$$\vec{Q}_{\alpha}^{+}|_{Noslip} = \begin{bmatrix} \rho_{\alpha}^{-} \\ 2\rho_{\alpha}^{-} v_{r}^{wall} - \rho_{\alpha}^{-} u_{\alpha r}^{-} \\ 2\rho_{\alpha}^{-} v_{\theta}^{wall} - \rho_{\alpha}^{-} u_{\alpha\theta}^{-} \\ 2\rho_{\alpha}^{-} v_{z}^{wall} - \rho_{\alpha}^{-} u_{\alpha z}^{-} \\ \epsilon_{\alpha}^{-} \end{bmatrix} \tag{2.132}$$

$$\vec{Q}_{\alpha}^{+}|_{Freeslip} = \begin{bmatrix} \rho_{\alpha}^{-} \\ 2\rho_{\alpha}^{-} v_{r}^{wall} - \rho_{\alpha}^{-} u_{\alpha r}^{-} \\ \rho_{\alpha}^{-} u_{\alpha\theta}^{-} \\ \rho_{\alpha}^{-} u_{\alpha z}^{-} \\ \epsilon_{\alpha}^{-} \end{bmatrix} \tag{2.133}$$

2.4.4 Outflow Open Boundary Conditions

In outflow open boundary conditions, either temperature or pressure is set as a Dirichlet boundary condition and other primary variables have homogeneous Neumann boundary conditions.

$$\vec{U}_\alpha^+ = \begin{bmatrix} \rho_\alpha^- \\ -u_{\alpha r}^- \\ -u_{\alpha\theta}^- \\ -u_{\alpha z}^- \\ 2P_\alpha^{wall} - P_\alpha^- \end{bmatrix} \tag{2.134}$$

$$\vec{U}_{\alpha T}^+ = \begin{bmatrix} \rho_\alpha^- \\ -u_{\alpha r}^- \\ -u_{\alpha\theta}^- \\ -u_{\alpha z}^- \\ 2T_\alpha^{wall} - T_\alpha^- \end{bmatrix} \tag{2.135}$$

2.5 Runge-Kutta Method for Time Evolution

WARPXM integrates the governing equations in time using the Runge-Kutta (RK) methods.[13, 33] Eq. (2.16) can be epressed as ordinary differential equations (ODEs)

$$\frac{d\vec{Q}_l^k}{dt} = \mathscr{L}(\vec{Q}_l^k, t) \tag{2.136}$$

where $\mathscr{L}$ is the operator that represents the remaining terms in Eq. (2.16), and performing intermediate calculations can achieve small residuals $\vec{\mathscr{R}} \simeq 0$. The Taylor expansion for $\vec{Q}_l^k$ gives

$$\begin{aligned} \vec{Q}_l^k(\vec{x}_l^k, t+\Delta t) &= \vec{Q}_l^k(\vec{x}_l^k, t) + \frac{1}{1!}\frac{d\vec{Q}_l^k}{dt}\Delta t + \frac{1}{2!}\frac{d^2\vec{Q}_l^k}{dt^2}(\Delta t)^2 + \frac{1}{3!}\frac{d^3\vec{Q}_l^k}{dt^3}(\Delta t)^3 + \frac{1}{4!}\frac{d^4\vec{Q}_l^k}{dt^4}(\Delta t)^4 + O\left((\Delta t)^5\right) \\ &= \vec{Q}_l^k(\vec{x}_l^k, t) + \mathscr{L}\Delta t + \frac{1}{2!}\frac{d\mathscr{L}}{dt^2}(\Delta t)^2 + \frac{1}{3!}\frac{d^2\mathscr{L}}{dt^2}(\Delta t)^3 + \frac{1}{4!}\frac{d^3\mathscr{L}}{dt^4}(\Delta t)^4 + O\left((\Delta t)^5\right) \end{aligned} \tag{2.137}$$

where $\mathscr{L} = \mathscr{L}(\vec{Q}_l^k, t)$ for simplicity. In the RK method, Eq. (2.137) is assumed to be expressed in terms of the following known terms

$$\vec{Q}_l^k(\vec{x}_l^k, t_{n+1}) = \vec{Q}_l^k(\vec{x}_l^k, t_n) + \sum_{i=1}^{s} b_i \mathscr{L}(\vec{\mathscr{Q}}_i, t_n + c_i \Delta t)\Delta t \tag{2.138}$$

where s indicates the number of stages, $\Delta t = t_{n+1} - t_n$, and

$$\vec{\mathscr{Q}}_i = \vec{Q}_l^k(\vec{x}_l^k, t_n) + \sum_{j=1}^{i-1} a_{ij} \mathscr{L}(\vec{\mathscr{Q}}_j, t_n + c_j \Delta t)\Delta t \tag{2.139}$$

$$\vec{\mathscr{Q}}_1 = \vec{Q}_l^k(\vec{x}_l^k, t_n) \tag{2.140}$$

$$a_{11} = c_1 = 0 \tag{2.141}$$

a_{ij} is known as the RK matrix, b_i and c_i are constant vectors. From Eq. (2.137), the ODE solved with first order of accuracy is

$$\frac{d\vec{Q}_l^k}{dt} = \frac{\vec{Q}_l^k(\vec{x}_l^k, t_{n+1}) - \vec{Q}_l^k(\vec{x}_l^k, t_n)}{\Delta t} + O(\Delta t) \tag{2.142}$$

which leads the discretized equations in the exact form as

$$\vec{Q}_l^k(\vec{x}_l^k, t_{n+1}) = \vec{Q}_l^k(\vec{x}_l^k, t_n) + \mathscr{L}(\vec{Q}_l^k, t_n)\Delta t + O\left((\Delta t)^2\right) \tag{2.143}$$

From Eq. (2.138), the first-stage RK method produces

$$\vec{Q}_l^k(\vec{x}_l^k, t_{n+1}) = \vec{Q}_l^k(\vec{x}_l^k, t_n) + b_1 \mathscr{L}(\vec{\mathscr{Q}}_1, t_n + c_1 \Delta t)\Delta t \tag{2.144}$$

Using Eqs. (2.140) and (2.141), $\mathscr{L}(\vec{\mathscr{Q}}_1, t_n + c_1 \Delta t)$ becomes

$$\mathscr{L}(\vec{\mathscr{Q}}_1, t_n + c_1 \Delta t) = \mathscr{L}(\vec{Q}_l^k, t_n) \tag{2.145}$$

Substituting Eq. (2.145) into Eq. (2.144),

$$\vec{Q}_l^k(\vec{x}_l^k, t_{n+1}) = \vec{Q}_l^k(\vec{x}_l^k, t_n) + b_1 \mathscr{L}(\vec{Q}_l^k, t_n)\Delta t \tag{2.146}$$

Comparing Eq. (2.146) with Eq. (2.143),

$$b_1 = 1 \tag{2.147}$$

provides the consistent first order of accuracy for the first-stage RK method. Notice that the first-stage and first-order explicit RK method correspond to the forward Euler method.

On the other hand, those constant values are not unique in higher-stage and higher-order RK methods; hence, the choice of constants determines the type of the scheme. The second order time derivative of $\vec{Q}_l^k$ is

$$\frac{d^2\vec{Q}_l^k}{dt^2} = \frac{d\mathscr{L}}{dt} = \frac{\partial \mathscr{L}}{\partial t} + \frac{\partial \mathscr{L}}{\partial \vec{Q}_l^k}\frac{d\vec{Q}_l^k}{dt} = \frac{\partial \mathscr{L}}{\partial t} + \frac{\partial \mathscr{L}}{\partial \vec{Q}_l^k}\mathscr{L} \tag{2.148}$$

Thus, Eq. (2.137) expanded about $t = t_n$ gives

$$\vec{Q}_l^k(\vec{x}_l^k, t_{n+1}) = \vec{Q}_l^k(\vec{x}_l^k, t_n)\Delta t + \mathscr{L}\Delta t + \frac{1}{2}\left(\frac{\partial \mathscr{L}}{\partial t} + \frac{\partial \mathscr{L}}{\partial \vec{Q}_l^k}\mathscr{L}\right)(\Delta t)^2 + O\left((\Delta t)^3\right) \tag{2.149}$$

In the second-stage RK method, Eq (2.138) gives

$$\vec{Q}_l^k(\vec{x}_l^k, t_{n+1}) = \vec{Q}_l^k(\vec{x}_l^k, t_n) + b_1\mathscr{L}\Delta t + b_2\mathscr{L}(\vec{\mathscr{Q}}_2, t_n + c_2\Delta t)\Delta t \tag{2.150}$$

$\mathscr{L}(\vec{\mathscr{Q}}_2, t_n + c_2\Delta t)$ can be expressed by applying a Taylor expansion around $(\vec{Q}_l^k, t_n)$ such that

$$\begin{aligned}\mathscr{L}(\vec{\mathscr{Q}}_2, t_n + c_2\Delta t) &= \mathscr{L}(\vec{Q}_l^k + a_{21}\mathscr{L}(\vec{\mathscr{Q}}_1, t_n)\Delta t, t_n + c_2\Delta t)\\ &= \mathscr{L} + \frac{1}{1!}\left(c_2\Delta t\frac{\partial}{\partial t} + a_{21}\mathscr{L}(\vec{\mathscr{Q}}_1, t_n)\Delta t\frac{\partial}{\partial \vec{Q}_l^k}\right)\mathscr{L} + O\left((\Delta t)^2\right)\\ &= \mathscr{L} + \frac{\partial \mathscr{L}}{\partial t}c_2\Delta t + \frac{\partial \mathscr{L}}{\partial \vec{Q}_l^k}a_{21}\mathscr{L}(\vec{Q}_l^k, t_n)\Delta t + O\left((\Delta t)^2\right)\end{aligned} \tag{2.151}$$

where

$$\vec{\mathscr{Q}}_2 = \vec{Q}_l^k(\vec{x}_l^k, t_n) + a_{21}\mathscr{L}(\vec{\mathscr{Q}}_1, t_n) \tag{2.152}$$

Substituting Eq. (2.151) into Eq. (2.150),

$$\vec{Q}_l^k(\vec{x}_l^k, t_{n+1}) = \vec{Q}_l^k(\vec{x}_l^k, t_n) + (b_1+b_2)\mathscr{L}\Delta t + b_2\left(c_2\frac{\partial \mathscr{L}}{\partial t} + a_{21}\frac{\partial \mathscr{L}}{\partial \vec{Q}_l^k}\mathscr{L}\right)(\Delta t)^2 + O\left((\Delta t)^3\right) \tag{2.153}$$

Comparing Eq. (2.153) with Eq. (2.149), the following constants provide the consistent second order of accuracy in the second-stage RK method

$$b_1 + b_2 = 1 \tag{2.154}$$

$$b_2c_2 = \frac{1}{2} \tag{2.155}$$

$$a_{21} = c_2 \tag{2.156}$$

Since there are only three equations but four unknowns, those constants cannot be determined uniquely. WARPXM adopts Heun's method as the second order Total Variation Diminishing Runge-Kutta method (TVDRK2)

$$(a_{21}, b_1, b_2, c_2) = (1, \frac{1}{2}, \frac{1}{2}, 1) \tag{2.157}$$

Another possible and popular scheme is the midpoint method called "RK2" in WARPXM

$$(a_{21}, b_1, b_2, c_2) = (\frac{1}{2}, 0, 1, \frac{1}{2}) \tag{2.158}$$

The third- and fourth-order RK methods can be derived in a similar manner (see Appendix C). In WARPXM, the third-stage third-order RK method called as Strong-Stability Preserving Runge-Kutta method (SSPRK3) uses

$$(a_{21}, a_{31}, a_{32}, b_1, b_2, b_3, c_2, c_3) = (1, \frac{1}{4}, \frac{1}{4}, \frac{1}{6}, \frac{1}{6}, \frac{2}{3}, 1, \frac{1}{2}) \tag{2.159}$$

Another possible and common scheme is called "RK3" in WARPXM using

$$(a_{21}, a_{31}, a_{32}, b_1, b_2, b_3, c_2, c_3) = (\frac{1}{2}, -1, -2, \frac{1}{6}, \frac{2}{3}, \frac{1}{6}, \frac{1}{2}, 1) \tag{2.160}$$

The fourth-stage fourth-order RK method (RK4) uses

$$(a_{21}, a_{31}, a_{32}, a_{41}, a_{42}, a_{43}, b_1, b_2, b_3, b_4, c_2, c_3, c_4) = (\frac{1}{2}, 0, \frac{1}{2}, 0, 0, 1, \frac{1}{6}, \frac{1}{3}, \frac{1}{3}, \frac{1}{6}, \frac{1}{2}, \frac{1}{2}, 1) \tag{2.161}$$

2.6 Courant-Friedrichs-Lewy (CFL) Numbers

WARPXM defines the default CFL number as

$$CFL_{max} = a_{max}\frac{\Delta t}{\Delta x} = \frac{1}{2k+1} \tag{2.162}$$

where a_{max} is the fastest characteristic speed, k is the polynomial degree and $k+1$ corresponds to the order of accuracy in space. This maximum CFL number is analytically proven by

Cockburn and Shu for $k = 0$ and $k = 1$ in the RKDG method[34, 35, 36]. For RK methods of order $\nu \geq k+1$, Cockburn and Shu numerically obtained the maximum CFL numbers which are greater than $1/(2k+1)$. For $\nu < k+1$, the numerically obtained maximum CFL number is smaller; it is necessary to set more strict CFL limit to achieve the stable results. For first and second order RK methods, the results are stable only if $\nu \geq k+1$. These analytical and numerical stability analysis are obtained for the homogeneous hyperbolic equations, particularly for convection-dominated problems[34] and summarized in Tab. 2.1.

Table 2.1: $\frac{CFL_{numerical}}{CFL_{max}}$ for convection-dominated problems[34]

		k				
		0	1	2	3	4
ν	1	1.00	-	-	-	-
	2	1.00	1.00	-	-	-
	3	1.256	1.227	1.045	0.91	0.801
	4	1.392	1.392	1.175	1.015	0.9

On the other hand, the governing hyperbolic equations for plasma often include inhomogeneous source terms. Also, there exist some characteristic frequencies (i.e., plasma frequency, cyclotron frequency, and collision frequency) in plasmas that limit the time steps to resolve the details of physics in numerical calculations. For example in the ideal $5N$-moment two-fluid model, WARPXM adopts the following maximum time step

$$\Delta t_{max} = \min\left(CFL_{max}\frac{\Delta x}{c}, CFL_{max}\frac{\Delta x}{c_{si}}, CFL_{max}\frac{\Delta x}{c_{se}}, \frac{0.1}{\omega_{pe}}, \frac{0.1}{\omega_{pi}}, \frac{0.1}{\omega_{ce}}, \frac{0.1}{\omega_{ci}}\right) \tag{2.163}$$

where $c_{s\alpha}$ is the speed of sound and $\omega_{c\alpha}$ is a cyclotron frequency for species α. In particular, the following two characteristic time steps set the maximum time step in the ideal $5N$-moment two-fluid model.

$$\Delta t_{max} = \min\left(CFL_{max}\frac{\Delta x}{c}, \frac{0.1}{\omega_{pe}}\right) \tag{2.164}$$

If the governing equations only include Maxwell equations,

$$\Delta t_{max} = CFL_{max}\frac{\Delta x}{c} \tag{2.165}$$

Also, if a problem considers only neutral fluids,

$$\Delta t_{max} = CFL_{max}\frac{\Delta x}{c_{sn}} \tag{2.166}$$

Fo most plasma problems, $\frac{0.1}{\omega_{pe}} < CFL_{max}\frac{\Delta x}{c}$. However, since the default maximum CFL number decreases as the spatial order of accuracy increases and the choice of Δx depends on the desired accuracy and resolution, it is possible to have $\frac{0.1}{\omega_{pe}} > CFL_{max}\frac{\Delta x}{c}$. Table. 2.2 indicates the possible CFL numbers for the stable Z-pinch in the radial equilibrium using the ideal two-fluid model via WARPXM. The details of the Z-pinch in the radial equilibrium are described in Section 3.5. All calculations use small enough Δx to satisfy $\frac{0.1}{\omega_{pe}} > CFL_{max}\frac{\Delta x}{c}$.

Table 2.2: $\frac{CFL_{numerical}}{CFL_{max}}$ for the radial equilibrium z-pinch in two-fluid model

		k				
		0	1	2	3	4
ν	1	-	-	-	-	-
	2	-	1.00	-	-	-
	3	-	1.00	1.00	0.91	0.80
	4	-	1.00	1.00	1.00	0.89

Note WARPXM does not allow CFL numbers larger than the default CFL_{max}, and thus $\frac{CFL_{numerical}}{CFL_{max}}$ cannot exceed unity. The possible maximum CFL numbers in WARPXM match well with the results shown in Table 2.1. Using first order of accuracy in space $k = 0$ with first or second order of RK methods $\nu \leq 2$, Ho[37] has numerically proven that the calculations can be unconditionally unstable due to the imaginary eigenvalues obtained from the inhomogeneous source terms in the ideal two-fluid model without fluxes. With the third or fourth order accuracy in time $\nu \geq 3$ and first order in space $k = 0$, the results are too diffusive and cannot sustain the equilibrium conditions well.

Chapter 3

BENCHMARK TESTS FOR GEOMETRIC SOURCE TERMS

The analytically described geometric source terms are numerically tested for several benchmark problems by using purely Maxwell's equations in Section 3.1, purely Euler equations in Section 3.2. Sections 3.3 and 3.4 test the viscosity tensor for the neutral fluid with the geometric source terms, and the ideal $5N$-moment two-fluid model and the ideal MHD model are tested in Section 3.5.

3.1 Transverse Electro (TE), Transverse Magnetic (TM), and Transverse ElectroMagnetic (TEM) modes in a Cylindrical Waveguide

The dynamics of EM fields propagating through a vacuum waveguide are described by Maxwell's equations. As the benchmark tests for the geometric source terms in Maxwell's equations, an axisymmetric hollow cylindrical waveguide with the perfect conducting wall is used to study vacuum EM field propagation. It is useful to assume that the EM fields propagate into the positive axial direction such that

$$\vec{E}(\vec{r},t) = \vec{E}_0(r,\theta)e^{i(k_z z-\omega t)} \tag{3.1}$$

$$\vec{B}(\vec{r},t) = \vec{B}_0(r,\theta)e^{i(k_z z-\omega t)} \tag{3.2}$$

where $\vec{k} = k_z\hat{z}$ is the wave vector. In vacuum, Maxwell equations can be simply expressed in the form of wave equations

$$\left(\frac{1}{c^2}\frac{\partial^2}{\partial t^2} - \nabla^2\right)\begin{bmatrix}\vec{E}\\ \vec{B}\end{bmatrix} = 0 \tag{3.3}$$

which reduces to

$$\left(\omega^2 + c^2\nabla^2\right)\begin{bmatrix}\vec{E}\\ \vec{B}\end{bmatrix} = 0 \tag{3.4}$$

The waveguide modes with only transverse $\vec{E}$ ($\vec{E}_z = 0$) are called TE waves and modes with only transverse $\vec{B}$ ($\vec{B}_z = 0$) are called TM waves.[31] Transverse ElectroMagnetic (TEM) modes have both $\vec{E}$ and $\vec{B}$ that are transverse to the axial direction and $\vec{E}_z = \vec{B}_z = 0$. Solving Faraday's law and Ampère's law in vacuum for the transverse (r, θ) components of the EM fields in terms of the axial components,

$$\begin{bmatrix} E_r \\ E_\theta \\ B_r \\ B_\theta \end{bmatrix} = \frac{i}{\left(\frac{\omega}{c}\right)^2 - k_z^2} \begin{bmatrix} k_z \frac{\partial E_z}{\partial r} + \omega \frac{1}{r} \frac{\partial B_z}{\partial \theta} \\ k_z \frac{1}{r} \frac{\partial E_z}{\partial \theta} - \omega \frac{\partial B_z}{\partial r} \\ k_z \frac{\partial B_z}{\partial r} - \frac{\omega}{c^2} \frac{1}{r} \frac{\partial E_z}{\partial \theta} \\ k_z \frac{1}{r} \frac{\partial B_z}{\partial \theta} + \frac{\omega}{c^2} \frac{\partial E_z}{\partial r} \end{bmatrix} \tag{3.5}$$

If $E_z = B_z = 0$ but the transverse EM fields exist (i.e., $\vec{E}_t \neq 0$ and $\vec{B}_t \neq 0$), the frequency ω satisfies $\omega = ck_z$, and Eq. (3.4) reduces to a two-dimensional form

$$\nabla_t^2 \begin{bmatrix} \vec{E}_t \\ \vec{B}_t \end{bmatrix} = 0 \tag{3.6}$$

where ∇_t^2 is the Laplacian operator for the transverse part

$$\nabla_t^2 = \nabla^2 - \frac{\partial^2}{\partial z^2} \tag{3.7}$$

Also, the Gauss's law for the transverse part

$$\nabla_t \cdot \vec{E}_t = -\frac{\partial E_z}{\partial z} \tag{3.8}$$

$$\nabla_t \cdot \vec{B}_t = -\frac{\partial B_z}{\partial z} \tag{3.9}$$

and the Ampère's law and Faraday's law yield

$$\nabla_t \times \vec{E}_t = 0 \tag{3.10}$$

$$\nabla_t \times \vec{B}_t = 0 \tag{3.11}$$

Eqs. (3.6), (3.8), (3.9), (3.10) and (3.11) imply that $\vec{E}_t$ and $\vec{B}_t$ are solutions of an electrostatic and a magnetostatic problems, respectively. The TEM mode does not exist in a cylindrical vacuum waveguide surrounded by a single perfectly conducting wall since the electrostatic fields vanish at the equipotential boundary. Note that the TEM mode can be supported in a cylindrical waveguide only if there exist multiple and non-equipotential boundaries, for example coaxial cables.[31]

Considering the general solutions of wave equations Eq. (3.3) in cylindrical coordinates (see Appendix D), the axisymmetric ($m = 0$) TM mode is given by

$$\begin{bmatrix} E_r \\ E_\theta \\ E_z \\ B_r \\ B_\theta \\ B_z \end{bmatrix} = \begin{bmatrix} i\frac{k_z}{k_c^2}\left(k_c J_{m-1}(k_c r) - \frac{mJ_m(k_c r)}{r}\right) \\ 0 \\ J_m(k_c r) \\ 0 \\ i\frac{\omega}{c^2 k_c^2}\left(k_c J_{m-1}(k_c r) - \frac{mJ_m(k_c r)}{r}\right) \\ 0 \end{bmatrix} e^{i(k_z z - \omega t)} = \begin{bmatrix} -i\frac{k_z}{k_c} J_1(k_c r) \\ 0 \\ J_0(k_c r) \\ 0 \\ -i\frac{\omega}{c^2 k_c} J_1(k_c r) \\ 0 \end{bmatrix} e^{i(k_z z - \omega t)} \tag{3.12}$$

where J_m is the Bessel function of the first kind and

$$k_c^2 = \left(\frac{\omega}{c}\right)^2 - k_z^2 \tag{3.13}$$

Similarly, the axisymmetric TE mode becomes

$$\begin{bmatrix} E_r \\ E_\theta \\ E_z \\ B_r \\ B_\theta \\ B_z \end{bmatrix} = \begin{bmatrix} 0 \\ -i\frac{\omega}{k_c^2}\left(k_c J_{m-1}(k_c r) - \frac{mJ_m(k_c r)}{r}\right) \\ 0 \\ i\frac{k_z}{k_c^2}\left(k_c J_{m-1}(k_c r) - \frac{mJ_m(k_c r)}{r}\right) \\ 0 \\ J_m(k_c r) \end{bmatrix} e^{i(k_z z - \omega t)} = \begin{bmatrix} 0 \\ i\frac{\omega}{k_c} J_1(k_c r) \\ 0 \\ -i\frac{k_z}{k_c} J_1(k_c r) \\ 0 \\ J_0(k_c r) \end{bmatrix} e^{i(k_z z - \omega t)} \tag{3.14}$$

Using the perfectly conducting wall boundary conditions at $r = L_r$, TM modes satisfy $E_z(r = L_r) = J_0(k_c L_r) = 0$ such that

$$k_c L_r = x_{0n} \tag{3.15}$$

where x_{0n} is nth root of the Bessel function of the first kind such that $J_0(x_{0n}) = 0$. The choice of $m = 0$ and n identifies the modes of the waves as TM$_{mn}$ mode, and thus Eq. (3.12) indicates one possible solution of TM_{0n} mode. On the other hand, TE_{0n} mode requires $\frac{\partial B_z}{\partial r}|_{r=L_r} = -k_c J_1(k_c L_r) = 0$ such that

$$k_c L_r = x_{1n} \tag{3.16}$$

For TEM waves, the perfectly conducting wall boundary conditions yield $E_\theta = B_r = 0$. Using Eqs. (3.8) and (3.10), the simple and possible solutions of E_r and B_θ are

$$E_r = \frac{1}{r} e^{i(k_z z - \omega t)} \tag{3.17}$$

$$B_\theta = \frac{1}{r} e^{i(k_z z - \omega t)} \tag{3.18}$$

The numerical results for each components of EM fields in TM_{01} modes are given in Figs. 3.1, 3.2, and 3.3 that are compared with the analytical solutions in Fig. 3.4 along $z = 0$. Figs. 3.5, 3.6, and 3.7 are the numerical results of TE_{01} modes that are compared with the analytical solutions in Fig. 3.8 along $z = 0$. The numerical results of EM fields in TEM_{01} modes are given in Figs. 3.9 and 3.10 that are compared with the analytical solutions along $z = 0$ in Fig. 3.11. Those benchmark tests have the third order of accuracy in time and space, and 40 and 10 elements in axial and radial directions, respectively.

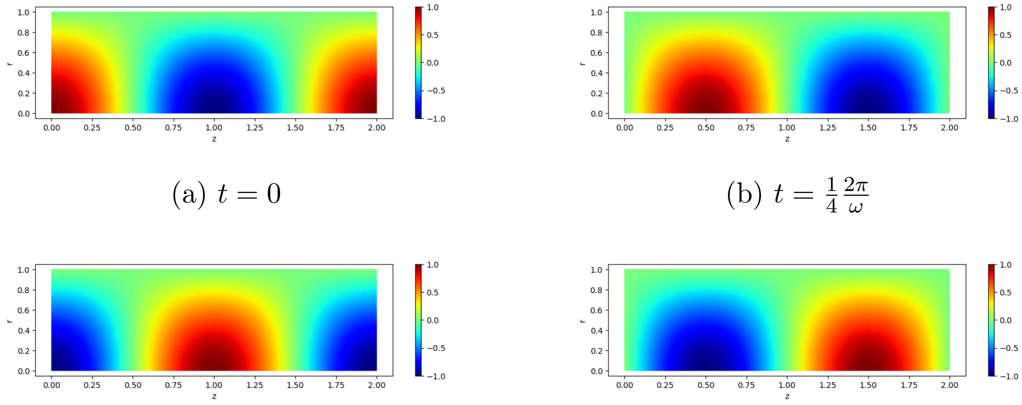

(a) $t = 0$

(b) $t = \frac{1}{4}\frac{2\pi}{\omega}$

(c) $t = \frac{1}{2}\frac{2\pi}{\omega}$

(d) $t = \frac{3}{4}\frac{2\pi}{\omega}$

Figure 3.1: Numerical results from WARPXM showing contours of E_z of a TM_{01} mode in a waveguide that is benchmarked to the analytical solution. The longitudinal component of electric fields E_z propagates through the cylindrical waveguide with the expected frequency ω. (Simulations of TM_{01} mode in a waveguide are performed with WARPXM version 1.5.9 using input file TE_TM_waveguide_modes.py)

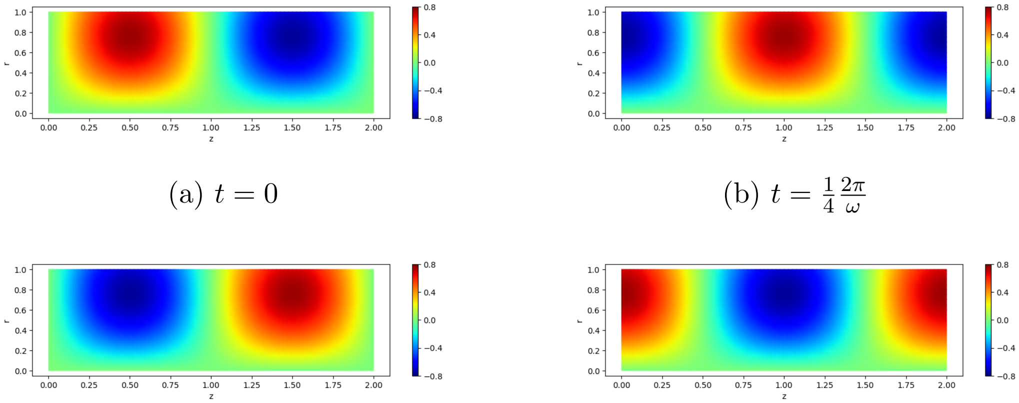

(a) $t = 0$

(b) $t = \frac{1}{4}\frac{2\pi}{\omega}$

(c) $t = \frac{1}{2}\frac{2\pi}{\omega}$

(d) $t = \frac{3}{4}\frac{2\pi}{\omega}$

Figure 3.2: Numerical results from WARPXM showing contours of E_r of a TM_{01} mode in a waveguide that is benchmarked to the analytical solution. The transverse component of electric fields E_r is induced and propagates through the cylindrical waveguide with the expected frequency ω. (Simulations of TM_{01} mode in a waveguide are performed with WARPXM version 1.5.9 using input file TE_TM_waveguide_modes.py)

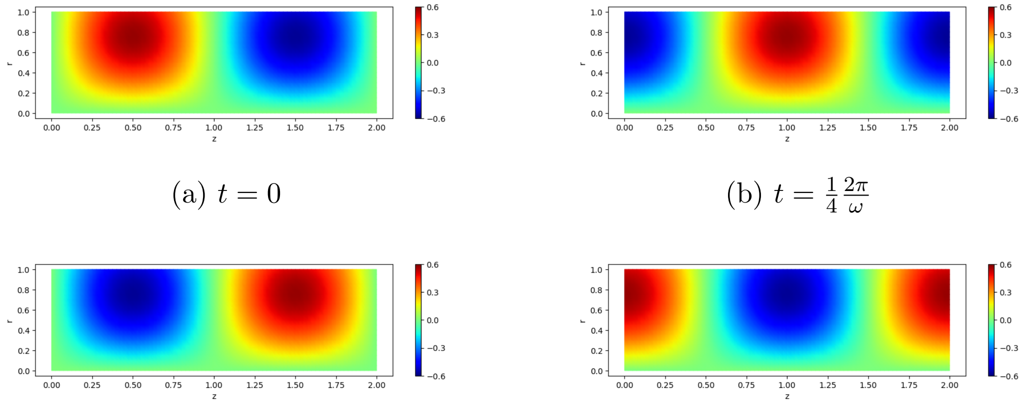

(a) $t = 0$

(b) $t = \frac{1}{4}\frac{2\pi}{\omega}$

(c) $t = \frac{1}{2}\frac{2\pi}{\omega}$

(d) $t = \frac{3}{4}\frac{2\pi}{\omega}$

Figure 3.3: Numerical results from WARPXM showing contours of B_θ of a TM_{01} mode in a waveguide that is benchmarked to the analytical solution. The transverse component of magnetic fields B_θ is induced and propagates through the cylindrical waveguide with the expected frequency ω. (Simulations of TM_{01} mode in a waveguide are performed with WARPXM version 1.5.9 using input file TE_TM_waveguide_modes.py)

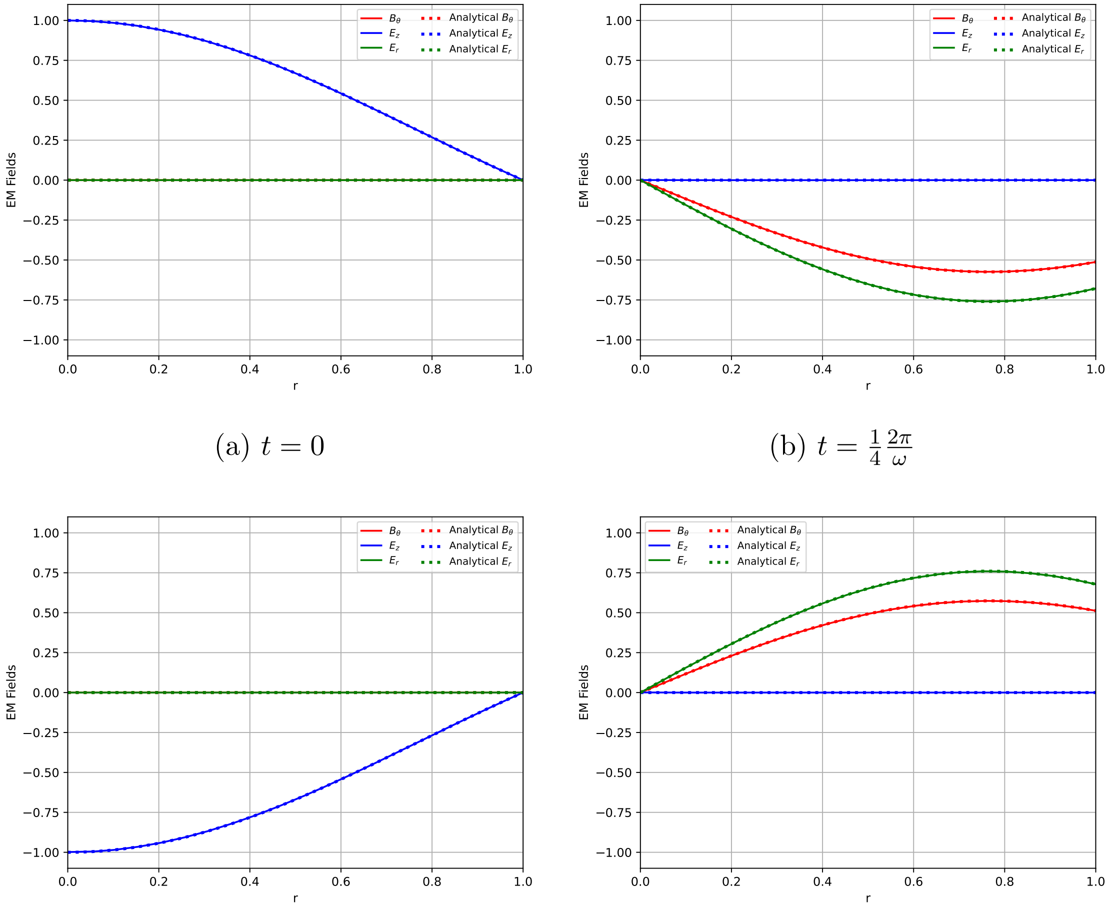

(a) $t = 0$

(b) $t = \frac{1}{4}\frac{2\pi}{\omega}$

(c) $t = \frac{1}{2}\frac{2\pi}{\omega}$

(d) $t = \frac{3}{4}\frac{2\pi}{\omega}$

Figure 3.4: Comparison of numerical solutions (solid lines) and analytical solutions (dotted lines) of TM_{01} mode in a waveguide at $z = 0$. As the longitudinal electric fields propagates, the transverse electromagnetic fields are induced. Numerical results obtained by using geometric source terms in Maxwell equations match well with analytical solutions

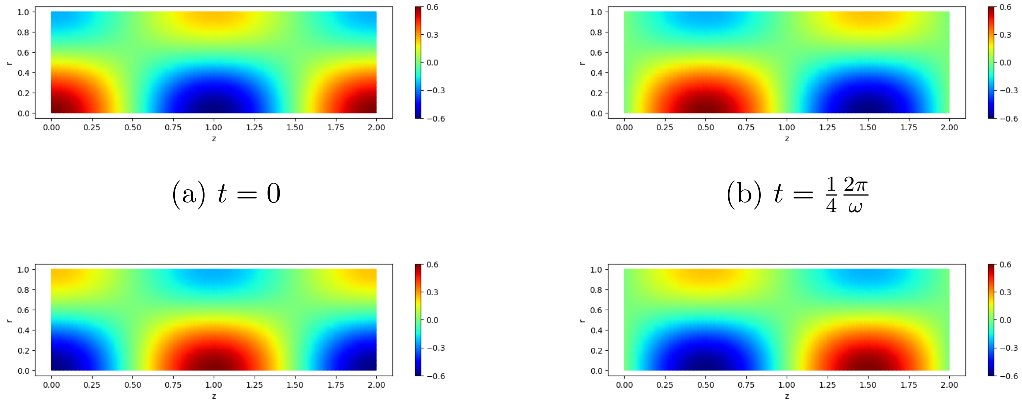

(a) $t = 0$

(b) $t = \frac{1}{4}\frac{2\pi}{\omega}$

(c) $t = \frac{1}{2}\frac{2\pi}{\omega}$

(d) $t = \frac{3}{4}\frac{2\pi}{\omega}$

Figure 3.5: Numerical results from WARPXM showing contours of B_z of a TE_{01} mode in a waveguide that is benchmarked to the analytical solution. The longitudinal component of magnetic fields B_z propagates through the cylindrical waveguide with the expected frequency ω. (Simulations of TE_{01} mode in a waveguide are performed with WARPXM version 1.5.9 using input file TE_TM_waveguide_modes.py)

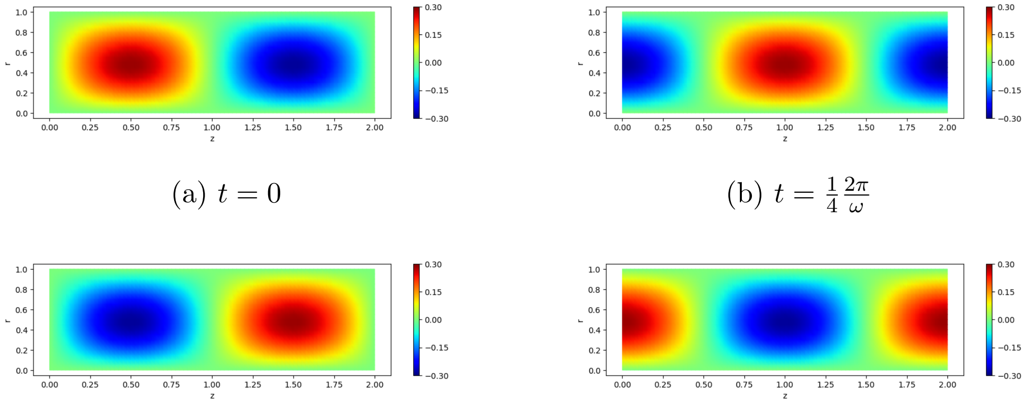

(a) $t = 0$

(b) $t = \frac{1}{4}\frac{2\pi}{\omega}$

(c) $t = \frac{1}{2}\frac{2\pi}{\omega}$

(d) $t = \frac{3}{4}\frac{2\pi}{\omega}$

Figure 3.6: Numerical results from WARPXM showing contours of B_r of a TE$_{01}$ mode in a waveguide that is benchmarked to the analytical solution. The transverse component of magnetic fields B_r is induced and propagates through the cylindrical waveguide with the expected frequency ω. (Simulations of TE$_{01}$ mode in a waveguide are performed with WARPXM version 1.5.9 using input file TE_TM_waveguide_modes.py)

(a) $t = 0$

(b) $t = \frac{1}{4}\frac{2\pi}{\omega}$

(c) $t = \frac{1}{2}\frac{2\pi}{\omega}$

(d) $t = \frac{3}{4}\frac{2\pi}{\omega}$

Figure 3.7: Numerical results from WARPXM showing contours of E_θ of a TE$_{01}$ mode in a waveguide that is benchmarked to the analytical solution. The transverse component of electric fields E_θ is induced and propagates through the cylindrical waveguide with the expected frequency ω. (Simulations of TE$_{01}$ mode in a waveguide are performed with WARPXM version 1.5.9 using input file TE_TM_waveguide_modes.py)

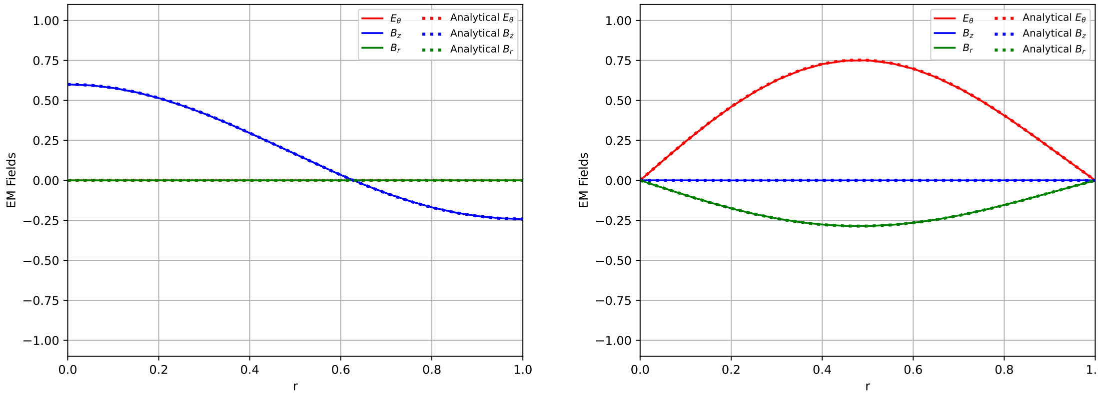

(a) $t = 0$

(b) $t = \frac{1}{4}\frac{2\pi}{\omega}$

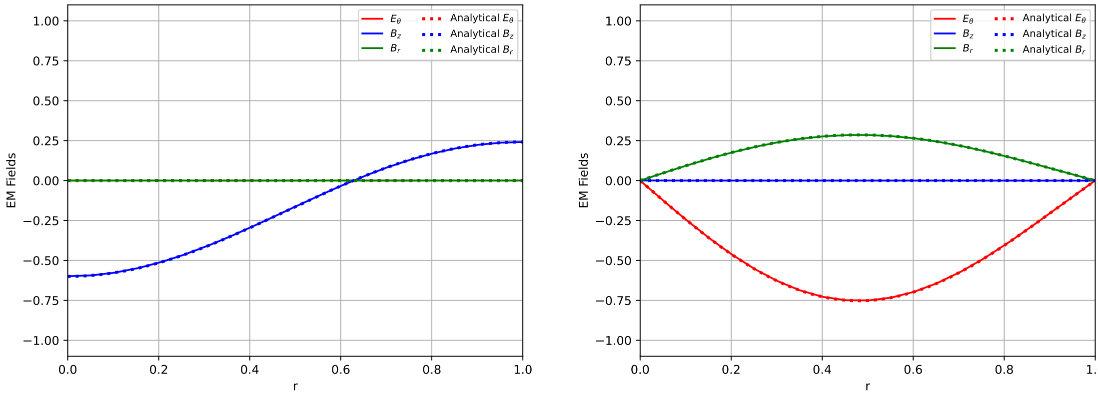

(c) $t = \frac{1}{2}\frac{2\pi}{\omega}$

(d) $t = \frac{3}{4}\frac{2\pi}{\omega}$

Figure 3.8: Comparison of numerical solutions (solid lines) and analytical solutions (dotted lines) of a TE_{01} mode in a waveguide at $z = 0$. As the longitudinal magnetic fields propagates, the transverse electromagnetic fields are induced. Numerical results obtained by using geometric source terms in Maxwell equations match well with analytical solutions

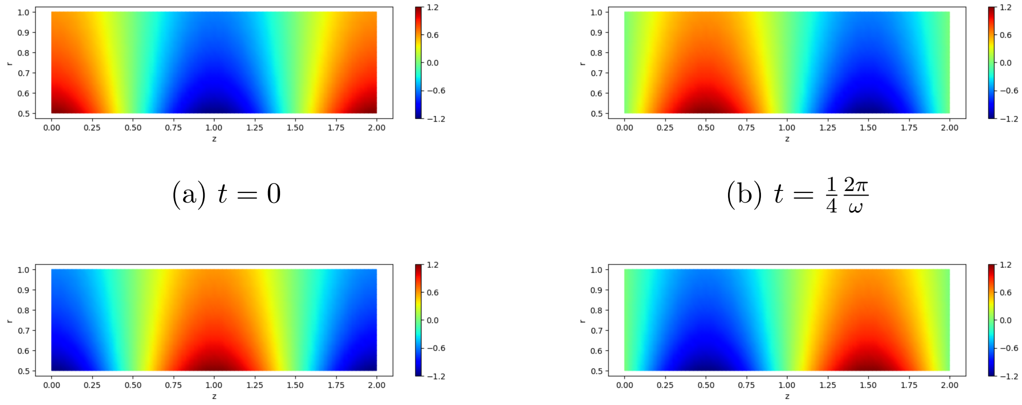

(a) $t = 0$

(b) $t = \frac{1}{4}\frac{2\pi}{\omega}$

(c) $t = \frac{1}{2}\frac{2\pi}{\omega}$

(d) $t = \frac{3}{4}\frac{2\pi}{\omega}$

Figure 3.9: Numerical results from WARPXM showing contours of B_θ of a TEM$_{01}$ mode in a waveguide that is benchmarked to the analytical solution. The transverse component of magnetic fields B_θ propagates through the cylindrical waveguide with the expected frequency ω. (Simulations of TEM$_{01}$ mode in a waveguide are performed with WARPXM version 1.5.9 using input file TE_TM_waveguide_modes.py)

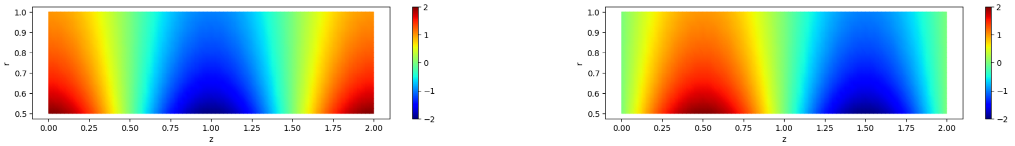

(a) $t = 0$

(b) $t = \frac{1}{4}\frac{2\pi}{\omega}$

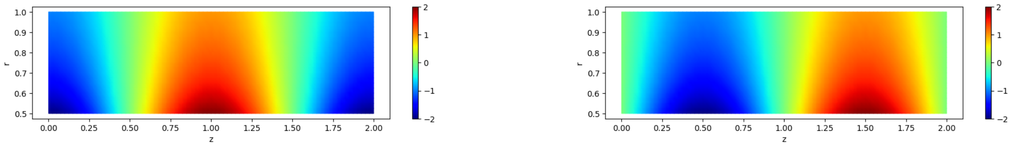

(c) $t = \frac{1}{2}\frac{2\pi}{\omega}$

(d) $t = \frac{3}{4}\frac{2\pi}{\omega}$

Figure 3.10: Numerical results from WARPXM showing contours of E_r of a TEM$_{01}$ mode in a waveguide that is benchmarked to the analytical solution. . The transverse component of electric fields E_r is propagates through the cylindrical waveguide with the expected frequency ω. (Simulations of TEM$_{01}$ mode in a waveguide are performed with WARPXM version 1.5.9 using input file TE_TM_waveguide_modes.py)

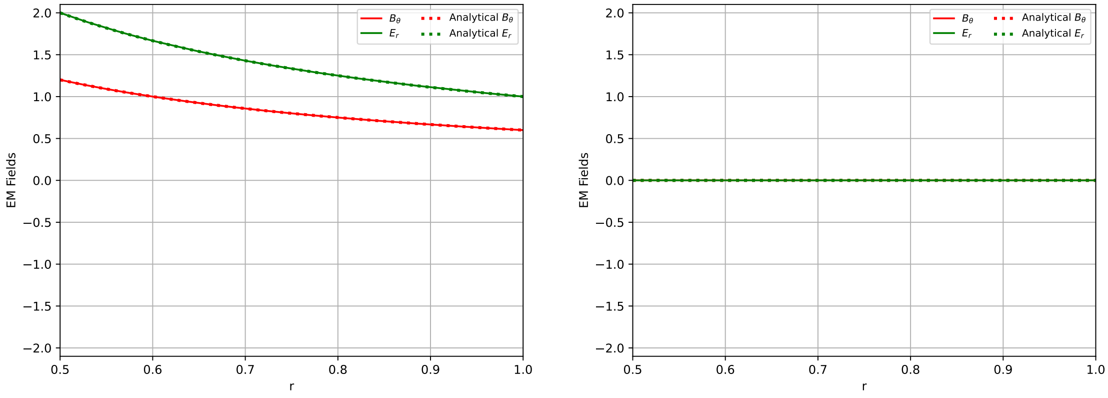

(a) $t = 0$

(b) $t = \frac{1}{4}\frac{2\pi}{\omega}$

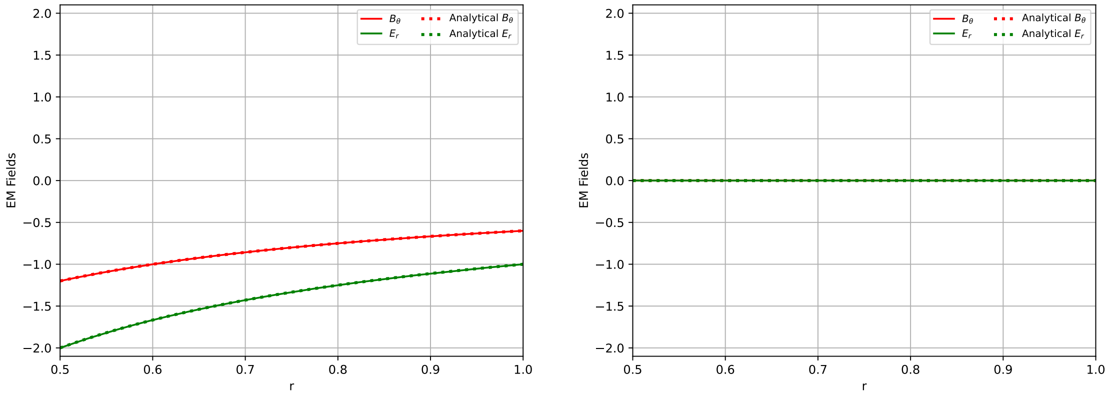

(c) $t = \frac{1}{2}\frac{2\pi}{\omega}$

(d) $t = \frac{3}{4}\frac{2\pi}{\omega}$

Figure 3.11: Comparison of numerical solutions (solid lines) and analytical solutions (dotted lines) in TEM_{01} mode at $z = 0$. Numerical results obtained by using geometric source terms in Maxwell equations match well with analytical solutions. Although TE_{01} or TM_{01} modes require to apply L'Hôpital's rule at $r = 0$ for the geometric source terms, TEM_{01} mode works as the benchmark test for the geometric source terms without using L'Hôpital's rule due to the hollow cylindrical configuration.

3.2 Rotational Hydrostatic Pressure

Considering the rotating, inviscid and neutral flow in equilibrium conditions with a constant angular velocity ω, the governing equation is

$$\rho_n(\vec{u}_n \cdot \nabla)\vec{u}_n + \nabla P_n = 0 \tag{3.19}$$

where

$$\vec{u}_n = u_{n\theta}\hat{\theta} = r\omega\hat{\theta} \tag{3.20}$$

Thus, Eq. (3.19) becomes

$$\frac{\partial P_n}{\partial r} = \rho_n r\omega^2 \tag{3.21}$$

Assuming the uniform density,

$$P_n(r) = \frac{1}{2}\rho_n\omega^2 r^2 + C \tag{3.22}$$

where C is the constant of integration. On the other hand, assuming the uniform temperature T_n,

$$\rho_n(r) = Ce^{\frac{\omega^2 r^2}{2k_B T_n}} \tag{3.23}$$

$$P_n(r) = C\frac{k_B T_n}{m_n}e^{\frac{\omega^2 r^2}{2k_B T_n}} \tag{3.24}$$

where k_B is Boltzmann constant and

$$P_n = n_n k_B T_n \tag{3.25}$$

The typical rotational hydrostatic analysis includes a gravity with the assumption of uniform density that yields a parabolic pressure profile. However, a gravity and the uniform density are not necessary in the ideal $5N$-moment fluid model. The assumption of the uniform temperature is useful to eliminate the heat flux term in the energy equation. The numerical results are compared with the analytical results in Fig. 3.12 where the benchmark test has the third order of accuracy in time and space with 32 elements.

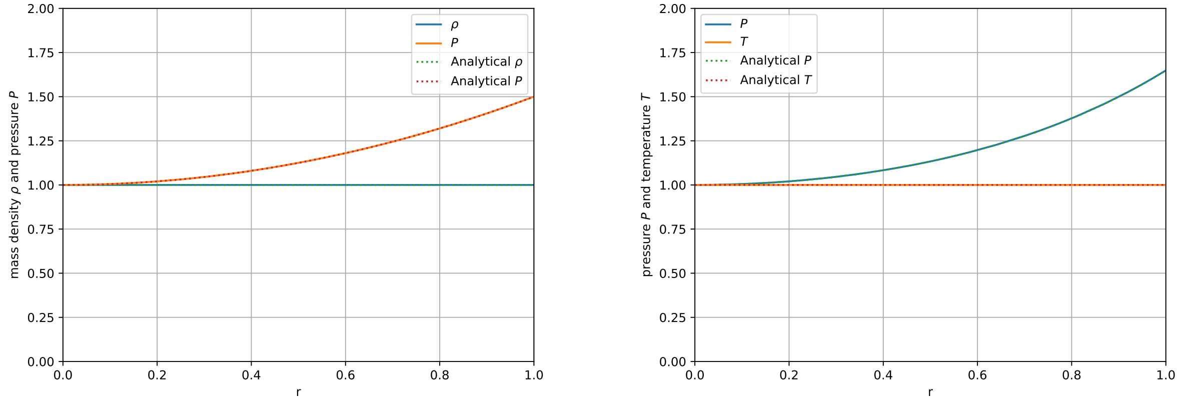

(a) uniform ρ_n

(b) uniform T_n

Figure 3.12: Radial profiles of mass density and temperature for a rotational hydrostatic flow. Numerical results (solid lines) are compared with analytical results (dotted line) that are benchmark tests for the geometric source terms in fluid Euler equations works. (Simulation of a rotational hydrodynamic flow is performed with WARPXM version 1.5.9 using input file rotating_flow.py)

3.3 Taylor-Couette Flow

The Taylor-Couette flow is the result of viscous fluid flow between two rotating coaxial cylinders. If the viscous fluid is between parallel plates instead of coaxial cylinders, the viscous flow is known as the Couette flow where one plate moves tangentially and the other one is fixed. In 1890, Couette described a viscometer to measure the viscosity of fluid experimentally by rotating an outer cylinder[38]. Taylor mathematically investigated the transition of the instability by increasing the rotational speed of the inner cylinder in 1923[39]. The governing equations are

$$\frac{\partial \rho_n}{\partial t} + \nabla \cdot (\rho_n \vec{u}_n) = 0 \tag{3.26}$$

$$\frac{\partial (\rho_n \vec{u}_n)}{\partial t} + \nabla \cdot (\rho_n \vec{u}_n \vec{u}_n) + \nabla P_n + \nabla \cdot \overleftrightarrow{\Pi}_n = 0 \tag{3.27}$$

$$\frac{\partial \epsilon_n}{\partial t} + \nabla \cdot ((\epsilon_n + P_n)\vec{u}_n + \vec{u}_n \cdot \overleftrightarrow{\Pi}_n) = 0 \tag{3.28}$$

where the index n indicates neutral fluid and the heat flux $\vec{h}_n$ is assumed to be zero. Assuming Newtonian fluid and constant viscosity coefficients,

$$\begin{aligned}\overset{\leftrightarrow}{\Pi}_n &= -\mu(\nabla\vec{u}_n + (\nabla\vec{u}_n)^T) - \lambda(\nabla\cdot\vec{u}_n)\overset{\leftrightarrow}{I} \\ &= -\mu(\nabla\vec{u}_n + (\nabla\vec{u}_n)^T) + \left(\frac{2}{3}\mu - \mu^{'}\right)(\nabla\cdot\vec{u}_n)\overset{\leftrightarrow}{I}\end{aligned} \tag{3.29}$$

where μ is the shear viscosity coefficient, λ is the second coefficient of viscosity and $\mu^{'}$ is the bulk viscosity coefficient[40]

$$\mu^{'} = \frac{2}{3}\mu + \lambda \tag{3.30}$$

The assumption of an incompressible flow can simplify the divergence of $\overset{\leftrightarrow}{\Pi}_n$ as

$$\begin{aligned}\nabla\cdot\overset{\leftrightarrow}{\Pi}_n &= -\mu\nabla^2\vec{u}_n - \left(\frac{1}{3}\mu + \mu^{'}\right)\nabla\left(\nabla\cdot\vec{u}_n\right) \\ &= -\mu\nabla^2\vec{u}_n - (\mu+\lambda)\nabla\left(\nabla\cdot\vec{u}_n\right) \\ &= -\mu\nabla^2\vec{u}_n\end{aligned} \tag{3.31}$$

where

$$\nabla\cdot\vec{u}_n = 0 \tag{3.32}$$

As a benchmark test of the geometric source terms for a neutral viscous fluid, the steady state azimuthal flow is described by

$$\vec{u}_n(\vec{r}) = u_{n\theta}(r)\hat{\theta} \tag{3.33}$$

$$P_n(\vec{r}) = P_n(r) \tag{3.34}$$

where the solution is assumed to be axisymmetric and independent on z. Eqs. (3.26), (3.27) and (3.31) give

$$\rho_n\left(\vec{u}_n\cdot\nabla\right)\vec{u}_n + \nabla P_n - \mu\nabla^2\vec{u}_n = 0 \tag{3.35}$$

which yields

$$-\rho_n\frac{u_{n\theta}^2}{r} + \frac{\partial P_n}{\partial r} = 0 \tag{3.36}$$

$$\mu\left(\nabla^2 u_{n\theta} - \frac{u_{n\theta}}{r^2}\right) = \mu\left(\frac{1}{r}\frac{\partial}{\partial r}\left(r\frac{\partial u_{n\theta}}{\partial r}\right) - \frac{u_{n\theta}}{r^2}\right) = 0 \tag{3.37}$$

Solving for P_n and $u_{n\theta}$,

$$u_{n\theta}(r) = rC_1 + \frac{C_2}{r} \tag{3.38}$$

$$P_n(r) = 2C_1C_2\rho_n \ln(r) + \frac{1}{2}\rho_n\left(r^2C_1^2 - \frac{C_2^2}{r^2}\right) + C_3 \tag{3.39}$$

where C_3 is an integral constant, and C_1 and C_2 are constants and can be determined by using boundary conditions; for example, the no-slip wall boundary conditions yield

$$C_1 = \frac{\Omega_o - \Omega_i\left(\frac{R_i}{R_o}\right)^2}{1-\left(\frac{R_i}{R_o}\right)^2} \tag{3.40}$$

$$C_2 = R_i^2\frac{\Omega_i - \Omega_o}{1-\left(\frac{R_i}{R_o}\right)^2} \tag{3.41}$$

R_i and R_o are the radii of an inner wall and an outer wall. Ω is a wall angular velocity. Using the perturbation theory, Chandrasekhar[41] summarized the transition of the instability in terms of a Taylor number T_a

$$\mathrm{T}_a = \frac{4\Omega_i^2R_i^4}{\nu^2}\frac{(1-\mu_\Omega)\left(1-\frac{\mu_\Omega}{\eta^2}\right)}{(1-\eta^2)^2} \tag{3.42}$$

where ν is a kinematic viscosity and

$$\mu_\Omega \equiv \frac{\Omega_o}{\Omega_i} \tag{3.43}$$

$$\eta \equiv \frac{R_i}{R_o} \tag{3.44}$$

With a narrow gap, $1-\eta \ll \frac{1+\eta}{2}$, the Taylor number and the critical Taylor number T_{cri} are

$$\mathrm{T}_a = -\frac{4C_1\Omega_i}{\nu^2}(R_o - R_i)^4 \tag{3.45}$$

$$T_{cri} = \frac{3430}{1+\mu_\Omega}, \tag{3.46}$$

respectively[41]. The stable and unstable numerical results are compared in Figs. 3.13 and 3.14 that are compared with the analytical solutions along $z = 0$ in Fig. 3.15 where the benchmark tests have the third order of accuracy in time and space, and 40 and 20 elements in axial and radial directions, respectively.

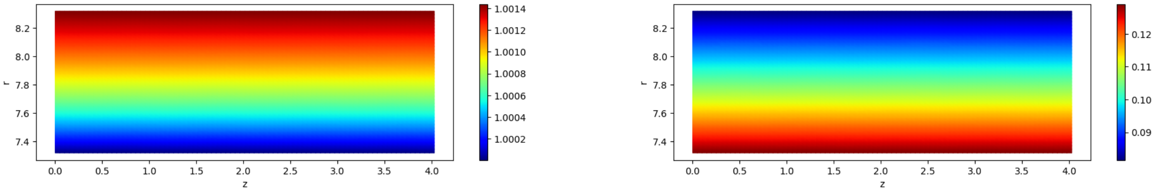

(a) Pressure

(b) u_θ

Figure 3.13: Contour maps of stable equlibrium solutions of hydrodynamic pressure and hydrodynamic azimuthal velocity for Taylor-Couette flow that has the smaller Taylor number than the critical Taylor number, $T_a = 1733 < T_{cri} = 2205$. This is one benchmark test for viscosity with geometric source terms in LGL nodes. (Simulations of Taylor-Couette flow are performed with WARPXM version 1.5.9 using input file Taylor_Couette_flow.py)

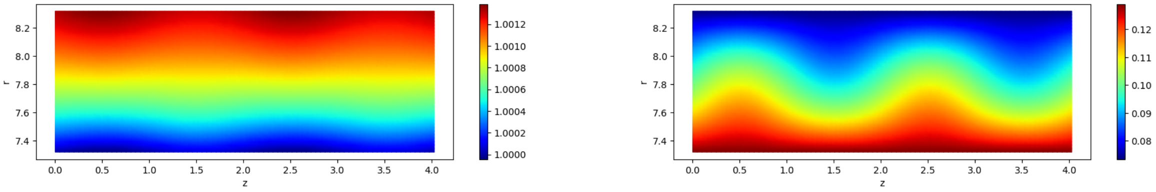

(a) Pressure

(b) u_θ

Figure 3.14: Contour maps of ustable solutions of hydrodynamic pressure and hydrodynamic azimuthal velocity for Taylor-Couette flow that has the larger Taylor number than the critical Taylor number, $T_a = 2684 > T_{cri} = 2286$ .This is another benchmark test for viscosity with geometric source terms in LGL nodes. (Simulations of Taylor-Couette flow are performed with WARPXM version 1.5.9 using input file Taylor_Couette_flow.py)

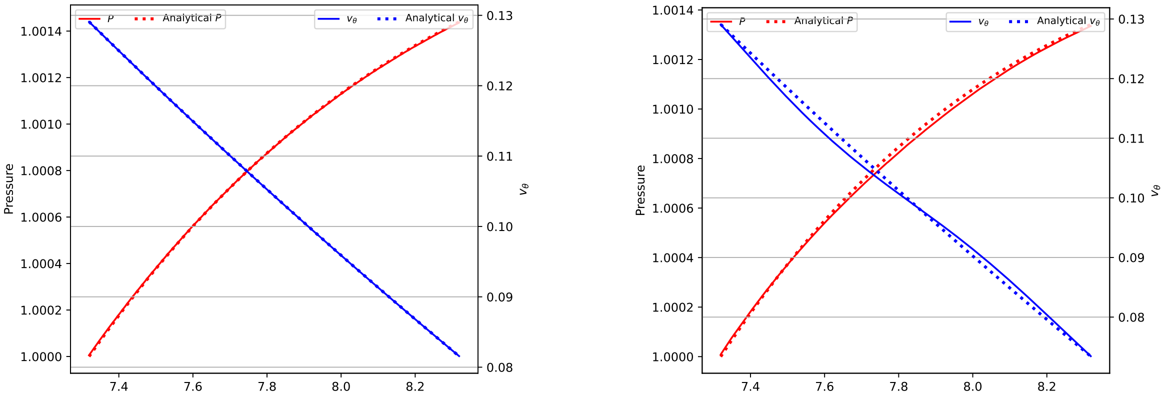

(a) $T_a = 1733 < T_{cri} = 2205$

(b) $T_a = 2684 > T_{cri} = 2286$

Figure 3.15: Comparison of radial profile of pressure and azimuthal velocities in (a) stable and (b) unstable Taylor-Couette flow at $z = 0$. Numerical results (solid lines) and analytical results (dotted lines) are compared as the benchmark test for viscosity with geometric source terms.

3.4 Hagen-Poiseuille Flow

The Hagen-Poiseuille flow results from a pressure drop due to the viscosity of a Newtonian fluid thorough the cylindrical pipe is found by Poiseuille and Hagen in 1840[42, 43, 44]. The theoretical analysis assumes incompressible and laminar flow. Since Taylor-Couette flow does not include $r = 0$ in the calculation domain, the Hagen-Poiseuille flow provides a useful benchmark test of the geometric source terms including $r = 0$ with viscosity. To avoid using the second order derivatives by applying L'Hôpital's rule at $r = 0$, Gauss-Legendre quadrature[45] for 1D simulations or Gaussian quadrature[46] for 2D simulations are used instead of using Legendre-Gauss-Lobatto quadrature[2]. Assuming that the axisymmetric solution in steady state can be expressed as

$$\vec{u}_n(\vec{r}) = u_{nz}(r)\hat{z} \tag{3.47}$$

$$P_n(\vec{r}) = P_n(z) \tag{3.48}$$

the governing equation, Eq. (3.35), reduces to

$$\frac{\partial P_n}{\partial z} - \mu \frac{1}{r} \frac{\partial}{\partial r} \left(r \frac{\partial u_{nz}}{\partial r} \right) = 0 \tag{3.49}$$

For a constant axial pressure gradient, the first term and the second term in the left hand side must be constant such that

$$\frac{\partial P_n}{\partial z} = \mu \frac{1}{r} \frac{\partial}{\partial r} \left(r \frac{\partial u_{nz}}{\partial r} \right) = G \tag{3.50}$$

Solving for u_{nz} and P_n,

$$u_{nz}(r) = \frac{G}{4\mu} r^2 + C_1 \ln(r) + C_2 \tag{3.51}$$

$$P_n(z) = Gz + C_3 \tag{3.52}$$

The assumption of the finite $u_{nz}(r = 0)$ gives $C_1 = 0$. Using fixed no-slip wall boundary conditions,

$$C_2 = -\frac{G}{4\mu} R_o^2 \tag{3.53}$$

The numerical equilibrium results are shown in Fig. 3.16 that are compared with the analytical results in 3.17. The benchmark tests have the third order of accuracy in time and space, and 30 and 10 elements in axial and radial directions, respectively.

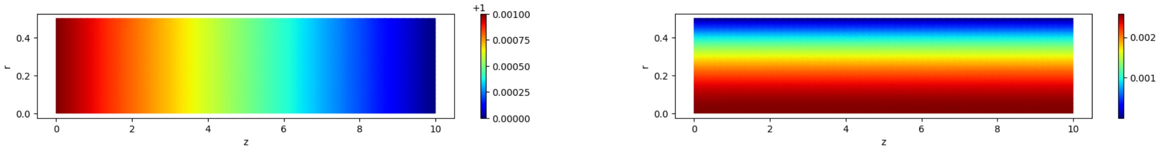

(a) Pressure

(b) u_z

Figure 3.16: Contour maps of equilibrium solutions of hydrodynamic pressure and hydrodynamic axial velocity that derive Hagen-Poiseuille flow as the benchmark test with viscosity in Gaussian quadrature nodes. (Simulations of Hagen-Poiseuille flow are performed with WARPXM version 1.5.9 using input file Hagen_Poiseuille_flow.py)

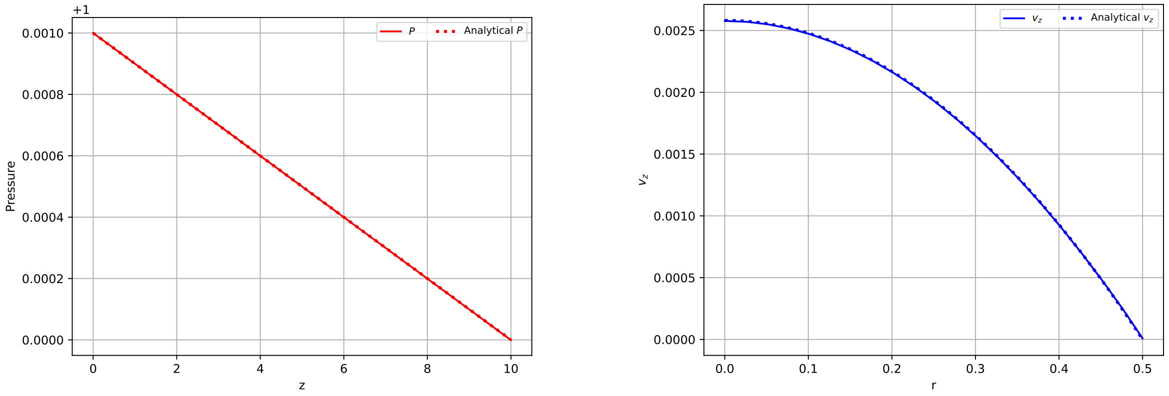

(a) Axial profile of pressure

(b) Radial profile of axial velocity

Figure 3.17: Axial profile of pressure at $r = 0$ and radial profile of velocity at $z = 0$ for Hagen-Poiseuille flow. Numerical results (solid lines) obtained by initiating uniform velocity with pressure gradient reaches the equilibrium analytical results (dotted lines).

3.5 1D Z-Pinch in Radial Equilibrium

3.5.1 Z-pinch in Ideal 5N-moment Two-fluid Model

The radial equilibrium conditions for the Z-pinch in two-fluid model in a frame of reference with no electric field satisfy

$$\nabla P_\alpha = \vec{J}_\alpha \times \vec{B} \tag{3.54}$$

$$\nabla \times \vec{B} = \mu_0 \vec{J} \tag{3.55}$$

The following Bennett profile[47, 48] is one possible and well-known solution for the equilibrium Z-pinch

$$n_\alpha = \frac{n_0}{\left(1 + \frac{r^2}{r_p^2}\right)^2} \tag{3.56}$$

$$J_{\alpha z} = n_\alpha q_\alpha u_{\alpha z} \tag{3.57}$$

$$B_\theta = B_0 \frac{2\frac{r}{r_p}}{1 + \frac{r^2}{r_p^2}} \tag{3.58}$$

where n_0 and B_0 are the peak number density and peak azimuthal magnetic fields, respectively, and r_p is the pinch radius defined as the radial position at the peak magnetic field. The numerical results are compared with the analytical solutions in Fig. 3.18 and The benchmark test has the third order of accuracy in time and space with 40 elements.

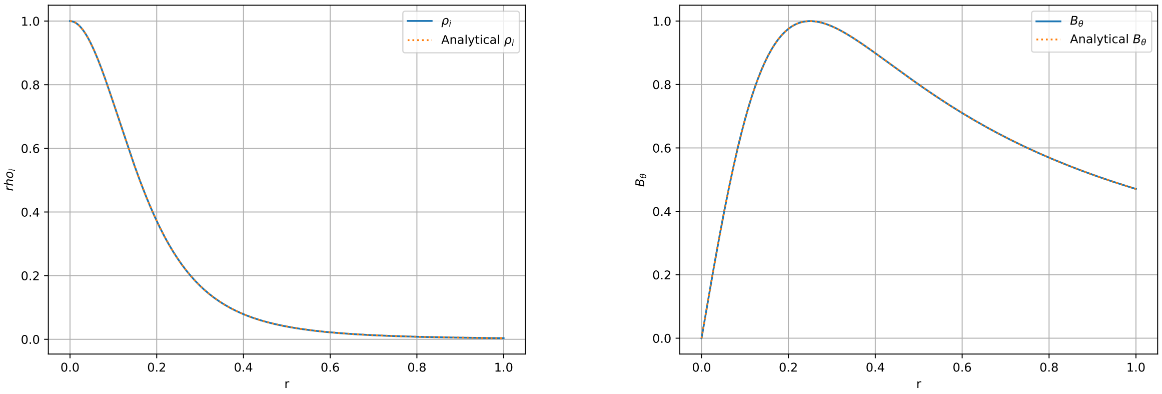

(a) ρ_i

(b) B_θ

Figure 3.18: 1D radial equilibrium Z pinch in the ideal two-fluid model. Numerical results (solid lines) match with the analytical results (dotted lines). The geometric source terms work well in the ideal $5N$-moment two-fluid plasma model. (Simulation of 1D equilibrium Z pinch in the ideal two-fluid model is performed with WARPXM version 1.5.9 using input file zpinch_5moment_1D.py)

3.5.2 Z-pinch in ideal MHD model

In the ideal MHD model, the Bennett profile is

$$n = \frac{n_0}{\left(1 + \frac{r^2}{r_p^2}\right)^2} \tag{3.59}$$

$$B_\theta = B_0 \frac{2\frac{r}{r_p}}{1 + \frac{r^2}{r_p^2}} \tag{3.60}$$

The numerical results in the ideal MHD model are compared with the analytical solutions in Fig. 3.19. The benchmark test has the third order of accuracy in time and space with 40 elements.

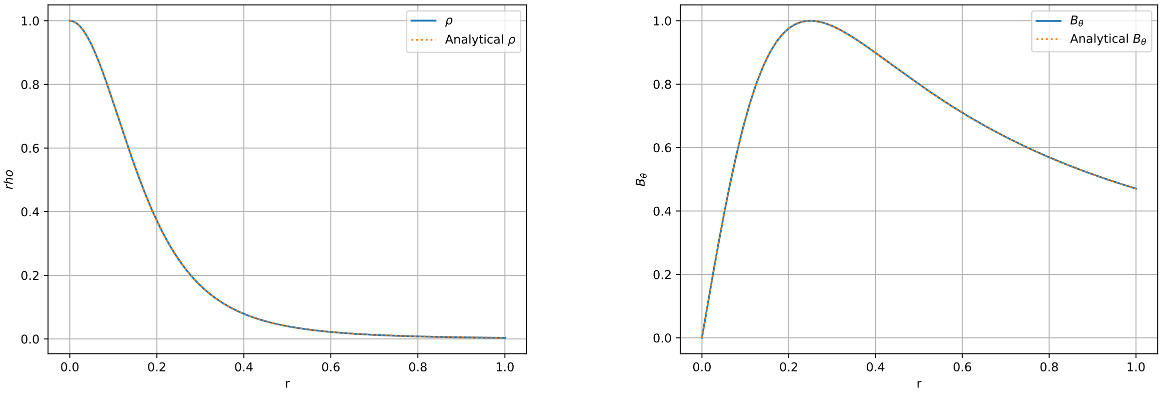

(a) ρ

(b) B_θ

Figure 3.19: 1D radial equilibrium Z-pinch in the ideal MHD model. Numerical results (solid lines) match with the analytical results (dotted lines). The geometric source terms works well in the ideal MHD plasma model. (Simulation of 1D equilibrium Z pinch in the ideal MHD model is performed with WARPXM version 1.5.9 using input file zpinch_mhd_1D.py)

3.6 Summary of the Benchmark Tests

The benchmark tests of purely Maxwell's equations, the neutral fluid equations, the ideal $5N$-moment two-fluid model and the ideal MHD model demonstrate that the geometric source terms have been implemented correctly. The numerical results match quite well with the analytical solutions including $r = 0$ in cylindrical coordinates where L'Hôpital's rule is applied. In the following chapters, WARPXM with the geometric source terms is used to solve more complicated axisymmetric problems to understand the Z-pinch plasma dynamics.

Chapter 4

$m = 0$ SAUSAGE INSTABILITY IN 2D AXISYMMETRIC Z-PINCH

The linear stability analysis for the pinch studied by Kruskal and Schwarzchild[49] and Taylor[39] have indicated that a Z-pinch is sensitive to the pressure-driven $m = 0$ sausage instability and the current-driven $m = 1$ kink instability. In 1995, Shumlak and Hartman demonstrated the stabilizing effects of a sheared-flow on Z-pinch equilibrium[50]. Scheffel et al. utilized the Vlasov-fluid model where ions are described in the kinetic model, but electrons are treated as fluid to observe the finite Larmor radius effects in 1997.[51] In 2002, Sotnikov et al. numerically investigated the physics of the shear-free and sheared Z-pinch by using the ideal and Hall MHD model.[52] In 2018, Tummel et al. applied fully kinetic model to investigate Fusion Z-pinch Experiment (FuZE) configurations.[8, 53] Note that kinetic results fundamentally include nonlinear dynamics; however, Tummel's work, while also nonlinear studies, only follows the evolution through the linear phase, when perturbations remained small, and observes only the early nonlinear physics. In 2021, Meier and Shumlak[54] obtained nonlinear saturated results for $m = 0$ sausage instabilities in the FuZE configurations by using $5N$-moment two-fluid model with Braginskii transport. A viable fusion device must operate for durations much longer than the time to reach nonlinear saturation. To observe the stable nonlinear physics and fusion reactions in an axisymmetric Z-pinch, it is important to investigate the sheared-flow stabilizing effects and Braginskii non-ideal transport effects for the $m = 0$ sausage instability in WARPXM. The all numerical results shown in Ch. 4 have the third order accuracy in time and space, and 40 and 10 elements in axial and radial directions, respectively.

4.1 *Shear-free Axisymmetric Z-pinch in Ideal Two-fluid and Ideal MHD Models*

4.1.1 Initial Conditions

The equilibrium conditions follow the Bennett profile and the initial perturbations are applied as follows.

$$n_\alpha = \frac{n_0}{\left(1+\frac{r^2}{r_p^2}\right)^2}\left(1+\epsilon\cos\left(kz\right)\right) \tag{4.1}$$

$$J_z = \frac{n_0}{\left(1+\frac{r^2}{r_p^2}\right)^2} q u_z \left(1-0.5\epsilon\cos\left(kz\right)\right) \tag{4.2}$$

where the axial velocities for each species are the same but opposite, which establishes a frame of reference with no initial electric field

$$u_{iz} = -u_{ez} = \frac{1}{2}u_z \tag{4.3}$$

The azimuthal magnetic fields are not perturbed

$$B_\theta = B_0 \frac{2\frac{r}{r_p}}{1+\frac{r^2}{r_p^2}} \tag{4.4}$$

and uniform temperature assumptions for each species give

$$T_i = T_e = T_0 \tag{4.5}$$

The pinch current I_p is obtained by integrating the axial current density from $r = 0$ to the pinch radius r_p

$$I_p = 2\pi\int_0^{r_p} r J_z dr \tag{4.6}$$

The characteristic physical parameters in FuZE configurations used for normalizations in WARPXM are given in Table 4.1.

Table 4.1: Characteristic physical parameters for FuZE configurations

n_0 [m^{-3}]	T_0 [keV]	I_p [kA]	r_p [mm]
4.25×10^{24}	1.27	150	0.91

4.1.2 Results

The growth rates obtained by using the ideal $5N$-moment two-fluid model for the shear-free Z-pinch with $r_p/r_{Li} = 5.8$ are larger compared with the ideal MHD simulations but comparable to the Hall MHD simulations with $r_p/r_{Li} = 2.36$ presented by Sotnikov et al.[52] at the small-k modes (see Fig. 4.1). As increasing the wave number k, the growth rates show the peak at $kr_p \approx 10$. While the values of those growth rates are larger than the results obtained by the former numerical studies done by Tummel et al.[48] with $r_p/r_{Li} = 5.8$ and Scheffel et al.[51] with $r_p/r_{Li} = 5$, the two-fluid results also show the further stabilizing effects at the large-k modes. To reduce computational costs, it is useful to use larger electron mass ratio $A_e = 1/25$ instead of using $A_e = 1/1836$ at small-k modes. However, the effects of the electron mobility appears significant if $kr_p > 5$. Using the ideal MHD model in WARPXM, the growth rates match well with the results from Sotnikov et al.[52] and saturate around $\gamma\frac{r_p}{V_A} \approx 0.8$ with increasing k. The numerical results obtained by using the ideal $5N$-moment two-fluid model are given in Fig. 4.2 and Fig. 4.3 shows the ideal MHD results.

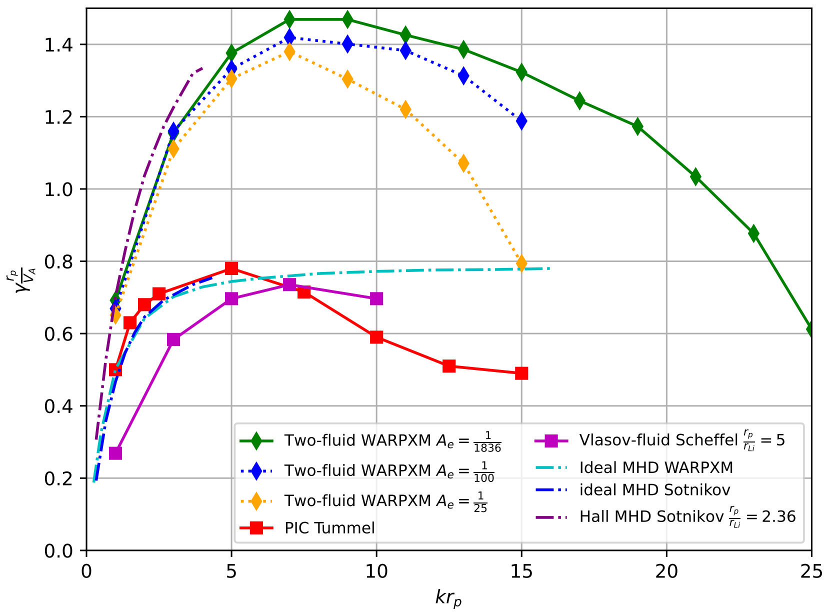

Figure 4.1: Numerical results of the growth rates γ for the sausage instabilities in 2D axisymmetric Z pinch with various different axial wavevector k for the axial perturbations obtained by using various different plasma models. Two-fluid results (diamond markers) show higher growth rates compared with both ideal MHD (blue dashdotted lines) and high-fidelity kinetic results (square markers). However, the Hall MHD results (purple dashdotted line) indicate comparable growth rates to those obtained by using the two-fluid model (diamond markers).

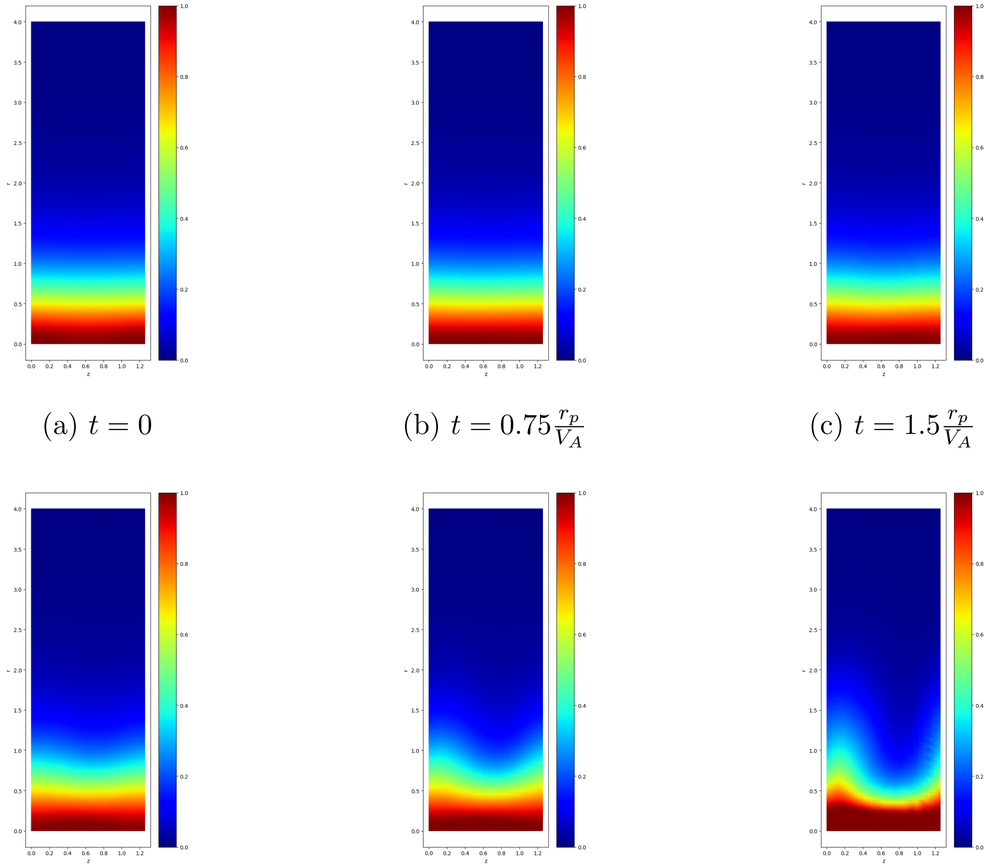

(a) $t = 0$

(b) $t = 0.75\frac{r_p}{V_A}$

(c) $t = 1.5\frac{r_p}{V_A}$

(d) $t = 2.25\frac{r_p}{V_A}$

(e) $t = 3.0\frac{r_p}{V_A}$

(f) $t = 3.75\frac{r_p}{V_A}$

Figure 4.2: Contour maps of ion mass density ρ_i with $kr_p = 5$ and $A_e = 1/1836$ obtained by using ideal two-fluid model. The sausage instabilities grow rapidly and the numerical solutions diverge at 4 Alfven transit time. (Simulations of 2D Z pinch in the ideal two-fluid model are performed with WARPXM version 1.5.9 using input file zpinch_5moment_2D.py)

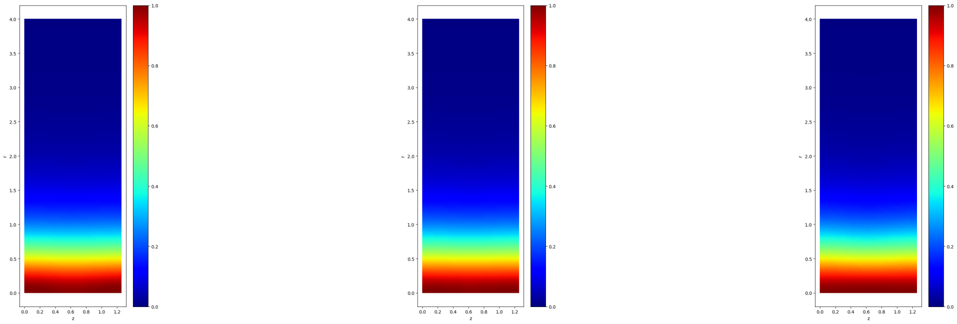

(a) $t = 0$ (b) $t = 0.75\frac{r_p}{V_A}$ (c) $t = 1.5\frac{r_p}{V_A}$

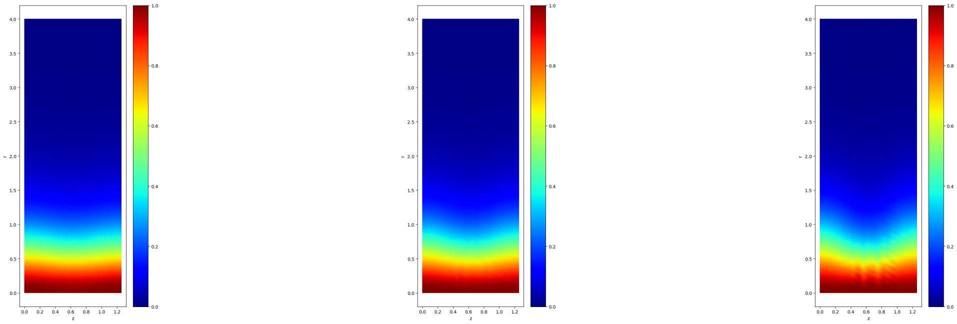

(d) $t = 2.25\frac{r_p}{V_A}$ (e) $t = 3.0\frac{r_p}{V_A}$ (f) $t = 3.75\frac{r_p}{V_A}$

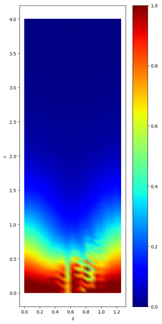

(g) $t = 4.5\frac{r_p}{V_A}$

Figure 4.3: Contour maps of mass density ρ with $kr_p = 5$ obtained by using the ideal MHD model. The slower growth of sausage instabilities in the axisymmetric Z pinch from the ideal MHD model indicates the higher stabilizing effects compared with the ideal two-fluid results, and the calculations can be sustained until 4.5 Alfven transit time. (Simulations of 2D Z pinch in the ideal MHD model are performed with WARPXM version 1.5.9 using input file zpinch_mhd_2D.py)

It is interesting that the growth rates from the ideal $5N$-moment two-fluid model present larger values compared with the Tummel's kinetic model and Sheffel's Vlasov-fluid model. This indicates that the kinetic ion has some stabilizing effects and the non-ideal terms in the $5N$-moment two-fluid model, for example Braginskii viscosity tensor, are anticipated to produce similar stabilizing effects. While there are not enough information for the kinetic electron effects at large-k modes, the both Vlasov-fluid and two-fluid results indicate shifted peaks and monotonically decrease without having an inflection point. On the other hand, the Sotnokov's Hall MHD results show larger growth rates than the ideal MHD results, but comparable to the ideal $5N$-moment two-fluid results. This suggests that Hall effects (or the mobility of electrons) are expected to produce some destabilizing effects at small-k modes.

4.2 Shear-Flow-Stabilized (SFS) Z Pinch in Ideal Two-fluid Model

A linear sheared flow profile is given to ions and electrons in addition to the initial conditions for the shear-free cases.

$$u_{iz} = -u_{ez} = \frac{1}{2}u_{z0} + u_{zs}\frac{r}{r_p} \tag{4.7}$$

Since the number density and magnetic fields start with the Bennett equilibrium for the shear-free Z pinch, the initial conditions do not satisfy equilibrium. Thereby, Maxwell's equations and momentum equations are expected to generate a radial electric field. Similar to Tummel's results, the stronger stabilizing effects and an improvement of the plasma confinement is observed for increasing velocity shear u_{zs} (see Fig. 4.4). However, it is difficult to achieve nonlinear saturation in the ideal two-fluid model due to the larger growth rates and the lack of dissipation. The numerical contour maps for ion mass density with different sheared flows are given in Figs. 4.5, 4.6, and 4.7.

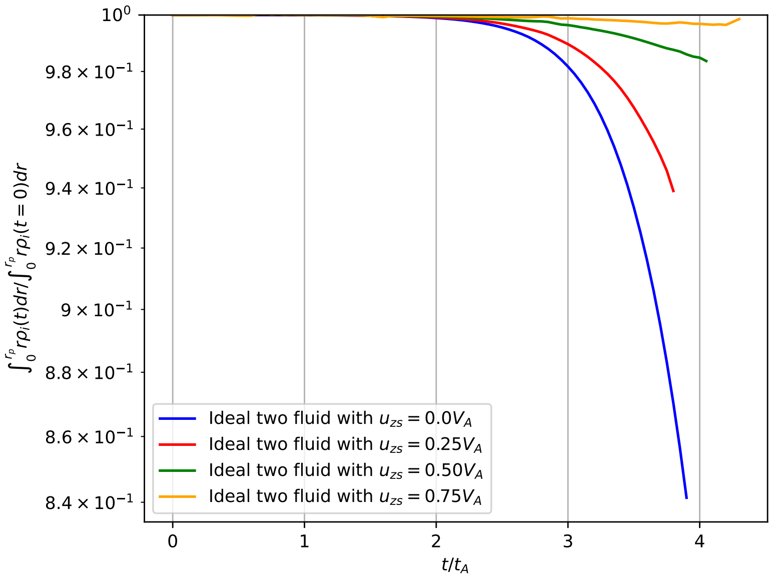

Figure 4.4: Total mass confined in the shear-free (blue line) and SFS Z pinches (red, green and orange lines) with various different shear flow. The larger sausage instabilities lead to more plasma losses; however the stronger shear profile improves the plasma confinement.

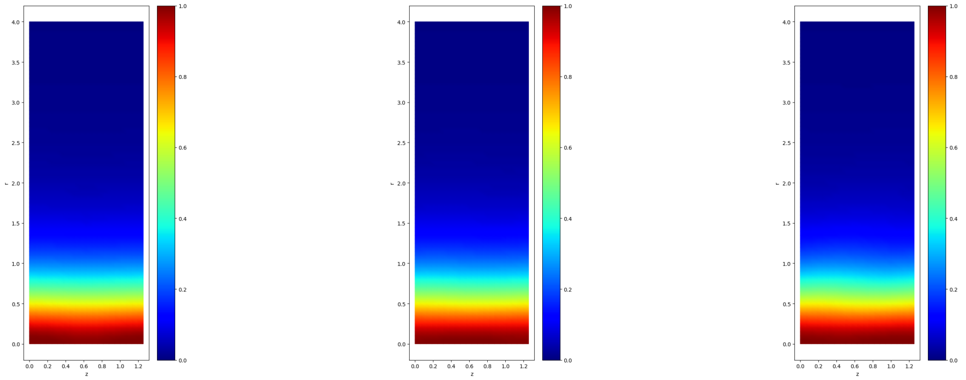

(a) $t = 0$ (b) $t = 0.75\frac{r_p}{V_A}$ (c) $t = 1.5\frac{r_p}{V_A}$

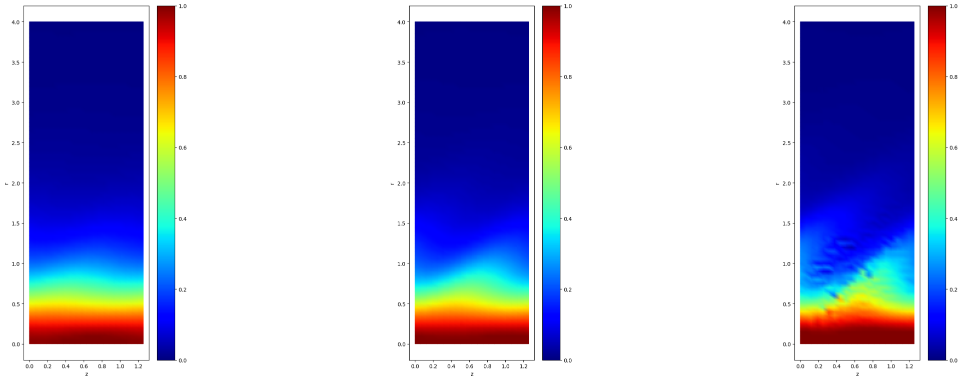

(d) $t = 2.25\frac{r_p}{V_A}$ (e) $t = 3.0\frac{r_p}{V_A}$ (f) $t = 3.75\frac{r_p}{V_A}$

Figure 4.5: Contour maps of ion mass density ρ_i of Z pinch with $kr_p = 5$ and $T_0 = 1270$ eV including sheared flow $u_{zs} = 0.25V_A$. While the shear profile with $u_{zs} = 0.25V_A$ cannot stabilize the sausage instability, the sheared flow starts to improve the plasma confinement compared with the shear-free case in Fig. 4.2 (Simulations of 2D SFS Z pinch in the ideal two-fluid model are performed with WARPXM version 1.5.9 using input file zpinch_5moment_2D.py)

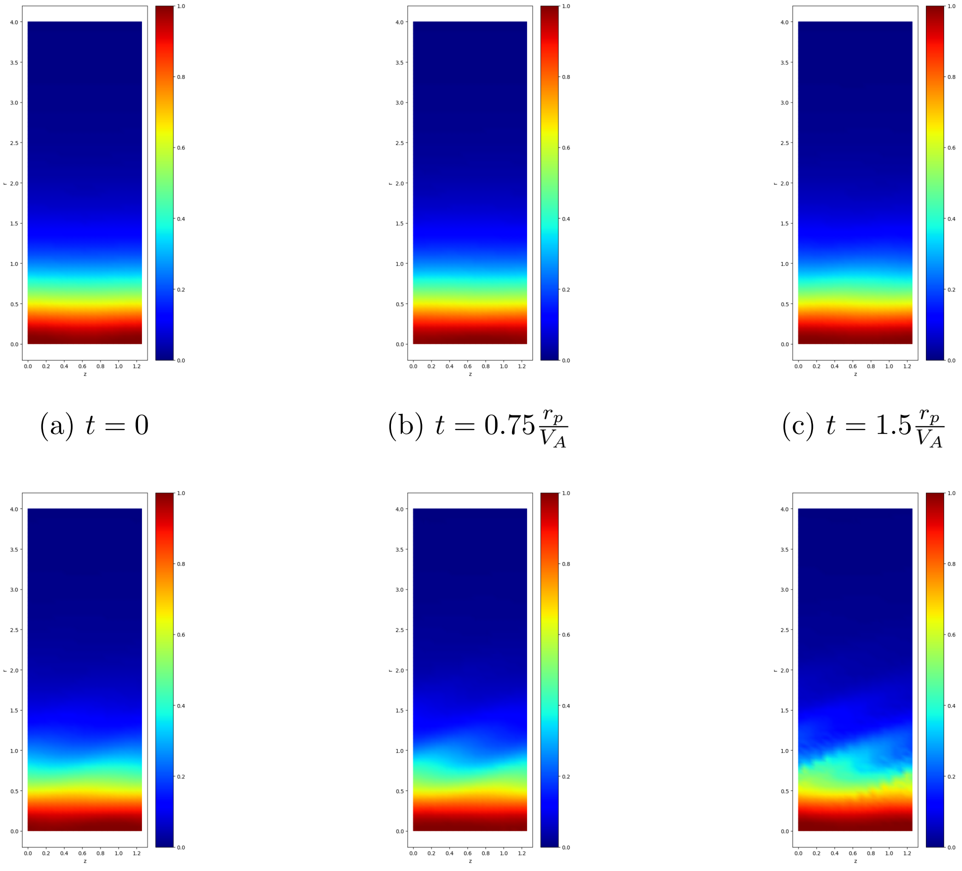

(a) $t = 0$ (b) $t = 0.75\frac{r_p}{V_A}$ (c) $t = 1.5\frac{r_p}{V_A}$

(d) $t = 2.25\frac{r_p}{V_A}$ (e) $t = 3.0\frac{r_p}{V_A}$ (f) $t = 3.75\frac{r_p}{V_A}$

Figure 4.6: Contour maps of ion mass density ρ_i of Z pinch with $kr_p = 5$ and $T_0 = 1270$ eV including sheared flow $u_{zs} = 0.50V_A$. The shear profile with $u_{zs} = 0.50V_A$ starts to stabilize the sausage instability and further improves the plasma confinement

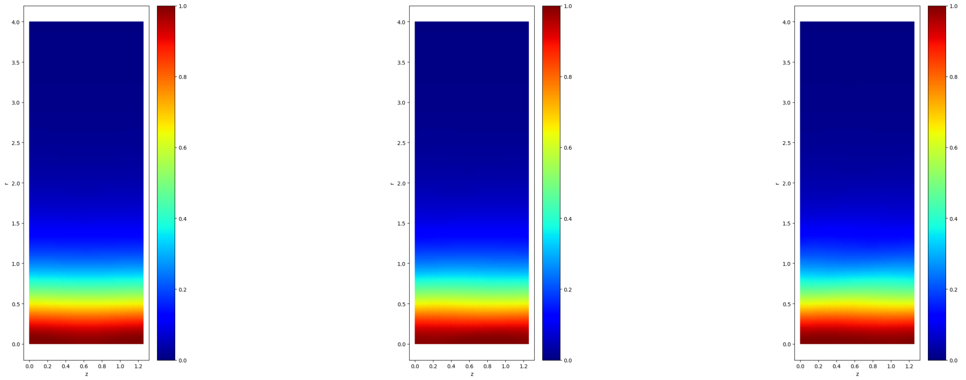

(a) $t = 0$ (b) $t = 0.75\frac{r_p}{V_A}$ (c) $t = 1.5\frac{r_p}{V_A}$

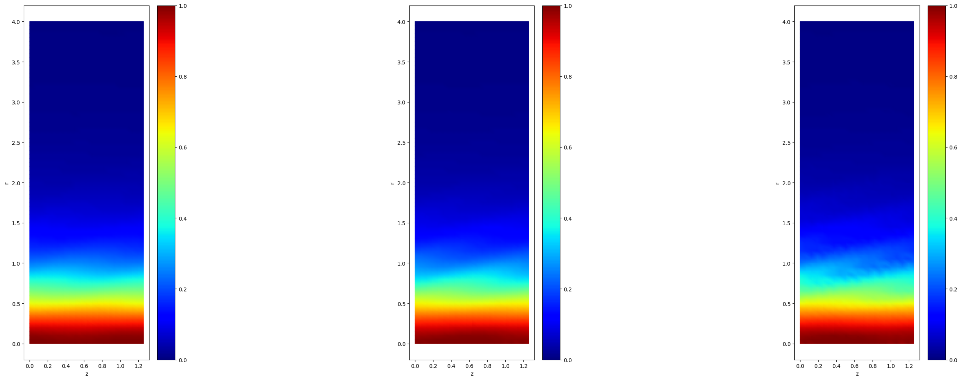

(d) $t = 2.25\frac{r_p}{V_A}$ (e) $t = 3.0\frac{r_p}{V_A}$ (f) $t = 3.75\frac{r_p}{V_A}$

Figure 4.7: Contour maps of ion mass density ρ_i of Z pinch with $kr_p = 5$ and $T_0 = 1270$ eV including sheared flow $u_{zs} = 0.75V_A$. The strong sheared profile with $u_{zs} = 0.75V_A$ stabilizes the sausage instability; however, the non-dissipative ideal two-fluid model cannot reach the nonlinear saturation

4.3 Axisymmetric Z pinch with Braginskii Viscosity and Thermal Conductivity

Braginskii[10] analyzed general the plasma transport by using a moment approach in 1965. The summary of the derivations of Braginskii equations are given in Appendix C. In the axisymmetric cylindrical coordinates, Braginskii viscosity and thermal conductivity are, respectively,

$$\overleftrightarrow{\Pi} = \begin{bmatrix} \Pi_{rr} & \Pi_{r\theta} & \Pi_{rz} \\ \Pi_{\theta r} & \Pi_{\theta\theta} & \Pi_{\theta z} \\ \Pi_{zr} & \Pi_{z\theta} & \Pi_{zz} \end{bmatrix} \tag{4.8}$$

and

$$\vec{h}_\alpha = -\kappa_\perp^\alpha \nabla_\perp T_\alpha \pm \kappa_\wedge^\alpha \left(\hat{b} \times \nabla T_\alpha\right) \tag{4.9}$$

where the positive sign of $\kappa_\wedge^\alpha$ is for ions and the negative sign is for electrons due to the opposite cyclotron direction. The azimuthal direction is parallel to the magnetic field, $\hat{\theta} \parallel \vec{B}$. The each components of the viscosity stress tensor $\overleftrightarrow{\Pi}$ and heat flux $\vec{h}_\alpha$ are

$$\Pi_{\theta\theta} = -\eta_0 W_{\theta\theta} \tag{4.10}$$

$$\Pi_{zz} = -\eta_0 \frac{1}{2}\left(W_{zz} + W_{rr}\right) - \eta_1 \frac{1}{2}\left(W_{zz} - W_{rr}\right) - \eta_3 W_{zr} \tag{4.11}$$

$$\Pi_{rr} = -\eta_0 \frac{1}{2}\left(W_{zz} + W_{rr}\right) - \eta_1 \frac{1}{2}\left(W_{rr} - W_{zz}\right) - \eta_3 W_{zr} \tag{4.12}$$

$$\Pi_{z\theta} = \Pi_{\theta z} = 0 \tag{4.13}$$

$$\Pi_{r\theta} = \Pi_{\theta r} = 0 \tag{4.14}$$

where

$$\overleftrightarrow{W} = \nabla \vec{u}_\alpha + \left(\nabla \vec{u}_\alpha\right)^{\mathrm{T}} - \frac{2}{3}\left(\nabla \cdot \vec{u}_\alpha\right) \overleftrightarrow{I} \tag{4.15}$$

and

$$\vec{h}_\perp = \left(\hat{b} \times \vec{h}\right) \times \hat{b} \tag{4.16}$$

$$\vec{h}_\wedge = \hat{b} \times \vec{h} \tag{4.17}$$

The transport coefficients for viscosity and thermal conductivity are

$$\eta_0^i = 0.96 n_i T_i \tau_{ii} \tag{4.18}$$

$$\eta_2^i = n_i T_i \tau_{ii} \frac{\left(\frac{6}{5} x_i^2 + 2.23\right)}{\Delta_{\eta i}} \tag{4.19}$$

$$\eta_4^i = n_i T_i \tau_{ii} x_i \frac{(x_i^2 + 2.28)}{\Delta_{\eta i}} \tag{4.20}$$

$$\eta_1^i = \eta_2^i(2x_i) \tag{4.21}$$

$$\eta_3^i = \eta_4^i(2x_i) \tag{4.22}$$

$$\eta_0^e = 0.733 n_e T_e \tau_{ei} \tag{4.23}$$

$$\eta_2^e = n_e T_e \tau_{ei} \frac{(2.05 x_e^2 + 8.50)}{\Delta_{\eta e}} \tag{4.24}$$

$$\eta_4^e = n_e T_e \tau_{ei} x_e \frac{(x_e^2 + 7.91)}{\Delta_{\eta e}} \tag{4.25}$$

$$\eta_1^e = \eta_2^e(2x_e) \tag{4.26}$$

$$\eta_3^e = \eta_4^e(2x_e) \tag{4.27}$$

and

$$\kappa_\perp^i = \frac{n_i T_i \tau_{ii}}{m_i} \frac{(2x_i^2 + 2.645)}{\Delta_{\kappa i}} \tag{4.28}$$

$$\kappa_\wedge^i = \frac{n_i T_i \tau_{ii}}{m_i} x_i \frac{\left(\frac{5}{2} x_i^2 + 4.65\right)}{\Delta_{\kappa i}} \tag{4.29}$$

$$\kappa_\perp^e = \frac{n_e T_e \tau_{ei}}{m_e} \frac{(4.664 x_e^2 + 11.92)}{\Delta_{\kappa i}} \tag{4.30}$$

$$\kappa_\wedge^e = \frac{n_e T_e \tau_{ei}}{m_e} x_e \frac{\left(\frac{5}{2} x_i^2 + 21.67\right)}{\Delta_{\kappa i}} \tag{4.31}$$

where the ions are assumed to be singly ionized $Z_i = 1$ and

$$x_\alpha = \omega_{c\alpha}\tau_{\alpha i} \tag{4.32}$$

$$\Delta_{\eta i} = x_i^4 + 4.03x_i^2 + 2.33 \tag{4.33}$$

$$\Delta_{\eta e} = x_e^4 + 13.8x_e^2 + 11.6 \tag{4.34}$$

$$\Delta_{\kappa i} = x_i^4 + 2.70x_i^2 + 0.677 \tag{4.35}$$

$$\Delta_{\kappa e} = x_e^4 + 14.79x_e^2 + 3.7703 \tag{4.36}$$

$$\tau_{ei} = \frac{1}{\nu_{ei}} = \frac{3\left(4\pi\epsilon_0\right)^2\sqrt{m_e}T_e^{\frac{3}{2}}}{4\sqrt{2\pi}n_iZ_i^2q^4\ln\Lambda} \tag{4.37}$$

$$\tau_{ii} = \frac{1}{\nu_{ii}} = \frac{3\left(4\pi\epsilon_0\right)^2\sqrt{m_i}T_i^{\frac{3}{2}}}{4\sqrt{\pi}n_iZ_i^4q^4\ln\Lambda} \tag{4.38}$$

The odd coefficients for viscosity, η_1^α and η_3^α, can be obtained by replacing x_α with $2x_\alpha$. Considering the applicability of Braginskii equations, FuZE configurations, which have $\log_{10}(\mathrm{Kn}) = 0.888$, are in a collisional transition or collisionless regime that is out of the formal applicability of Braginskii equations.

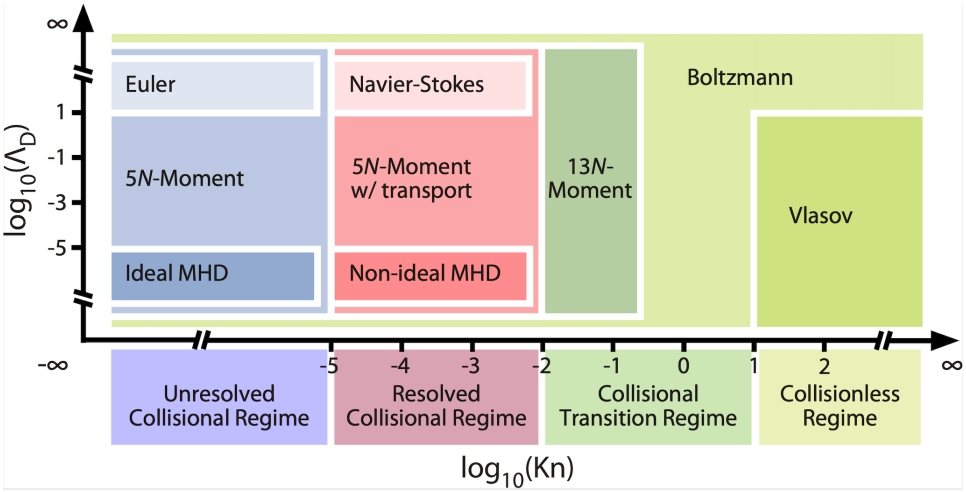

Figure 4.8: Applicability of plasma models based on the collisionality and charge separation[2].

As Knudsen number increases (as plasma becomes collisionless), although Braginskii resistivity α decreases, viscosity coefficient η and thermal conductivity κ increase (see in Fig. 4.9). In a collisionless regime, the viscosity and thermal conductivity become unphysically large. Thereby, Meier and Shumlak[54] extended the applicability of Braginskii equations by applying several physics-based corrections for the transport coefficients.

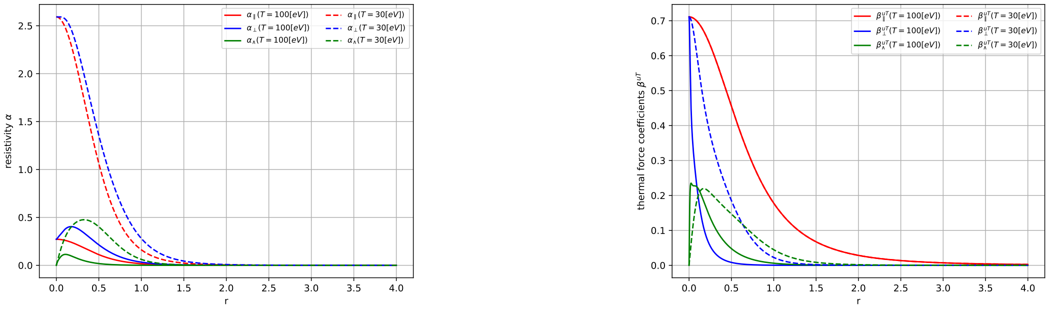

(a) Resistivity α

(b) Thermal force coefficients β

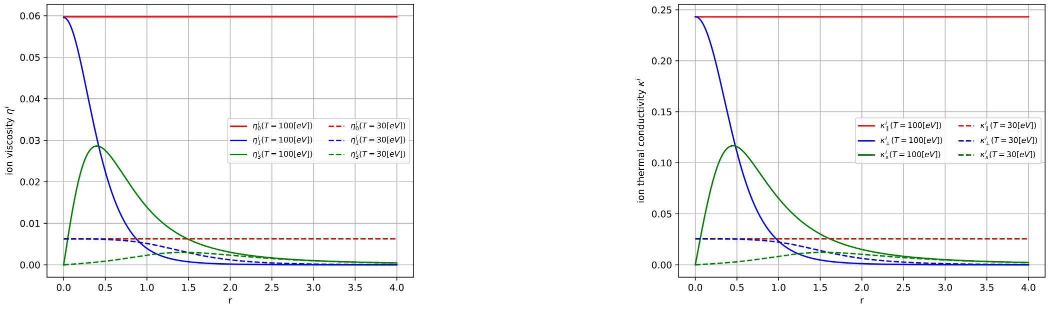

(c) Ion viscosity η^i

(d) Ion thermal conductivity κ^i

Figure 4.9: The radial profile of Braginskii transport coefficients for $T = 100$ eV (solid lines) and $T = 30$ eV (dashed lines) Z pinch plasma satisfying the Bennett equilibrium. While the resistive coefficients α decrease as temperature increases, the transport coefficients of viscosity η and thermal conductivity κ increase. The magnitude of the coefficient β for Nernst effect and Ettingshausen effect do not change with temperature; however, the magnetization $\omega_c\tau_{ei}$ changes the profiles of β around $r = 0$.

In a resolved collisional regime where Braginskii equations are applicable, Braginskii viscosity tensor $\overset{\leftrightarrow}{\Pi} \propto \nabla\vec{u}$ and conductive thermal heat flux $\vec{h} \propto \nabla T$ are found to suppress the $m = 0$ sausage instability (see Fig. 4.10). To increase Knudsen number, the initial conditions are modified as shown in Table. 4.2. At large-k modes, the growth rates with $T_0 = 10[eV]$ start to be overdamped from PIC results. Hence, some corrections for the coefficients of viscosity and thermal conductivity are required as Knudsen number further increases. Considering the results obtained by using $T_0 = 30[eV]$ and $T_0 = 100[eV]$ with the correction factors proposed by Meier and Shumlak[54], the effects of diffusivity in the collisional transition regime is weakened. However, there still exists stronger diffusion at large-k modes since the correction factors related with the collisionality work effectively if the Knudsen number is greater than unity, Kn > 1. The contour maps of ion mass density with Braginskii viscosity and thermal conductivity are shown in Fig. 4.11.

$$f^{\tau}_{corr} = \frac{1}{1+\frac{\tau_{ii}}{\tau_{dyn}}} = \frac{1}{1+\mathrm{Kn}} \tag{4.39}$$

Table 4.2: Initial conditions with different temperatures lead various different regimes

	$n_0[m^{-3}]$	$T_0[eV]$	$I_p[kA]$	$r_p[mm]$	$log_{10}\,(\mathrm{Kn})$
FuZE (collisionless)	4.25×10^{24}	1270	150	0.910	0.888
collisional case1	4.25×10^{24}	1	4.21	0.910	-4.57
collisional case2	4.25×10^{24}	10	13.3	0.910	-3.01
collisional case3	4.25×10^{24}	20	18.8	0.910	-2.49
collisional case4	4.25×10^{24}	30	23.1	0.910	-2.17
transition case1	4.25×10^{24}	50	29.8	0.910	-1.77
transition case2	4.25×10^{24}	100	42.1	0.910	-1.21

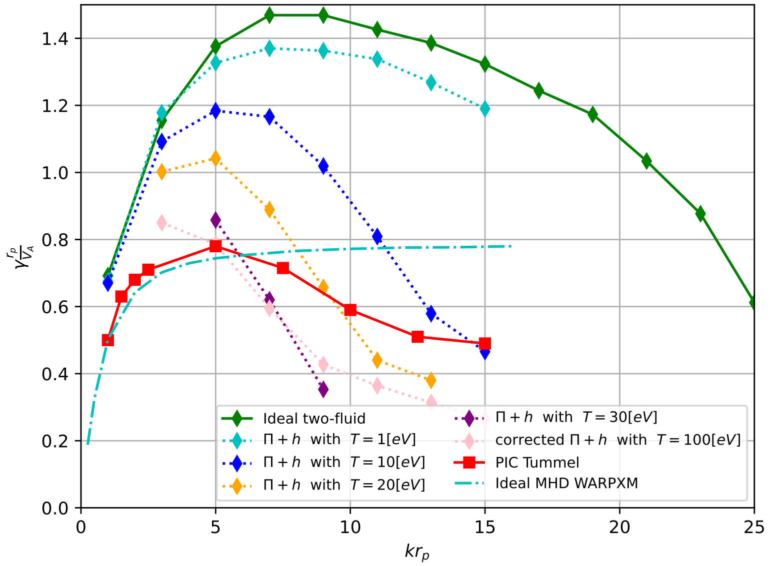

Figure 4.10: Numerical results of the growth rates γ for the sausage instabilities in 2D axisymmetric Z pinch with various different axial wavevector k for the axial perturbations obtained by using $5N$-moment two-fluid model with various different temperature compared with the published results from a PIC kinetic model and ideal MHD results obtained by using WARPXM. The diamond markers with dotted lines indicate the Braginskii results including viscosity and thermal conductivity. As temperature increases, the stronger viscosity and thermal conductivity mitigate the sausage instabilities and decrease the growth rates.

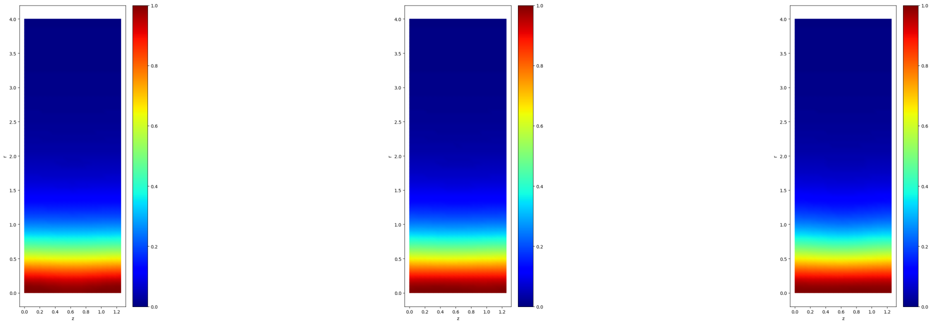

(a) $t = 0$ (b) $t = 0.75\frac{r_p}{V_A}$ (c) $t = 1.5\frac{r_p}{V_A}$

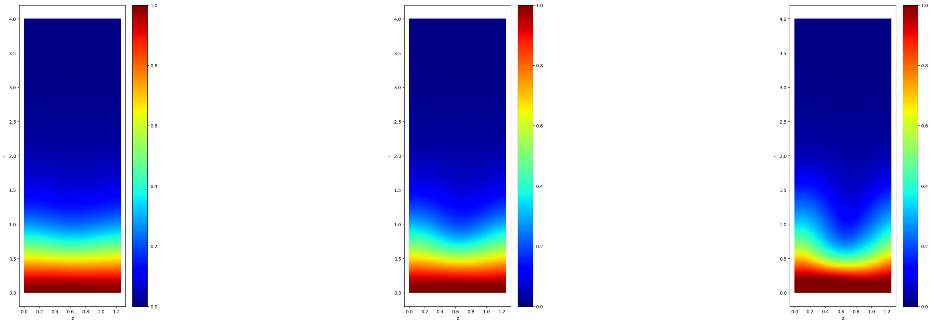

(d) $t = 2.25\frac{r_p}{V_A}$ (e) $t = 3.0\frac{r_p}{V_A}$ (f) $t = 3.75\frac{r_p}{V_A}$

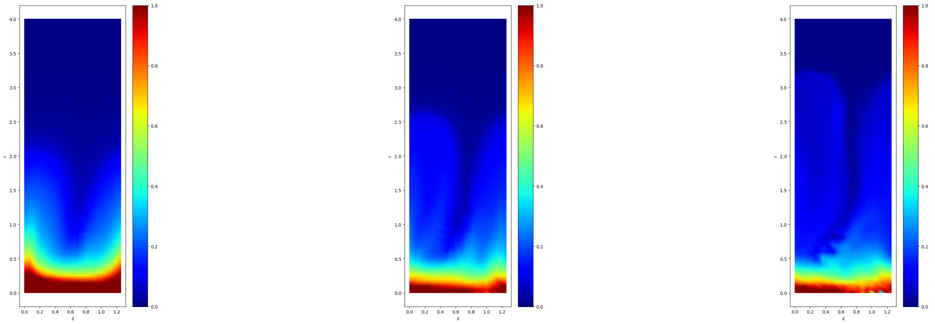

(g) $t = 4.50\frac{r_p}{V_A}$ (h) $t = 5.25\frac{r_p}{V_A}$ (i) $t = 6.0\frac{r_p}{V_A}$

Figure 4.11: Contour maps of ion mass density ρ_i of Z pinch with $kr_p = 5$ and $T_0 = 10$ eV including viscosity and thermal conductivity. The dissipation due to the viscosity and thermal conductivity cannot fully stabilize the sausage instabilities; however those diffusion help to sustain the core of Z pinch and mitigate the plasma losses. (Simulations of 2D Z pinch with viscosity and thermal conductivity are performed with WARPXM version 1.5.9 using input file zpinch_5moment_2D.py)

4.4 Axisymmetric Z pinch with Braginskii Resistivity and Heat Generation

Braginskii resistivity for each species in the axisymmetric Z pinch are

$$\vec{R}_u^{ei} = -\alpha_\perp \left(\vec{u}_e - \vec{u}_i\right)_\perp + \alpha_\wedge \left[\hat{b} \times \left(\vec{u}_e - \vec{u}_i\right)\right] \tag{4.40}$$

$$\vec{R}_u^{ie} = -\vec{R}_u^{ei} \tag{4.41}$$

where the transport coefficients for resistivity for a singly ionized plasma $Z_i = 1$ are

$$\alpha_\perp = \frac{m_e n_e}{\tau_{ei}} \left(1 - \frac{6.416 x_e^2 + 1.836}{\Delta_{\kappa e}}\right) \tag{4.42}$$

$$\alpha_\wedge = \frac{m_e n_e}{\tau_{ei}} x_e \frac{1.704 x_e^2 + 0.7796}{\Delta_{\kappa e}} \tag{4.43}$$

The heat generation terms $Q_{\alpha\beta}$ for each species are

$$Q_{ie} = 3 n_e \frac{m_e}{m_i} \nu_{ei} \left(T_e - T_i\right) \tag{4.44}$$

$$Q_{ei} = -\vec{R}_{ei} \cdot \left(\vec{u}_e - \vec{u}_i\right) - Q_{ie} \tag{4.45}$$

Since the both resistivity and heat generation terms decrease as plasma becomes collisionless, the growth rates increase as temperature increases (see Fig. 4.12). In a collisional regime, it is difficult to evaluate linear growth rates since resistivity rapidly dissipates the Z-pinch equilibrium (see Fig. 4.14). It is necessary to initialize with small perturbations or deviations from initial equilibrium conditions to apply a linear stability analysis appropriately. The rapid dissipation of Z-pinch plasmas yields the poor plasma confinement (see Fig. 4.13). In the collisional transition regime, resistivity is low enough to observe linear growth and indicate some stabilizing effects until the Knudsen number reaches Kn ~ 0.06. The contour maps of ion mass density with resistivity and the sausage instability are given in Fig. 4.15.

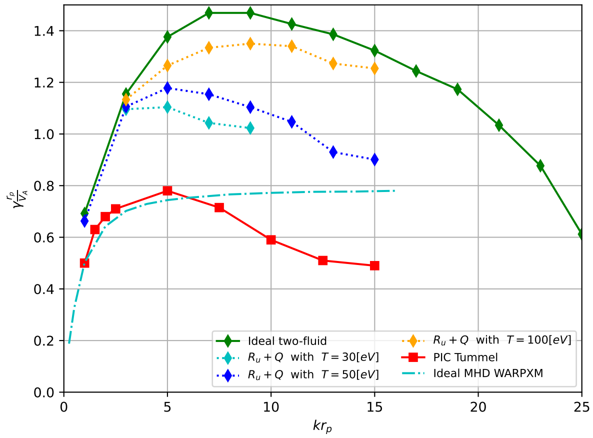

Figure 4.12: Numerical results of the growth rates γ for the sausage instabilities in 2D axisymmetric Z pinch with various different axial wavevector k for the axial perturbations obtained by using $5N$-moment two-fluid model with various different temperature compared with the published results from a PIC kinetic model and ideal MHD results obtained by using WARPXM. The diamond markers with dotted lines indicate the Braginskii results including resistivity and heat generation. As temperature increases, the growth rates increase due to the weaker resistivity.

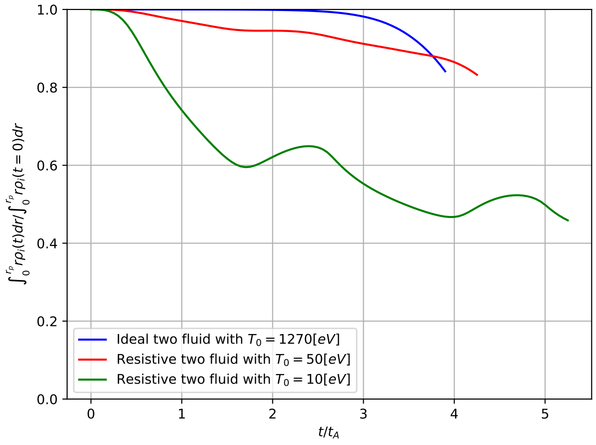

Figure 4.13: Total mass confined in the Z pinch with sausage instabilities by using ideal two-fluid model (blue line) and resistive two-fluid model with different temperature (red and green lines). The strong resistivity (green) diffuses plasmas significantly and leads more plasma losses compared with the ideal two-fluid case (blue)

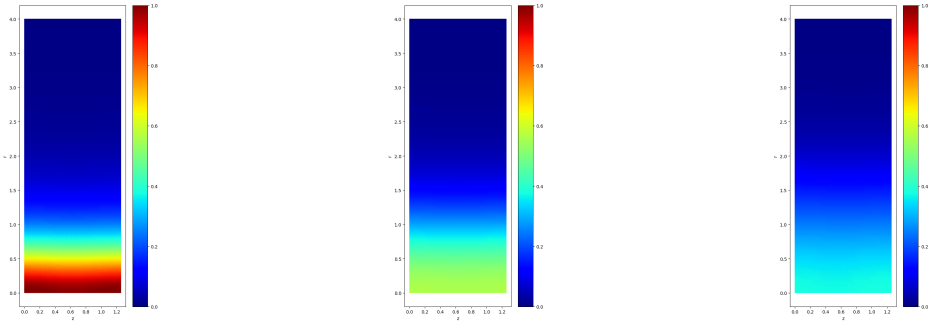

(a) $t = 0$ (b) $t = 0.75\frac{r_p}{V_A}$ (c) $t = 1.5\frac{r_p}{V_A}$

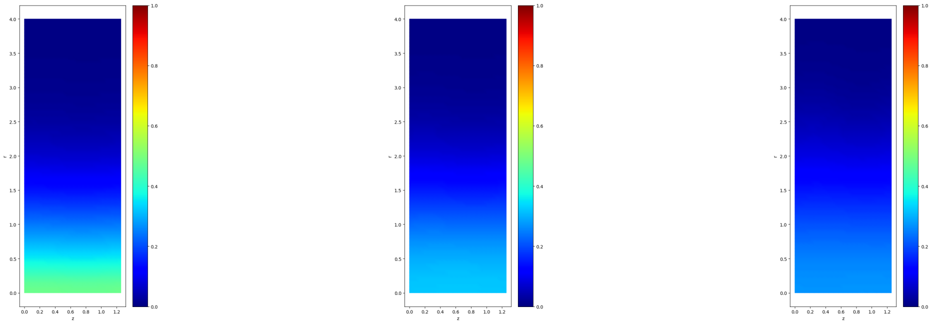

(d) $t = 2.25\frac{r_p}{V_A}$ (e) $t = 3.0\frac{r_p}{V_A}$ (f) $t = 3.75\frac{r_p}{V_A}$

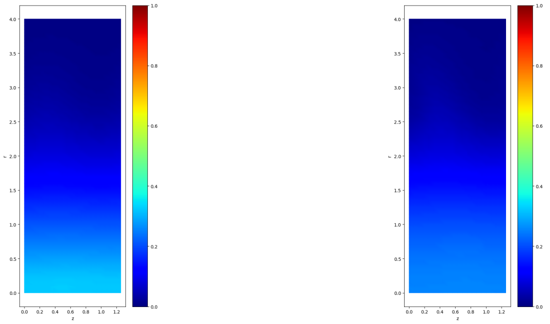

(g) $t = 4.50\frac{r_p}{V_A}$ (h) $t = 5.25\frac{r_p}{V_A}$

Figure 4.14: Contour maps of ion mass density ρ_i in Z pinch with $kr_p = 5$ and $T_0 = 10$ eV including resistivity and heat generation. The stronger resistivity in a collisional regime diffuses plasmas significantly and it is difficult to observe the sausage instability. (Simulations of 2D Z pinch with resistivity and heat generation are performed with WARPXM version 1.5.9 using input file zpinch_5moment_2D.py)

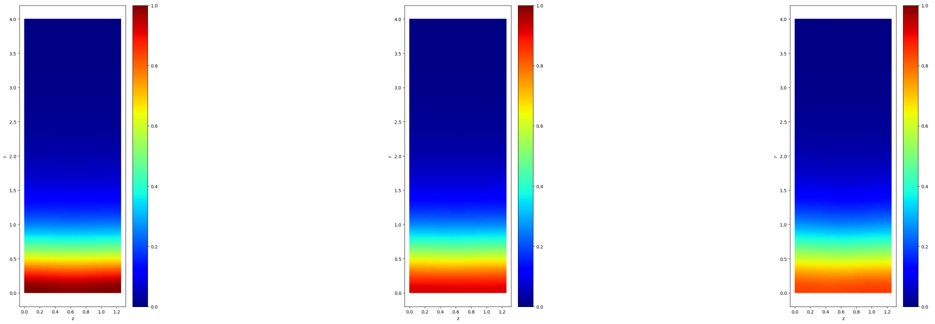

(a) $t = 0$ (b) $t = 0.75\frac{r_p}{V_A}$ (c) $t = 1.5\frac{r_p}{V_A}$

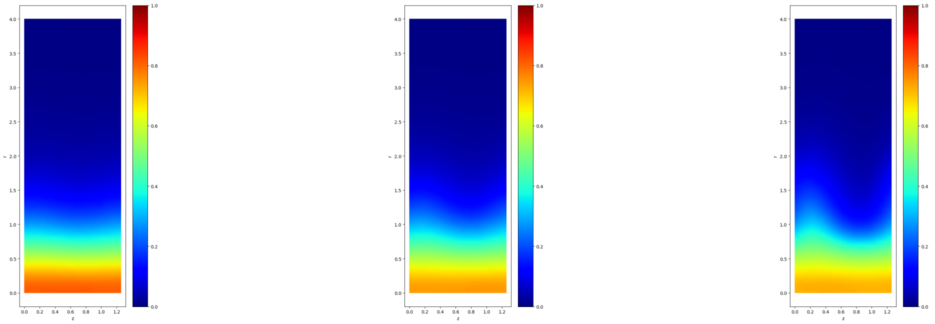

(d) $t = 2.25\frac{r_p}{V_A}$ (e) $t = 3.0\frac{r_p}{V_A}$ (f) $t = 3.75\frac{r_p}{V_A}$

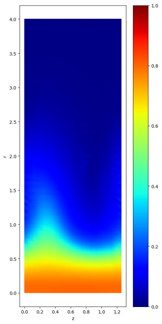

(g) $t = 4.25\frac{r_p}{V_A}$

Figure 4.15: Contour map of ion mass density ρ_i with $kr_p = 5$ and $T_0 = 50$ eV including resistivity and heat generation. In the beginning of the collisional transition regime, the resistivity still has some diffusive and stabilizing effects for the sausage instability. (Simulations of 2D Z pinch with resistivity and heat generation are performed with WARPXM version 1.5.9 using input file zpinch_5moment_2D.py)

4.5 Axisymmetric Z pinch with Full Braginskii Non-ideal Terms

The Braginskii equations include electron heat flux $\vec{h}_u^e$ and thermal force $\vec{R}_T$, which are known as Ettingshausen effect and Nernst effect, respectively

$$\vec{h}_u^e = \beta_\perp^{Tu}\left(\vec{u}_e - \vec{u}_i\right)_\perp + \beta_\wedge^{Tu}\left[\hat{b}\times\left(\vec{u}_e - \vec{u}_i\right)\right] \tag{4.46}$$

$$\vec{R}_T = -\beta_\perp^{uT}\nabla_\perp T_e - \beta_\wedge^{uT}\left(\hat{b}\times\nabla T_e\right) \tag{4.47}$$

The transport coefficients for the electron heat flux and thermal force for a singly ionized plasma $Z_i = 1$ are

$$\beta_\perp^{Tu} = T_e\beta_\perp^{uT} \tag{4.48}$$

$$\beta_\wedge^{Tu} = T_e\beta_\wedge^{uT} \tag{4.49}$$

$$\beta_\perp^{uT} = n_e\frac{5.101x_e^2 + 2.681}{\Delta_{\kappa e}} \tag{4.50}$$

$$\beta_\wedge^{uT} = n_e x_e\frac{\frac{3}{2}x_e^2 + 3.053}{\Delta_{\kappa e}} \tag{4.51}$$

The Nernst effect can drive a current flow if there is a temperature gradient. Conversely, the Ettingshausen effect can yield a temperature gradient if there is a current flow. These two effects are known as the Onsager reciprocal relations[55, 56]. In the Bennett profile with a uniform temperature, the Ettingshausen effect starts to provide the advection of the energy flux that yields negative gradients of temperature in axial and radial directions. Combining with the Nernst effects, the produced negative gradients of temperature drives a radial motion of the plasma and decreases the axial current that eventually yields further destabilizing effects of the sausage instability. Since the Ettingshausen effect does not lead to diffusion behavior unlike resistivity, viscosity, and thermal conductivity, the Ettingshausen effect is ignored in the following discussion to avoid including a large deviations from the Bennett equilibrium condition.

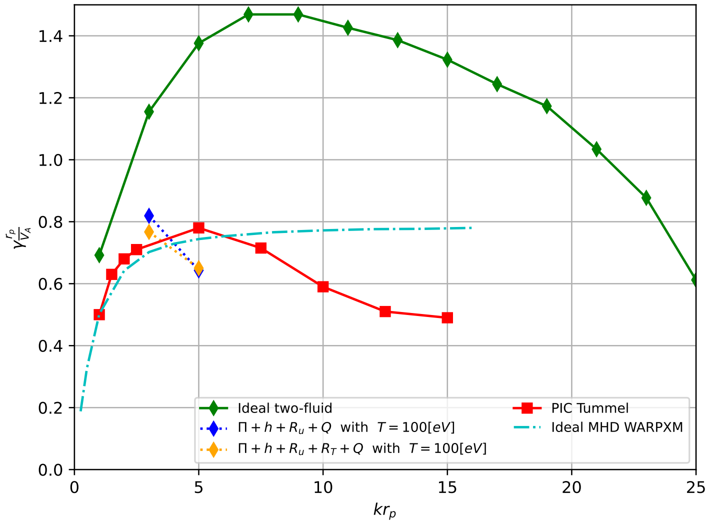

Figure 4.16: Numerical results of the growth rates γ for the sausage instabilities in 2D axisymmetric Z pinch with various axial wavevector k for the axial perturbations obtained by using $5N$-moment two-fluid model compared with the published results from a PIC kinetic model and ideal MHD results obtained by using WARPXM. The coefficients for viscosity and thermal conductivity are corrected. The results using full Braginskii transport yield the comparable growth rates to those obtained by using the kinetic model at $kr_p = 3$. However, the diffusive effects become significantly larger in larger wavenumbers due to the weaker corrections in a collisional transition regime.

As shown in Sec. 4.4, the strong resistivity dissipates the Z-pinch equilibrium rapidly; therefore, it is necessary to implement simulations within the collisional transition regime to observe the full Braginskii effects. However, the corrected viscosity and thermal conductivity still has a larger diffusion effect in the collisional transition regime, particularly at large-k modes. Combining with the resistivity, while the results with $kr_p = 3$ get closer to PIC results, $kr_p \geq 5$ modes are overdamped in Fig. 4.16. The contour maps of ion mass density with full Braginskii transport are shown in Fig. 4.17.

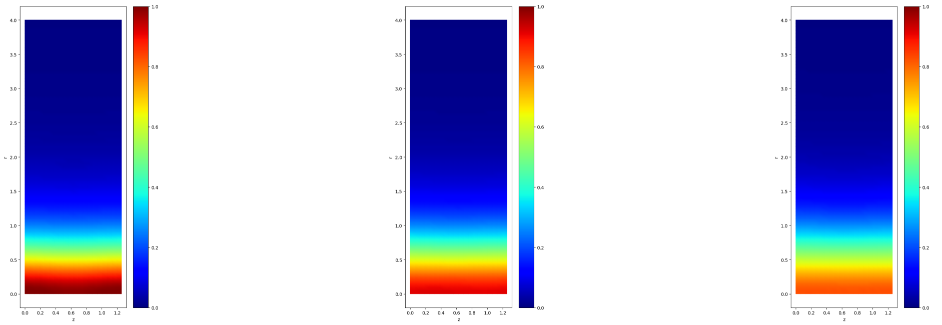

(a) $t = 0$ (b) $t = 0.75\frac{r_p}{V_A}$ (c) $t = 1.5\frac{r_p}{V_A}$

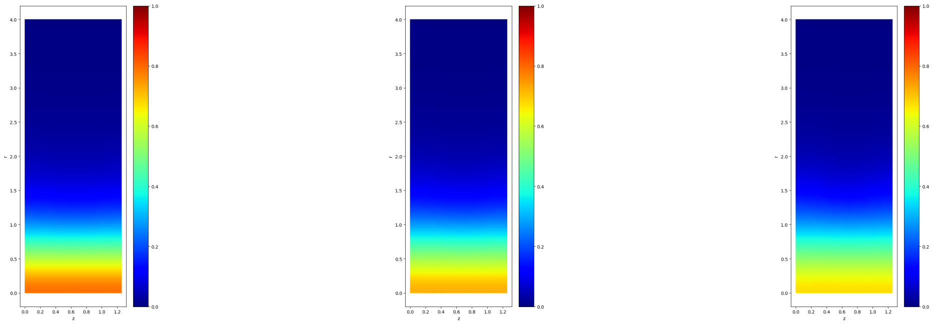

(d) $t = 2.25\frac{r_p}{V_A}$ (e) $t = 3.0\frac{r_p}{V_A}$ (f) $t = 3.75\frac{r_p}{V_A}$

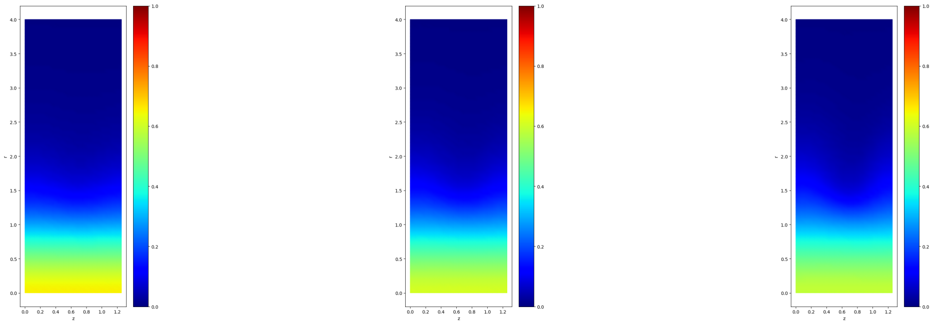

(g) $t = 4.50\frac{r_p}{V_A}$ (h) $t = 5.25\frac{r_p}{V_A}$ (i) $t = 6.00\frac{r_p}{V_A}$

Figure 4.17: Contour maps of ion mass density ρ_i in the Z pinch with $kr_p = 5$ and $T_0 = 100$ eV including full Braginskii non-ideal terms except for Ettingshausen effect. The strong diffusions lead large plasma losses and it is difficult to observe the sausage instability. (Simulations of 2D Z pinch with the full Braginskii transport are performed with WARPXM version 1.5.9 using input file zpinch_5moment_2D.py)

Chapter 5

DEUTERIUM-TRITIUM Z-PINCH FUSION REACTIONS

Fusion reactions and alpha heating in an axisymmetric, D-T-fueled Z pinch are numerically investigated using the $5N$-moment multi-fluid plasma model. The Z pinch is modeled as a four-fluid system (deuterons, tritons, alphas, and electrons) with self-consistent electromagnetic fields. Conservation of charge (0th moment), momentum (1st moment), and energy (2nd moment) are described in terms of 5N-moment fluid variables and fusion reactivity. The fusion reactivity is obtained by using a R-matrix fitting approach described by Bosch and Hale[57]. At sufficiently high plasma currents, fusion alphas can be magnetically confined[58]. The confined alphas collide with the Z-pinch plasma and lead to bulk plasma heating, which is modeled using a Fokker-Planck collision operator for the fast alphas and the Maxwellian Z-pinch plasma while preserving total energy. Several interesting physical phenomena occur as a result of energetic alpha particle production from the fusion reactions.

5.1 Fusion Collision Operator

5.1.1 Boltzmann Collision Operator

The Boltzmann equation is

$$\frac{\partial f_\alpha}{\partial t} + \frac{\vec{p}}{m_\alpha} \cdot \frac{\partial f_\alpha}{\partial \vec{x}} + \frac{\vec{F}}{m_\alpha} \cdot \frac{\partial f_\alpha}{\partial \vec{v}} = \left(\frac{\delta f_\alpha}{\delta t} \right)_{coll} \tag{5.1}$$

where $f_\alpha = f_\alpha(t, \vec{x}, \vec{v})$ is velocity distribution function for a species s, $\vec{p} = m_\alpha \vec{v}$ is momentum, m_α is mass, and $\vec{F}$ is force. The right hand side accounts for the time evolution of the distribution function due to correlations, in particular, collisions with other species of particles or particle generation through fusion or atomic reactions. The Boltzmann collision operator[59] between an incident particle a and a target (or background) particle b is

$$\left(\frac{\delta f_a}{\delta t}\right)_{coll} \equiv C_a^{coll}(f_a, f_b) = \iint v_{rel}\left(f_a(\vec{v}'_a)f_b(\vec{v}'_b) - f_a(\vec{v}_a)f_b(\vec{v}_b)\right)\frac{d\sigma}{d\Omega}d\Omega d\vec{v}_b \tag{5.2}$$

where the primed velocities $\vec{v}'_s$ are post-collision velocities, Ω is a solid angle in a velocity space for scattered particles, $\frac{d\sigma}{d\Omega}$ is a differential scattering cross section, and v_{rel} is a magnitude of relative velocity

$$v_{rel} \equiv |\vec{v}_{rel}| = |\vec{v}_b - \vec{v}_a| \tag{5.3}$$

For a fusion reaction, post-collision scattered velocities do not exist and a fusion cross section σ_{fus} can be empirically obtained such that

$$C_a^{cons}(f_a, f_b) = -\int f_a(\vec{v}_a)f_b(\vec{v}_b)\sigma_{fus}(v_{rel})v_{rel}d\vec{v}_b \tag{5.4}$$

where the negative sign indicates the consumption of species a, which produces a sink.

5.1.2 0th moment

The 0th moment of the consumptive fusion collision operator is

$$\int C_a^{cons}(f_a, f_b)d\vec{v}_a = -\iint f_a(\vec{v}_a)f_b(\vec{v}_b)\sigma_{fus}(v_{rel})v_{rel}d\vec{v}_b d\vec{v}_a \tag{5.5}$$

Suppose that the fuel plasma species a and b have drifting Maxwellian distributions and thermal velocity $v_{ths} \equiv \sqrt{\frac{2T_s}{m_s}}$ is much faster than bulk fluid velocity u_s i.e., $v_{ths} \gg u_s$, the Taylor series of the drifting Maxwellian distribution function of species s with temperature $T_s[eV]$ and number density n_s is

$$\begin{aligned} f_s(\vec{v}_s) &= n_s\left(\frac{m_s}{2\pi T_s}\right)^{\frac{3}{2}} e^{-\frac{m_s|\vec{v}_s - \vec{u}_s|}{2T_s}} \\ &\simeq n_s\left(\frac{m_s}{2\pi T_s}\right)^{\frac{3}{2}} e^{-\frac{m_s v_s^2}{2T_s}}\left[1 + 2\frac{\vec{v}_s \cdot \vec{u}_s}{v_{ths}^2} + \mathcal{O}\left(\left(\frac{u_s}{v_{ths}^2}\right)^2\right)\right] \end{aligned} \tag{5.6}$$

which then leads to

$$\begin{aligned} f_a(\vec{v}_a)f_b(\vec{v}_b) &\simeq \frac{n_a n_b}{(2\pi T)^3}(m_a m_b)^{\frac{3}{2}} e^{-\frac{m_a v_a^2 + m_b v_b^2}{2T}} \left(1 + 2\frac{\vec{v}_a \cdot \vec{u}_a}{v_{tha}^2}\right)\left(1 + 2\frac{\vec{v}_b \cdot \vec{u}_b}{v_{thb}^2}\right) + \mathcal{O}\left(\left(\frac{u_s}{v_{ths}^2}\right)^2\right) \\ &= \frac{n_a n_b}{(2\pi T)^3}(m_a m_b)^{\frac{3}{2}} e^{-\frac{m_a v_a^2 + m_b v_b^2}{2T}} \left[1 + 2\left(\frac{\vec{v}_a \cdot \vec{u}_a}{v_{tha}^2} + \frac{\vec{v}_b \cdot \vec{u}_b}{v_{thb}^2}\right)\right] + \mathcal{O}\left(\left(\frac{u_s}{v_{ths}^2}\right)^2\right) \end{aligned} \tag{5.7}$$

where temperature for incident and target particles are assumed to be approximately same, $T = T_a \simeq T_b$. Since the cross-section area is a function of the relative velocity v_{rel}, it is more convenient to express $\vec{v}_a$ and $\vec{v}_b$ in terms of the center-of-mass velocity $\vec{v}_{cm}$ and the relative velocity $\vec{v}_{rel}$ such that

$$\vec{v}_a = \vec{v}_{cm} - \frac{m_{red}}{m_a}\vec{v}_{rel} \tag{5.8}$$

$$\vec{v}_b = \vec{v}_{cm} + \frac{m_{red}}{m_b}\vec{v}_{rel} \tag{5.9}$$

$$d\vec{v}_a d\vec{v}_b = \det \overset{\leftrightarrow}{J} d\vec{v}_{cm} d\vec{v}_{rel} \tag{5.10}$$

where

$$\vec{v}_{cm} \equiv \frac{m_a \vec{v}_a + m_b \vec{v}_b}{m_a + m_b}, \tag{5.11}$$

$\overset{\leftrightarrow}{J}$ is Jacobian

$$det \overset{\leftrightarrow}{J} = \frac{\partial \vec{v}_a}{\partial \vec{v}_{cm}}\frac{\partial \vec{v}_b}{\partial \vec{v}_{rel}} - \frac{\partial \vec{v}_a}{\partial \vec{v}_{rel}}\frac{\partial \vec{v}_b}{\partial \vec{v}_{cm}} = m_{red}\left(\frac{1}{m_b} + \frac{1}{m_a}\right) = 1, \tag{5.12}$$

and m_{red} is reduced mass

$$m_{red} \equiv \frac{m_a m_b}{m_a + m_b} \tag{5.13}$$

Hence, Eq. (5.5) becomes

$$\begin{aligned} &\int C_a^{cons}(f_a, f_b) d\vec{v}_a \simeq -\frac{n_a n_b}{(2\pi T)^3}(m_a m_b)^{\frac{3}{2}} \\ &\qquad \iint \sigma_{fus}(v_{rel}) v_{rel} e^{-\frac{m_{tot} v_{cm}^2 + m_{red} v_{rel}^2}{2T}} \left[1 + \frac{m_{tot}}{T}\vec{u}_{cm} \cdot \vec{v}_{cm} + \frac{m_{red}}{T}\vec{u}_{rel} \cdot \vec{v}_{rel}\right] d\vec{v}_{cm} d\vec{v}_{rel} \end{aligned} \tag{5.14}$$

where m_{tot} is a total mass

$$m_{tot} \equiv m_a + m_b \tag{5.15}$$

and $\vec{u}_{cm}$ and $\vec{u}_{rel}$ are center-of-mass fluid velocity and relative fluid velocity, respectively

$$\vec{u}_{cm} = \frac{m_a \vec{u}_a + m_b \vec{u}_b}{m_a + m_b} \tag{5.16}$$

$$\vec{u}_{rel} = \vec{u}_b - \vec{u}_a \tag{5.17}$$

Note that

$$\frac{1}{2} m_a v_a^2 + \frac{1}{2} m_b v_b^2 = \frac{1}{2} m_{tot} v_{cm}^2 + \frac{1}{2} m_{red} v_{rel}^2 \tag{5.18}$$

$$\begin{aligned} 2\left(\frac{\vec{v}_a \cdot \vec{u}_a}{v_{tha}^2} + \frac{\vec{v}_b \cdot \vec{u}_b}{v_{thb}^2}\right) &= 2\left(\frac{\vec{u}_a}{v_{tha}^2} + \frac{\vec{u}_b}{v_{thb}^2}\right) \cdot \vec{v}_{cm} - 2\frac{m_{red}}{m_a} \vec{v}_{rel} \cdot \frac{\vec{u}_a}{v_{tha}^2} + 2\frac{m_{red}}{m_b} \vec{v}_{rel} \cdot \frac{\vec{u}_b}{v_{thb}^2} \\ &= \frac{1}{T}(m_a \vec{u}_a + m_b \vec{u}_b) \cdot \vec{v}_{cm} + \frac{m_{red}}{T}(\vec{u}_b - \vec{u}_a) \cdot \vec{v}_{rel} \\ &= \frac{m_{tot}}{T} \vec{u}_{cm} \cdot \vec{v}_{cm} + \frac{m_{red}}{T} \vec{u}_{rel} \cdot \vec{v}_{rel} \end{aligned} \tag{5.19}$$

Considering the second and third terms of the integral in Eq. (5.14),

$$\frac{m_{tot}}{T} \vec{u}_{cm} \cdot \int \vec{v}_{cm} e^{-\frac{m_{tot} v_{cm}^2}{2T}} d\vec{v}_{cm} \int \sigma_{fus}(v_{rel}) v_{rel} e^{-\frac{m_{red} v_{rel}^2}{2T}} d\vec{v}_{rel} = 0 \tag{5.20}$$

$$\frac{m_{red}}{T} \vec{u}_{rel} \cdot \int \vec{v}_{rel} \sigma_{fus}(v_{rel}) v_{rel} e^{-\frac{m_{red} v_{rel}^2}{2T}} d\vec{v}_{rel} \int e^{-\frac{m_{tot} v_{cm}^2}{2T}} d\vec{v}_{cm} = 0 \tag{5.21}$$

because the following integrands are both odd functions

$$\vec{v}_{cm} e^{-\frac{m_{tot} v_{cm}^2}{2T}} : \text{ odd function}$$

$$\vec{v}_{rel} \sigma_{fus}(v_{rel}) v_{rel} e^{-\frac{m_{red} v_{rel}^2}{2T}} : \text{ odd function}$$

Thus, only the first term remains

$$\begin{aligned} \int C_a^{cons}(f_a, f_b) d\vec{v}_a &\simeq -\frac{n_a n_b}{(2\pi T)^3} (m_a m_b)^{\frac{3}{2}} \int_{-\infty}^{\infty} e^{-\frac{m_{tot} v_{cm}^2}{2T}} d\vec{v}_{cm} \int_{-\infty}^{\infty} \sigma_{fus}(v_{rel}) v_{rel} e^{-\frac{m_{red} v_{rel}^2}{2T}} d\vec{v}_{rel} \\ &= -\frac{n_a n_b}{(2\pi T)^3} (m_a m_b)^{\frac{3}{2}} \left(\frac{2\pi T}{m_{tot}}\right)^{\frac{3}{2}} \int_{-\infty}^{\infty} \sigma_{fus}(v_{rel}) v_{rel} e^{-\frac{m_{red} v_{rel}^2}{2T}} d\vec{v}_{rel} \\ &= -n_a n_b \left(\frac{m_{red}}{2\pi T}\right)^{\frac{3}{2}} \int_{-\infty}^{\infty} \sigma_{fus}(v_{rel}) v_{rel} e^{-\frac{m_{red} v_{rel}^2}{2T}} d\vec{v}_{rel} \\ &= -n_a n_b < \sigma_{fus} v_{rel} > \end{aligned} \tag{5.22}$$

where

$$\int_{-\infty}^{\infty} e^{-\frac{m_{tot}v_{cm}^2}{2T}} d\vec{v}_{cm} = \int_{0}^{\infty} 4\pi v_{cm}^2 e^{-\frac{m_{tot}v_{cm}^2}{2T}} dv_{cm} = \left(\frac{2\pi T}{m_{tot}}\right)^{\frac{3}{2}} \tag{5.23}$$

and $< \sigma_{fus} v_{rel} >$ is an average reactivity

$$< \sigma_{fus} v_{rel} > \equiv \left(\frac{m_{red}}{2\pi T}\right)^{\frac{3}{2}} \int_{-\infty}^{\infty} \sigma_{fus}(v_{rel}) v_{rel} e^{-\frac{m_{red}v_{rel}^2}{2T}} d\vec{v}_{rel} \tag{5.24}$$

It is important to note that for reactions between the same species, for example D−D fusion, the factor of half is introduced because collisions between incident and target particles are indistinguishable. Since two nuclei are consumed through a single reaction, Eq. (5.22) can be rewritten as

$$\int C_a^{cons}(f_a, f_b) d\vec{v}_a \simeq -\frac{1+\delta_{ab}}{1+\delta_{ab}} n_a n_b < \sigma_{fus} v_{rel} > = -(1+\delta_{ab})\mathcal{S}_{ab} \tag{5.25}$$

where δ_{ab} is the Kronecker delta and $\mathcal{S}_{ab}$ is a reactive source term in fluid equations

$$\mathcal{S}_{ab} \equiv -\frac{1}{(1+\delta_{ab})} \int C_a^{cons}(f_a, f_b) d\vec{v}_a \simeq \frac{1}{(1+\delta_{ab})} n_a n_b < \sigma_{fus} v_{rel} > \tag{5.26}$$

Note that the reactive source term is proportional to the reaction rate, and the 0th moment of a fusion collision operator represents a rate of a consumption of nuclei.

5.1.3 1st moment

The 1st moment of the consumptive fusion collision operator multiplied by m_a for reactions of dissimilar species is

$$m_a \int \vec{v}_a C_a^{cons}(f_a, f_b) d\vec{v}_a \simeq -\frac{n_a n_b}{(2\pi T)^3}(m_a m_b)^{\frac{3}{2}}$$
$$\iint (m_a \vec{v}_{cm} - m_{red}\vec{v}_{rel}) \sigma_{fus}(v_{rel}) v_{rel} e^{-\frac{m_{tot}v_{cm}^2 + m_{red}v_{rel}^2}{2T}} \left[1 + \frac{m_{tot}}{T}\vec{u}_{cm}\cdot\vec{v}_{cm} + \frac{m_{red}}{T}\vec{u}_{rel}\cdot\vec{v}_{rel}\right] d\vec{v}_{cm} d\vec{v}_{rel} \tag{5.27}$$

Again, since

$$\vec{v}_{cm} e^{-\frac{m_{tot}v_{cm}^2}{2T}} : \text{ odd function}$$

$$\vec{v}_{rel}\sigma_{fus}(v_{rel})v_{rel}e^{-\frac{m_{red}v_{rel}^2}{2T}}: \text{ odd function}$$

only the following two terms remain

$$\begin{aligned}m_a\int\vec{v}_aC_a^{cons}(f_a,f_b)d\vec{v}_a &\simeq -\frac{n_an_b}{(2\pi T)^3}(m_am_b)^{\frac{3}{2}}\\ &\left[m_a\int\frac{m_{tot}}{T}\vec{v}_{cm}(\vec{u}_{cm}\cdot\vec{v}_{cm})e^{-\frac{m_{tot}v_{cm}^2}{2T}}d\vec{v}_{cm}\int\sigma_{fus}(v_{rel})v_{rel}e^{-\frac{m_{red}v_{rel}^2}{2T}}d\vec{v}_{rel}\right.\\ &\left.-m_{red}\int e^{-\frac{m_{tot}v_{cm}^2}{2T}}d\vec{v}_{cm}\int\frac{m_{red}}{T}\vec{v}_{rel}(\vec{u}_{rel}\cdot\vec{v}_{rel})\sigma_{fus}(v_{rel})v_{rel}e^{-\frac{m_{red}v_{rel}^2}{2T}}d\vec{v}_{rel}\right]\end{aligned}\tag{5.28}$$

Using integration by parts with Eq. (5.23)

$$\begin{aligned}&m_a\int\frac{m_{tot}}{T}\vec{v}_{cm}(\vec{u}_{cm}\cdot\vec{v}_{cm})e^{-\frac{m_{tot}v_{cm}^2}{2T}}d\vec{v}_{cm}\int\sigma_{fus}(v_{rel})v_{rel}e^{-\frac{m_{red}v_{rel}^2}{2T}}d\vec{v}_{rel}\\ &=m_a\left(-\int(\vec{u}_{cm}\cdot\vec{v}_{cm})\nabla_{\vec{v}_{cm}}e^{-\frac{m_{tot}v_{cm}^2}{2T}}d\vec{v}_{cm}\right)\left(\frac{2\pi T}{m_{red}}\right)^{\frac{3}{2}}<\sigma_{fus}v_{rel}>\\ &=m_a\left(\frac{2\pi T}{m_{red}}\right)^{\frac{3}{2}}\left\{\vec{u}_{cm}\int e^{-\frac{m_{tot}v_{cm}^2}{2T}}d\vec{v}_{cm}-\int\nabla_{\vec{v}_{cm}}\left[(\vec{u}_{cm}\cdot\vec{v}_{cm})e^{-\frac{m_{tot}v_{cm}^2}{2T}}\right]d\vec{v}_{cm}\right\}<\sigma_{fus}v_{rel}>\\ &=m_a\frac{(2\pi T)^3}{(m_{red}m_{tot})^{\frac{3}{2}}}<\sigma_{fus}v_{rel}>\vec{u}_{cm}\end{aligned}\tag{5.29}$$

where $\nabla_{\vec{v}_{cm}}$ is a vector differential operator with respect to the center of mass velocity

$$-\nabla_{\vec{v}_{cm}}e^{-\frac{m_{tot}v_{cm}^2}{2T}}=\frac{m_{tot}}{T}\vec{v}_{cm}e^{-\frac{m_{tot}v_{cm}^2}{2T}}\tag{5.30}$$

and

$$\int\nabla_{\vec{v}_{cm}}\left[(\vec{u}_{cm}\cdot\vec{v}_{cm})e^{-\frac{m_{tot}v_{cm}^2}{2T}}\right]d\vec{v}_{cm}=0\tag{5.31}$$

Similarly,

$$\begin{aligned}
&-m_{red}\int e^{-\frac{m_{tot}v_{cm}^2}{2T}}d\vec{v}_{cm}\int\frac{m_{red}}{T}\vec{v}_{rel}(\vec{u}_{rel}\cdot\vec{v}_{rel})\sigma_{fus}(v_{rel})v_{rel}e^{-\frac{m_{red}v_{rel}^2}{2T}}d\vec{v}_{rel}\\
&\quad=m_{red}\left(\frac{2\pi T}{m_{tot}}\right)^{\frac{3}{2}}\int(\vec{u}_{rel}\cdot\vec{v}_{rel})\sigma_{fus}(v_{rel})v_{rel}\nabla_{\vec{v}_{rel}}e^{-\frac{m_{red}v_{rel}^2}{2T}}d\vec{v}_{rel}\\
&\quad=-m_{red}\left(\frac{2\pi T}{m_{tot}}\right)^{\frac{3}{2}}\left\{\vec{u}_{rel}\int\sigma_{fus}(v_{rel})v_{rel}e^{-\frac{m_{red}v_{rel}^2}{2T}}d\vec{v}_{rel}\right.\\
&\qquad\qquad+\int(\vec{u}_{rel}\cdot\vec{v}_{rel})\nabla_{\vec{v}_{rel}}(\sigma_{fus}(v_{rel})v_{rel})e^{-\frac{m_{red}v_{rel}^2}{2T}}d\vec{v}_{rel}\\
&\qquad\qquad\left.-\int\nabla_{\vec{v}_{rel}}\left[(\vec{u}_{rel}\cdot\vec{v}_{rel})\sigma_{fus}(v_{rel})v_{rel}e^{-\frac{m_{red}v_{rel}^2}{2T}}\right]d\vec{v}_{rel}\right\}\\
&\quad=-m_{red}\frac{(2\pi T)^3}{(m_{red}m_{tot})^{\frac{3}{2}}}<\sigma_{fus}v_{rel}>\vec{u}_{rel}\\
&\qquad\qquad-m_{red}\left(\frac{2\pi T}{m_{tot}}\right)^{\frac{3}{2}}\int(\vec{u}_{rel}\cdot\vec{v}_{rel})\nabla_{\vec{v}_{rel}}(\sigma_{fus}v_{rel})e^{-\frac{m_{red}v_{rel}^2}{2T}}d\vec{v}_{rel}
\end{aligned} \tag{5.32}$$

where

$$\int\nabla_{\vec{v}_{rel}}\left[(\vec{u}_{rel}\cdot\vec{v}_{rel})\sigma_{fus}(v_{rel})v_{rel}e^{-\frac{m_{red}v_{rel}^2}{2T}}\right]d\vec{v}_{rel}=0 \tag{5.33}$$

Hence,

$$\begin{aligned}
m_a\int\vec{v}_aC_a^{cons}(f_a,f_b)d\vec{v}_a&\simeq-\frac{n_an_b}{(2\pi T)^3}(m_am_b)^{\frac{3}{2}}\left[(m_a\vec{u}_{cm}-m_{red}\vec{u}_{rel})\frac{(2\pi T)^3}{(m_{red}m_{tot})^{\frac{3}{2}}}<\sigma_{fus}v_{rel}>\right.\\
&\qquad\left.-m_{red}\left(\frac{2\pi T}{m_{tot}}\right)^{\frac{3}{2}}\int(\vec{u}_{rel}\cdot\vec{v}_{rel})\nabla_{\vec{v}_{rel}}(\sigma_{fus}v_{rel})e^{-\frac{m_{red}v_{rel}^2}{2T}}d\vec{v}_{rel}\right]\\
&=-m_a\vec{u}_an_an_b<\sigma_{fus}v_{rel}>+m_{red}n_an_b\left(\frac{m_{red}}{2\pi T}\right)^{\frac{3}{2}}\int(\vec{u}_{rel}\cdot\vec{v}_{rel})\nabla_{\vec{v}_{rel}}(\sigma_{fus}v_{rel})e^{-\frac{m_{red}v_{rel}^2}{2T}}d\vec{v}_{rel}
\end{aligned} \tag{5.34}$$

Note

$$m_a\vec{u}_{cm}-m_{red}\vec{u}_{rel}=m_a\frac{m_a\vec{u}_a+m_b\vec{u}_b}{m_{tot}}-\frac{m_am_b}{m_{tot}}(\vec{u}_b-\vec{u}_a)=m_a\vec{u}_a \tag{5.35}$$

Including the effects of the collisions between same species of particles, the general form of the 1st moment of the consumptive fusion collision operator is

$$m_a\int\vec{v}_aC_a^{cons}(f_a,f_b)d\vec{v}_a\simeq-(1+\delta_{ab})m_a\vec{u}_a\mathcal{S}_{ab}-(1+\delta_{ab})\vec{\mathcal{R}}_{ab} \tag{5.36}$$

where $\vec{\mathcal{R}}_{ab}$ is a rate of momentum transfer through fusion reactions

$$\begin{aligned}\vec{\mathcal{R}}_{ab} &\equiv -\frac{1}{1+\delta_{ab}} m_{red} n_a n_b \left(\frac{m_{red}}{2\pi T}\right)^{\frac{3}{2}} \int (\vec{u}_{rel}\cdot\vec{v}_{rel}) \nabla_{\vec{v}_{rel}} (\sigma_{fus} v_{rel}) e^{-\frac{m_{red} v_{rel}^2}{2T}} d\vec{v}_{rel} \\ &= \frac{1}{1+\delta_{ab}} m_{red} n_a n_b \left(\frac{m_{red}}{2\pi T}\right)^{\frac{3}{2}} \int (\vec{w}_{rel}\cdot\vec{v}_{rel}) \nabla_{\vec{v}_{rel}} (\sigma_{fus} v_{rel}) e^{-\frac{m_{red} v_{rel}^2}{2T}} d\vec{v}_{rel}\end{aligned} \tag{5.37}$$

and $\vec{w}_{rel}$ is relative random velocity

$$\vec{w}_{rel} = \vec{w}_b - \vec{w}_a = \vec{v}_{rel} - \vec{u}_{rel} \tag{5.38}$$

$$\vec{w}_s \equiv \vec{v}_s - \vec{u}_s \tag{5.39}$$

Note that $\vec{\mathcal{R}}_{ab}$ vanishes if $\vec{u}_{rel} \simeq 0$ or $\vec{v}_{rel} \simeq \vec{w}_{rel}$. One possible case for $\vec{u}_{rel} \simeq 0$ is that the incident and target particles are the same species, for example D−D fusion. For the interspecies fusion reaction, for example D−T fusion, the approximation of $\vec{v}_{rel} \simeq \vec{w}_{rel}$ is reasonable since the most fusion reactions occur at the tail of distributions. In Meier's plasma-neutral model[60], the same approximation $\vec{v}_{rel} \simeq \vec{w}_{rel}$ is used for an atomic reaction. Note that $\vec{\mathcal{R}}_{ba} = -\vec{\mathcal{R}}_{ab}$ because $\vec{v}_b$ has the opposite sign for $\vec{v}_{rel}$ compared with $\vec{v}_a$ in Eqs. (5.8) and (5.9).

5.1.4 2nd moment

The 2nd moment of the consumptive fusion collision operator with $\frac{1}{2}m_a$ for dissimilar particles is

$$\begin{aligned}\frac{1}{2} m_a \int v_a^2 C_a^{cons}(f_a, f_b) d\vec{v}_a \simeq -\frac{n_a n_b}{(2\pi T)^3} (m_a m_b)^{\frac{3}{2}} \\ \iint \frac{1}{2} m_a \left[v_{cm}^2 - 2\frac{m_{red}}{m_a} \vec{v}_{rel}\cdot\vec{v}_{cm} + \left(\frac{m_{red}}{m_a}\right)^2 v_{rel}^2 \right] \sigma_{fus}(v_{rel}) v_{rel} e^{-\frac{m_{tot} v_{cm}^2 + m_{red} v_{rel}^2}{2T}} \\ \left[1 + \frac{m_{tot}}{T} \vec{u}_{cm}\cdot\vec{v}_{cm} + \frac{m_{red}}{T} \vec{u}_{rel}\cdot\vec{v}_{rel} \right] d\vec{v}_{cm} d\vec{v}_{rel}\end{aligned} \tag{5.40}$$

Since there are four odd functions,

$$\vec{v}_{cm} e^{-\frac{m_{tot} v_{cm}^2}{2T}} : \text{ odd function}$$

$$\vec{v}_{rel}\sigma_{fus}(v_{rel})v_{rel}e^{-\frac{m_{red}v_{rel}^2}{2T}}: \text{ odd function}$$

$$\vec{v}_{cm}v_{cm}^2e^{-\frac{m_{tot}v_{cm}^2}{2T}}: \text{ odd function}$$

$$\vec{v}_{rel}v_{rel}^2\sigma_{fus}(v_{rel})v_{rel}e^{-\frac{m_{red}v_{rel}^2}{2T}}: \text{ odd function}$$

only two terms survive

$$\begin{aligned}\frac{1}{2}m_a\int v_a^2C_a^{cons}(f_a,f_b)d\vec{v}_a \simeq{}& -\frac{n_an_b}{(2\pi T)^3}(m_am_b)^{\frac{3}{2}}\\ &\iint\frac{1}{2}m_a\left[v_{cm}^2+\left(\frac{m_{red}}{m_a}\right)^2v_{rel}^2\right]\sigma_{fus}(v_{rel})v_{rel}e^{-\frac{m_{tot}v_{cm}^2+m_{red}v_{rel}^2}{2T}}d\vec{v}_cd\vec{v}_{rel}\end{aligned} \tag{5.41}$$

The first term is

$$\begin{aligned}\frac{1}{2}m_a\int v_{cm}^2e^{-\frac{m_{tot}v_{cm}^2}{2T}}d\vec{v}_{cm}&\int\sigma_{fus}(v_{rel})v_{rel}e^{-\frac{m_{red}v_{rel}^2}{2T}}d\vec{v}_{rel}\\ &=\frac{1}{2}m_a\frac{3T}{m_{tot}}\left(\frac{2\pi T}{m_{tot}}\right)^{\frac{3}{2}}\left(\frac{2\pi T}{m_{red}}\right)^{\frac{3}{2}}<\sigma_{fus}v_{rel}> \\ &=\frac{3}{2}\frac{m_a}{m_{tot}}T\frac{(2\pi T)^3}{(m_{tot}m_{red})^{\frac{3}{2}}}<\sigma_{fus}v_{rel}>\end{aligned} \tag{5.42}$$

where

$$\int_{-\infty}^{\infty}v_{cm}^2e^{-\frac{m_{tot}v_{cm}^2}{2T}}d\vec{v}_{cm}=\int_0^{\infty}4\pi v_{cm}^4e^{-\frac{m_{tot}v_{cm}^2}{2T}}dv_{cm}=6\sqrt{2}\pi^{\frac{3}{2}}\left(\frac{T}{m_{tot}}\right)^{\frac{5}{2}} \tag{5.43}$$

The second term combined with Eq. (5.23) is

$$\begin{aligned}\frac{1}{2}m_a\left(\frac{m_{red}}{m_a}\right)^2\int e^{-\frac{m_{tot}v_{cm}^2}{2T}}d\vec{v}_{cm}&\int\sigma_{fus}(v_{rel})v_{rel}^3e^{-\frac{m_{red}v_{rel}^2}{2T}}d\vec{v}_{rel}\\ &=\frac{m_{red}}{m_a}\left(\frac{2\pi T}{m_{tot}}\right)^{\frac{3}{2}}\left(\frac{2\pi T}{m_{red}}\right)^{\frac{3}{2}}<\frac{1}{2}m_{red}v_{rel}^2\sigma_{fus}v_{rel}> \\ &=\frac{m_{red}}{m_a}\frac{(2\pi T)^3}{(m_{tot}m_{red})^{\frac{3}{2}}}<\frac{1}{2}m_{red}v_{rel}^2\sigma_{fus}v_{rel}>\end{aligned} \tag{5.44}$$

where $<\frac{1}{2}m_{red}v_{rel}^2\sigma_{fus}v_{rel}>$ is an average kinetic energy transfer rate in the center-of-mass frame

$$<\frac{1}{2}m_{red}v_{rel}^2\sigma_{fus}v_{rel}>\equiv\left(\frac{m_{red}}{2\pi T}\right)^{\frac{3}{2}}\int\frac{1}{2}m_{red}v_{rel}^2\sigma_{fus}(v_{rel})v_{rel}e^{-\frac{m_{red}v_{rel}^2}{2T}}d\vec{v}_{rel} \tag{5.45}$$

Hence,

$$\begin{aligned}
&\frac{1}{2}m_a \int v_a^2 C_a^{cons}(f_a, f_b) d\vec{v}_a \simeq -\frac{n_a n_b}{(2\pi T)^3}(m_a m_b)^{\frac{3}{2}} \\
&\left[\frac{3}{2}\frac{m_a}{m_{tot}} T \frac{(2\pi T)^3}{(m_{tot} m_{red})^{\frac{3}{2}}} < \sigma_{fus} v_{rel} > + \frac{m_{red}}{m_a} \frac{(2\pi T)^3}{(m_{tot} m_{red})^{\frac{3}{2}}} < \frac{1}{2} m_{red} v_{rel}^2 \sigma_{fus} v_{rel} > \right] \\
&= -\frac{3}{2}\frac{m_a}{m_{tot}} T n_a n_b < \sigma_{fus} v_{rel} > - \frac{m_b}{m_{tot}} n_a n_b < \frac{1}{2} m_{red} v_{rel}^2 \sigma_{fus} v_{rel} >
\end{aligned} \tag{5.46}$$

Including the effects of collisions between the same species of particles and accounting for internal degrees of freedom, the general form of the 2nd moment of the consumptive fusion collision operator is

$$\frac{1}{2}m_a \int v_a^2 C_a^{cons}(f_a, f_b) d\vec{v}_a \simeq -(1+\delta_{ab})\frac{1}{\gamma - 1}\frac{m_a}{m_{tot}} T \mathcal{S}_{ab} - (1+\delta_{ab})\frac{m_b}{m_{tot}} \mathcal{Q}_{ab} \tag{5.47}$$

where γ is the specific heat capacity ratio and $\mathcal{Q}_{ab}$ is energy transfer rate

$$\begin{aligned}
\mathcal{Q}_{ab} &\equiv \frac{1}{1+\delta_{ab}} n_a n_b \left(\frac{m_{red}}{2\pi T}\right)^{\frac{3}{2}} \int \frac{1}{2} m_{red} v_{rel}^2 \sigma_{fus}(v_{rel}) v_{rel} e^{-\frac{m_{red} v_{rel}^2}{2T}} d\vec{v}_{rel} \\
&= \frac{1}{1+\delta_{ab}} n_a n_b < \frac{1}{2} m_{red} v_{rel}^2 \sigma_{fus} v_{rel} >
\end{aligned} \tag{5.48}$$

Notice that the center-of-mass kinetic energy $\frac{1}{2}m_{tot}v_{cm}^2$ is consumed in the form of the thermal energy loss, and the relative kinetic energy in the frame moving with the center of mass $\frac{1}{2}m_{red}v_{rel}^2$ is lost by transferring $\mathcal{Q}_{ab}$.

5.2 Conservation Laws with Fusion Reactions

It is known that conservation of the number of particles is obtained by using a Hamiltonian formulation and Liouville's theorem, which is valid for conservative forces, such as the Lorentz force, for a collisionless Boltzmann equation[59, 61, 62]. As in Eq. (5.2), the Boltzmann collision operator includes the effects of reversible collisions in time and space by considering post-collision velocity distribution functions, and thus the conservation of the number of particles is guaranteed. However, since the consumptive fusion collision operator decreases post-collision particles in Eq. (5.4), the conservation of the number of particles is not necessarily satisfied for each species during a fusion reaction and must be explicitly accounted. Similarly, the conservations of momentum and energy in a fluid model can be obtained by taking the 1st and 2nd moment of the collisionless Boltzmann equation. With the typical Boltzmann collision operator, the total momentum and energy in a multi-fluid model can be conserved by transferring the change of momentum and energy into other fluids[1]. Again, however, the momentum and energy transfer cannot be obtained by taking the moments of the consumptive fusion collision operator due to the loss of particles. In this section, the correlations between consumed and produced fluids through fusion reactions is discussed by considering the conservation of total mass, total momentum, and total energy in an adiabatic system.

5.2.1 Conservation of Total Mass (0th moment)

While the number of particles of a given species is not necessarily conserved through a fusion reaction, the total number of protons and neutrons (and thereby the total mass) is conserved

$$\mathscr{A}_a + \mathscr{A}_b = \sum_{s \neq a,b} \mathscr{A}_s p_s^{sn} p_s^{br} \tag{5.49}$$

where $\mathscr{A}_s$ is atomic mass number, p_s^{sn} is stoichiometry coefficient, and $p_{br}(\sigma_{fus})$ is a branching ratio for a fusion reaction, for example, $p_\alpha^{sn} = 3$ and $p_{br} = 1$ for $p - {}^{11}\mathrm{B}$ fusion

$$\mathrm{p} + {}^{11}\mathrm{B} \xrightarrow[p_\alpha^{br} = 1]{} 3 (= p_\alpha^{sn})\, {}^4\mathrm{He} + 8.7 \text{ MeV} \tag{5.50}$$

For D−D fusion, $p_s^{sn} = 1$ and $p_s^{br} = 0.5$ if deuteron energy is high enough to achieve the peak of the fusion crosssection[65],

$$\mathrm{D} + \mathrm{D} \xrightarrow[p_T^{br} = p_p^{br} = 0.5]{} \mathrm{T}(1.01 \text{ MeV}) + \mathrm{p}(3.02 \text{ MeV}) \tag{5.51}$$

$$\mathrm{D} + \mathrm{D} \xrightarrow[p_{{}^3\mathrm{He}}^{br} = p_n^{br} = 0.5]{} {}^3\mathrm{He}(0.82 \text{ MeV}) + n(2.45 \text{ MeV}) \tag{5.52}$$

---

[1] Although the rigorous derivations of the conservation of momentum and energy require applying Noether's theorem in Hamiltonian fluid mechanics[63, 64], those discussions are beyond the scope of this dissertation.

Considering consumption and formation rates of nuclei through a fusion reaction,

$$(\mathcal{A}_a + \mathcal{A}_b)\mathcal{S}_{ab} = \sum_{s \neq a,b} \mathcal{A}_s \int C_s^{form} d\vec{v}_s \tag{5.53}$$

where C_s^{form} is a formative fusion collision operator. Using Eqs. (5.49) and (5.53),

$$\int C_s^{form} d\vec{v}_s = p_s^{sn} p_s^{br} \mathcal{S}_{ab} \tag{5.54}$$

Therefore, the 5N-moment continuity equations for D-T fusion are

$$\frac{\partial n_D}{\partial t} + \nabla \cdot (n_D \vec{u}_D) = -\mathcal{S}_{DT} \tag{5.55}$$

$$\frac{\partial n_T}{\partial t} + \nabla \cdot (n_T \vec{u}_T) = -\mathcal{S}_{DT} \tag{5.56}$$

$$\frac{\partial n_\alpha}{\partial t} + \nabla \cdot (n_\alpha \vec{u}_\alpha) = \mathcal{S}_{DT} \tag{5.57}$$

$$\frac{\partial n_n}{\partial t} + \nabla \cdot (n_n \vec{u}_n) = \mathcal{S}_{DT} \tag{5.58}$$

$$\mathcal{S}_{DT} = n_D n_T < \sigma_{DT} v_{rel} > \tag{5.59}$$

$$p_\alpha^{br} = p_n^{br} = 1 \tag{5.60}$$

$$p_\alpha^{sn} = p_n^{sn} = 1 \tag{5.61}$$

For D-D fusion with a branching ratio of 1/2,

$$\frac{\partial n_D}{\partial t} + \nabla \cdot (n_D \vec{u}_D) = -2\mathcal{S}_{DD} \tag{5.62}$$

$$\frac{\partial n_T}{\partial t} + \nabla \cdot (n_T \vec{u}_T) = \frac{1}{2}\mathcal{S}_{DD} \tag{5.63}$$

$$\frac{\partial n_p}{\partial t} + \nabla \cdot (n_p \vec{u}_p) = \frac{1}{2}\mathcal{S}_{DD} \tag{5.64}$$

$$\frac{\partial n_{^3\mathrm{He}}}{\partial t} + \nabla \cdot (n_{^3\mathrm{He}} \vec{u}_{^3\mathrm{He}}) = \frac{1}{2}\mathcal{S}_{DD} \tag{5.65}$$

$$\frac{\partial n_n}{\partial t} + \nabla \cdot (n_n \vec{u}_n) = \frac{1}{2}\mathcal{S}_{DD} \tag{5.66}$$

$$\mathcal{S}_{DD} = \frac{1}{2} n_D^2 < \sigma_{DD} v_{rel} > \tag{5.67}$$

$$p_T^{br} = p_p^{br} = p_{^3\mathrm{He}}^{br} = p_n^{br} = \frac{1}{2} \tag{5.68}$$

$$p_T^{sn} = p_p^{sn} = p_{^3\mathrm{He}}^{sn} = p_n^{sn} = 1 \tag{5.69}$$

5.2.2 Conservation of Total Momentum (1st moment)

To conserve the total momentum,

$$(m_a\vec{u}_a + m_b\vec{u}_b)\mathcal{S}_{ab} = \sum_{s\neq a,b}\int m_s\vec{v}_s C_s^{form} d\vec{v}_s \tag{5.70}$$

If a-b fusion produces a single species of nucleus c, for example $p - {}^{11}\text{B}$ fusion, the above equation is sufficient to find the 1st moment of a formative fusion collision operator. However, if a-b fusion produces multiple species like D−T fusion or ^{3}He−T fusion, it is necessary to evaluate the 1st moment for each product satisfying Eq. (5.70). Suppose that a-b fusion produces nuclei c and d

$$\text{a} + \text{b} \xrightarrow[p_c^{br}[\%] = p_d^{br}[\%]]{} p_c^{sn}\text{c} + p_d^{sn}\text{d} \tag{5.71}$$

$$\vec{v}_c = \vec{v}'_{cm} - \frac{m'_{red}}{m_c}\vec{v}'_{rel} \tag{5.72}$$

$$\vec{v}_d = \vec{v}'_{cm} + \frac{m'_{red}}{m_d}\vec{v}'_{rel} \tag{5.73}$$

$$\vec{v}'_{cm} \equiv \frac{m_c\vec{v}_c + m_d\vec{v}_d}{m_c + m_d} \tag{5.74}$$

$$\vec{v}'_{rel} \equiv \vec{v}_d - \vec{v}_c \tag{5.75}$$

$$m'_{red} \equiv \frac{m_c m_d}{m_c + m_d} \tag{5.76}$$

$$m'_{tot} \equiv m_c + m_d \tag{5.77}$$

where the prime denotes post-collision properties. Assuming a formative fusion collision operator is expressed in terms of a common integrand C' such that

$$C_c^{form} = p_c^{sn} p_c^{br} \int C' d\vec{v}_d \tag{5.78}$$

$$C_d^{form} = p_d^{sn} p_d^{br} \int C' d\vec{v}_c \tag{5.79}$$

where p_s^{br} is assumed as constant and $d\vec{v}_c d\vec{v}_d \propto d\vec{v}_{cm} d\vec{v}_{rel}$, the right hand side of Eq. (5.70) becomes

$$\sum_{s\neq a,b}\int m_s\vec{v}_s C_s^{form} d\vec{v}_s = \iint (p_c^{sn} p_c^{br} m_c\vec{v}_c + p_d^{sn} p_d^{br} m_d\vec{v}_d) C' d\vec{v}_c d\vec{v}_d \tag{5.80}$$

Considering the momentum and kinetic energy conservation,

$$m_a\vec{v}_a + m_b\vec{v}_b = m_c\vec{v}_c + m_d\vec{v}_d \tag{5.81}$$

$$\frac{1}{2}m_a v_a^2 + \frac{1}{2}m_b v_b^2 = \frac{1}{2}m_c v_c^2 + \frac{1}{2}m_d v_d^2 \tag{5.82}$$

In the classic hard sphere elastic collision with $m_a = m_c$ and $m_b = m_d$, Eqs. (5.81) and (5.82) yield

$$\vec{v}'_{cm} = \vec{v}_{cm} \tag{5.83}$$

$$\vec{v}'_{rel} = -\vec{v}_{rel} \tag{5.84}$$

In fusion reactions, $m_a \neq m_c$ and $m_b \neq m_d$ lead to

$$\vec{v}'_{cm} = \frac{m_{tot}}{m'_{tot}}\vec{v}_{cm} \tag{5.85}$$

$$v'^2_{rel} = \frac{m_{red}}{m'_{red}}v^2_{rel} + \left(1 - \frac{m_{tot}}{m'_{tot}}\right)\frac{m_{tot}}{m'_{red}}v^2_{cm} \tag{5.86}$$

In general, a thermonuclear fusion reaction has a small mass defect $m'_{tot} \simeq m_{tot}$ so that the approximated expressions become

$$\vec{v}'_{cm} \simeq \vec{v}_{cm} \tag{5.87}$$

$$\vec{v}'_{rel} \simeq -\sqrt{\frac{m_{red}}{m'_{red}}}\vec{v}_{rel} \tag{5.88}$$

$$\vec{v}_c \simeq \vec{v}_{cm} + \frac{\sqrt{m_{red}m'_{red}}}{m_c}\vec{v}_{rel} \tag{5.89}$$

$$\vec{v}_d \simeq \vec{v}_{cm} - \frac{\sqrt{m_{red}m'_{red}}}{m_d}\vec{v}_{rel} \tag{5.90}$$

$$d\vec{v}_c d\vec{v}_d \simeq -\sqrt{\frac{m_{red}}{m'_{red}}}d\vec{v}_{cm}d\vec{v}_{rel} \tag{5.91}$$

where the negative sign is selected in Eq. (5.88) as an analogy to the elastic collision in Eq. (5.84). Hence, one possible expression of the integrand C' for a formative fusion collision operator satisfying Eq. (5.54) is

$$C' = -\sqrt{\frac{m'_{red}}{m_{red}}}f_a f_b \sigma_{fus} v_{rel} \tag{5.92}$$

Note that including the mass defect is academic since the value is negligible. The 1st moment of the formative collision operator for c and d are

$$\int m_c\vec{v}_c C_c^{form} d\vec{v}_c \simeq p_c^{sn}p_c^{br} \iint (m_c\vec{v}_{cm} + \sqrt{m_{red}m'_{red}}\vec{v}_{rel}) f_a f_b \sigma_{fus} v_{rel} d\vec{v}_{cm} d\vec{v}_{rel}$$
$$= p_c^{sn}p_c^{br}\left[(m_c\vec{u}_{cm} + \sqrt{m_{red}m'_{red}}\vec{u}_{rel})(1+\delta_{ab})\mathcal{S}_{ab} - (1+\delta_{ab})\sqrt{\frac{m'_{red}}{m_{red}}}\vec{\mathcal{R}}_{ba}\right] \tag{5.93}$$

$$\int m_d\vec{v}_d C_d^{form} d\vec{v}_d \simeq p_d^{sn}p_d^{br} \iint (m_d\vec{v}_{cm} - \sqrt{m_{red}m'_{red}}\vec{v}_{rel}) f_a f_b \sigma_{fus} v_{rel} d\vec{v}_{cm} d\vec{v}_{rel}$$
$$= p_d^{sn}p_d^{br}\left[(m_d\vec{u}_{cm} - \sqrt{m_{red}m'_{red}}\vec{u}_{rel})(1+\delta_{ab})\mathcal{S}_{ab} - (1+\delta_{ab})\sqrt{\frac{m'_{red}}{m_{red}}}\vec{\mathcal{R}}_{ab}\right] \tag{5.94}$$

Notice that the set of the above equations satisfy Eq. (5.70). Therefore, the 5N-moment momentum equations for D−T fusion with the assumptions of the total momentum conservation and negligble mass defect are

$$\frac{\partial(\rho_D\vec{u}_D)}{\partial t} + \nabla\cdot(\rho_D\vec{u}_D\vec{u}_D) + \nabla P_D - n_D q_D(\vec{E} + \vec{u}_D \times \vec{B}) = -m_D\vec{u}_D\mathcal{S}_{DT} - \vec{\mathcal{R}}_{DT} \tag{5.95}$$

$$\frac{\partial(\rho_T\vec{u}_T)}{\partial t} + \nabla\cdot(\rho_T\vec{u}_T\vec{u}_T) + \nabla P_T - n_T q_T(\vec{E} + \vec{u}_T \times \vec{B}) = -m_T\vec{u}_T\mathcal{S}_{DT} + \vec{\mathcal{R}}_{DT} \tag{5.96}$$

$$\frac{\partial(\rho_\alpha\vec{u}_\alpha)}{\partial t} + \nabla\cdot(\rho_\alpha\vec{u}_\alpha\vec{u}_\alpha) + \nabla P_\alpha - n_\alpha q_\alpha(\vec{E} + \vec{u}_\alpha \times \vec{B}) = \left(m_\alpha\vec{u}_{cm} + \sqrt{m_{red}m'_{red}}\vec{u}_{rel}\right)\mathcal{S}_{DT} + \sqrt{\frac{m'_{red}}{m_{red}}}\vec{\mathcal{R}}_{DT} \tag{5.97}$$

$$\frac{\partial(\rho_n\vec{u}_n)}{\partial t} + \nabla\cdot(\rho_n\vec{u}_n\vec{u}_n) + \nabla P_n - n_n q_n(\vec{E} + \vec{u}_n \times \vec{B}) = \left(m_n\vec{u}_{cm} - \sqrt{m_{red}m'_{red}}\vec{u}_{rel}\right)\mathcal{S}_{DT} - \sqrt{\frac{m'_{red}}{m_{red}}}\vec{\mathcal{R}}_{DT} \tag{5.98}$$

$$\vec{\mathcal{R}}_{DT} = -m_{red}n_D n_T \left(\frac{m_{red}}{2\pi T}\right)^{\frac{3}{2}} \int (\vec{u}_{rel}\cdot\vec{v}_{rel})\nabla_{\vec{v}_{rel}}(\sigma_{fus}v_{rel}) e^{-\frac{m_{red}v_{rel}^2}{2T}} d\vec{v}_{rel} \tag{5.99}$$

5.2.3 *Conservation of Total Energy (2nd moment)*

The conservation of the total fluid energy is

$$\frac{1}{\gamma-1}T\mathcal{S}_{ab} + \mathcal{Q}_{ab} = \sum_{s\neq a,b}\int \frac{1}{2}m_s v_s^2 C_s^{form} d\vec{v}_s \tag{5.100}$$

Similar to the 1st moment, assuming that a-b fusion produces nuclei c and d with negligble mass defect, the right hand side of the above equation becomes

$$\sum_{s\neq a,b}\int \frac{1}{2}m_s v_s^2 C_s^{form} d\vec{v}_s = \iint \left(p_c^{sn}p_c^{br}\frac{1}{2}m_c v_c^2 + p_d^{sn}p_d^{br}\frac{1}{2}m_d v_d^2\right) C' d\vec{v}_c d\vec{v}_d \tag{5.101}$$

The 2nd moments of the formative collision operator for c and d with constant p_s^{br} are

$$\int \frac{1}{2}m_c v_c^2 C_c^{form} d\vec{v}_c \simeq p_c^{sn}p_c^{br}(1+\delta_{ab})\left[\frac{1}{\gamma-1}\frac{m_c}{m_{tot}}T\mathcal{S}_{ab} + \frac{m'_{red}}{m_c}\mathcal{Q}_{ab}\right] \tag{5.102}$$

$$\int \frac{1}{2}m_d v_d^2 C_d^{form} d\vec{v}_d \simeq p_d^{sn}p_d^{br}(1+\delta_{ab})\left[\frac{1}{\gamma-1}\frac{m_d}{m_{tot}}T\mathcal{S}_{ab} + \frac{m'_{red}}{m_d}\mathcal{Q}_{ab}\right] \tag{5.103}$$

and the summation of these two equations satisfies Eq. (5.100). Therefore, the 5N-moment fluid energy equations for D−T fusion with the assumptions of the total energy conservation and negligble mass defect are

$$\frac{\partial \epsilon_D}{\partial t} + \nabla\cdot[(\epsilon_D + P_D)\vec{u}_D] - n_D q_D \vec{u}_D\cdot\vec{E} = -\frac{1}{\gamma-1}\frac{m_D}{m_{tot}}T\mathcal{S}_{DT} - \frac{m_T}{m_{tot}}\mathcal{Q}_{DT} \tag{5.104}$$

$$\frac{\partial \epsilon_T}{\partial t} + \nabla\cdot[(\epsilon_T + P_T)\vec{u}_T] - n_T q_T \vec{u}_T\cdot\vec{E} = -\frac{1}{\gamma-1}\frac{m_T}{m_{tot}}T\mathcal{S}_{DT} - \frac{m_D}{m_{tot}}\mathcal{Q}_{DT} \tag{5.105}$$

$$\frac{\partial \epsilon_\alpha}{\partial t} + \nabla\cdot[(\epsilon_\alpha + P_\alpha)\vec{u}_\alpha] - n_\alpha q_\alpha \vec{u}_\alpha\cdot\vec{E} = \frac{1}{\gamma-1}\frac{m_\alpha}{m_{tot}}T\mathcal{S}_{DT} + \frac{m_n}{m'_{tot}}\mathcal{Q}_{DT} \tag{5.106}$$

$$\frac{\partial \epsilon_n}{\partial t} + \nabla\cdot[(\epsilon_n + P_n)\vec{u}_n] - n_n q_n \vec{u}_n\cdot\vec{E} = \frac{1}{\gamma-1}\frac{m_n}{m_{tot}}T\mathcal{S}_{DT} + \frac{m_\alpha}{m'_{tot}}\mathcal{Q}_{DT} \tag{5.107}$$

$$\mathcal{Q}_{DT} = n_D n_T < \frac{1}{2}m_{red}v_{rel}^2\sigma_{fus}v_{rel} > \tag{5.108}$$

$$< \frac{1}{2}m_{red}v_{rel}^2\sigma_{fus}v_{rel} > \equiv \left(\frac{m_{red}}{2\pi T}\right)^{\frac{3}{2}}\int \frac{1}{2}m_{red}v_{rel}^2\sigma_{fus}v_{rel}e^{-\frac{m_{red}v_{rel}^2}{2T}}d\vec{v}_{rel} \tag{5.109}$$

Notice that fusion energy is not introduced in this section, but it is considered in the next section, since Boltzmann collision operator does not describe mass defect.

5.2.4 Mass Defect and Nuclear Binding Energy

Through a fusion reaction, nuclei combine and release some nuclear binding energy to achieve a lower energy state. Considering the relation between nuclear binding energy $\mathcal{E}_{sBin}$ and rest mass energy $m_s c^2$ for a particle s,

$$\mathcal{E}_{sBin} = \Delta m_s c^2 = \left[Z_s m_p + \left(\mathcal{A}_s - Z_s\right) m_n\right] c^2 - m_s c^2 \tag{5.110}$$

where c is the speed of light and the relativistic effect is assumed to be negligible. Also Z_s is atomic number satisfying a conservation of charge

$$Z_a + Z_b = \sum_{s \neq a,b} Z_s p_s^{sn} p_s^{br} \tag{5.111}$$

Assuming that the released binding energy is converted into isotropic kinetic energy of reaction product particles,

$$\sum_{s \neq a,b} \mathcal{E}_{sBin} p_s^{sn} p_s^{br} - \left(\mathcal{E}_{aBin} + \mathcal{E}_{bBin}\right) = \sum_{s \neq a,b} p_s^{sn} p_s^{br} \frac{1}{2} m_s v_{sBir}^2 = \sum_{s \neq a,b} p_s^{sn} p_s^{br} \frac{1}{\gamma - 1} T_{sBir} \tag{5.112}$$

Using Eqs. (5.49), (5.110), and (5.111),

$$\begin{aligned}
\sum_{s \neq a,b} \mathcal{E}_{sBin} p_s^{sn} p_s^{br} - \left(\mathcal{E}_{aBin} + \mathcal{E}_{bBin}\right) &= \left[\sum_{s \neq a,b} Z_s p_s^{sn} p_s^{br} - \left(Z_a + Z_b\right)\right] m_p c^2 \\
&+ \left[\sum_{s \neq a,b} \mathcal{A}_s p_s^{sn} p_s^{br} - \left(\mathcal{A}_a + \mathcal{A}_b\right) - \sum_{s \neq a,b} Z_s p_s^{sn} p_s^{br} + \left(Z_a + Z_b\right)\right] m_n c^2 \\
&- \left[\sum_{s \neq a,b} m_s p_s^{sn} p_s^{br} - \left(m_a + m_b\right)\right] c^2 \\
&= \left[\left(m_a + m_b\right) - \sum_{s \neq a,b} m_s p_s^{sn} p_s^{br}\right] c^2
\end{aligned} \tag{5.113}$$

Hence, Eqs. (5.112) and (5.113) yield the conservation of the total rest mass energy through a fusion reaction such that

$$(m_a + m_b) c^2 = \sum_{s \neq a,b} \left(m_s c^2 + \frac{1}{\gamma - 1} T_{sBir}\right) p_s^{sn} p_s^{br} \tag{5.114}$$

Since the fluid energy equations obtained by taking the 2nd moment of Boltzmann equation do not include the effects of the change of rest mass energy, it is necessary to explicitly add it as the additional change of the internal energy. Thus, the energy equations for D−T fusion with the assumptions of the total fluid and rest mass energy conservations and a negligible mass defect become

$$\frac{\partial}{\partial t}\left(\epsilon_D+\rho_D c^2\right)+\nabla\cdot[(\epsilon_D+\rho_D c^2+P_D)\vec{u}_D]-n_D q_D\vec{u}_D\cdot\vec{E}=-\left(\frac{1}{\gamma-1}\frac{m_D}{m_{tot}}T+m_D c^2\right)\mathcal{S}_{DT}-\frac{m_T}{m_{tot}}\mathcal{Q}_{DT} \tag{5.115}$$

$$\frac{\partial}{\partial t}\left(\epsilon_T+\rho_T c^2\right)+\nabla\cdot[(\epsilon_T+\rho_T c^2+P_T)\vec{u}_T]-n_T q_T\vec{u}_T\cdot\vec{E}=-\left(\frac{1}{\gamma-1}\frac{m_T}{m_{tot}}T+m_T c^2\right)\mathcal{S}_{DT}-\frac{m_D}{m_{tot}}\mathcal{Q}_{DT} \tag{5.116}$$

$$\frac{\partial}{\partial t}\left(\epsilon_\alpha+\rho_\alpha c^2\right)+\nabla\cdot[(\epsilon_\alpha+\rho_\alpha c^2+P_\alpha)\vec{u}_\alpha]-n_\alpha q_\alpha\vec{u}_\alpha\cdot\vec{E}=\left[\frac{1}{\gamma-1}\left(\frac{m_\alpha}{m_{tot}}T+T_{\alpha Bir}\right)+m_\alpha c^2\right]\mathcal{S}_{DT}+\frac{m_n}{m'_{tot}}\mathcal{Q}_{DT} \tag{5.117}$$

$$\frac{\partial}{\partial t}\left(\epsilon_n+\rho_n c^2\right)+\nabla\cdot[(\epsilon_n+\rho_n c^2+P_n)\vec{u}_n]=\left[\frac{1}{\gamma-1}\left(\frac{m_n}{m_{tot}}T+T_{nBir}\right)+m_n c^2\right]\mathcal{S}_{DT}+\frac{m_\alpha}{m'_{tot}}\mathcal{Q}_{DT} \tag{5.118}$$

Using continuity equations multiplied by $m_s c^2$, the final form of the 5N-moment energy equations for D−T fusion are

$$\frac{\partial\epsilon_D}{\partial t}+\nabla\cdot[(\epsilon_D+P_D)\vec{u}_D]-n_D q_D\vec{u}_D\cdot\vec{E}=-\left(\frac{1}{\gamma-1}\frac{m_D}{m_{tot}}T\right)\mathcal{S}_{DT}-\frac{m_T}{m_{tot}}\mathcal{Q}_{DT} \tag{5.119}$$

$$\frac{\partial\epsilon_T}{\partial t}+\nabla\cdot[(\epsilon_T+P_T)\vec{u}_T]-n_T q_T\vec{u}_T\cdot\vec{E}=-\left(\frac{1}{\gamma-1}\frac{m_T}{m_{tot}}T\right)\mathcal{S}_{DT}-\frac{m_D}{m_{tot}}\mathcal{Q}_{DT} \tag{5.120}$$

$$\frac{\partial\epsilon_\alpha}{\partial t}+\nabla\cdot[(\epsilon_\alpha+P_\alpha)\vec{u}_\alpha]-n_\alpha q_\alpha\vec{u}_\alpha\cdot\vec{E}=\frac{1}{\gamma-1}\left(\frac{m_\alpha}{m_{tot}}T+T_{\alpha Bir}\right)\mathcal{S}_{DT}+\frac{m_n}{m'_{tot}}\mathcal{Q}_{DT} \tag{5.121}$$

$$\frac{\partial\epsilon_n}{\partial t}+\nabla\cdot[(\epsilon_n+P_n)\vec{u}_n]=\frac{1}{\gamma-1}\left(\frac{m_n}{m_{tot}}T+T_{nBir}\right)\mathcal{S}_{DT}+\frac{m_\alpha}{m'_{tot}}\mathcal{Q}_{DT} \tag{5.122}$$

5.3 Fokker-Planck Collision Operator for Alpha Heating

The alpha heating can be obtained by considering the Fokker-Planck collision operator. Assuming that the background plasma species have non-drifting Maxwellian distributions,

$$\begin{aligned}C_\alpha^{scat}(f_\alpha,f_{M\beta})=&\frac{m_\alpha}{m_\alpha+m_\beta}\frac{\partial}{\partial\vec{v}}\cdot\left(\nu_s^{\alpha\backslash\beta}\vec{v}f_\alpha\right)\\&+\frac{1}{2}\frac{\partial}{\partial\vec{v}}\cdot\left[\frac{1}{2}\nu_\perp^{\alpha\backslash\beta}\left(v^2\overleftrightarrow{I}-\vec{v}\vec{v}\right)\cdot\frac{\partial f_\alpha}{\partial\vec{v}}+\nu_\parallel^{\alpha\backslash\beta}\left(\vec{v}\vec{v}\cdot\frac{\partial f_\alpha}{\partial\vec{v}}\right)\right]\end{aligned} \tag{5.123}$$

where the first term represents the momentum loss (slowing-down effect) and the second and third terms indicate the energy diffusion

$$\frac{<\Delta\vec{v}>^{\alpha\backslash\beta}}{\Delta t} \equiv -\nu_s^{\alpha\backslash\beta}\vec{v} \tag{5.124}$$

$$\frac{<\Delta\vec{v}\Delta\vec{v}>^{\alpha\backslash\beta}}{\Delta t} \equiv \frac{1}{2}\nu_\perp^{\alpha\backslash\beta}(v^2\overset{\leftrightarrow}{I} - \vec{v}\vec{v}) + \nu_\parallel^{\alpha\backslash\beta}\vec{v}\vec{v} \tag{5.125}$$

The parallel and perpendicular directions are evaluated based on the velocity of the incident particle. In spherical velocity space, $\vec{v} = (v, v_\theta, v_\phi) = (v, 0, 0)$ and Fokker-Planck collision operator becomes

$$\begin{aligned} C_\alpha^{scat}(f_\alpha, f_{M\beta}) = {} & \frac{m_\alpha}{m_\alpha + m_\beta}\frac{1}{v^2}\frac{\partial}{\partial v}\left(v^3\nu_s^{\alpha\backslash\beta}f_\alpha\right) \\ & + \frac{1}{2}\left[\frac{1}{2}\nu_\perp^{\alpha\backslash\beta}\frac{\partial}{\partial\vec{v}}\cdot\left(v^2\overset{\leftrightarrow}{I} - \vec{v}\vec{v}\right)\cdot\frac{\partial f_\alpha}{\partial\vec{v}} + \frac{1}{v^2}\frac{\partial}{\partial v}\left(v^4\nu_\parallel^{\alpha\backslash\beta}\frac{\partial f_\alpha}{\partial v}\right)\right] \end{aligned} \tag{5.126}$$

Within the fluid context, a monoenergetic alpha distribution cannot be fully modeled. Thus, similar to the Braginskii approach, an approximate Maxwellian is expanded by associated Laguerre polynomials (or Sonine polynomials) $L_l^{(k)}$ for the alphas

$$f_\alpha = \frac{n_\alpha}{\pi^{\frac{3}{2}}v_{th\alpha}^3}e^{-X}\sum_{l=0}^{\infty}a_l^{(k)}L_l^{(k)}(X) \tag{5.127}$$

where

$$X = \frac{v^2}{v_{th\alpha}^2} \tag{5.128}$$

While it is understood that the alphas are poorly represented by an approximate Maxwellian distribution, it is chosen to evaluate first-order effects of energetic fusion alphas on the bulk plasma. Taking 0th moment and 2nd moment,

$$\begin{aligned} n_\alpha = \int f_\alpha d\vec{v} &= 4\pi\int v^2 f_\alpha dv \\ &= 2\pi\int v f_\alpha 2v dv \\ &= 2\pi\int v_{th\alpha}X^{\frac{1}{2}}f_\alpha v_{th\alpha}^2 dX \\ &= 2\pi v_{th\alpha}^3\int X^{\frac{1}{2}}f_\alpha dX \end{aligned} \tag{5.129}$$

$$\begin{aligned}\epsilon_\alpha = \int \frac{1}{2} m_\alpha v^2 f_\alpha d\vec{v} &= 2\pi m_\alpha \int v^4 f_\alpha dv \\ &= \pi m_\alpha \int v_{th\alpha}^3 X^{\frac{3}{2}} f_\alpha v_{th\alpha}^2 dX \\ &= 2\pi T_\alpha v_{th\alpha}^3 \int X^{\frac{3}{2}} f_\alpha dX\end{aligned} \tag{5.130}$$

Using the orthogonality of Laguerre polynomials,

$$\begin{aligned}\int X^{\frac{1}{2}} f_\alpha dX &= \frac{n_\alpha}{\pi^{\frac{3}{2}} v_{th\alpha}^3} \int X^{\frac{1}{2}} e^{-X} \sum_{l=0}^{\infty} a_l^{\left(\frac{1}{2}\right)} L_l^{\left(\frac{1}{2}\right)} dX \\ &= \frac{n_\alpha}{\pi^{\frac{3}{2}} v_{th\alpha}^3} \int X^{\frac{1}{2}} e^{-X} a_0^{\left(\frac{1}{2}\right)} L_0^{\left(\frac{1}{2}\right)} L_0^{\left(\frac{1}{2}\right)} dX \\ &= \frac{n_\alpha}{\pi^{\frac{3}{2}} v_{th\alpha}^3} \frac{\sqrt{\pi}}{2} a_0^{\left(\frac{1}{2}\right)}\end{aligned} \tag{5.131}$$

$$\begin{aligned}\int X^{\frac{3}{2}} f_\alpha dX &= \frac{n_\alpha}{\pi^{\frac{3}{2}} v_{th\alpha}^3} \int X^{\frac{3}{2}} e^{-X} \sum_{l=0}^{\infty} a_l^{\left(\frac{1}{2}\right)} L_l^{\left(\frac{1}{2}\right)} dX \\ &= \frac{n_\alpha}{\pi^{\frac{3}{2}} v_{th\alpha}^3} \int \left(\frac{3}{2} - L_1^{\left(\frac{1}{2}\right)}\right) X^{\frac{1}{2}} e^{-X} \sum_{l=0}^{\infty} a_l^{\left(\frac{1}{2}\right)} L_l^{\left(\frac{1}{2}\right)} dX \\ &= \frac{n_\alpha}{\pi^{\frac{3}{2}} v_{th\alpha}^3} \frac{3\sqrt{\pi}}{4} \left(a_0^{\left(\frac{1}{2}\right)} - a_1^{\left(\frac{1}{2}\right)}\right)\end{aligned} \tag{5.132}$$

Hence, the Laguerre coefficients become

$$a_0^{\left(\frac{1}{2}\right)} = 1 \tag{5.133}$$

$$a_1^{\left(\frac{1}{2}\right)} = -\frac{2}{3} \frac{u_\alpha^2}{v_{th\alpha}^2} \tag{5.134}$$

Ignoring $l \geq 2$ coefficients, the approximate Maxwellian distribution for alphas can be written as

$$f_\alpha = \frac{n_\alpha}{\pi^{\frac{3}{2}} v_{th\alpha}^3} e^{-\frac{v^2}{v_{th\alpha}^2}} \left(1 - \frac{2}{3} \frac{u_\alpha^2}{v_{th\alpha}^2} L_1^{\left(\frac{1}{2}\right)}\right) \tag{5.135}$$

Since the distribution function of alphas is isotropic in velocity space i.e., $f_\alpha(\vec{v}) = f_\alpha(v)$, the perpendicular diffusion term in Fokker-Planck collision operator becomes negligible

$$\begin{aligned}\left(v^2\overset{\leftrightarrow}{I} - \vec{v}\vec{v}\right)\cdot\frac{\partial f_\alpha}{\partial \vec{v}} &= \left(\vec{v}\times\frac{\partial f_\alpha}{\partial\vec{v}}\right)\times\vec{v}\\ &= \left(\vec{v}\times\frac{\partial f_\alpha(v)}{\partial v}\frac{\partial v}{\partial\vec{v}}\right)\times\vec{v}\\ &= \frac{\partial f_\alpha(v)}{\partial v}(\vec{v}\times\hat{v})\times\vec{v}\\ &= \vec{0}\end{aligned} \tag{5.136}$$

which yields

$$C_\alpha^{scat}(f_\alpha, f_{M\beta}) = \frac{m_\alpha}{m_\alpha+m_\beta}\frac{1}{v^2}\frac{\partial}{\partial v}\left(v^3\nu_s^{\alpha\backslash\beta}f_\alpha\right) + \frac{1}{2}\frac{1}{v^2}\frac{\partial}{\partial v}\left(v^4\nu_\parallel^{\alpha\backslash\beta}\frac{\partial f_\alpha}{\partial v}\right) \tag{5.137}$$

Using the Maxwell integral $\Psi\left(x^{\alpha\backslash\beta}\right)$[66], the collision frequencies for the slowing-down effect and energy diffusion can be written as

$$\nu_s^{\alpha\backslash\beta} = \left(1+\frac{m_\alpha}{m_\beta}\right)\Psi\nu_0^{\alpha\backslash\beta} \tag{5.138}$$

$$\nu_\parallel^{\alpha\backslash\beta} = \frac{\Psi}{x^{\alpha\backslash\beta}}\nu_0^{\alpha\backslash\beta} \tag{5.139}$$

where

$$\Psi\left(x^{\alpha\backslash\beta}\right) \equiv \frac{2}{\sqrt{\pi}}\int_0^{x^{\alpha\backslash\beta}}\sqrt{y}e^{-y}dy \tag{5.140}$$

$$x^{\alpha\backslash\beta} \equiv \frac{v^2}{v_{th\beta}^2} \tag{5.141}$$

$$\nu_0^{\alpha\backslash\beta}(v) \equiv \frac{4\pi n_\beta q_\alpha^2 q_\beta^2}{\left(4\pi\epsilon_0\right)^2 m_\alpha^2 v^3}\ln\Lambda \tag{5.142}$$

Assuming $v_{thi} \ll v \ll v_{the}$ for the fast alphas,

$$\nu_s^{\alpha\backslash e} \simeq \frac{v^3}{v_c^3}\frac{m_\alpha}{m_i}\nu_0^{\alpha\backslash e}(v) = \frac{4}{3\sqrt{\pi}}\frac{m_\alpha}{m_e}\nu_0^{\alpha\backslash e}(v_{the}) \tag{5.143}$$

$$\nu_\parallel^{\alpha\backslash e} \simeq \frac{4}{3\sqrt{\pi}}\frac{v}{v_{the}}\nu_0^{\alpha\backslash e}(v) \tag{5.144}$$

$$\nu_s^{\alpha\backslash i} \simeq \left(1+\frac{m_\alpha}{m_i}\right)\nu_0^{\alpha\backslash i}(v) \tag{5.145}$$

$$\nu_{\parallel}^{\alpha\backslash i} \simeq \frac{v_{thi}^2}{v^2}\nu_0^{\alpha\backslash i}(v) \tag{5.146}$$

where

$$v_c^3 \equiv \frac{3\sqrt{\pi}}{4}\frac{m_e}{m_i}v_{the}^3 \tag{5.147}$$

The assumption of $v \ll v_{the}$ for monoenergetic alphas can be violated if $v_{the} \simeq v_{th\alpha}$ such that

$$T_e = \frac{m_e}{m_\alpha}T_\alpha = 476.6 \text{ eV} \tag{5.148}$$

However, this electron temperature is not realistic for thermonuclear fusion reactions where $T_e \sim T_i \geq 10[keV]$. Thus, it is reasonable to assume $v \ll v_{the}$. On the other hand, the energetic alphas slow down through collisions with the bulk 10 keV plasma. Thus, the assumption of $v \gg v_{thi}$ is not always valid, and the non-approximate equations, Eqs. (5.138) and (5.139), are used for alpha-ion collisions. The Fokker-Planck collision operators for alpha-electron and alpha-ion collisions are

$$\begin{aligned}
C_\alpha^{scat}(f_\alpha, f_{Me}) &\simeq \frac{1}{v^2}\frac{\partial}{\partial v}\left(v^3\nu_s^{\alpha\backslash e}f_\alpha\right) + \frac{1}{2}\frac{1}{v^2}\frac{\partial}{\partial v}\left(v^4\frac{4}{3\sqrt{\pi}}\frac{v}{v_{the}}\nu_0^{\alpha\backslash e}\frac{\partial f_\alpha}{\partial v}\right) \\
&= \nu_s^{\alpha\backslash e}\frac{1}{v^2}\frac{\partial}{\partial v}\left(v^3 f_\alpha\right) + \frac{1}{2}\frac{v_{the}^2}{v^2}\frac{\partial}{\partial v}\left(v^2\frac{4}{3\sqrt{\pi}}\nu_0^{\alpha\backslash e}(v_{the})\frac{\partial f_\alpha}{\partial v}\right) \\
&= \nu_s^{\alpha\backslash e}\left[\frac{1}{v^2}\frac{\partial}{\partial v}\left(v^3 f_\alpha\right) + \frac{1}{2}\frac{m_e}{m_\alpha}\frac{v_{the}^2}{v^2}\frac{\partial}{\partial v}\left(v^2\frac{\partial f_\alpha}{\partial v}\right)\right]
\end{aligned} \tag{5.149}$$

and

$$\begin{aligned}
C_\alpha^{scat}(f_\alpha, f_{Mi}) &\simeq \frac{1}{v^2}\frac{\partial}{\partial v}\left(v^3\frac{m_\alpha}{m_i}\Psi\nu_0^{\alpha\backslash i}f_\alpha\right) + \frac{1}{2}\frac{1}{v^2}\frac{\partial}{\partial v}\left(v^4\frac{v_{thi}^2}{v^2}\Psi\nu_0^{\alpha\backslash i}\frac{\partial f_\alpha}{\partial v}\right) \\
&= \frac{1}{v^2}\frac{\partial}{\partial v}\left(v_{the}^3\frac{m_\alpha}{m_i}\frac{n_i Z_i^2}{n_e}\nu_0^{\alpha\backslash e}(v_{the})\Psi f_\alpha\right) + \frac{1}{2}\frac{v_{thi}^2}{v^2}\frac{\partial}{\partial v}\left(\frac{v_{the}^3}{v}\frac{n_i Z_i^2}{n_e}\nu_0^{\alpha\backslash e}(v_{the})\Psi\frac{\partial f_\alpha}{\partial v}\right) \\
&= \frac{n_i Z_i^2}{n_e}\left[\frac{1}{v^2}\frac{\partial}{\partial v}\left(v_{the}^3\frac{m_\alpha}{m_i}\frac{3\sqrt{\pi}}{4}\frac{m_e}{m_\alpha}\nu_s^{\alpha\backslash e}\Psi f_\alpha\right) + \frac{1}{2}\frac{v_{thi}^2}{v^2}\frac{\partial}{\partial v}\left(\frac{v_{the}^3}{v}\frac{3\sqrt{\pi}}{4}\frac{m_e}{m_\alpha}\nu_s^{\alpha\backslash e}\Psi\frac{\partial f_\alpha}{\partial v}\right)\right] \\
&= \nu_s^{\alpha\backslash e}\frac{n_i Z_i^2}{n_e}v_c^3\left[\frac{1}{v^2}\frac{\partial}{\partial v}\left(\Psi f_\alpha\right) + \frac{1}{2}\frac{m_i}{m_\alpha}\frac{v_{thi}^2}{v^2}\frac{\partial}{\partial v}\left(\frac{1}{v}\Psi\frac{\partial f_\alpha}{\partial v}\right)\right],
\end{aligned} \tag{5.150}$$

respectively. Taking the 2nd moment and using integration by parts

$$\begin{aligned}
Q_{\alpha e} &= \int \frac{1}{2} m_\alpha v^2 C_\alpha^{scat}(f_\alpha, f_{Me}) d\vec{v} \\
&= \nu_s^{\alpha\backslash e} 4\pi \int \frac{1}{2} m_\alpha v^2 \left[\frac{\partial}{\partial v}\left(v^3 f_\alpha\right) + \frac{1}{2}\frac{m_e}{m_\alpha} v_{the}^2 \frac{\partial}{\partial v}\left(v^2 \frac{\partial f_\alpha}{\partial v}\right)\right] dv \\
&= 2\pi m_\alpha \nu_s^{\alpha\backslash e} \left[\int v^2 \frac{\partial}{\partial v}\left(v^3 f_\alpha\right) dv + \frac{1}{2}\frac{m_e}{m_\alpha} v_{the}^2 \int v^2 \frac{\partial}{\partial v}\left(v^2 \frac{\partial f_\alpha}{\partial v}\right) dv\right] \\
&= -2\pi m_\alpha \nu_s^{\alpha\backslash e} \left[\int v^3 f_\alpha 2v dv + \frac{1}{2}\frac{m_e}{m_\alpha} v_{the}^2 \int 2v^3 \frac{\partial f_\alpha}{\partial v} dv\right] \\
&= -2\pi m_\alpha \nu_s^{\alpha\backslash e} \left[\int v_{th\alpha}^5 X^{\frac{3}{2}} f_\alpha dX - \frac{3}{2}\frac{m_e}{m_\alpha} v_{the}^2 \int v f_\alpha 2v dv\right] \\
&= -2\pi m_\alpha v_{th\alpha}^5 \nu_s^{\alpha\backslash e} \left[\int X^{\frac{3}{2}} f_\alpha dX - \frac{3}{2}\frac{m_e}{m_\alpha}\frac{v_{the}^2}{v_{th\alpha}^2} \int X^{\frac{1}{2}} f_\alpha dX\right] \\
&= -m_\alpha v_{th\alpha}^2 \nu_s^{\alpha\backslash e} \left[\frac{\epsilon_\alpha}{T_\alpha} - \frac{3}{2}\frac{T_e}{T_\alpha} n_\alpha \right] \\
&= -3 n_\alpha \nu_s^{\alpha\backslash e} \left[(T_\alpha - T_e) + \frac{2}{3} T_\alpha \frac{u_\alpha^2}{v_{th\alpha}^2} \right]
\end{aligned} \tag{5.151}$$

and

$$\begin{aligned}
Q_{\alpha i} &= \int \frac{1}{2} m_\alpha v^2 C_\alpha^{scat}(f_\alpha, f_{Mi}) d\vec{v} \\
&= \nu_s^{\alpha\backslash e} \frac{n_i Z_i^2}{n_e} v_c^3 4\pi \int \frac{1}{2} m_\alpha v^2 \left[\frac{\partial}{\partial v}\left(\Psi f_\alpha\right) + \frac{1}{2}\frac{m_i}{m_\alpha} v_{thi}^2 \frac{\partial}{\partial v}\left(\frac{1}{v}\Psi \frac{\partial f_\alpha}{\partial v}\right)\right] dv \\
&= -2\pi \frac{n_i Z_i^2}{n_e} m_\alpha v_c^3 \nu_s^{\alpha\backslash e} \left[\int \Psi f_\alpha 2v dv + \frac{m_i}{m_\alpha} v_{thi}^2 \int \Psi \frac{\partial f_\alpha}{\partial v} dv \right] \\
&= -2\pi \frac{n_i Z_i^2}{n_e} m_\alpha v_c^3 \nu_s^{\alpha\backslash e} \left[v_{th\alpha}^2 \int \Psi f_\alpha dX - \frac{m_i}{m_\alpha} v_{thi}^2 \int \Psi' \frac{\partial x^{\alpha\backslash i}}{\partial v} f_\alpha dv \right] \\
&= -2\pi \frac{n_i Z_i^2}{n_e} m_\alpha v_c^3 v_{th\alpha}^2 \nu_s^{\alpha\backslash e} \left[\int \Psi f_\alpha dX - \frac{m_i}{m_\alpha} \int \Psi' f_\alpha dX \right]
\end{aligned} \tag{5.152}$$

The first term becomes

$$\begin{aligned}
\int \Psi f_\alpha dX &= \frac{n_\alpha}{\pi^{\frac{3}{2}} v_{th\alpha}^3} \int \Psi e^{-X} \left(1 - \frac{2}{3}\frac{u_\alpha^2}{v_{th\alpha}^2} L_1^{\left(\frac{1}{2}\right)}\right) dX \\
&= \frac{n_\alpha}{\pi^{\frac{3}{2}} v_{th\alpha}^3} \int \Psi \frac{\partial}{\partial X}\left(-e^{-X}\right) \left(1 - \frac{2}{3}\frac{u_\alpha^2}{v_{th\alpha}^2} L_1^{\left(\frac{1}{2}\right)}\right) dX \\
&= \frac{n_\alpha}{\pi^{\frac{3}{2}} v_{th\alpha}^3} \int e^{-X} \left[\Psi' \frac{v_{th\alpha}^2}{v_{thi}^2} \left(1 - \frac{2}{3}\frac{u_\alpha^2}{v_{th\alpha}^2} L_1^{\left(\frac{1}{2}\right)}\right) + \frac{2}{3}\frac{u_\alpha^2}{v_{th\alpha}^2} L_0^{\left(\frac{3}{2}\right)} \Psi\right] dX \\
&= \frac{n_\alpha}{\pi^{\frac{3}{2}} v_{th\alpha}^3} \frac{T_\alpha}{T_i}\frac{m_i}{m_\alpha} \int e^{-X}\Psi' \left[1 + \frac{2}{3}\frac{u_\alpha^2}{v_{th\alpha}^2} - \frac{2}{3}\frac{u_\alpha^2}{v_{th\alpha}^2} L_1^{\left(\frac{1}{2}\right)}\right] dX
\end{aligned} \tag{5.153}$$

Also

$$\begin{aligned}
\int e^{-X}\Psi' dX &= \frac{2}{\sqrt{\pi}} \int e^{-X} \sqrt{x^{\alpha\backslash i}} e^{-x^{\alpha\backslash i}} dX \\
&= \frac{2}{\sqrt{\pi}} \int e^{-v^2\left(\frac{1}{v_{th\alpha}^2} + \frac{1}{v_{thi}^2}\right)} \frac{v}{v_{thi}} \frac{2v}{v_{th\alpha}^2} dv \\
&= \frac{2}{\sqrt{\pi}} \frac{1}{v_{thi} v_{th\alpha}^2} \frac{v_{th\alpha}^3 v_{thi}^3}{\left(v_{th\alpha}^2 + v_{thi}^2\right)^{\frac{3}{2}}} \int e^{-z^{\alpha\backslash i}} \sqrt{z^{\alpha\backslash i}} dz^{\alpha\backslash i} \\
&= \frac{v_{thi}^2}{v_{th\alpha}^2} \frac{v_{th\alpha}^3}{v_{th\alpha i}^3}
\end{aligned} \tag{5.154}$$

and

$$\begin{aligned}
\int e^{-X}\Psi' L_1^{\left(\frac{1}{2}\right)} dX &= \frac{2}{\sqrt{\pi}} \int e^{-v^2\left(\frac{1}{v_{th\alpha}^2} + \frac{1}{v_{thi}^2}\right)} \frac{v}{v_{thi}} \left(\frac{3}{2} - \frac{v^2}{v_{th\alpha}^2}\right) \frac{2v}{v_{th\alpha}^2} dv \\
&= \frac{2}{\sqrt{\pi}} \frac{1}{v_{thi} v_{th\alpha}^2} \frac{v_{th\alpha}^3 v_{thi}^3}{\left(v_{th\alpha}^2 + v_{thi}^2\right)^{\frac{3}{2}}} \int e^{-z^{\alpha\backslash i}} \sqrt{z^{\alpha\backslash i}} \left(\frac{3}{2} - z^{\alpha\backslash i} \frac{v_{thi}^2}{v_{th\alpha}^2 + v_{thi}^2}\right) dz^{\alpha\backslash i} \\
&= \frac{3}{2} \frac{v_{thi}^2}{v_{th\alpha}^2} \frac{v_{th\alpha}^3}{v_{th\alpha i}^3} \left(1 - \frac{v_{thi}^2}{v_{th\alpha i}^2}\right) \\
&= \frac{3}{2} \frac{v_{thi}^2}{v_{th\alpha i}^2} \frac{v_{th\alpha}^3}{v_{th\alpha i}^3}
\end{aligned} \tag{5.155}$$

where

$$z^{\alpha\backslash i} \equiv v^2 \left(\frac{1}{v_{th\alpha}^2} + \frac{1}{v_{thi}^2}\right) \tag{5.156}$$

$$v_{th\alpha i} \equiv \sqrt{v_{th\alpha}^2 + v_{thi}^2} \tag{5.157}$$

Thus, Eq. (5.152) can be expressed as

$$
\begin{aligned}
Q_{\alpha i} &= -2\pi \frac{n_i Z_i^2}{n_e} m_\alpha v_c^3 v_{th\alpha}^2 \nu_s^{\alpha\backslash e} \frac{n_\alpha}{\pi^{\frac{3}{2}} v_{th\alpha}^3} \frac{m_i}{m_\alpha} \\
&\quad \left[\frac{T_\alpha}{T_i} \int \Psi' e^{-X} \left(1 + \frac{2}{3}\frac{u_\alpha^2}{v_{th\alpha}^2} - \frac{2}{3}\frac{u_\alpha^2}{v_{th\alpha}^2} L_1^{(\frac{1}{2})}\right) dX - \int \Psi' e^{-X} \left(1 - \frac{2}{3}\frac{u_\alpha^2}{v_{th\alpha}^2} L_1^{(\frac{1}{2})}\right) dX\right] \\
&= -3 \frac{m_e}{m_\alpha} \frac{n_i Z_i^2}{n_e} \frac{v_{the}^3}{v_{th\alpha}^3} n_\alpha T_\alpha \nu_s^{\alpha\backslash e} \\
&\quad \left[\left\{\frac{T_\alpha}{T_i}\left(1 + \frac{2}{3}\frac{u_\alpha^2}{v_{th\alpha}^2}\right) - 1\right\} \int \Psi' e^{-X} dX - \frac{2}{3}\frac{u_\alpha^2}{v_{th\alpha}^2}\left(\frac{T_\alpha}{T_i} - 1\right) \int \Psi' e^{-X} L_1^{(\frac{1}{2})} dX\right] \\
&= -3 \frac{m_e}{m_\alpha} \frac{n_i Z_i^2}{n_e} \frac{v_{the}^3}{v_{th\alpha}^3} n_\alpha T_\alpha \nu_s^{\alpha\backslash e} \frac{v_{thi}^2}{v_{th\alpha}^2} \frac{v_{th\alpha}^3}{v_{th\alpha i}^3} \left[\left(\frac{T_\alpha}{T_i} - 1\right)\left(1 - \frac{u_\alpha^2}{v_{th\alpha i}^2}\right) + \frac{2}{3}\frac{T_\alpha}{T_i}\frac{u_\alpha^2}{v_{th\alpha}^2}\right] \\
&= -3 n_\alpha \nu_s^{\alpha\backslash e} \cdot \frac{m_e}{m_i} \frac{n_i Z_i^2}{n_e} \frac{v_{the}^3}{v_{th\alpha i}^3} \left[(T_\alpha - T_i)\left(1 - \frac{u_\alpha^2}{v_{th\alpha i}^2}\right) + \frac{2}{3} T_\alpha \frac{u_\alpha^2}{v_{th\alpha}^2}\right]
\end{aligned}
\tag{5.158}
$$

Similar to Braginskii equations, the slowing-down collision frequency $\nu_s^{\alpha\backslash e}$ is expressed in terms of the typical collision frequency $\nu_{e\alpha}$ such that

$$
Q_{\alpha e} = -3 n_e \frac{m_e}{m_\alpha} \nu_{e\alpha} \left[(T_\alpha - T_e) + \frac{2}{3} T_\alpha \frac{u_\alpha^2}{v_{th\alpha}^2}\right] \tag{5.159}
$$

$$
Q_{\alpha i} = -3 n_e \frac{m_e}{m_\alpha} \nu_{e\alpha} \cdot \frac{m_e}{m_i} \frac{n_i Z_i^2}{n_e} \frac{v_{the}^3}{v_{th\alpha i}^3} \left[(T_\alpha - T_i)\left(1 - \frac{u_\alpha^2}{v_{th\alpha i}^2}\right) + \frac{2}{3} T_\alpha \frac{u_\alpha^2}{v_{th\alpha}^2}\right] \tag{5.160}
$$

where

$$
\nu_s^{\alpha\backslash e} \simeq \frac{4}{3\sqrt{\pi}} \frac{m_\alpha}{m_e} \nu_0^{\alpha\backslash e}(v_{the}) = \frac{n_e}{n_\alpha} \frac{m_e}{m_\alpha} \nu_{e\alpha} \tag{5.161}
$$

and

$$
\nu_{e\alpha} = \frac{4\sqrt{2\pi} n_\alpha Z_\alpha^2 q^4}{3 \left(4\pi\epsilon_0\right)^2 \sqrt{m_e} T_e^{\frac{3}{2}}} \ln \Lambda \tag{5.162}
$$

The previous analysis has assumed a non-drifting Maxwellian distribution for the bulk plasma ions and electrons. However, since the Coulomb collision operator is Galilean invariant (see Appendix E), adding an average flow to the Maxwellian distributions results in

$$
Q_{\alpha e} = -3 n_e \frac{m_e}{m_\alpha} \nu_{e\alpha} \left[(T_\alpha - T_e) + \frac{2}{3} T_\alpha \frac{\left|\vec{u}_\alpha - \vec{u}_e\right|^2}{v_{th\alpha}^2}\right] \tag{5.163}
$$

$$
Q_{\alpha i} = -3 n_e \frac{m_e}{m_\alpha} \nu_{e\alpha} \cdot \frac{m_e}{m_i} \frac{n_i Z_i^2}{n_e} \frac{v_{the}^3}{v_{th\alpha i}^3} \left[(T_\alpha - T_i)\left(1 - \frac{\left|\vec{u}_\alpha - \vec{u}_i\right|^2}{v_{th\alpha i}^2}\right) + \frac{2}{3} T_\alpha \frac{\left|\vec{u}_\alpha - \vec{u}_i\right|^2}{v_{th\alpha}^2}\right] \tag{5.164}
$$

5.4 1D D-T Z-pinch Fusion Simulation

5.4.1 Initial Conditions

Studying the dynamical evolution of a D-T Z-pinch plasma undergoing fusion reactions requires initializing an equilibrium. Initial conditions satisfy the equilibrium Bennett profile for four fluids

$$n_e(r) = \frac{n_0}{\left(1 + \frac{r^2}{r_p^2}\right)^2} \tag{5.165}$$

$$n_D(r) = n_T(r) = \frac{1}{2}\left[\frac{n_0}{\left(1 + \frac{r^2}{r_p^2}\right)^2} - Z_\alpha n_{\alpha 0}\right] \tag{5.166}$$

For numerical reasons, a low amplitude uniform and stationary alpha population with $n_\alpha/n_0 \ll 1$ is initialized, so the ion number densities are slightly modified to maintain the quasineutrality. Typical values for the following numerical simulations are $n_\alpha/n_0 = 10^{-30}$. The azimuthal magnetic fields are the same as the two-fluid case

$$B_\theta = B_0 \frac{2\frac{r}{r_p}}{1 + \frac{r^2}{r_p^2}} \tag{5.167}$$

where the axial electron velocity is uniform

$$u_{ez} = -\frac{1}{2} u_{z0} \tag{5.168}$$

but

$$u_{Dz}(r) = u_{Tz}(r) = \frac{1}{2} u_{z0} \frac{1}{1 - Z_\alpha \frac{n_{\alpha 0}}{n_0}\left(1 + \frac{r^2}{r_p^2}\right)^2} \tag{5.169}$$

Initial temperature is uniform

$$T_i = T_e = T_0 \tag{5.170}$$

The characteristic physical constants compared with the FuZE configurations are summarized in Table 5.1. The 1D numerical results shown in the following sections have the third order accuracy in time and space with 40 elements.

Table 5.1: Initial conditions for D-T fusion configurations

	$n_0[\mathrm{m}^{-3}]$	$T_0[\mathrm{keV}]$	$I_p[\mathrm{kA}]$	$r_p[\mathrm{mm}]$
FuZE	4.25×10^{24}	1.27	150	0.91
D-T fusion	10^{26}	10.0	1350	0.60

5.4.2 Radial Expansion of Alphas and Alpha Driving Effect

The time evolution of primary fluid variables of alphas are given in Fig. 5.1. Due to the continuous fusion reactions with $\mathcal{S}_{DT}$, the alpha number density n_α increases. The expected increment of the density in $\Delta t = \tau_A = 0.617[ns]$ at $r = 0$ is

$$\frac{\Delta n_\alpha}{n_0} = \mathcal{S}_{DT}\frac{\tau_A}{n_0} = 6.17 \times 10^{-36} n_D n_T < \sigma_{fus} v_{rel} >\sim 1.54 \times 10^{-6} \tag{5.171}$$

In an early phase (orange lines at $t = 0.048\tau_A$ in Fig. 5.1), radially expanding alphas leave the calculation domain through the open boundary at $r = 4r_p$ and the expansion wave causes the alpha temperature to drop. It is interesting that the alphas develop an axial velocity due to the Lorentz force $\vec{u}_{\alpha r} \times \vec{B}_\theta$. Then, the interaction between the axial motion of alphas and sufficiently strong azimuthal magnetic fields restricts the radially outward motion of alphas (red lines at $t = 0.288\tau_A$ in Fig. 5.1). This axial motion of alphas carries a portion of the axial current which is called the alpha current in this dissertation.

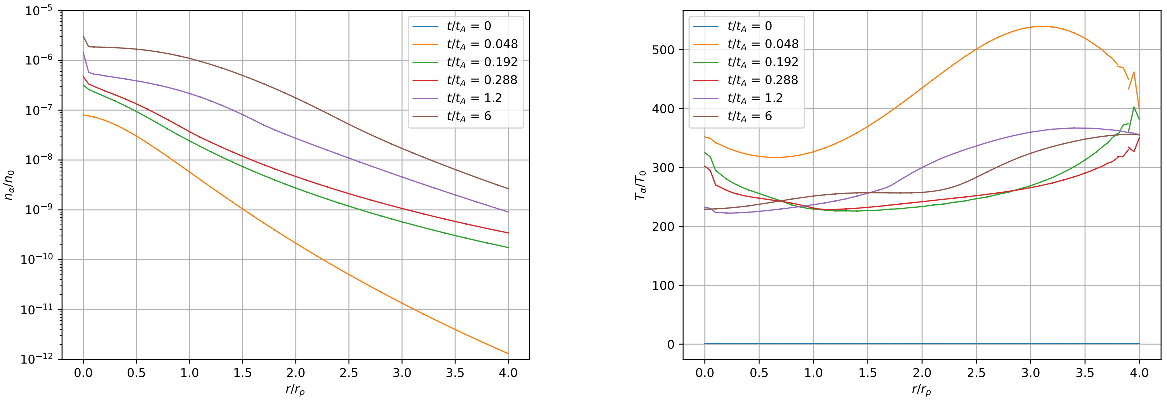

(a) Normalized n_α (b) Normalized T_α

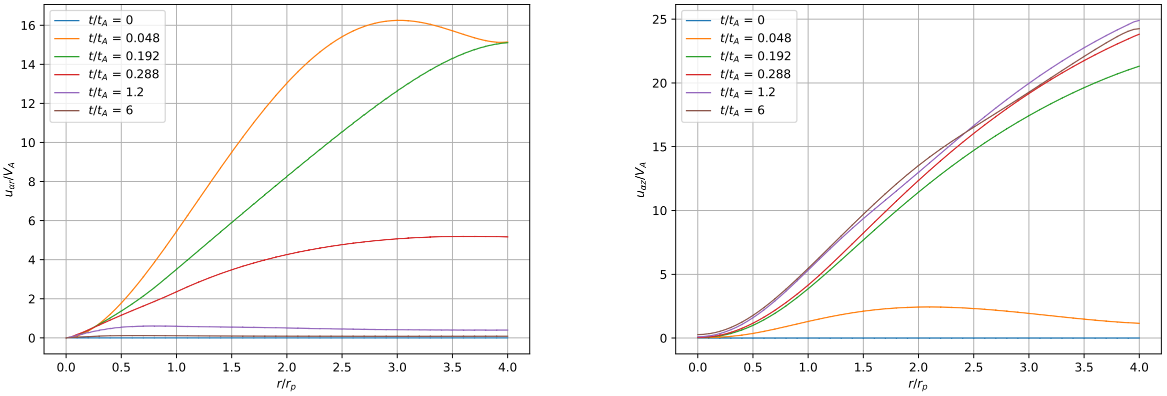

(c) Normalized $u_{\alpha r}$ (d) Normalized $u_{\alpha z}$

Figure 5.1: Time evolution of the radial profile of (a) number density n_α (b) temperature T_α, (c) radial velocity $u_{\alpha r}$, and (d) axial velocity $u_{\alpha z}$ of alphas in 1D axisymmetric D-T four-fluid Z pinch. Fusion reactions produce more alphas and fusion energy leads to radial expansion of alphas that decreases the alpha temperature and increases radial velocity. The radial motion of alphas interacts with the azimuthal magnetic field that produces an axial velocity of alphas (orange lines in (c) and (d)). The axial motion of alphas produces a current and interacts with azimuthal magnetic fields that results in a confining force on the alphas and decreases their radial velocity. (Simulations of 1D D-T Z-pinch fusion in the four-fluid model are performed with WARPXM version 1.5.9 using input file multifluid_zpinch_1D.py)

5.4.3 Alpha Heating and Energy Cascade

Comparing the collision frequencies for slowing down and energy diffusion in Tab. 5.2, the slowing-down effect is found to be the primary effect in the Fokker-Planck collision operator with 10 keV of plasma. Hence, to observe alpha heating, it is necessary to calculate until the slowing-down period

$$\frac{\tau_s^{\alpha\backslash e}}{\tau_A} = \frac{1}{\nu_s^{\alpha\backslash e}\tau_A} \simeq 1023.2 \tag{5.172}$$

where the Alfvén transit time is approximately one nanosecond, $\tau_A = \frac{r_p}{V_A} = 0.617$ ns, and the slowing-down time is approximately one microsecond, $\tau_s^{\alpha\backslash e} = 0.631$ μs. From Eq. (5.144), the energy diffusion time is approximately one millisecond, $\tau_{\|}^{\alpha\backslash e} = 0.221$ ms. Thus, it is important to note that the alpha distribution can reach Maxwellian only if the energetic alphas are confined for approximately one millisecond. However, the assumption of an approximate Maxwellian distribution for alphas is still useful to capture first-order effects of collisional interactions between the energetic fusion alphas and the bulk plasma. The comparison of slowing-down frequency and energy diffusion frequency is summarized in Tab. 5.2.

Table 5.2: Comparison of frequencies for slowing-down and energy diffusion rates for 10 keV plasma

	$\nu_s^{\alpha\backslash\beta}/\nu_0^{\alpha\backslash\beta}$	$\nu_{\|}^{\alpha\backslash\beta}/\nu_0^{\alpha\backslash\beta}$
alpha-electron	57.5	0.164
alpha-deuterium	3.00	5.71×10^{-3}
alpha-tritium	2.33	3.81×10^{-3}

Multi-fluid plasma simulations of high density plasmas are computationally expensive since the electron plasma frequency becomes large and must be resolved by using an artificially heavier electron mass $m_i/m_p = 0.01 \ll 1$. In the early phase of the simulations (at $t = 0.4\tau_A$ in Fig. 5.2), 95.43%, 2.363%, and 2.208% of energy from alphas into electrons, deuterons, and tritons, respectively. As the electron temperature increases beyond the ion temperature, electrons transfer energy to ions but alpha energy transfer to ions remains low. The deuteron-electron and triton-electron energy transfer rates are 2.85 and 1.97 times higher than the alpha-deuteron and alpha-triton energy transfers, respectively. As the alphas slow down and their alpha temperature decreases, the energy transfer rate increases from alphas to ions. Thus, the primary energy cascade flows from energetic alphas to electrons, and then from electrons to deuterons and tritons.

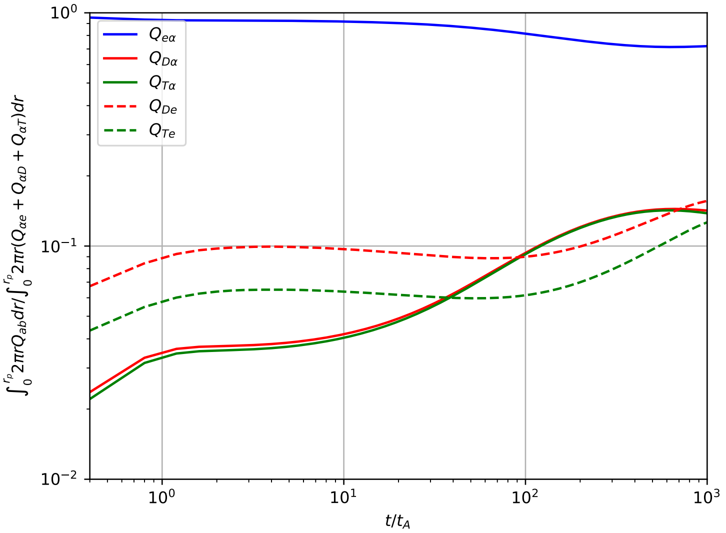

Figure 5.2: Comparison of the fraction of the volume integrated energy transfer rates for each species: solid lines for energy transfer from alphas to electrons and ions: dashed lines for energy transfer from electrons to ions. The primary energy transfer initiates from alphas to electrons (blue solid line). The energy transfer rates from electrons to ions (dashed red and green lines) are higher than those from alphas to ions (solid red and green lines). The results demonstrate the energy cascade from alphas to electrons and from electrons to ions.

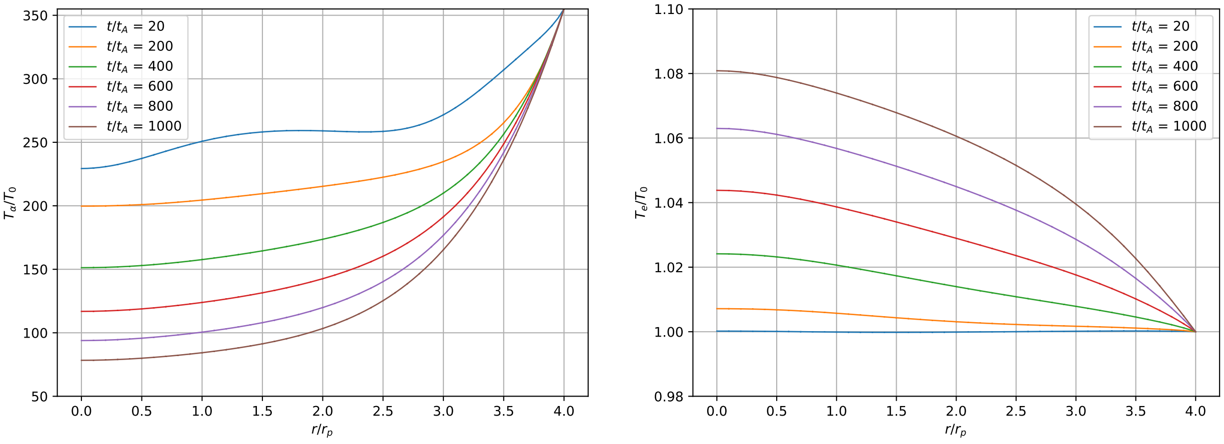

(a) Normalized T_α (b) Normalized T_e

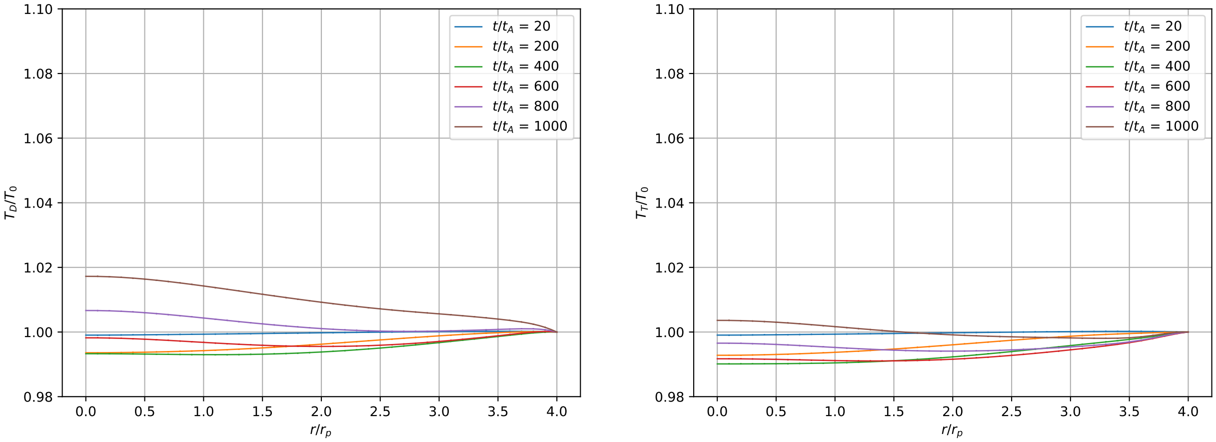

(c) Normalized T_D (d) Normalized T_T

Figure 5.3: Time evolution of the radial profile of (a) alpha T_α, (b) electron T_e, (c) deuterium T_D, and (d) tritium T_T of alphas in 1D axisymmetric D-T four-fluid Z pinch. Most of energetic alphas leave the Z pinch and the small amount of confined alphas start to transfer their energy into electrons so that T_α decreases and T_e increases. As electron temperature increases, the energy transfers from electrons in ions that leads the increment of T_D and T_T. (Simulations of 1D D-T Z-pinch fusion in the four-fluid model are performed with WARPXM version 1.5.9 using input file multifluid_zpinch_1D.py)

5.4.4 Bremsstrahlung Radiation

In classical electromagnetic theory, it is known that the acceleration or deceleration of a charged particle results in the emission of electromagnetic radiation. The radiation produced by electrons through Coulomb scattering with the ions is called bremsstrahlung radiation[31]. According to Goldston and Rutherford[67], the radiative power loss per unit volume can be expressed as

$$p_{rad} = 0.75 \sum_i \frac{2\pi^2 n_i n_e Z_i^2 q^6 T_e^{\frac{1}{2}}}{3^{\frac{1}{2}} (4\pi\epsilon_0)^3 m^{\frac{3}{2}} c^3 \hbar} \tag{5.173}$$

where $\hbar$ is reduced Planck constant $\hbar = \frac{h}{2\pi}$ and lowercase p_{rad} indicates the power per unit volume. Including bremsstrahlung radiation as the loss term in the electron energy equation, the electron temperature slightly decreases, and the amount of energy transfer from electrons to ions become comparable to the energy transfer from energetic alphas to ions (see Fig. 5.4).

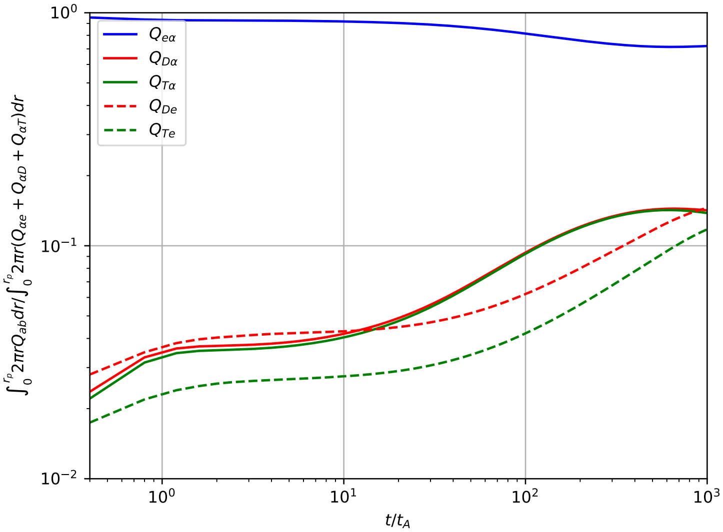

Figure 5.4: Comparison of the fraction of the volume integrated energy transfer rates for each species: solid lines for energy transfer from alphas into electrons and ions: dashed lines for energy transfer from electrons into ions. The radiation energy loss of electrons leads lower energy transfer from electrons to ions (dashed red and green lines)

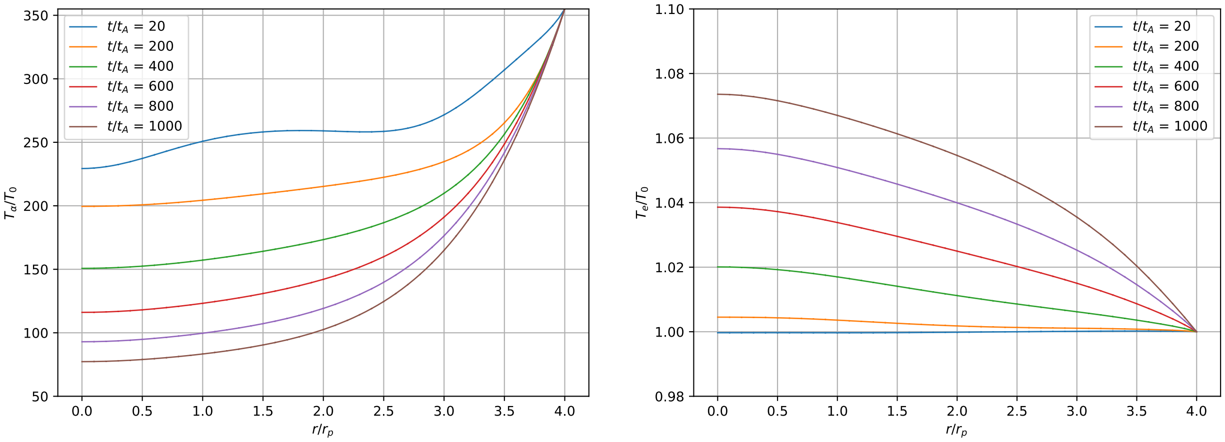

(a) Normalized T_α (b) Normalized T_e

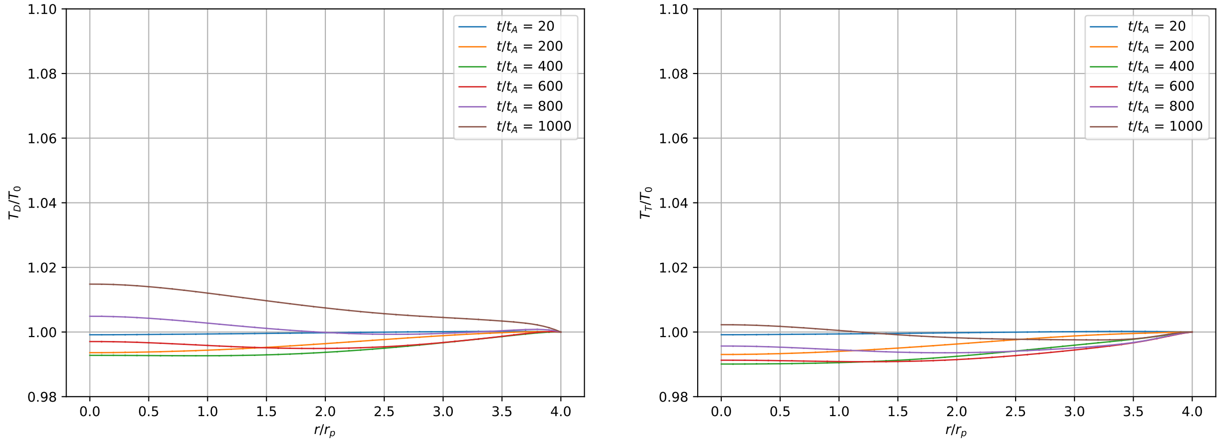

(c) Normalized T_D (d) Normalized T_T

Figure 5.5: Time evolution of the radial profile of (a) alpha T_α, (b) electron T_e, (c) deuterium T_D, and (d) tritium T_T of alphas in 1D axisymmetric D-T four-fluid Z pinch including Bremsstrahlung radiation. Comparing with Fig. (5.3), the Z pinch plasmas (electrons, deuterons and tritons) have slightly lower temperature due to the radiation energy loss of electrons. (Simulations of 1D D-T Z-pinch fusion with bremsstrahlung radiation are performed with WARPXM version 1.5.9 using input file multifluid_zpinch_1D.py)

5.5 Ignition Conditions of D-T Z Pinch Fusion

The scientific feasibility of a fusion reactor can be evaluated in terms of the fusion gain Q_{sci}

$$Q_{sci} \equiv \frac{\text{fusion power}}{\text{external power input}} = \frac{P_F}{P_{in}} \tag{5.174}$$

P_F is the power released from the D-T fusion reaction

$$\begin{aligned} P_F &= P_{Fn} + P_{F\alpha} \\ &= \int \frac{1}{\gamma - 1} \left(T_\alpha^{fus} + T_n^{fus} \right) \mathcal{S}_{DT} dV \\ &= \frac{2\pi L_z}{\gamma - 1} \left(T_\alpha^{fus} + T_n^{fus} \right) \int_0^{r_p} n_D n_T < \sigma_{fus} v_{rel} > r dr \end{aligned} \tag{5.175}$$

where $T_\alpha^{fus} = 3.5$ MeV and $T_n^{fus} = 14.1$ MeV are used for the resulting temperature of alphas and neutrons, through fusion reactions. The volume integral is evaluated with the axisymmetric assumption and 50-cm long Z pinch, $L_z = 50[cm]$. The required input power to sustain sheared-flow-stabilized (SFS) Z pinch is discussed by Shumlak et al.[58],

$$P_{in} = P_{th} + P_{flow} + P_{rad} \tag{5.176}$$

where P_{th} and P_{flow} are thermal power and flow power, respectively, to compensate for losses of thermal energy and kinetic energy. The primary thermal energy losses are a radial thermal conduction to the surrounding wall and axial advection to the electrodes

$$P_{th} = \frac{1}{\tau_E} \frac{2\pi L_z}{\gamma - 1} \int_0^{r_p} \sum_{s \neq \alpha, n} n_s T_s r dr \tag{5.177}$$

where τ_E is a characteristic energy confinement time

$$\frac{1}{\tau_E} = \frac{1}{\tau_E^0} + \frac{1}{\tau_{flow}} \tag{5.178}$$

and τ_E^0 and τ_{flow} are a thermal conduction time and a characteristic advection time. Since the Z pinch makes physical contact with the electrodes and the radial thermal conduction must traverse a long distance through low plasma density and across a strong magnetic field, the thermal energy loss due to the advection becomes more significant $\tau_E^0 \gg \tau_{flow}$ so that

$$\tau_E \simeq \tau_{flow} = \frac{L_z}{u_z} \tag{5.179}$$

The kinetic energy loss is

$$P_{flow} = \frac{1}{\tau_{flow}} 2\pi L_z \int_0^{r_p} \sum_{s \neq \alpha, n} \frac{1}{2} \rho_s u_s^2 r dr \tag{5.180}$$

In Eq. (5.176), the radiative power loss represents the bremsstrahlung radiation. Taking the volume integral of Eq. (5.173),

$$P_{rad} = 2\pi L_z \int_0^{r_p} 0.75 \sum_i \frac{2\pi^2 n_i n_e Z_i^2 q^6 T_e^{\frac{1}{2}}}{3^{\frac{1}{2}} (4\pi\epsilon_0)^3 m^{\frac{3}{2}} c^3 \hbar} r dr \tag{5.181}$$

The alpha heating discussed in Sec. 5.4 can partially offset the power losses and decrease the required input power.

$$Q = \frac{P_F}{P_{th} + P_{flow} + P_{rad} - P_{\alpha h}} \tag{5.182}$$

where $P_{\alpha h}$ is the total energy transfer from energetic alphas to the Z-pinch plasma

$$P_{\alpha h} = 2\pi L_z \int_0^{r_p} \sum_{s \neq \alpha, n} Q_{s\alpha} r dr \tag{5.183}$$

It is important to note that the true ignition condition $Q_{sci} = \infty$ is never achieved since the SFS Z pinch configurations always require an external power source to drive the plasma flow. Thus, the maximum scientific fusion gain is

$$Q_{max} = \frac{P_F}{P_{flow}} \tag{5.184}$$

Using the given initial conditions in Tab. 5.1, the fusion gain Q achieves breakeven $Q = 8.14 > 1$. The primary energy losses are thermal conduction and radiation. Although the alpha heating does not completely compensate for the energy losses, it provides the higher fusion gain $Q \simeq 15$ (see Fig. 5.6). Increasing pinch current from $I_p = 1.35$ MA to $I_p = 2.55$ MA, shown in Tab. 5.3, the fusion gain Q is further amplified to $Q = 151.8$ (see Fig. 5.10).

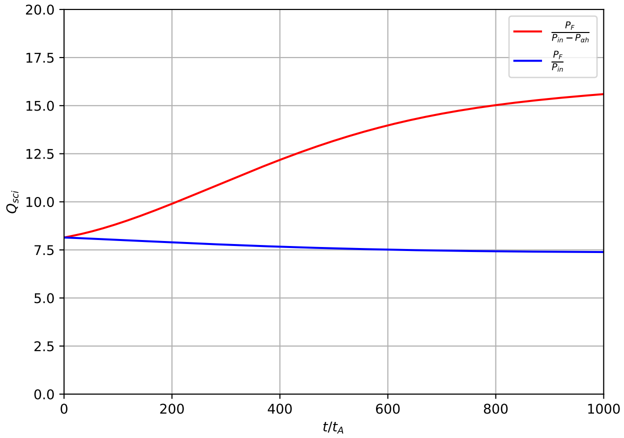

Figure 5.6: Comparison of scientific fusion gain Q_{sci} obtained from D-T Z-pinch fusion reactions with alpha heating. Without including alpha heating (blue line), the fusion gain Q slightly decreases since the expansion of the Z pinch due to the fuel consumptions decreases ion temperature. The alpha heating effect (red line) contributes to increase fusion gain.

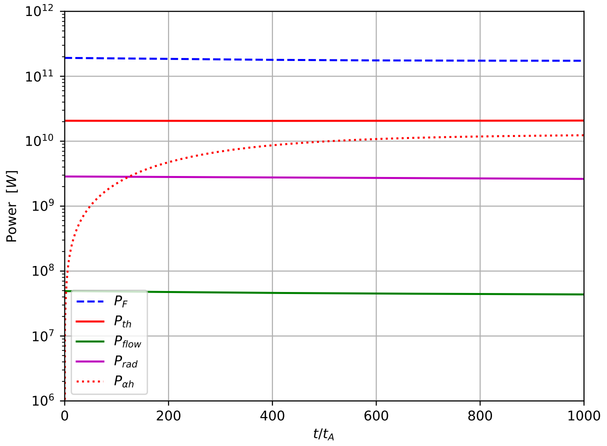

Figure 5.7: Time evolution of the various different volume integrated power that are used to evaluate the scientific fusion gain Q in the Z pinch. The primary energy losses are thermal conduction (red solid line) and radiation (purple solid line) losses. Alpha heating (red dotted line) partially compensates for the energy losses.

The fraction of alpha heating f_c can be evaluated as

$$f_c = \frac{P_{\alpha h}}{P_F} \tag{5.185}$$

that is increased by confining more alphas resulting in the higher probability of collisional interactions. The amount of magnetically confined alphas can be estimated by considering $r_{L\alpha}/r_p$

$$\frac{r_{L\alpha}}{r_p} = \frac{2\pi m_\alpha v_{th\alpha}}{\mu_0 q}\frac{1}{I_p} \tag{5.186}$$

Hence, f_c increases as pinch current I_p increases with the decreasing $r_{L\alpha}/r_p$ shown in Tab. 5.3. Interestingly, f_c tends to saturate around $f_c \simeq 0.07$ in Fig. 5.8. Considering the energy equation for alphas without including the energy transfer from fuel plasmas,

$$\frac{\partial \epsilon_\alpha}{\partial t} + \nabla\cdot\left[\left(\epsilon_\alpha + P_\alpha\right)\vec{u}_\alpha\right] - n_\alpha q_\alpha \vec{u}_\alpha \cdot \vec{E} = \frac{1}{\gamma - 1} T_\alpha^{fus} \mathcal{S}_{DT} + \sum_\beta Q_{\alpha\beta} \tag{5.187}$$

The contribution of kinetic energy can be eliminated by taking dot product of the momentum equation with $\vec{u}_\alpha$ such that

$$\frac{1}{\gamma-1}\frac{dP_\alpha}{dt}=\frac{1}{\gamma-1}T_\alpha^{fus}\mathcal{S}_{DT}+\sum_\beta Q_{\alpha\beta} \tag{5.188}$$

Subtracting the continuity equation multiplied by $T_\alpha/\left(\gamma-1\right)$,

$$\frac{1}{\gamma-1}n_\alpha\frac{dT_\alpha}{dt}=\frac{1}{\gamma-1}\left(T_\alpha^{fus}-T_\alpha\right)\mathcal{S}_{DT}+\sum_\beta Q_{\alpha\beta} \tag{5.189}$$

The above equation suggests that the steady state alpha temperature becomes $T_\alpha=T_\alpha^{fus}$ if there is not energy transfer $\sum_\beta Q_{\alpha\beta}=0$. If fusion alphas are confined and collisional interactions occur, the steady state solutions is achieved with

$$\sum_\beta Q_{\alpha\beta}=-\frac{1}{\gamma-1}\left(T_\alpha^{fus}-T_\alpha\right)\mathcal{S}_{DT}=-\sum_\beta Q_{\beta\alpha} \tag{5.190}$$

Considering the maximum possible value of f_c with the assumption of uniform and constant plasma density and temperature,

$$\begin{aligned} f_c &\simeq \frac{\sum_\beta Q_{\beta\alpha}}{\frac{1}{\gamma-1}\left(T_\alpha^{fus}+T_n^{fus}\right)\mathcal{S}_{DT}} \\ &= \frac{T_\alpha^{fus}}{\left(T_\alpha^{fus}+T_n^{fus}\right)}-\frac{T_\alpha}{\left(T_\alpha^{fus}+T_n^{fus}\right)} \\ &= 0.2-\frac{T_\alpha}{\left(T_\alpha^{fus}+T_n^{fus}\right)} \end{aligned} \tag{5.191}$$

While the fluid simulations do not reach steady state, the finite value of alpha temperature limits the maximum value of f_c. In the fluid simulations, alpha thermal energy confinement time $\tau_{\alpha th}$ can be evaluated as

$$\tau_{\alpha th}\equiv\frac{\int_0^{r_p}rn_\alpha T_\alpha dr}{\left(T_\alpha^{fus}+T_n^{fus}\right)\int_0^{r_p}r\mathcal{S}_{DT}dr} \tag{5.192}$$

which is compared with various pinch current in Fig. 5.8. With the larger pinch current, a higher density n_α and a higher temperature T_α lead to a higher energy transfer rate, and then increase the alpha cooling rate. Hence, the increased n_α and the decreased T_α result in the saturation of f_c.

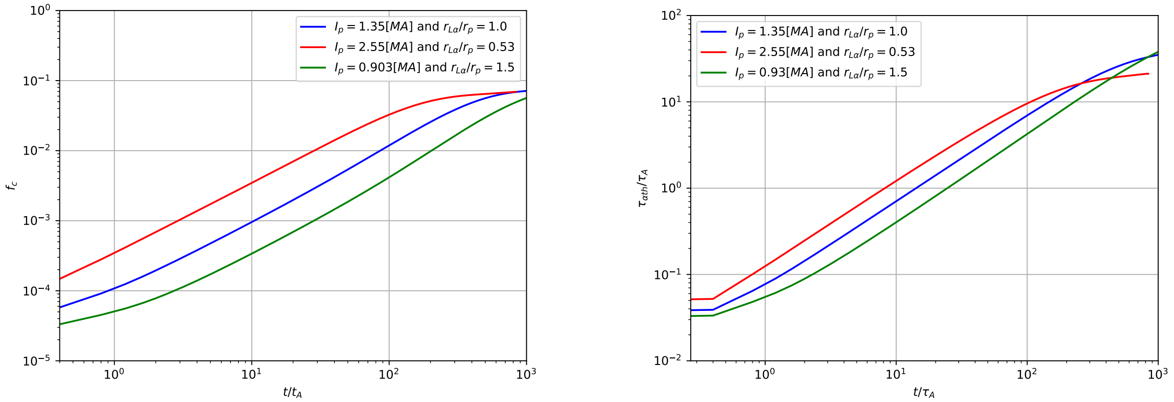

(a) f_c

(b) $\tau_{\alpha th}/\tau_A$

Figure 5.8: (a) Alpha heating fraction f_c and (b) alpha thermal energy confinement time $\tau_{\alpha th}/\tau_A$. In these simulations, $\tau_A = 4.11 \times 10^{-10}$ sec for $I_p = 0.903$ MA: $\tau_A = 6.17 \times 10^{-10}$ sec for $I_p = 1.35$ MA: $\tau_A = 1.16 \times 10^{-9}$ sec for $I_p = 2.55$ MA. The sufficiently strong magnetic fields with the $\vec{J}_{z\alpha} \times \vec{B}_\theta$ force confine more alphas and increase f_c and $\tau_{\alpha th}$. The increased density n_α and decreased temperature T_α from alpha heating leads to a saturation of f_c. (Simulations of 1D D-T Z-pinch fusion in the four-fluid model with different pinch current are performed with WARPXM version 1.5.9 using input file multifluid_zpinch_1D.py)

The alpha current that results from their axial motion can be evaluated in terms of $f_{J\alpha}$ such that

$$f_{J\alpha} = \frac{\int_0^{r_p} r J_{\alpha z}(t) dr}{\int_0^{r_p} r \sum_{s=D,T} J_{sz}(t=0) dr} \tag{5.193}$$

While the current driven by electrons is expected to be constant in well-confined Z-pinch plasmas, the current driven by ions decreases due to the ion consumption through fusion reactions. Hence, $f_{J\alpha}$ can be interpreted as the portion of ion current compensated by the alpha current. A larger $f_{J\alpha}$ contributes to sustaining the magnetic field and confining more alphas. The fraction of current driven by ion, electron, and the total current are calculated as

$$f_{Ji} = \frac{\int_0^{r_p} r J_{iz}(t) dr}{\int_0^{r_p} r J_{iz}(t=0) dr} \tag{5.194}$$

$$f_{Je} = \frac{\int_0^{r_p} r J_{ez}(t) dr}{\int_0^{r_p} r J_{ez}(t=0) dr} \tag{5.195}$$

$$f_{Jtot} = \frac{\int_0^{r_p} r \sum_s J_{sz}(t) dr}{\int_0^{r_p} r \sum_s J_{sz}(t=0) dr} \tag{5.196}$$

As pinch current increases, confined alphas better compensate for ion current decrease due to consumption. Interestingly, the alpha current fraction $f_{J\alpha}$ tends to saturate around $f_{J\alpha} \simeq 0.1$. Due to the ion current decrease from fusion reactions, the total current decreases and the entire plasma expands. While more alphas are confined as time evolves, the expansion of the pinch radius due to the total current decrease leads to a deceleration of alphas and electrons. Thus, increasing n_α with decreasing $u_{\alpha z}$ provides the saturation of the alpha current fraction $f_{J\alpha}$. The alpha current contributes to produce thrust in a Z-pinch fusion thruster such as

$$F_{thrust} = \dot{m}\bar{u}_{\alpha z} = \bar{u}_{\alpha z} \int \rho_\alpha \vec{u}_\alpha \cdot d\vec{S} = 2\pi \bar{u}_{\alpha z} \int_0^{r_p} r \rho_\alpha u_{\alpha z} dr \tag{5.197}$$

where $\bar{u}_{\alpha z}$ is radially-averaged axial velocity

$$\bar{u}_{\alpha z} = \frac{1}{\pi r_p^2} \int \vec{u}_\alpha \cdot d\vec{S} = \frac{2}{r_p^2} \int_0^{r_p} r u_{\alpha z} dr \tag{5.198}$$

Considering specific impulse I_{sp},

$$I_{sp} = \frac{F_{thrust}}{\dot{m} g_0} = \frac{\bar{u}_{\alpha z}}{g_0} \tag{5.199}$$

where $g_0 = 9.8067$ m/s^2 is the gravitational acceleration constant. The time evolutions of axial momentum and axial velocity of alphas are shown in Fig. 5.11. In Fig. 5.12, mass flow rate, radially-averaged axial velocity, thrust, and specific impulse for deuterons, tritons and alphas are provided. While the alpha density is smaller than the Z-pinch ion densities, the higher alpha axial velocity produces higher thrust and longer specific impulse. Fig.

5.13 indicates that the thrust and specific impulse produced by alphas increases with the increasing pinch current.

	n_0 [m^{-3}]	T_0 [keV]	I_p [kA]	r_p [mm]	$r_{L\alpha}/r_p$	Q	f_c	$f_{J\alpha}$
fusion case1	10^{26}	10.0	1350	0.60	1.0	15.0	0.068	0.062
fusion case2	10^{26}	10.0	2550	1.14	0.53	151.8	0.069	0.12
fusion case3	10^{26}	10.0	903	0.40	1.5	6.90	0.047	0.024

Table 5.3: Characteristic physical properties with different pinch current. The fusion gain Q including alpha heating, the fractions f_c and $f_{J\alpha}$ are evaluated at $t = 800\tau_A$

It is important to note that pinch current is increased with the increasing pinch radius and constant density and temperature that leads to constant peak magnetic field B_0. In a Bennett pinch, the pinch current is calculated as

$$I_p = \int \vec{J} \cdot d\vec{S} = \frac{2\pi}{\mu_0} r_p B_0 \tag{5.200}$$

where the peak magnetic field B_0 can be obtained by considering the force balance equation $\nabla P = \vec{J} \times \vec{B}$ and Ampère's law such that

$$\frac{B_0^2}{\mu_0} = n_0 T_0 \tag{5.201}$$

The typical approach to obtain higher pinch current is increasing the magnetic field and decreasing pinch radius; however, if the rate of magnetic field increase and the rate of pinch radius decrease are identical, pinch current remains the same. In the simulations discussed in this dissertation, the rate of pinch current increase is same to the rate of pinch radius increase that leads to the magnetic fields remain the same in the Bennett Z pinch. Those configurations can be achieved, for example, by using larger electrodes. Despite the unusual configurations, it is important to remember that the increase of fusion gain can be obtained by decreasing $r_{L\alpha}/r_p$ that yields high density of alphas and high collisionality within the pinch radius.

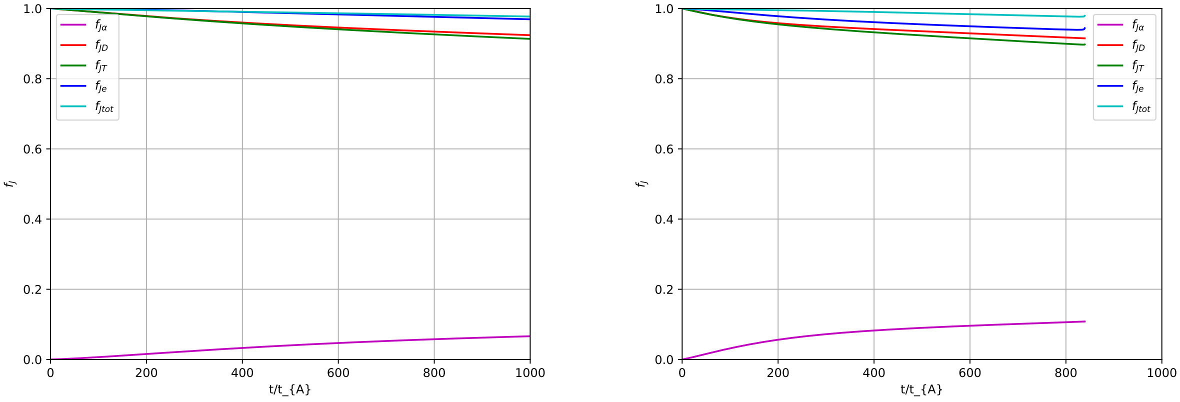

(a) Case1 (b) Case2

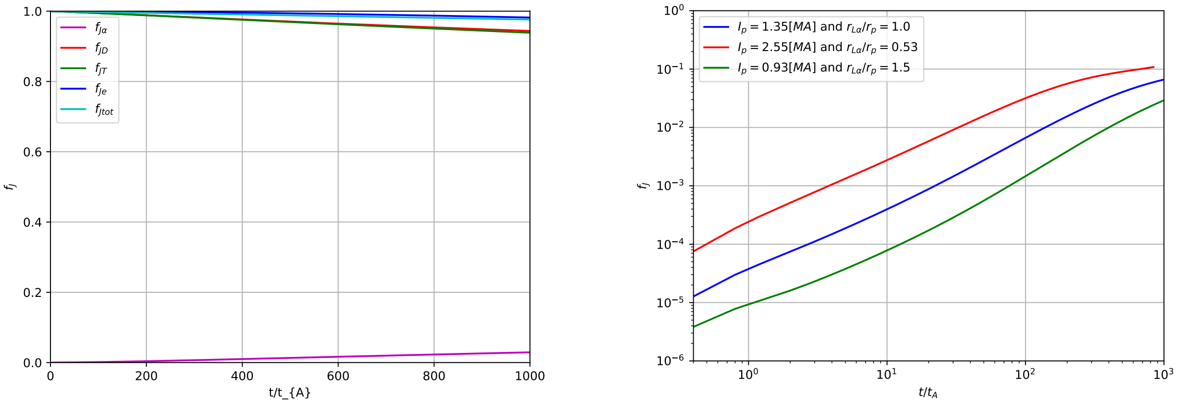

(c) Case3 (d) $f_{J\alpha}$

Figure 5.9: Comparison of current fraction for the three different cases (a) - (c) described in Tab. 5.3. (d) shows an expanded view of the alpha current fraction $f_{J\alpha}$ which is larger for higher pinch currents. The decreasing total current leads to an expansion of the pinch radius. As time evolves, more alphas are confined and the plasma continues to expand so that increasing n_α with decreasing $u_{z\alpha}$ produces the saturation of $f_{J\alpha}$.

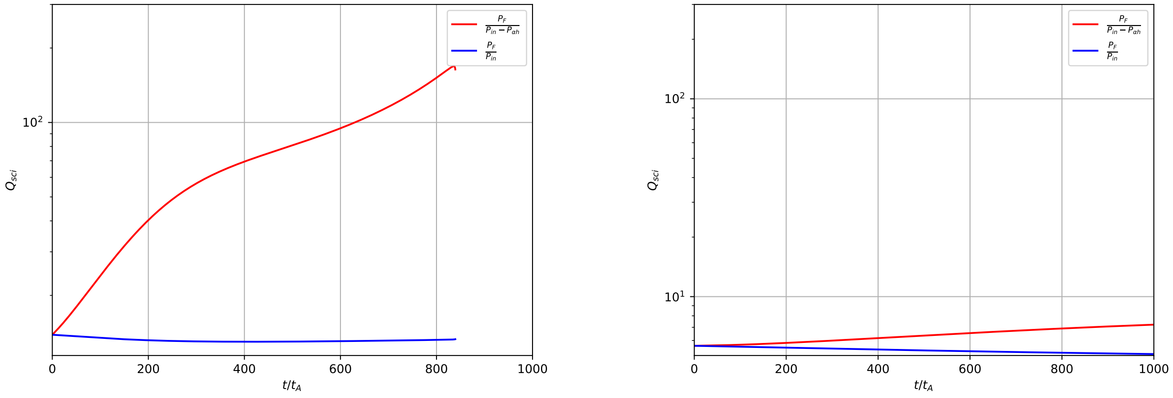

(a) Q_{sci} for case2 (b) Q_{sci} for case3

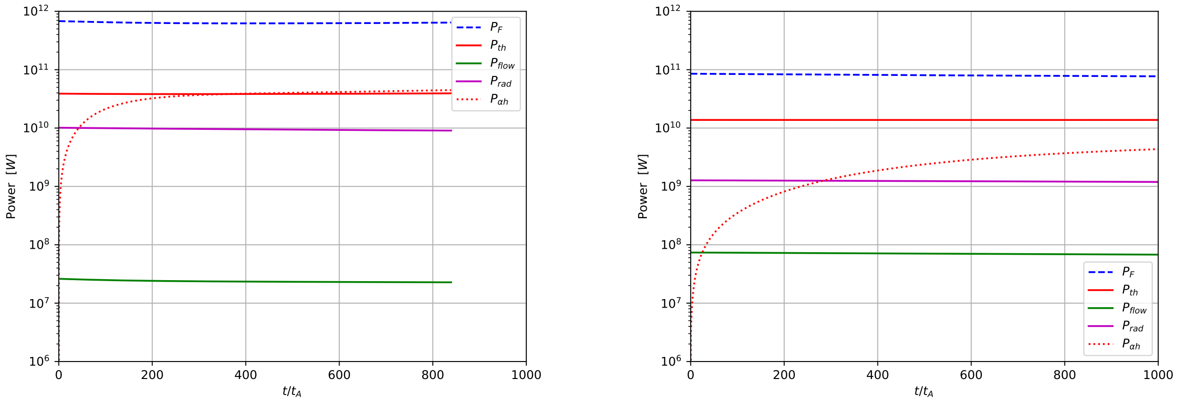

(c) Volume integrated power for case2 (d) Volume integrated power for case3

Figure 5.10: Comparison of fusion gains Q_{sci} and various different powers P to evaluate the fusion gain with two different pinch current of Z pinch. (a) and (c) are for the case2 with $I_p = 2.55$ MA and $r_{L\alpha}/r_p = 0.53$. (b) and (d) are for the case3 with $I_p = 0.903$ MA and $r_{L\alpha}/r_p = 1.5$. As pinch current increases, the fusion gain significantly increases due to the larger alpha heating effects.

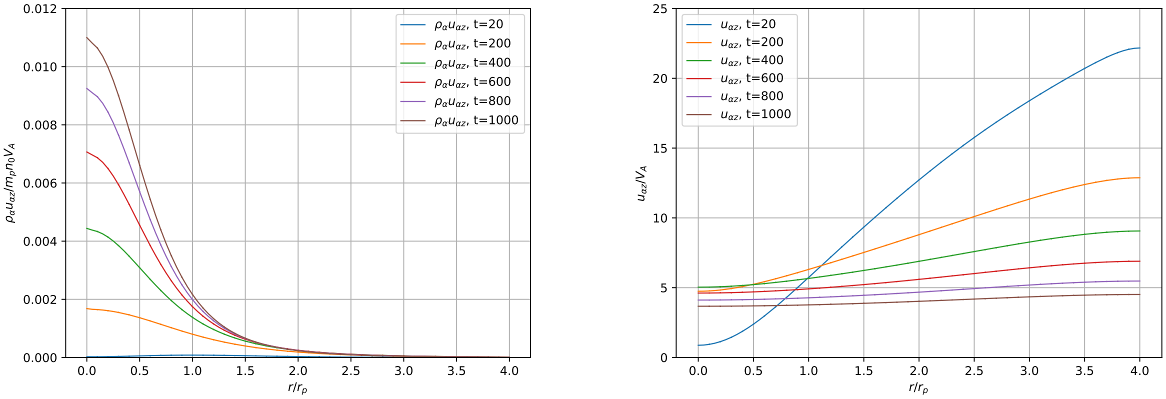

(a) Normalized alpha axial momentum

(b) Normalized alpha axial velocity

Figure 5.11: Time evolution of (a) axial momentum of alphas and (b) axial velocity of alphas in the Z pinch with $I_p = 1.35$ MA and $r_{L\alpha}/r_p = 1.0$. The axial velocity tends to become uniform and slows down due to viscosity and the expansion of the Z pinch. While the axial velocity is high, the axial momentum remains low due to the low density of alphas.

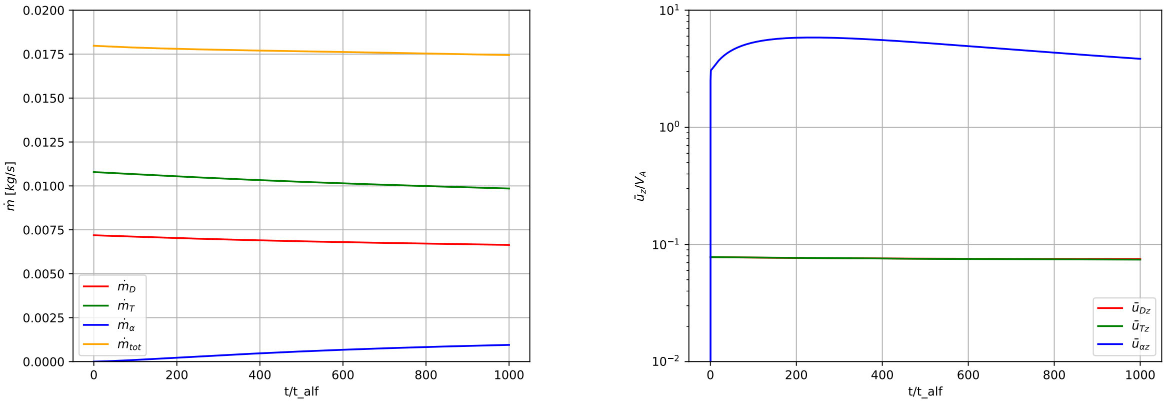

(a) Mass flow rate (b) Normalized radially-averaged axial velocity

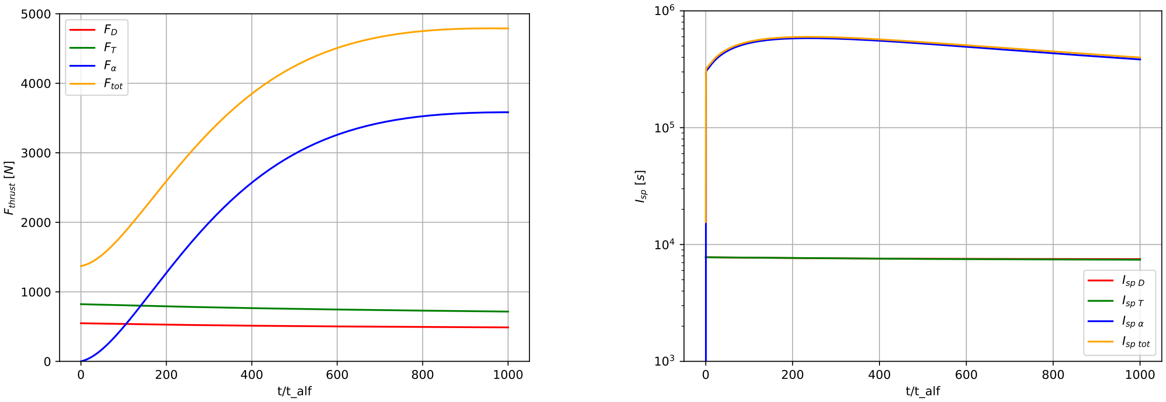

(c) Thrust (d) Specific impulse

Figure 5.12: Comparison of (a) mass flow rate, (b) normalized radially-averaged axial velocity, (c) thrust, and (d) specific impulse for deuterons (red line), tritons (green line), alphas (blue line), and the entire ions (orange line) in the Z pinch with $I_p = 1.35$ MA and $r_{L\alpha}/r_p = 1.0$. The radially-averaged axial velocity of alphas is significantly higher than that of Z-pinch ions resulting in a significantly higher specific impulse for alphas. Ion thrust decreases through fusion reactions; however, the axial motion of alphas with high velocity produces larger thrust. Deuterons and tritons exhibit similar radially-averaged velocity and specific impulse.

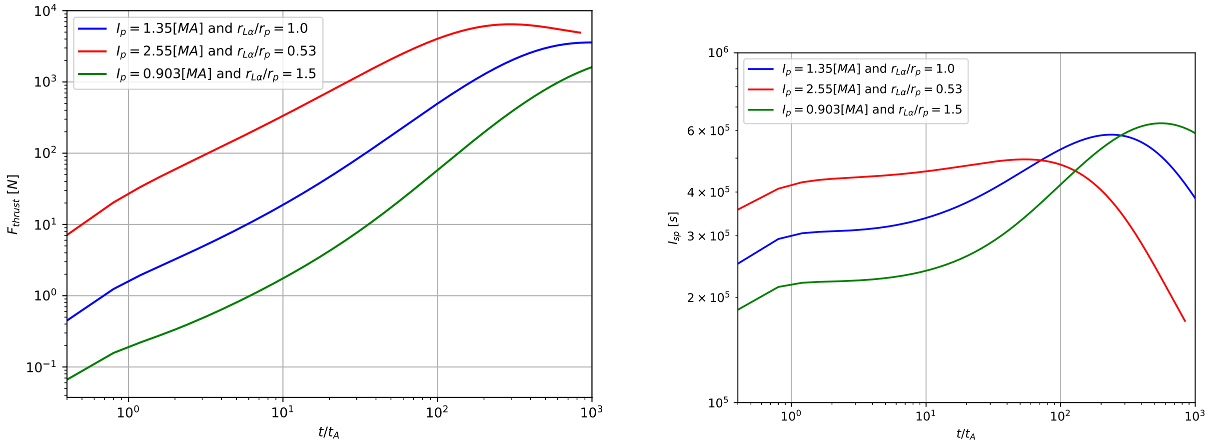

(a) Thrust

(b) Specific impulse

Figure 5.13: Comparison of thrust and specific impulse produced by alphas for three different cases as described in Tab. 5.3. As pinch current increases, both thrust and specific impulse resulting from the alpha current increases.

Chapter 6

CONCLUSIONS

6.1 Summary of the Dissertation

The SFS Z pinch is a promising concept for terrestrial fusion energy production and future space exploration. In this dissertation, three main contributions have been made to extend the capabilities of WARPXM simulation framework and to investigate the effects of fusion reactions in D-T Z-pinch plasma. First, the geometric source terms which are originally introduced by Srinivasan for WARPX are implemented into the WARPXM to model axisymmetric problems in cylindrical coordinates. Second, the full Braginskii transport except for Ettingshausen effect are developed and implemented to investigate the $m = 0$ sausage instability in the axisymmetric Z pinch and to study the impact of plasma collisionality. Third, the thermonuclear fusion process in a D-T Z pinch is investigated by developing the multi-component, deuterium-tritium-helium-electron, plasma model that includes fusion reactions and interspecies collisions to observe physical phenomena related with energetic alpha particles.

6.1.1 Geometric Source Terms

WARPXM has been originally developed for a computational mesh and governing equations described in Cartesian coordinates. To solve axisymmetric problems, the general expression of the geometric source terms are introduced and several analytical benchmark tests are implemented in multiple different models. For Maxwell's equations, the TE, TM, and TEM modes in a cylindrical waveguide are tested. The singular problem of the geometric source terms are resolved by applying L'Hôpital's rule at $r = 0$. As for Euler fluid equations, the rotational hydrostatic pressure problem is implemented. To verify the implementation of viscosity with the geometric source terms, Taylor-Couette flow and Hagen-Poiseulle flow are tested with Gaussian quadrature. To benchmark the plasma models, the Bennett equilibrium of 1D Z pinch in ideal MHD and ideal $5N$-moment two-fluid models are implemented. The benchmark tests demonstrate correct implementation with numerical results that match the analytical results.

6.1.2 Braginskii Transport Equations

The $m = 0$ sausage instability in the 2D axisymmetric Z pinch is investigated in ideal MHD and $5N$-moment two-fluid model with Braginskii transport. Comparing with the PIC kinetic results, while the ideal MHD model provides comparable linear growth rates for the $m = 0$ sausage instability, the ideal $5N$-moment two-fluid model indicates higher linear growth rates that are comparable to Hall MHD results for the shear-free Z pinch. Thus, Hall effect or some effects related to the electron mobility are expected to produce destabilizing effects. While the SFS Z pinch in the ideal $5N$-moment two-fluid model indicates the stronger stabilizing effects and improves the plasma confinement with increasing shear velocity, nonlinear saturation is not observed due to the large growth rates and the lack of dissipative effects. Braginskii transports are introduced to more accurately model the expected physics, which tends to mitigate the higher growth rates. Since the FuZE configuration is in a collisionless regime due to the high temperature, the Braginskii equations are implemented within the collisional or collisional transition regimes. In the collisional regime, the high resistivity dissipates the Z pinch current. Resistive effects become negligible if $\mathrm{Kn} > 0.1$ in a collisional transition regime. The viscosity and thermal conductivity are found to have stabilizing effects for the shear-free Z pinch. However, as temperature increases (as plasma becomes collisionless), the transport coefficients for the viscosity and thermal conductivity become large so that the growth rates become overdamped. The correction factors proposed by Meier are not accurate in the collisional transition regime due to the small Knudsen number $\mathrm{Kn} \simeq 10^{-2} - 10^{0}$ compared with a collisionless case where $\mathrm{Kn} \geq 10$. Hence, appropriate correction factors for plasmas in a collisional transition regime with a smooth transition to

Meier's correction factors need to be developed.

6.1.3 D-T Z-pinch Fusion

As a novel contribution of this research, 1D 5N-moment four-fluid (deuterium-tritium-alpha-electron) plasma model is developed. The fusion reactivities are obtained by using a R-matrix fitting approach described by Bosch and Hale. The collisional interactions of the energetic alphas and Maxwellian Z-pinch plasmas are modeled by using a Fokker-Planck collision operator. While it lowers the fidelity of the model, an approximate Maxwellian distribution is used to represent the energetic fusion alphas and to understand the first-order effects of collisional interactions. With sufficiently high magnetic fields, the energetic alphas can be magnetically confined. In an early phase, radially expanding alphas interact with the azimuthal magnetic fields, which drives an axial motion of alphas. This alpha current can compensate for the ion current decrease due to ion consumption by fusion reactions and can mitigate the radial expansion of the pinch by producing a restoring $\vec{J}_{z\alpha} \times \vec{B}_\theta$ force. The alpha heating can be observed by simulating for sufficiently long durations, which approximately corresponds to a slowing-down period. The primary energy cascade is observed to initiate from energetic alphas to electrons, and eventually the electron energy transfers to deuterons and tritons. Using a pinch current of $I_p = 1.35$ MA, which corresponds to a pinch radius equal to the gyroradius of alphas, the fraction of alpha heating to fusion energy f_c reaches to 10%, which amplifies the fusion gain Q increases from 5.43 to 10. Interestingly, the alpha current compensate for 6% of the original ion current; however, the decreasing total current leads to an expansion of the pinch. The higher pinch current of $I_p = 2.55$ MA provides a saturated $f_c \simeq 7\%$. While the alpha heating fraction f_c is similar to the lower pinch current case with the smaller pinch radius, the significantly higher fusion gain $Q = 151.8$ is obtained.

6.2 Future Work

While this research enhances the capabilities of WARPXM and presents multiple contributions, there are several topics requiring additional work. The following sections highlight the possible future directions.

6.2.1 Hall MHD Model

The linear growth rates in the Hall MHD model are obtained by Sotnikov[52] with $\frac{r_p}{r_{Li}} = 2.36$. To compare with the ideal two-fluid WARPXM results with $\frac{r_p}{r_{Li}} = 5.8$, it is necessary to develop the geometric source terms for the Hall MHD model in WARPXM including hyperviscosity to stabilize the whistler waves.

6.2.2 Braginskii Transports in a Collisional Transition Regime

Prior to reaching fusion conditions, the SFS Z pinch confines plasmas with increasing temperature during the Z-pinch assembly process[68, 69]. To mitigate the unphysically large viscosity and thermal conductivity in the collisional transition regime, more accurate correction factors with smooth transitions to correction factors will be required to investigate the dynamics of the SFS Z pinch.

6.2.3 Onsager's Reciprocal Terms

The Onsager's reciprocal terms, in particular Ettingshausen effect, are not investigated in the Z-pinch simulations. Implementing rigorous benchmark tests for Onsager's reciprocal terms including Nernst effect will enhance the capabilities of WARPXM and produce more physically accurate simulations.

6.2.4 Non-Maxwellian Alpha Distribution

Within the fluid context, a monoenergetic alpha distribution or slowing-down distribution cannot be fully modeled. While a fully kinetic model has the highest fidelity, the computational cost becomes quite expensive for long-duration simulations to observe alpha heating effects. Maxwellian approximations allow a computationally efficient fluid model and help develop insight into how collisional interactions effect the plasma dynamics. Using a more realistic distribution function of energetic alphas, for example a delta function or slowing-down distribution, will improve the fidelity of alpha heating simulations.

6.2.5 2D Z-pinch Fusion Simulations

Understanding the physics of alpha current is important to increase fusion gain, and it has the potential to provide insights for achieving the ignition conditions in a SFS Z pinch. 2D simulations will provide more detailed dynamics of alphas and help to determine a nonlinear saturation.

6.2.6 High-Fidelity Kinetic and Multi-Fluid Models

The hybrid kinetic and multi-fluid model developed by Datta[70] or a hybrid multi-fluid and Vlasov-Maxwell model developed by Ho[71] haves the potential to provide more detailed and accurate descriptions of alpha current in the core of the Z pinch. The collisional interactions with computed distributions will also yield rigorous insight for alpha heating.

6.2.7 D-D Z-pinch Fusion

D-T Z-pinch fusion is investigated in this work to observe alpha heating with feasible temperatures. At the University of Washington, an experimental device known as FuZE[53] achieved D-D fusion reactions. Comparing numerical results using D-D Z-pinch fusion with the experimental results will be helpful to validate the numerical investigations.

6.2.8 Boundary Conditions for Z-pinch Fusion Thruster

For space propulsion applications, it is important to estimate the lifetime of electrodes due to erosion. Developing boundary conditions for plasma-facing electrodes will help to investigate the potential performance of a Z-pinch fusion thruster. Also, non-perfectly conducting wall boundary conditions will be useful to enhance the capabilities of WARPXM and to perform more physically accurate simulations.

BIBLIOGRAPHY

[1] M. R. Gordlinear et al. Nuclear fusion power. *Encyclopedia of Physical Science and Technology*, pages 671–699, 2003.

[2] S. Miller. *Modeling collisional processes in plasmas using discontinuous numerical methods*. PhD thesis, University of Washington, 2016.

[3] W. M. Stacey Jr. *Fusion: An Introduction to the Physics and Technology of Magnetic Confinement Fusion*. A Wiley-Interscience Publication, Canada, 1984.

[4] A. K. Hyder, R. L. Wiley, and G. Halpert et al. *Spacecraft Power Technologies*. Imperial College Press, London, 2000.

[5] J. Cassibry, R. Cortez, and M. Stanic et al. Case and development path for fusion propulsion. *Journal of Spacecraft and Rockets*, 52(2):595–612, 2015.

[6] W. C. Elmore, J. L. Tuck, and K. M. Watson. On the inertial-electrostatic confinement of a plasma. *Physics of Fluids*, 2(3):239–246, 1959.

[7] S. Atzeni and J. Meyer ter Vehn. *The Physics of Inertial Fusion: Beam Plasma Interaction, Hydrodynamics, Hot Dense Matter*. Oxford University Press, Incorporated, Oxford, 2004.

[8] U. Shumlak. Z-pinch fusion. *Journal of Applided Physics*, 127, 2020.

[9] U. Shumlak, R. C. Lilly, and C. S. Adams et al. Advanced space propulsion based on the flow-stabilized z-pinch fusion concept. Number 3. 42nd AIAA/ASME/SAE/ASEE Joint Propulsion Conference, 2006.

[10] S. I. Braginskii. Transport process in a plasma. *Review of Plasma Physics*, 1:205–311, 1965.

[11] U. Shumlak, R. Lilly, N. Reddell, E. Sousa, and B. Srinivasan. Advanced physics calculations using a multi-fluid plasma model. *Computer Physics Communications*, 182(9):1767–1770, 2011. Computer Physics Communications Special Edition for Conference on Computational Physics Trondheim, Norway, June 23-26, 2010.

[12] Bhuvana Srinivasan. *Numerical Methods for 3-dimensional Magnetic Confinement Configurations using Two-Fluid Plasma Equations.* PhD thesis, University of Washington, 2010.

[13] Charles Hirsch. *Numerical Computation of Internal and External Flows: Fundamentals of Computational Fluid Dynamics*, volume 1. Butterworth-Heinemann, Oxford, 2nd edition, 2007.

[14] Olaf Kolditz. *Computational Methods in Environmental Fluid Mechanics.* Springer-Verlag, NY, 2002.

[15] A. Hrennikoff. Solution of problems of elasticity by the framework method. *Journal of Applied Mechanics*, 8(4):169–175, 1941.

[16] D. McHenry. A lattice analogy for the solution of plane stress problems. *Journal of Institution of Civil Engineers*, 21(4):59–82, 1943.

[17] B. A. Suzabo and G. C. Lee. Derivation of stiffness matrices for problems in plane elasticity by galerkin's method. *International Journal of Numerical Methods in Engineering*, 1:301–310, 1969.

[18] Jan S. Hesthaven and Tim Warburton. *Nodal Discontinuous Galerkin Methods: Algorithms, Analysis, and Applications.* Springer Science+Business Media, NY, 2008.

[19] W. H. Reed and T. Hill, editors. *Triangular Mesh Methods for the Neutron Transport Equation.* Proceedings of the American Nuclear Society, 1973.

[20] Emil de Souza Sánchez Filho. *Tensor Calculus for Engineers and Physicists.* Springer International Publishing, AG Switzerland, 2016.

[21] George B. Arfken, Hans J. Weber, and Frank E. Harris. *Mathematical Methods for Physicists.* Elsevier Inc., MA, 7th edition, 2013.

[22] Dwight E. Neuenschwander. *Tensor Calculus for Physics: A Concise Guide.* Jhons Hopkins University Press, MD, 2015.

[23] Murray R. Spiegel. *Vector Analysis and an Introduction to Tensor Analysis: Schaum's Outline of Theory and Problems.* Schaum Publishing Company, 1959.

[24] Bruce R. Kusse and Erik A. Westwig. *Mathematical Physics: Applied Mathematics for Scientists and Engineers.* WILEY-VCH Verlag GmbH & Co. KGaA, Weinheim, 2006.

[25] Robert S. Cohen, Lyman Spitzer, and Paul McR. Routly. The electrical conductivity of an ionized gas. *Physical Review*, 80(2):230–238, 1950.

[26] Lyman Spitzer and Richard Härm. Transport phenomena in a completely ionized gas. *Physical Review*, 89(5):977–981, 1953.

[27] Lyman Spitzer. *Physics of Fully Ionized Gases*. Interscience Publishers, Inc., NY, 1956.

[28] Bernardo Cockburn and Chi-Wang Shu. The local discontinuous galerkin method for time-dependent convection-diffusion systems. *SIAM Journal of Numerical Analysis*, 35(6):2440–2463, 1998.

[29] J. Douglas and T. Dupont. Interior penalty procedures for elliptic and parabolic galerkin methods. In *Lecture Notes in Physics: Computing Methods in Applied Sciences*, volume 58, pages 207–216. Springer-Verlag, Berlin, 1976.

[30] Douglas N. Arnold. An interior penalty finite element method with discontinuous elements. *SIAM Journal of Numerical Analysis*, 19(4):742–760, 1982.

[31] John David Jackson. *Classical Electrodynamics*. John Wiley & Sons, Inc., NY, 3rd edition, 1999.

[32] John D. Anderson Jr. *Computational Fluid Dynamics: The Basics with Applications*. McGraw-Hill, Inc., Singapore, 1995.

[33] C. William Gear. *Numerical Initial Value Problems in Ordinary Differential Equations*. Prentice-Hall, Inc., NJ, 1971.

[34] Bernardo Cockburn and Chi-Wang Shu. Runge-kutta discontinuous galerkin methods for convection-dominated problems. *Journal of Scientific Computing*, 16(3):173–261, 2001.

[35] Bernardo Cockburn and Chi-Wang Shu. The runge-kutta local projection p^1-discontinuous-galerkin finite element method for scalar conservation laws. *RAIRO Modél. Math. Anal. Numér*, 25(3):337–361, 1991.

[36] Guy Chavent and Bernardo Cockburn. The local projection p^0-p^1-discontinuous-galerkin finite element method for scalar conservation laws. *RAIRO Modél. Math. Anal. Numér*, 23(4):565–592, 1989.

[37] Andrew Ho. *Modeling plasma systems using a domain-hybridized physical model*. PhD thesis, [University of Washington], 2022.

[38] M. M. Couette. études sur le frottement des liquides. *Ann. Chim. Phys.*, 6(21):433–510, 1890.

[39] G. I. Taylor. Stability of viscous liquid contained between two rotating cylinders. *Philosophical Transactions of the Royal Society of London. Series A, Containing Papers of a Mathematical or Physical Character*, 223:289–343, 1923.

[40] Pijush K. Kundu and Ira M. Cohen. *Fluid Mechanics*. Elsevier Inc., MA, 4th edition, 2008.

[41] S. Chandrasekhar. *Hydrodynamic and Hydromagnetic Stability*. Oxford University Press, Great Britain, 1961.

[42] Salvatore P. Sutera and Richard Skalak. The history of poiseuille's law. *Annu. rev. Fluid Mech.*, 25:1–19, 1993.

[43] G. H. L. Hagen. Uber die bewegung des wassers in engen cylindrischen röhren. *Poggendorf's Annalen der Physik und Chemie*, 46, 1839.

[44] J. L. M. Poiseuille. Recherches expérimentales sur le mouvement des liquides dans les tubes de très-petits diamètres. *Mèmoires presentés par divers savants à l' Acadèmie Royal des Sciences de l'Institut de France*, 9:433–544, 1846.

[45] Olek C Zienkiewicz, Robert L Taylor, and J.Z Zhu. *Finite Element Method - Its Basis and Fundamentals (6th Edition)*. Elsevier, sixth edition edition, 2005.

[46] D. A. Dunavant. High degree efficient symmetrical gaussian quadrature rules for the triangle. *International Journal for Numerical Methods in Engineering*, 21, 1985.

[47] Willard H. Bennett. Magnetically self-focussing streams. *Physical Review*, 45:890–897, 1934.

[48] K. Tummel, D. P. Higginson, and A. J. Link et al. Kinetic simulations of sheared flow stabilization in high-temperature z-pinch plasmas. *Physics of Plasmas*, 26, 2019.

[49] M. Kruskal and M. Schwarzschild. Some instabilities of a completely ionized plasma. *Proceeding of the Royal Society of London Series A, Mathematical and Physical Sciences*, 223, 1954.

[50] U. Shumlak and C. W. Hartman. Sheared flow stabilization of the $m = 1$ kink mode in z pinches. *Physical Review Letters*, 75(18), 1995.

[51] J. Scheffel, T. D. Arber, M. Coppins, and P. G. F. Russel. Kinetic stability of the finite electron temperature z-pinch. *Plasma Phys. Control. Fusion*, 39:559–568, 1997.

[52] V. I. Sotnikov, I. Paraschiv, and V. Makhin et al. Linear analysis of sheared flow stabilization of global magnetohydrodynamic instabilities based on the hall fluid model. *Physics of Plasmas*, 9(3):913–922, 2002.

[53] Y. Zhang et al. Sustained neutron production from a sheared-flow stabilized z pinch. *Phys. Rev. Lett.*, 122, 2019.

[54] E. T. Meier and U. Shumlak. Development of five-moment two-fluid modeling for z-pinch physics. *Physics of Plasmas*, 28, 2021.

[55] L. Onsager. Reciprocal relations in irreversible processes ii. *Physical Review*, 38, 1931.

[56] P. W. Bridgman. The connections between the four transverse galvanomagnetic and thermomagnetic phenomena. *Physical Review*, 24, 1924.

[57] H. S. Bosch and G. M. Hale. Improved formulas for fusion cross-sections and thermal reactivities. *Nucl. Fusion*, 32, 1992.

[58] U. Shumlak, Meier E.T., and B. J. Levitt. Fusion gain and triple product for the sheared-flow-stabilized z pinch. *Fusion Science and Technology*, 2023.

[59] D. C. Montgomery and D. A. Tidman. *Plasma Kinetic Theory.* McGraw-Hill Book Company, NY, 1964.

[60] E. T. Meier and U. Shumlak. A general nonlinear fluid model for reacting plasma-neutral mixtures. *Physics of Plasmas*, 19, 2012.

[61] I. P. Shakarofsky, T. W. Johnston, and M. P. Bachynsky. *The Particle Kinetics of Plasmas.* Addison-Wesley Publishing Company, Netherlands, 1966.

[62] R. Balescu. *Transport Processes in Plasmas.* Academic Press, NY, 1973.

[63] R. Salmon. Hamiltonian fluid mechanics. *Annual review of fluid mechanics*, 20, 1988.

[64] P. J. Morrison and J. M. Greene. Noncanonical hamiltonian density formulation of hydrodynamics and ideal magnetohydrodynamics. *Physics review letters*, 45(10), 1980.

[65] Francis K. McGowan and William T. Milner. *Charged-particle reaction list, 1948-1971.* Academic Press, NY, 1973.

[66] B. A. Trubnikov. Particle interactions in a fully ionized plasma. *Reviews of Plasma Physics*, 1, 1965.

[67] R. J. Goldston and P. H. Rutherford. *Introduction to Plasma Physics*. Taylor and Francis Group, LLC., NY, 1995.

[68] U. Shumlak et al. Sheared flow stabilization experiments in the zap flow z pinch. *Physics of Plasmas*, 10, 2003.

[69] U. Shumlak et al. Equilibrium, flow shear and stability measurements in the z pinch. *Nucler Fusion*, 49, 2009.

[70] I.A.M. Datta and U. Shumlak. Computationally efficient high-fidelity plasma simulations by coupling multi-species kinetic and multi-fluid models on decomposed domains. *Journal of Computational Physics*, 483:112073, 2023.

[71] A. Ho, I. A. M. Datta, and U. Shumlak. Physics-based-adaptive plasma model for high-fidelity numerical simulations. *Front. Phys.*, 21, 2018.

[72] U. Shumlak et al. Increasing plasma parameters using sheared flow stabilization of a z pinch. *Physics of Plasmas*, 24, 2017.

[73] Charles Hirsch. *Numerical Computation of Internal and External Flows: Computational Methods for Inviscid and Viscous Flows*, volume 2. John Wiley & Sons, West Sussex, 1990.

[74] Daryl L. Logan. *A First Course in the Finite Element Method*. Cengage Learning, MA, 6th edition, 2014.

[75] N. Copernicus. *De revolutionibus orbium coelestium*. Johannes Petreius, Nuremberg, 1543.

[76] J. Kepler. *De Stella Nova in Pede Serpentarii*. Paul Sessius, Prague, 1606.

[77] G. Galilei. *Dialogue Concerning the Two Chief World Systems*. Giovanni Battista Landini, Florence, 1632.

[78] I. Newton. *PhilosophiæNaturalis Principia Mathematica*. Edmund Halley, London, 1687.

[79] E. Harnett and R. Winglee. *Space and Space Travel*. Congnella, Inc., CA, 2015.

[80] B. Srinivasan and U. Shumlak. Analytical and computational study of the ideal full two-fluid plasma model and asymptotic approximations for hall-maggnetohydrodynamics. *Physics of Plasmas*, 18(9), 2011.

[81] J. P. Freidberg. Ideal magnetohydrodynamic theory of magnetic fusion systems. *Review of Modern Physics*, 54(3):801–903, 1982.

[82] R. J. Taylor. Hydromagnetic instabilities of an ideally conducting fluid. *Proceeding of the Physical Society Section B*, 70(1154):348–360, 1957.

[83] E. T. Meier. *Modeling Plasmas with Strong Anisotropy, Neutral Fluid Effects, and Open Boundaries.* PhD thesis, University of Washington, 2011.

[84] B. H. Duane. Fusion cross section theory. *Rept. BNWL-1685 (The Pacific Northwest Laboratory Annual Report on Controlled Thermonuclear Reactor Technology)*, 1972.

[85] G. H. Miley, H. Towner, and N. Ivich. Fusion cross sections and reactivities (rept. coo-2218-17). Technical report, University of Illinois, IL, 1974.

[86] U. Shumlak, R. C. Lilly, and C. S. Adams et al. Advanced space propulsion based on the flow-stabilized z-pinch fusion concept. Number 3. 42nd AIAA/ASME/SAE/ASEE Joint Propulsion Conference, 2006.

[87] S. Chapman and T. G. Cowling. *The Mathematical Theory of Non-Uniform Gases.* Cambridge University Press, United Kingdom, 2nd edition, 1953.

[88] H. Grad. On the kinetic theory of rarefied gases. *Comm. Pure appl. Math.*, 2, 1949.

[89] F. L. Hinton. *Collisional Transport in Plasma.* Fusion Research Center, Texas, 1983.

[90] S. P. Hirshman. Transport of a multiple-ion species plasma in the pfirsch-schluter regime. *The Physics of Fluids*, 20, 1977.

[91] S. P. Hirshman and D. J. Sigmar. *Neoclassical Transport of Impurities in Tokamak Plasmas.* Oak Ridge National Laboratory TM-7588, Tennessee, 1981.

Appendix A

TENSOR ANALYSIS IN CURVILINEAR COORDINATES

A.1 Coordinate Transformations

Suppose that there exist N independent relations between two different frames of references $(\{x^j|j=1,2,\cdots,N\})$ and $\left(\{X^k|k=1,2,\cdots,N\}\right)$ such that

$$\begin{aligned} X^1 &= X^1\left(x^1,x^2,\cdots,x^N\right) \\ X^2 &= X^2\left(x^1,x^2,\cdots,x^N\right) \\ &\vdots \\ X^N &= X^N\left(x^1,x^2,\cdots,x^N\right) \end{aligned} \tag{A.1}$$

where those involved functions are single-valued, continuous and have continuous spatial derivatives. In contrast,

$$\vec{x}^j = \begin{bmatrix} x^1\left(X^1,X^2,\cdots,X^N\right) \\ \vdots \\ x^N\left(X^1,X^2,\cdots,X^N\right) \end{bmatrix} \tag{A.2}$$

Eqs. (A.1) and (A.2) indicate transformations of coordinates (or vector space).

A.2 Covariance and Contravariance

The infinitesimal displacement $d\vec{\ell}$ in a vector space $(\{x^j|j=1,2,\cdots\})$ can be transformed in a different vector space $\left(\{X^k|k=1,2,\cdots\}\right)$ by using the change of basis

$$d\vec{\ell} = d\vec{\ell}\left(\{x^j|j=1,2,\cdots\}\right) = \sum_j^N dx^j\vec{b}_j = dx^j\vec{b}_j \tag{A.3}$$

$$d\vec{\ell} = d\vec{\ell}\left(\{X^k|k=1,2,\cdots\}\right) = \sum_k^N dX^k\vec{B}_k = dX^k\vec{B}_k \tag{A.4}$$

where the Einstein notation simplifies a summation, and $\vec{b}_j$ and $\vec{B}_k$ are basis vectors for the invariant $d\vec{\ell}$ under the change of basis such that

$$\vec{b}_j = \frac{\partial \vec{\ell}}{\partial x^j} \tag{A.5}$$

$$\vec{B}_k = \frac{\partial \vec{\ell}}{\partial X^k} = \frac{\partial x^j}{\partial X^k}\frac{\partial \vec{\ell}}{\partial x^j} = \frac{\partial x^j}{\partial X^k}\vec{b}_j \tag{A.6}$$

The invariance of $d\vec{\ell}$ under the choice of basis vectors also yields

$$dX^k = \frac{\partial X^k}{\partial x^j}dx^j \tag{A.7}$$

Applying this change of basis, Eq. (A.6), for an arbitrary and invariant vector $\vec{Q}$

$$\vec{Q} = q^j\vec{b}_j = Q^k\vec{B}_k = Q^k\frac{\partial x^j}{\partial X^k}\vec{b}_j \tag{A.8}$$

which yields

$$Q^k = \frac{\partial X^k}{\partial x^j}q^j \tag{A.9}$$

If certain quantity is transformed $(\{x^j|j = 1, 2, \cdots\}) \rightarrow \left(\{X^k|k = 1, 2, \cdots\}\right)$ by $\frac{\partial x^j}{\partial X^k}$ likewise Eq. (A.6), the transformation is referred as a covariant transformation and the quantity is called components of covariant tensor; $\vec{B}_k$ and $\vec{b}_j$ are covariant basis vector. On the other hand, if a transformation is ruled by $\frac{\partial X^k}{\partial x^j}$ like Eqs. (A.7) or (A.9), the transformation is referred as a contravariant transformation and the quantity is called components of contravariant tensor. Hence, the transformation of contravariant basis vector is

$$\vec{B}^k = \frac{\partial X^k}{\partial x^j}\vec{b}^j \tag{A.10}$$

Also,

$$\vec{Q} = q_j\vec{b}^j = Q_k\vec{B}^k = Q_k\frac{\partial X^k}{\partial x^j}\vec{b}^j \tag{A.11}$$

yields

$$Q_k = \frac{\partial x^j}{\partial X^k}q_j \tag{A.12}$$

Note the matrix form of coefficients for the covariant transformations is Jacobian matrix of x^j with respect to X^k

$$\overset{\leftrightarrow}{J}(X^1, \cdots, X^N) = \begin{bmatrix} \frac{\partial x^1}{\partial X^1} & \cdots & \frac{\partial x^1}{\partial X^N} \\ \vdots & \ddots & \vdots \\ \frac{\partial x^N}{\partial X^1} & \cdots & \frac{\partial x^N}{\partial X^N} \end{bmatrix} \tag{A.13}$$

A.3 Metric Tensor

Considering the square of infinitesimal displacement,

$$d\ell^2 = d\vec{\ell} \cdot d\vec{\ell} = (\vec{b}_j \cdot \vec{b}_k) dx^j dx^k = g_{jk} dx^j dx^k \tag{A.14}$$

where $\overset{\leftrightarrow}{g}$ is the metric tensor and g_{jk} is defined as

$$g_{jk} \equiv \vec{b}_j \cdot \vec{b}_k \tag{A.15}$$

Since a dot product is commutative, $\overset{\leftrightarrow}{g}$ is symmetric. The orthogonal basis vectors yields zero non-diagonal terms. Also, the general Riemannian space has a different metric tensor, in particular $g_{jj} = 1$ is known as Euclidean space. The magnitude of a basis vector is known as the scale factor and a normalized basis vector is called as a unit vector

$$\bar{b}_j = \frac{\vec{b}_j}{\sqrt{g_{jj}}} \tag{A.16}$$

In Cartesian coordinates (Euclidean space), the basis vector is identical to the unit vector since $g_{jj} = 1$, but generally not identical in curvilinear coordinates (Riemannian space). From Eq. (A.14),

$$d\ell^2 = g_{ij} dx^i dx^j = G_{kl} dX^k dX^l \tag{A.17}$$

Using Eqs. (A.7), (A.9) and (A.17),

$$G_{ik} Q^k = g_{nl} \frac{\partial x^n}{\partial X^i} \frac{\partial x^l}{\partial X^k} \frac{\partial X^k}{\partial x^j} q^j = g_{nl} \frac{\partial x^n}{\partial X^i} \delta^l{}_j q^j = g_{nl} \frac{\partial x^n}{\partial X^i} q^l \tag{A.18}$$

Suppose that $g_{nl} q^l$ is treated as a single quantity, Eq. (A.18) indicates the covariant transformation of the vector such that

$$Q_i = \frac{\partial x^n}{\partial X^i} q_n \tag{A.19}$$

where

$$q_n = g_{nl} q^l \tag{A.20}$$

Similarly for contravariant tensors,

$$q^n = g^{nl} q_l \tag{A.21}$$

Also, Eqs. (A.8) and (A.11) imply that the contravariant basis vector is dual basis for the covariant basis vector such that

$$\vec{b}^i \cdot \vec{b}_j = \delta^i_j \tag{A.22}$$

where δ^i_j is Kronecker delta. Hence

$$\vec{Q} \cdot \vec{b}^i = q^j \vec{b}_j \cdot \vec{b}^i = q^j \delta^i_j = q^i = g^{ik} q_k = g^{ik} g_{kj} q^j \tag{A.23}$$

yields the relationships between covariant and contravariant metric tensor

$$g^{ik} g_{kj} = g_{jk} g^{ki} = \delta^i_j \tag{A.24}$$

and the relationships between covariant and contravariant basis vectors

$$\vec{b}_i = g_{ij} \vec{b}^j \tag{A.25}$$

$$\vec{b}^i = g^{ij} \vec{b}_j \tag{A.26}$$

A.4 Christoffel Symbols

Considering spatial derivatives of vectors $\vec{A} = A^i \vec{B}_i$ with respect to general coordinates q^j,

$$\begin{aligned} \frac{\partial \vec{A}}{\partial q^j} &= \frac{\partial A^i}{\partial q^j} \vec{B}_i + A^i \frac{\partial \vec{B}_i}{\partial q^j} \\ &= \frac{\partial A^i}{\partial q^j} \vec{B}_i + A^i \Gamma^k_{ji} \vec{B}_k \end{aligned} \tag{A.27}$$

where Γ^k_{ji} is known as Christoffel symbols of the second kind satisfying

$$\frac{\partial \vec{B}_i}{\partial q^j} = \Gamma^k_{ji} \vec{B}_k \tag{A.28}$$

Dotting with $\vec{B}^l$,

$$\Gamma^k_{ji}\vec{B}_k \cdot \vec{B}^l = \Gamma^k_{ji}\delta^l_{\ k} = \Gamma^l_{ji} = \frac{\partial \vec{B}_i}{\partial q^j} \cdot \vec{B}^l = \frac{\partial^2 \vec{\ell}}{\partial q^j \partial q^i} \cdot \vec{B}^l \tag{A.29}$$

where

$$\vec{B}_i = \frac{\partial \vec{\ell}}{\partial q^i} \tag{A.30}$$

From Eq. (A.29), it is obvious

$$\Gamma^l_{ji} = \Gamma^l_{ij} \tag{A.31}$$

Interchanging the dummy indices i and k in Eq. (A.27),

$$\frac{\partial \vec{A}}{\partial q^j} = \left(\frac{\partial A^k}{\partial q^j} + A^i \Gamma^k_{ij} \right) \vec{B}_k \tag{A.32}$$

This parenthesized quantity is called as the covariant derivative of A^k and common expressions are

$$\nabla_j A^k \equiv A^k_{;j} \equiv \frac{\partial A^k}{\partial q^j} + A^i \Gamma^k_{ij} \tag{A.33}$$

On the other hand, the spatial derivatives of covariant vectors $\vec{A} = A_i \vec{B}^i$ are

$$\frac{\partial \vec{A}}{\partial q^j} = \frac{\partial A_i}{\partial q^j}\vec{B}^i + A_i \frac{\partial \vec{B}^i}{\partial q^j} \tag{A.34}$$

Using the dual basis relation,

$$\frac{\partial}{\partial q^j}\left(\vec{B}^i \cdot \vec{B}_i\right) = \frac{\partial}{\partial q^j}\delta^i_{\ k} = 0 \tag{A.35}$$

Also

$$\begin{aligned} \frac{\partial}{\partial q^j}\left(\vec{B}^i \cdot \vec{B}_i\right) &= \frac{\partial \vec{B}^i}{\partial q^j} \cdot \vec{B}_i + \vec{B}^i \cdot \Gamma^k_{ji}\vec{B}_k \\ &= \gamma^k_{ji}\vec{B}^k \cdot \vec{B}_i + \vec{B}^i \cdot \Gamma^k_{ji}\vec{B}_k \\ &= \gamma^k_{ji}\delta^k_{\ i} + \Gamma^k_{ji}\delta^i_{\ k} \end{aligned} \tag{A.36}$$

where

$$\frac{\partial \vec{B}^i}{\partial q^j} = \gamma^l_{ji}\vec{B}_l \tag{A.37}$$

Hence, Eq. (A.34) can be re-written as

$$\begin{aligned}\frac{\partial \vec{A}}{\partial q^j} &= \left(\frac{\partial A_k}{\partial q^j} + A_i \gamma^k_{ij}\right) \vec{B}^k \\ &= \left(\frac{\partial A_k}{\partial q^j} - A_i \Gamma^k_{ij}\right) \vec{B}^k\end{aligned} \tag{A.38}$$

Similar to Eq. (A.33), the parenthesized quantity is called as the covariant derivative of A_k and common expressions are

$$\nabla_j A_k \equiv A_{k;j} \equiv \frac{\partial A^k}{\partial q^j} - A^i \Gamma^k_{ij} \tag{A.39}$$

Christoffel symbols can also be expressed in terms of metric tensors. Considering the spatial derivative of Eq. (A.15),

$$\begin{aligned}\frac{\partial g_{ki}}{\partial q^j} &= \frac{\partial \vec{b}_k}{\partial q^j} \cdot \vec{b}_i + \vec{b}_k \cdot \frac{\partial \vec{b}_i}{\partial q^j} \\ &= \Gamma^l_{kj} \vec{b}_l \cdot \vec{b}_i + \vec{b}_k \cdot \Gamma^l_{ij} \vec{b}_l \\ &= \Gamma^l_{kj} g_{li} + \Gamma^l_{ij} g_{kl}\end{aligned} \tag{A.40}$$

Similarly,

$$\frac{\partial g_{jk}}{\partial q^i} = \Gamma^l_{ji} g_{lk} + \Gamma^l_{ki} g_{jl} \tag{A.41}$$

$$\frac{\partial g_{ij}}{\partial q^k} = \Gamma^l_{ik} g_{lj} + \Gamma^l_{jk} g_{il} \tag{A.42}$$

Eqs. (A.40), (A.41) and (A.42) lead Eq. (2.24)

$$\Gamma^l_{ij} \equiv \frac{1}{2} g^{lk} \left(\frac{\partial g_{jk}}{\partial q^i} + \frac{\partial g_{ki}}{\partial q^j} - \frac{\partial g_{ij}}{\partial q^k}\right) \tag{A.43}$$

where the half of parenthesized quantity is defined as the Christoffel symbols of the first kind Γ_{kij}

$$\Gamma_{kij} \equiv \frac{1}{2} \left(\frac{\partial g_{jk}}{\partial q^i} + \frac{\partial g_{ki}}{\partial q^j} - \frac{\partial g_{ij}}{\partial q^k}\right) \tag{A.44}$$

yielding

$$\Gamma^l_{ij} = g^{lk} \Gamma_{kij} \tag{A.45}$$

Appendix B

DERIVATIONS OF THE FLUID MODELS FOR PLASMA

B.1 5N-moment Multi-fluid Model

The multi-fluid model is derived by taking moments of Vlasov-Boltzmann equation. Vlasov-Boltzmann equation for species α is

$$\frac{\partial f_\alpha}{\partial t} + \vec{v} \cdot \frac{\partial f_\alpha}{\partial \vec{x}} + \frac{q_\alpha}{m_\alpha}\left(\vec{E} + \vec{v} \times \vec{B}\right) \cdot \frac{\partial f_\alpha}{\partial \vec{v}} = \left.\frac{\delta f_\alpha}{\delta t}\right|_{coll} \tag{B.1}$$

where $f_\alpha(t, \vec{x}, \vec{v})$ is the velocity distribution. The right hand side of Eq. (B.1) represents collisional interactions and binary collisions between incident particles α and background particles β can be expressed as

$$\left.\frac{\delta f_\alpha}{\delta t}\right|_{coll} = \sum_\beta C(f_\alpha, f_\beta) \tag{B.2}$$

Taking 0th moment,

$$\int \frac{\partial f_\alpha}{\partial t} d\vec{v} + \int \vec{v} \cdot \frac{\partial f_\alpha}{\partial \vec{x}} d\vec{v} + \int \frac{q_\alpha}{m_\alpha}\left(\vec{E} + \vec{v} \times \vec{B}\right) \cdot \frac{\partial f_\alpha}{\partial \vec{v}} d\vec{v} = \sum_\beta \int C(f_\alpha, f_\beta) d\vec{v} \tag{B.3}$$

which yields the continuity equation

$$\frac{\partial n_\alpha}{\partial t} + \nabla \cdot (n_\alpha \vec{u}_\alpha) = 0 \tag{B.4}$$

where number density n_α is defined as

$$n_\alpha \equiv \int f_\alpha d\vec{v} \tag{B.5}$$

and collisions are assumed not to create or destroy particles

$$\sum_\beta \int C(f_\alpha, f_\beta) d\vec{v} = 0 \tag{B.6}$$

The 1st moment is

$$\int \vec{v}\frac{\partial f_\alpha}{\partial t}d\vec{v} + \int \vec{v}\vec{v}\cdot\frac{\partial f_\alpha}{\partial \vec{x}}d\vec{v} + \int \vec{v}\frac{q_\alpha}{m_\alpha}\left(\vec{E}+\vec{v}\times\vec{B}\right)\cdot\frac{\partial f_\alpha}{\partial \vec{v}}d\vec{v} = \sum_\beta \int \vec{v}C(f_\alpha, f_\beta)d\vec{v} \tag{B.7}$$

which leads the momentum equation

$$\frac{\partial}{\partial t}(\rho_\alpha \vec{v}_\alpha) + \nabla\cdot(\rho_\alpha\vec{u}_\alpha\vec{u}_\alpha) + \nabla P_\alpha + \nabla\cdot\overset{\leftrightarrow}{\Pi}_\alpha - n_\alpha q_\alpha(\vec{E}+\vec{u}_\alpha\times\vec{B}) = \sum_{\beta\neq\alpha}\vec{R}_{\alpha\beta} \tag{B.8}$$

where ρ_α is mass density, P_α is isotropic scalar pressure, Π_α is Braginskii viscosity tensor, $\vec{w}$ is random velocity, and $\vec{R}_{\alpha\beta}$ is momentum change due to collisions

$$\rho_\alpha\vec{u}_\alpha \equiv \int \vec{v} f_\alpha d\vec{v} \tag{B.9}$$

$$P_\alpha \equiv \int \frac{m_\alpha w^2}{3} f_\alpha d\vec{v} \tag{B.10}$$

$$\overset{\leftrightarrow}{\Pi}_\alpha \equiv m_\alpha \int \left(\vec{w}\vec{w} - \frac{w^2}{3}\overset{\leftrightarrow}{I}\right) f_\alpha d\vec{v} \tag{B.11}$$

$$\vec{w} \equiv \vec{v} - \vec{u}_\alpha \tag{B.12}$$

$$\vec{R}_{\alpha\beta} \equiv m_\alpha \int \vec{w}C(f_\alpha, f_\beta)d\vec{v} \tag{B.13}$$

The 2nd moment is

$$\int \vec{v}\vec{v}\frac{\partial f_\alpha}{\partial t}d\vec{v} + \int \vec{v}\vec{v}\vec{v}\cdot\frac{\partial f_\alpha}{\partial \vec{x}}d\vec{v} + \int \vec{v}\vec{v}\frac{q_\alpha}{m_\alpha}\left(\vec{E}+\vec{v}\times\vec{B}\right)\cdot\frac{\partial f_\alpha}{\partial \vec{v}}d\vec{v} = \sum_\beta \int \vec{v}\vec{v}C(f_\alpha, f_\beta)d\vec{v} \tag{B.14}$$

Using the dyadic product $\frac{1}{2}m_\alpha\vec{v}\vec{v}$, the following energy equation for 13-moment multi-fluid model can be derived

$$\begin{aligned}\frac{\partial}{\partial t}\left(\frac{1}{\gamma-1}\overset{\leftrightarrow}{P}_\alpha + \frac{1}{2}\rho_\alpha\vec{u}_\alpha\vec{u}_\alpha\right) + \nabla\cdot\left[\left(\frac{1}{\gamma-1}\overset{\leftrightarrow}{P}_\alpha + \frac{1}{2}\rho_\alpha\vec{u}_\alpha\vec{u}_\alpha\right)\vec{u}_\alpha\right] + \nabla\cdot\overset{\leftrightarrow}{\vec{h}}_\alpha \\ - q_\alpha\left(n_\alpha\vec{E}\vec{u}_\alpha + \int f_\alpha(\vec{v}\times\vec{B})\vec{v}d\vec{v}\right) = \sum_{\beta\neq\alpha}(\vec{u}_\alpha\vec{R}_{\alpha\beta} + \overset{\leftrightarrow}{Q}_{\alpha\beta})\end{aligned} \tag{B.15}$$

The dot product $\frac{1}{2}m_\alpha\vec{v}\cdot\vec{v}$ yields $5N$-moment multi-fluid model

$$\begin{aligned}\frac{\partial}{\partial t}\left(\frac{1}{\gamma-1}P_\alpha + \frac{1}{2}\rho_\alpha u_\alpha^2\right) + \nabla\cdot\left[\left(\frac{1}{\gamma-1}P_\alpha + \frac{1}{2}\rho_\alpha u_\alpha^2\right)\vec{u}_\alpha\right] + \nabla\cdot(\vec{u}_\alpha\cdot\overset{\leftrightarrow}{P}_\alpha) + \nabla\cdot\vec{h}_\alpha \\ - q_\alpha n_\alpha\vec{u}_\alpha\cdot\vec{E} = \sum_{\beta\neq\alpha}(\vec{u}_\alpha\cdot\vec{R}_{\alpha\beta} + Q_{\alpha\beta})\end{aligned} \tag{B.16}$$

where $\overset{\leftrightarrow}{P}_\alpha$ is pressure tensor, $\overset{\overset{\rightarrow}{\leftrightarrow}}{h}$ and $\vec{h}$ are third-rank and first-rank heat flux tensor, $\overset{\leftrightarrow}{Q}_{\alpha\beta}$ and $Q_{\alpha\beta}$ are heat generations,

$$\overset{\leftrightarrow}{P}_\alpha \equiv \int \vec{w}\vec{w} f_\alpha d\vec{v} = P_\alpha \overset{\leftrightarrow}{I} + \overset{\leftrightarrow}{\Pi} \tag{B.17}$$

$$\overset{\overset{\rightarrow}{\leftrightarrow}}{h}_\alpha \equiv \frac{1}{2} m_\alpha \int \vec{w}\vec{w}\vec{w} f_\alpha d\vec{v} \tag{B.18}$$

$$\vec{h}_\alpha \equiv \frac{1}{2} m_\alpha \int w^2 \vec{w} f_\alpha d\vec{v} \tag{B.19}$$

$$\overset{\leftrightarrow}{Q}_{\alpha\beta} \equiv \frac{1}{2} m_\alpha \int \vec{w}\vec{w} C_{\alpha\beta} d\vec{v} \tag{B.20}$$

$$Q_{\alpha\beta} \equiv \frac{1}{2} m_\alpha \int w^2 C_{\alpha\beta} d\vec{v} \tag{B.21}$$

In WARPXM, the fluid total energy is defined as

$$\epsilon_\alpha \equiv \frac{1}{\gamma - 1} P_\alpha + \frac{1}{2} \rho_\alpha u_\alpha^2 \tag{B.22}$$

which simplifies the energy equation in the $5N$-moment multi-fluid model as the summation of the thermal energy and fluid kinetic energy

$$\begin{aligned} \frac{\partial \epsilon_\alpha}{\partial t} + \nabla \cdot \left[\left(\epsilon_\alpha + P_\alpha \right) \vec{u}_\alpha + (\vec{u}_\alpha \cdot \overset{\leftrightarrow}{\Pi}_\alpha) \right] + \nabla \cdot \vec{h}_\alpha - q_\alpha n_\alpha \vec{u}_\alpha \cdot \vec{E} \\ = \sum_{\beta \neq \alpha} (\vec{u}_\alpha \cdot \vec{R}_{\alpha\beta} + Q_{\alpha\beta}) \end{aligned} \tag{B.23}$$

Appendix C

DERIVATIONS OF BRAGINSKII TRANSPORT EQUATIONS

C.1 Chapman-Enskog Expansion

Considering the effect of collisional interactions in Vlasov-Boltzmann equation, Eq. (B.1), there are three characteristic normalized parameters

$$\frac{\frac{\partial f_\alpha}{\partial t}}{\left.\frac{\delta f_\alpha}{\delta t}\right|_{coll}} \sim \frac{\frac{f}{\tau}}{\frac{f}{\tau_{\alpha\beta}}} = \frac{\tau_{\alpha\beta}}{\tau} = \epsilon_t \tag{C.1}$$

$$\frac{\vec{v}\cdot\frac{\partial f_\alpha}{\partial \vec{x}}}{\left.\frac{\delta f_\alpha}{\delta t}\right|_{coll}} \sim \frac{v\frac{f}{L}}{\frac{f}{\tau_{\alpha\beta}}} = \frac{\lambda_{mfp}}{L} = \epsilon_L \tag{C.2}$$

$$\frac{\frac{q_\alpha}{m_\alpha}\vec{E}\cdot\frac{\partial f_\alpha}{\partial \vec{v}}}{\left.\frac{\delta f_\alpha}{\delta t}\right|_{coll}} \sim \frac{\frac{q}{m}E\frac{f}{v}}{\frac{f}{\tau_{\alpha\beta}}} = \frac{E}{\frac{mv_{th}}{q\tau_{\alpha\beta}}} = \frac{E}{E_D} = \epsilon_E \tag{C.3}$$

$$\frac{\frac{q_\alpha}{m_\alpha}\vec{v}\times\vec{B}\cdot\frac{\partial f_\alpha}{\partial \vec{v}}}{\left.\frac{\delta f_\alpha}{\delta t}\right|_{coll}} \sim \frac{\frac{qB}{m}f}{\frac{f}{\tau_{\alpha\beta}}} = \omega_c\tau_{\alpha\beta} = \epsilon_B \tag{C.4}$$

where both ϵ_t and ϵ_L indicate the scale of collisionality, E_D is known as Dreicer electric field, which is a critical electric field for runaway electrons, and ϵ_B represents the effect of magnetization. Thereby, the normalized Vlasov-Boltzmann equation can be written as

$$\frac{df_\alpha}{dt} = \frac{\partial f_\alpha}{\partial t} + \vec{v}\cdot\frac{\partial f_\alpha}{\partial \vec{x}} + \frac{q_\alpha}{m_\alpha}\left(\vec{E}+\vec{v}\times\vec{B}\right)\cdot\frac{\partial f_\alpha}{\partial \vec{v}} = \frac{1}{\epsilon}\left.\frac{\delta f_\alpha}{\delta t}\right|_{coll} \tag{C.5}$$

where ϵ has the order of $\epsilon \sim \epsilon_t \sim \epsilon_L \sim \epsilon_E \sim \epsilon_B$. Assuming $\epsilon \ll 1$ in a weakly magnetized plasma, the distribution function f_α can be expanded as

$$f_\alpha \simeq f_{\alpha 0} + f_{\alpha 1} + f_{\alpha 2} + \cdots \tag{C.6}$$

where the subscript denotes the order of ϵ. The linearized collision operator is

$$\begin{aligned}\left.\frac{\delta f_\alpha}{\delta t}\right|_{coll} &= \sum_\beta C(f_\alpha, f_\beta) \\ &\simeq \sum_\beta \left[C(f_{\alpha0}, f_{\beta0}) + C(f_{\alpha0}, f_{\beta1}) + C(f_{\alpha1}, f_{\beta0}) + C(f_{\alpha1}, f_{\beta1}) + \cdots\right]\end{aligned} \tag{C.7}$$

Hence, Vlasov-Boltzmann equation can be expanded order by order

$$\begin{aligned} &\epsilon^{-1} \text{ order:} && 0 = \sum_\beta C(f_{\alpha0}, f_{\beta0}) \\ &\epsilon^{0} \text{ order:} && \frac{df_{\alpha0}}{dt} = \sum_\beta \left[C(f_{\alpha0}, f_{\beta1}) + C(f_{\alpha1}, f_{\beta0})\right] \\ &\epsilon^{1} \text{ order:} && \frac{df_{\alpha1}}{dt} = \sum_\beta \left[C(f_{\alpha1}, f_{\beta1}) + C(f_{\alpha2}, f_{\beta0}) + \cdots\right] \\ &\quad\vdots && \vdots \end{aligned}$$

These expansions are known as Chapman-Enskog expansion[87]. From Boltzmann H theorem, it is known that Maxwellian distributions $f_{M\alpha}$ with a state of thermodynamic equilibrium, where temperature satisfies $\vec{u}_\alpha = \vec{u}_\beta$ and $T_\alpha = T_\beta$, become the solution of the ϵ^{-1} order of the equation.

$$f_{\alpha0}(t, \vec{x}, \vec{v}) = n_\alpha(\vec{x}, t) \left(\frac{m}{2\pi T_\alpha(\vec{x}, t)}\right)^{\frac{3}{2}} e^{-\frac{m|\vec{v}-\vec{u}_\alpha(\vec{x},t)|^2}{2T_\alpha(\vec{x},t)}} \tag{C.8}$$

In a strongly magnetized plasma, $\epsilon_B \gg 1$,

$$\begin{aligned} &\epsilon^{-1} \text{ order:} && \omega_c(\vec{v}\times\hat{b})\cdot\frac{\partial f_{\alpha0}}{\partial \vec{v}} = \sum_\beta C(f_{\alpha0}, f_{\beta0}) \\ &\epsilon^{0} \text{ order:} && \frac{\partial f_{\alpha0}}{\partial t} + \vec{v}\cdot\frac{\partial f_{\alpha0}}{\partial \vec{x}} + \frac{q_\alpha}{m_\alpha}\vec{E}\cdot\frac{\partial f_{\alpha0}}{\partial \vec{v}} + \omega_c(\vec{v}\times\hat{b})\cdot\frac{\partial f_{\alpha1}}{\partial \vec{v}} = \sum_\beta \left[C(f_{\alpha0}, f_{\beta1}) + C(f_{\alpha1}, f_{\beta0})\right] \\ &\quad\vdots && \vdots \end{aligned}$$

Note that the non-drifting Maxwellian distribution in the frame moving with the background fluid velocity $\vec{u}_\beta$ is still the solution of the ϵ^{-1} order of the equation.

$$\omega_c(\vec{v}\times\hat{b})\cdot\frac{\partial f_{\alpha0}}{\partial \vec{v}} = \omega_c(\vec{v}\times\hat{b})\cdot\frac{m_\alpha(\vec{u}_\alpha - \vec{u}_\beta)}{T_\alpha} f_{\alpha0} = 0 = \sum_\beta C(f_{\alpha0}, f_{\beta0}) \tag{C.9}$$

Considering the total derivative of the Maxwellian distribution function,

$$\frac{df_{\alpha 0}}{dt} = \frac{\partial f_{\alpha 0}}{\partial t} + \vec{v} \cdot \frac{\partial f_{\alpha 0}}{\partial \vec{x}} + \frac{q_\alpha}{m_\alpha} \left(\vec{E} + \vec{v} \times \vec{B} \right) \cdot \frac{\partial f_{\alpha 0}}{\partial \vec{v}} \tag{C.10}$$

Using the chain rule,

$$\frac{\partial f_{\alpha 0}}{\partial t} = \frac{\partial f_{\alpha 0}}{\partial n_\alpha} \frac{\partial n_\alpha}{\partial t} + \frac{\partial f_{\alpha 0}}{\partial \vec{u}_\alpha} \cdot \frac{\partial \vec{u}_\alpha}{\partial t} + \frac{\partial f_{\alpha 0}}{\partial T_\alpha} \frac{\partial T_\alpha}{\partial t} \tag{C.11}$$

$$\vec{v} \cdot \frac{\partial f_{\alpha 0}}{\partial \vec{x}} = \vec{v} \cdot \left(\frac{\partial f_{\alpha 0}}{\partial n_\alpha} \frac{\partial n_\alpha}{\partial \vec{x}} + \frac{\partial f_{\alpha 0}}{\partial \vec{u}_\alpha} \cdot \frac{\partial \vec{u}_\alpha}{\partial \vec{x}} + \frac{\partial f_{\alpha 0}}{\partial T_\alpha} \frac{\partial T_\alpha}{\partial \vec{x}} \right) \tag{C.12}$$

$$\frac{q_\alpha}{m_\alpha} \left(\vec{E} + \vec{v} \times \vec{B} \right) \cdot \frac{\partial f_{\alpha 0}}{\partial \vec{v}} = \frac{q_\alpha}{m_\alpha} \left(\vec{E} + \vec{v} \times \vec{B} \right) \cdot \left[-\frac{m \left(\vec{v} - \vec{u}_\alpha \right)}{T_\alpha} f_{\alpha 0} \right] \tag{C.13}$$

Since $f_{\alpha 0}$ is Maxwellian,

$$\frac{\partial f_{\alpha 0}}{\partial n_\alpha} = \frac{1}{n_\alpha} f_{\alpha 0} \tag{C.14}$$

$$\frac{\partial f_{\alpha 0}}{\partial \vec{u}_\alpha} \cdot \frac{\partial \vec{u}_\alpha}{\partial \vec{x}} = \frac{m_\alpha}{2T_\alpha} \vec{w} \cdot \left[\nabla \vec{u}_\alpha + \left(\nabla \vec{u}_\alpha \right)^{\mathrm{T}} \right] \tag{C.15}$$

$$\frac{\partial f_{\alpha 0}}{\partial T_\alpha} = \left(\frac{m_\alpha w_\alpha^2}{2T_\alpha} - \frac{3}{2} \right) \frac{f_{\alpha 0}}{T_\alpha} \tag{C.16}$$

where $\vec{w}$ is random velocity of alpha

$$\vec{w} = \vec{v} - \vec{u}_\alpha \tag{C.17}$$

Also, Maxwellian $f_{\alpha 0}$ allows to use the ideal $5N$-moment fluid equations such that

$$\frac{\partial n_\alpha}{\partial t} = -\nabla \cdot \left(n_\alpha \vec{u}_\alpha \right) = -\vec{u}_\alpha \cdot \nabla n_\alpha - n_\alpha \left(\nabla \cdot \vec{u}_\alpha \right) \tag{C.18}$$

$$\frac{\partial \vec{u}_\alpha}{\partial t} = -\left(\vec{u}_\alpha \cdot \nabla \right) \vec{u}_\alpha - \frac{\nabla P_\alpha}{m_\alpha} + \frac{q_\alpha}{m_\alpha} \left(\vec{E} + \vec{u}_\alpha \times \vec{B} \right) \tag{C.19}$$

$$\frac{\partial T_\alpha}{\partial t} = -\vec{u}_\alpha \cdot \nabla T_\alpha + \frac{2}{3} T_\alpha \left(\nabla \cdot \vec{u}_\alpha \right) \tag{C.20}$$

Collecting together all components for the total derivative of Maxwellian, $df_{\alpha 0}/dt$,

$$\frac{df_{\alpha 0}}{dt} = f_{\alpha 0} \left\{ \left(\frac{m_\alpha w^2}{2T_\alpha} - \frac{5}{2} \right) \vec{w} \cdot \frac{1}{T_\alpha} \nabla T_\alpha + \frac{m_\alpha}{2T_\alpha} \left(\vec{w}\vec{w} - \frac{w^2}{3} \overset{\leftrightarrow}{I} \right) : \left[\nabla \vec{u}_\alpha + \left(\nabla \vec{u}_\alpha \right)^{\mathrm{T}} \right] \right\} \tag{C.21}$$

Notice that the first and second terms represent heat flux and viscosity tensor, respectively. Since the Vlasov-Boltzmann equation can be expressed in terms of the total derivatives of Maxwellian distribution and off-Maxwellian part f_α^ℓ such that

$$\frac{df_\alpha}{dt} = \frac{df_{\alpha 0}}{dt} + \frac{df_\alpha^\ell}{dt} = \sum_\beta C(f_\alpha, f_\beta) \tag{C.22}$$

, the heat flux and viscosity are found to be related with the off-Maxwellian part (thermodynamic non-equilibrium condition) and collisional interactions

$$\begin{aligned} \frac{df_\alpha^\ell}{dt} - \sum_\beta C(f_\alpha, f_\beta) &= -\frac{df_{\alpha 0}}{dt} \\ &= -f_{\alpha 0}\left\{\left(\frac{m_\alpha w^2}{2T_\alpha} - \frac{5}{2}\right)\vec{w}\cdot\frac{1}{T_\alpha}\nabla T_\alpha + \frac{m_\alpha}{2T_\alpha}\left(\vec{w}\vec{w} - \frac{w^2}{3}\overset{\leftrightarrow}{I}\right) : \left[\nabla\vec{u}_\alpha + (\nabla\vec{u}_\alpha)^{\mathrm{T}}\right]\right\} \end{aligned} \tag{C.23}$$

C.2 Expansion of the Distributions around Maxwellian in terms of Legendre and Laguerre Polynomials

In the velocity space using spherical coordinates $\vec{v} = (v, \theta, \phi)$, the distribution function f can be expanded around the Maxwellian f_0[62]

$$\begin{aligned} f(\vec{v}) = f(v,\theta,\phi) &= f_0(v)\,(1+\mathcal{X}) \\ &= f_0 \sum_{l=0}^{\infty}\sum_{m=-l}^{l} b_l^{(m)} Y_l^{(m)}(\theta,\phi) \sum_{i=0}^{\infty} a_i^{(l+\frac{1}{2})} L_i^{(l+\frac{1}{2})}\left(\frac{w^2}{v_{th}^2}\right) \end{aligned} \tag{C.24}$$

where $\vec{w} = \vec{v} - \vec{u}$ is random velocity, $Y_l^{(m)}$ is spherical harmonics and $L_i^{(l+\frac{1}{2})}$ is the associated Laguerre polynomials, which is also known as Sonine polynomials. Using a real basis of spherical harmonics Y_{lm}[61],

$$f(v,\theta,\phi) = f_0 \sum_{l=0}^{\infty}\sum_{m=-l}^{l} b_{lm} Y_{lm}(\theta,\phi) \sum_{i=0}^{\infty} a_i^{(l+\frac{1}{2})} L_i^{(l+\frac{1}{2})}\left(\frac{w^2}{v_{th}^2}\right) \tag{C.25}$$

where

$$Y_l^{(m)}(\theta,\phi) = \sqrt{\frac{2l+1}{4\pi}\frac{(l-m)!}{(l+m)!}}P_l^{(m)}(cos\theta)e^{im\phi} \tag{C.26}$$

$$Y_{lm}(\theta,\phi)=\sqrt{\frac{2l+1}{4\pi}\frac{(l-|m|)!}{(l+|m|)!}}P_l^{(m)}(cos\theta)e^{im\phi} \tag{C.27}$$

and $P_l^{(m)}$ is the associated Legendre polynomials. Considering $l=0,1,2,\cdots$,

$$\begin{aligned}f(v,\theta,\phi)=f_0\Bigg[&b_{00}Y_{00}\sum_{i=0}^{\infty}a_i^{(\frac{1}{2})}L_i^{(\frac{1}{2})}+\sum_{m=-1}^{1}\vec{Y}_{1m}\cdot\vec{b}_{1m}\sum_{i=0}^{\infty}a_i^{(\frac{3}{2})}L_i^{(\frac{3}{2})}+\\&\sum_{m=-2}^{2}\overset{\leftrightarrow}{Y}_{2m}:\overset{\leftrightarrow}{b}_{2m}\sum_{i=0}^{\infty}a_i^{(\frac{5}{2})}L_i^{(\frac{5}{2})}+\cdots\Bigg]\end{aligned} \tag{C.28}$$

This form of the expression is useful due to the orthogonality of polynomials in the moment approach. Note that Grad[88] and Balescu[62] expanded the distribution in terms of Hermite polynomials. Showing more explicit and useful expressions,

$$\begin{aligned}f(v,\theta,\phi)=f_0\Bigg[&\left(N_0L_0^{(\frac{1}{2})}+N_1L_1^{(\frac{1}{2})}+\cdots\right)\\&+2\frac{\vec{w}}{v_{th}^2}\cdot\left(\vec{U}_0L_0^{(\frac{3}{2})}+\vec{U}_1L_1^{(\frac{3}{2})}+\cdots\right)\\&+\frac{12}{5}\frac{\vec{w}\vec{w}-\frac{w^2}{3}\overset{\leftrightarrow}{I}}{nmv_{th}^4}:\left(\overset{\leftrightarrow}{P}_0L_0^{(\frac{5}{2})}+\overset{\leftrightarrow}{P}_1L_1^{(\frac{5}{2})}+\cdots\right)+\cdots\Bigg]\end{aligned} \tag{C.29}$$

where the coefficients N_i, $\vec{U}_i$, and $\overset{\leftrightarrow}{P}_i$ can be obtained by taking moments. For example, considering 0th moment,

$$\int fd^3v\equiv n \tag{C.30}$$

Using the expanded function, the 0th moment becomes

$$\begin{aligned}\int fd^3v=\int Y_{00}L_0^{(\frac{1}{2})}fd^3w&=4\pi\int w^2f_0L_0^{(\frac{1}{2})}\left(N_0L_0^{(\frac{1}{2})}+N_1L_1^{(\frac{1}{2})}+\cdots\right)dw\\&=4\pi\frac{n}{\pi^{\frac{3}{2}}v_{th}^3}N_0\int e^{-X}L_0^{(\frac{1}{2})}L_0^{(\frac{1}{2})}\frac{1}{2}X^{\frac{1}{2}}v_{th}^3dX\\&=nN_0\end{aligned} \tag{C.31}$$

where $X \equiv w^2/v_{th}^2$. Thus, $N_0 = 1$. Similarly, taking a moment with $L_1^{(\frac{1}{2})}$

$$\begin{aligned}
\int L_1^{(\frac{1}{2})} f d^3v &= \int \left(\frac{3}{2} - \frac{mw^2}{2T}\right) f d^3v \\
&= \frac{3}{2}n - \frac{3}{2T}\int \frac{mw^2}{3} f d^3v \\
&= \frac{3}{2}\left(n - \frac{P}{T}\right) = 0
\end{aligned} \tag{C.32}$$

Using the expanded function,

$$\begin{aligned}
\int L_1^{(\frac{1}{2})} f d^3v = \int Y_{00} L_1^{(\frac{1}{2})} f d^3w &= 4\pi \int w^2 f_0 L_1^{(\frac{1}{2})} \left(N_0 L_0^{(\frac{1}{2})} + N_1 L_1^{(\frac{1}{2})} + \cdots\right) dw \\
&= \frac{2}{\sqrt{\pi}} n N_1 \int L_1^{(\frac{1}{2})} L_1^{(\frac{1}{2})} X^{\frac{1}{2}} e^{-X} dX \\
&= \frac{3}{2} n N_1 = 0
\end{aligned} \tag{C.33}$$

that leads $N_1 = 0$. The moment with the random velocity is simply

$$\int m\vec{w} f d^3v = 0 \tag{C.34}$$

Since $\vec{w} \propto \vec{Y}_{1m}$[61], the only diagonal terms of $\vec{w}\vec{w}$ tensor, $w_x^2 = w_y^2 = w_z^2 = w^2/3$, contribute from spherical harmonics such that

$$\begin{aligned}
\int m Y_{1m} L_0^{(\frac{3}{2})} f d^3v &= 4\pi m \int f_0 L_0^{(\frac{3}{2})} \frac{2\frac{w^2}{3}}{v_{th}^2} \overset{\leftrightarrow}{I} \cdot \left(\vec{U}_0 L_0^{(\frac{3}{2})} + \vec{U}_1 L_1^{(\frac{3}{2})} + \cdots\right) w^2 dw \\
&= \frac{4}{3\sqrt{\pi}} nm\vec{U}_0 \cdot \overset{\leftrightarrow}{I} \int \frac{w^2}{v_{th}^2} L_0^{(\frac{3}{2})} L_0^{(\frac{3}{2})} e^{-X} X^{\frac{1}{2}} dX \\
&= \frac{4}{3\sqrt{\pi}} nm\vec{U}_0 \cdot \overset{\leftrightarrow}{I} \int X^{\frac{3}{2}} L_0^{(\frac{3}{2})} L_0^{(\frac{3}{2})} e^{-X} dX \\
&= nm\vec{U}_0 = 0
\end{aligned} \tag{C.35}$$

Thus, $\vec{U}_0 = 0$. Taking a moment with $L_1^{(\frac{3}{2})}$,

$$\begin{aligned}
\int \vec{w} L_1^{(\frac{3}{2})} f d^3v &= \int \vec{w} \left(\frac{3}{2} - \frac{mw^2}{2T}\right) f d^3v \\
&= -\frac{1}{T}\int \frac{1}{2} m w^2 \vec{w} f d^3v \\
&= -\frac{1}{T}\vec{h}
\end{aligned} \tag{C.36}$$

where $\vec{h}$ is heat flux. Using the expanded distribution,

$$\begin{aligned}\int Y_{1m} L_1^{(\frac{3}{2})} f d^3v &= 4\pi \int f_0 L_1^{(\frac{3}{2})} \frac{2\frac{w^2}{3}}{v_{th}^2} \overset{\leftrightarrow}{I} \cdot \left(\vec{U}_0 L_0^{(\frac{3}{2})} + \vec{U}_1 L_1^{(\frac{3}{2})} + \cdots\right) w^2 dw \\ &= \frac{4}{3\sqrt{\pi}} n\vec{U}_1 \cdot \overset{\leftrightarrow}{I} \int X^{\frac{3}{2}} L_1^{(\frac{3}{2})} L_1^{(\frac{3}{2})} e^{-X} dX \\ &= \frac{5}{2} n\vec{U}_1\end{aligned} \tag{C.37}$$

Hence,

$$\vec{U}_1 = -\frac{2}{5nT}\vec{h} \tag{C.38}$$

The viscosity stress tensor $\overset{\leftrightarrow}{\Pi}$ can be obtained by

$$\overset{\leftrightarrow}{\Pi} = \int m \left(\vec{w}\vec{w} - \frac{w^2}{3}\overset{\leftrightarrow}{I}\right) f d^3v \tag{C.39}$$

Since $Y_{2m} \propto \vec{w}\vec{w} - \frac{w^2}{3}\overset{\leftrightarrow}{I}$, the only off-diagonal terms of Y_{2m} where $m = (-2, -1, 1)$ and $(w_x w_y, w_y w_z, w_x w_z)$ contribute

$$\begin{aligned}\int m Y_{sm} L_0^{(\frac{5}{2})} f d^3v &= \frac{4}{\sqrt{\pi}} \frac{6}{5} \int L_0^{(\frac{5}{2})} \frac{w_x^2 w_y^2}{v_{th}^4} \overset{\leftrightarrow}{P}_0 L_0^{(\frac{5}{2})} e^{-X} X^{\frac{1}{2}} dX \\ &= \frac{4}{\sqrt{\pi}} \frac{6}{5} \overset{\leftrightarrow}{P}_0 \int \frac{1}{9} \frac{w^4}{v_{th}^4} L_0^{(\frac{5}{2})} L_0^{(\frac{5}{2})} e^{-X} X^{\frac{1}{2}} dX \\ &= \frac{8}{15\sqrt{\pi}} \overset{\leftrightarrow}{P}_0 \int X^{\frac{5}{2}} L_0^{(\frac{5}{2})} L_0^{(\frac{5}{2})} e^{-X} X^{\frac{1}{2}} dX \\ &= \overset{\leftrightarrow}{P}_0 = \overset{\leftrightarrow}{\Pi}\end{aligned} \tag{C.40}$$

The other coefficients are related with higher moments or higher order of spherical harmonics and Laguerre polynomials. For $5N$-moment fluid model, it is enough to consider

$$f(v,\theta,\phi) \simeq f_0 \left[1 + 2\frac{\vec{w}}{v_{th}^2} \cdot \left(-\frac{2}{5nT}\vec{h} L_1^{(\frac{3}{2})}\right) + \frac{12}{5} \frac{\vec{w}\vec{w} - \frac{w^2}{3}\overset{\leftrightarrow}{I}}{nmv_{th}^4} : \overset{\leftrightarrow}{\Pi}\right] \tag{C.41}$$

Applying Taylor expansion of Maxwellian distribution with $w \ll v_{th}$,

$$f(v,\theta,\phi) \simeq \tilde{f}_0 \left[1 + 2\frac{\vec{v}}{v_{th}^2} \cdot \left(\vec{u} - \frac{2}{5nT}\vec{h} L_1^{(\frac{3}{2})}\right) + \frac{12}{5} \frac{\vec{v}\vec{v} - \frac{v^2}{3}\overset{\leftrightarrow}{I}}{nmv_{th}^4} : \overset{\leftrightarrow}{\Pi}\right] \tag{C.42}$$

where the distribution function now is expanded around the non-shifted Maxwellian distribution $\tilde{f}_0$

$$\tilde{f}_0 = n\left(\frac{m}{2\pi T}\right)^{\frac{3}{2}} e^{-\frac{mv^2}{2T}} \tag{C.43}$$

C.3 Approximated Fokker-Planck Collision Operator for Coulomb Scattering with the Assumption of Small Mass Ratio

The Fokker-Planck collision operator can be expressed in terms of Rosenbluth potentials $H_\beta(\vec{v})$ and $G_\beta(\vec{v})$

$$\begin{aligned} C(f_\alpha, f_\beta) &= -\frac{\partial}{\partial \vec{v}} \cdot \left(f \frac{< \Delta\vec{v} >}{\Delta t} \right) + \frac{1}{2} \frac{\partial^2}{\partial \vec{v} \partial \vec{v}} : \left(f \frac{< \Delta\vec{v}\Delta\vec{v} >}{\Delta t} \right) \\ &= -\frac{\partial}{\partial \vec{v}} \cdot \left\{ \Gamma_{\alpha\beta} \left[\frac{m_\alpha}{m_\alpha + m_\beta} f_\alpha \frac{\partial H_\beta}{\partial \vec{v}} - \frac{1}{2} \frac{\partial f_\alpha}{\partial \vec{v}} \cdot \frac{\partial^2 G_\beta}{\partial \vec{v} \partial \vec{v}} \right] \right\} \end{aligned} \tag{C.44}$$

where the first term is for momentum loss and the second term is for temperature (or energy) diffusion such that

$$\frac{< \Delta\vec{v} >}{\Delta t} = \Gamma_{\alpha\beta} \frac{\partial H_\beta}{\partial \vec{v}} \tag{C.45}$$

$$\frac{< \Delta\vec{v}\Delta\vec{v} >}{\Delta t} = \Gamma_{\alpha\beta} \frac{\partial^2 G_\beta}{\partial \vec{v} \partial \vec{v}} \tag{C.46}$$

$$H_\beta(\vec{v}) = \left(1 + \frac{m_\alpha}{m_\beta} \right) \int \frac{f_\beta(\vec{v}_\beta)}{|\vec{v} - \vec{v}_\beta|} d^3 v_\beta \tag{C.47}$$

$$G_\beta(\vec{v}) = \int f_\beta(\vec{v}_\beta) \, |\vec{v} - \vec{v}_\beta| \, d^3 v_\beta \tag{C.48}$$

$$\Gamma_{\alpha\beta} \equiv \frac{4\pi q_\alpha^2 q_\beta^2 \ln \Lambda}{(4\pi\epsilon_0)^2 m_\alpha^2} \tag{C.49}$$

Considering the linearized collision operator by using the linearized distributions around the non-shifted Maxwellian distributions,

$$C(f_\alpha, f_\beta) \simeq C(\tilde{f}_{\alpha 0}, \tilde{f}_{\beta 0}) + C^\ell_{\alpha\beta} \tag{C.50}$$

where the first term becomes zero only if $T_\alpha = T_\beta$. Assuming the small mass ratio (e.g., electron-ion collision), $m_\alpha/m_\beta \ll 1$, the first term in Eq. (C.44) involving H_β becomes negligible. According to Hinton[89], the second term can be evaluated as

$$\frac{\partial^2 G_\beta}{\partial \vec{v} \partial \vec{v}} \simeq n_\beta \frac{w_\beta^2 \overset{\leftrightarrow}{I} - \vec{w}_\beta \vec{w}_\beta}{w_\beta^3} \tag{C.51}$$

where the following approximation is applied for the relative velocity $\vec{v} - \vec{v}'$

$$|\vec{v} - \vec{v}'| \simeq |\vec{v} - \vec{u}_\beta| = w_\beta \tag{C.52}$$

Hence, the collision operator in the frame moving with the background fluid velocity $\vec{u}_\beta$ becomes

$$C(f_\alpha, f_\beta) \simeq \frac{1}{2} n_\beta \Gamma_{\alpha\beta} \frac{\partial}{\partial \vec{w}_\beta} \cdot \left[\frac{w_\beta^2 \overleftrightarrow{I} - \vec{w}_\beta \vec{w}_\beta}{w_\beta^3} \cdot \frac{\partial f_\alpha}{\partial \vec{w}_\beta} \right] \tag{C.53}$$

Assuming $u_\beta / v_{th\alpha} \ll 1$, the linearized collision operator with the first order terms can be written as

$$\begin{aligned} C(f_\alpha, f_\beta) &\simeq C^\ell(f_{\alpha 1}, \tilde{f}_{\beta 0}) + C^\ell(\tilde{f}_{\alpha 0}, f_{\beta 1}) \\ &= \frac{1}{2} \frac{n_\beta \Gamma_{\alpha\beta}}{v^3} \left[\frac{\partial}{\partial \vec{v}} \cdot \left(v^2 \overleftrightarrow{I} - \vec{v}\vec{v} \right) \cdot \frac{\partial f_{\alpha 1}}{\partial \vec{v}} + \frac{\vec{v} \cdot \vec{u}_\beta}{v_{th\alpha}^2} \tilde{f}_{\alpha 0} \right] \end{aligned} \tag{C.54}$$

As for the opposite interspecies collision (e.g., ion-electron collision), since the first term in Eq. (C.44) involving H_β is not negligible, the zeroth order term becomes negligible for small mass ratio $m_\alpha \ll m_\beta$ or identical temperature $T_\alpha = T_\beta$.

$$C(\tilde{f}_{\beta 0}, \tilde{f}_{\alpha 0}) = \frac{1}{\tau_{\alpha\beta}} \frac{n_\alpha m_\alpha}{n_\beta m_\beta} \left(1 - \frac{T_\alpha}{T_\beta} \right) \frac{\partial}{\partial \vec{v}} \cdot \left(\vec{v} \tilde{f}_{\beta 0} \right) \tag{C.55}$$

$$C_{\beta\alpha}^\ell \simeq \frac{1}{n_\beta m_\beta} \left(\vec{R}_{\alpha\beta} - \frac{n_\alpha m_\alpha \vec{u}_\beta}{\tau_{\alpha\beta}} \right) \cdot \frac{\partial \tilde{f}_{\beta 0}}{\partial \vec{v}} + \frac{n_\alpha m_\alpha}{n_\beta m_\beta \tau_{\alpha\beta}} \frac{\partial}{\partial \vec{v}} \cdot \left(\vec{v} f_{\beta 1} + \frac{T_\alpha}{m_\alpha} \frac{\partial f_{\beta 1}}{\partial \vec{v}} \right) \tag{C.56}$$

where $\tau_{\alpha\beta}$ is the momentum transfer time (slowing-down period)

$$\tau_{\alpha\beta} = \frac{4}{3\sqrt{\pi}} \frac{n_\beta \Gamma_{\alpha\beta}}{\left(v_{th\alpha}^2 + v_{th\beta}^2 \right)^{\frac{3}{2}}} \left(1 + \frac{m_\alpha}{m_\beta} \right) \tag{C.57}$$

and $\vec{R}_{\alpha\beta}$ is the momentum transfer rate obtained by taking the first moment of the linearized collision operator

$$\vec{R}_{\alpha\beta} \equiv \int m_\alpha \vec{v} C(f_\alpha, f_\beta) d^3 v = \frac{n_\alpha m_\alpha}{\tau_{\alpha\beta}} \vec{u}_\beta - n_\beta m_\alpha \Gamma_{\alpha\beta} \int \frac{\vec{v}}{v^3} f_{\alpha 1} d^3 v \tag{C.58}$$

C.4 Transport Coefficients Obtained by Taking Moments

Taking the first moment of ϵ_0 order equation for electrons in steady state $\partial f_e/\partial t = 0$ with different orders of associated Laguerre polynomials,

$$
\begin{aligned}
\int m_e \vec{v} \frac{d\tilde{f}_{e0}}{dt} \begin{bmatrix} L_0^{(\frac{3}{2})} \\ L_1^{(\frac{3}{2})} \\ L_2^{(\frac{3}{2})} \end{bmatrix} = \begin{bmatrix} \nabla P_e - n_e q_e \vec{E} \\ -\frac{5}{2} n_e \nabla T_e \\ 0 \end{bmatrix} \\
= \int m_e \vec{v} C_{ei}^{\ell} \begin{bmatrix} L_0^{(\frac{3}{2})} \\ L_1^{(\frac{3}{2})} \\ L_2^{(\frac{3}{2})} \end{bmatrix} d^3v + n_e q_e \begin{bmatrix} \vec{U}_{e0} \times \vec{B} \\ \frac{5}{2}\vec{U}_{e1} \times \vec{B} \\ \frac{35}{8}\vec{U}_{e2} \times \vec{B} \end{bmatrix} \\
= \begin{bmatrix} \vec{R}_{ei}^{(0)} \\ \vec{R}_{ei}^{(1)} \\ \vec{R}_{ei}^{(2)} \end{bmatrix} + n_e q_e \begin{bmatrix} \vec{U}_{e0} \times \vec{B} \\ \frac{5}{2}\vec{U}_{e1} \times \vec{B} \\ \frac{35}{8}\vec{U}_{e2} \times \vec{B} \end{bmatrix}
\end{aligned}
\tag{C.59}
$$

Dotting with $\hat{b}$,

$$
\begin{bmatrix} \nabla_{\parallel} P_e - n_e q_e E_{\parallel} \\ -\frac{5}{2} n_e \nabla_{\parallel} T_e \\ 0 \end{bmatrix} = \begin{bmatrix} \vec{R}_{ei}^{(0)} \\ \vec{R}_{ei}^{(1)} \\ \vec{R}_{ei}^{(2)} \end{bmatrix} \cdot \hat{b} \tag{C.60}
$$

where the parallel equation can be proceeded as in the Spitzer[26] problem. According to Hirshman and Sigmar[90, 91], the parallel components of the frictional force can be expressed as

$$
\begin{bmatrix} \vec{R}_{ei}^{(0)} \\ \vec{R}_{ei}^{(1)} \\ \vec{R}_{ei}^{(2)} \end{bmatrix} \cdot \hat{b} = \sum_{\beta} \left[\ell_{ij}^{e\beta} \right] \begin{bmatrix} U_{\beta 0\parallel} \\ U_{\beta 1\parallel} \\ U_{\beta 2\parallel} \end{bmatrix} \tag{C.61}
$$

where

$$
\ell_{ij}^{\alpha\beta} = \left(\sum_k n_\alpha m_\alpha \nu_{\alpha\beta} M_{\alpha k}^{ij} \right) \delta_{\alpha\beta} + n_\alpha m_\alpha \nu_{\alpha\beta} N_{\alpha\beta}^{ij} \tag{C.62}
$$

$$
n_\alpha \nu_{\alpha\beta} M_{\alpha\beta}^{ij} \equiv \int v_{\parallel} L_{i-1}^{(\frac{3}{2})} C^{\ell} \left(\frac{2 v_{\parallel}}{v_{th\alpha}^2} L_{j-1}^{(\frac{3}{2})} \tilde{f}_{\alpha 0}, \tilde{f}_{\beta 0} \right) d^3v \tag{C.63}
$$

$$n_\alpha \nu_{\alpha\beta} N^{ij}_{\alpha\beta} \equiv \int v_\parallel L^{(\frac{3}{2})}_{i-1} C^\ell \left(\tilde{f}_{\alpha 0}, \frac{2v_\parallel}{v^2_{th\beta}} L^{(\frac{3}{2})}_{j-1} \tilde{f}_{\beta 0}\right) d^3v \tag{C.64}$$

Hence, using the small mass ratio assumption $m_e \ll m_i$ in the $5N$-moment two-fluid model

$$\begin{aligned} \begin{bmatrix} \vec{R}^{(0)}_{ei} \\ \vec{R}^{(1)}_{ei} \\ \vec{R}^{(2)}_{ei} \end{bmatrix} \cdot \hat{b} = -n_e m_e \nu_{ee} \Bigg\{ & \begin{bmatrix} Z_i & \frac{3}{2}Z_i & \frac{15}{8}Z_i \\ \frac{3}{2}Z_i & \sqrt{2}+\frac{13}{4}Z_i & \frac{3\sqrt{2}}{4}+\frac{69}{16}Z_i \\ \frac{15}{8}Z_i & \frac{3\sqrt{2}}{4}+\frac{69}{16}Z_i & \frac{45\sqrt{2}}{16}+\frac{433}{64}Z_i \end{bmatrix} \begin{bmatrix} U_{e0\parallel} \\ U_{e1\parallel} \\ U_{e2\parallel} \end{bmatrix} \\ & - \begin{bmatrix} Z_i & 0 & 0 \\ \frac{3}{2}Z_i & 0 & 0 \\ \frac{15}{8}Z_i & 0 & 0 \end{bmatrix} \begin{bmatrix} U_{i0\parallel} \\ U_{i1\parallel} \\ U_{i2\parallel} \end{bmatrix} \Bigg\} \end{aligned} \tag{C.65}$$

which can be re-written as

$$\begin{bmatrix} \vec{R}^{(0)}_{ei} \\ \vec{R}^{(1)}_{ei} \\ \vec{R}^{(2)}_{ei} \end{bmatrix} \cdot \hat{b} = -n_e m_e \nu_{ei} \left[\mathcal{L}^e_{ij}\right] \begin{bmatrix} U_{e0\parallel} - U_{i0\parallel} \\ U_{e1\parallel} \\ U_{e2\parallel} \end{bmatrix} = -n_e m_e \nu_{ei} \left[\mathcal{L}^e_{ij}\right] \begin{bmatrix} u_{e\parallel} - u_{i\parallel} \\ -\frac{2}{5n_eT_e} h_{e\parallel} \\ U_{e2\parallel} \end{bmatrix} \tag{C.66}$$

where $\nu_{ei} = Z_i \nu_{ee}$ and

$$\left[\mathcal{L}^e_{ij}\right] = \begin{bmatrix} 1 & \frac{3}{2} & \frac{15}{8} \\ \frac{3}{2} & \frac{\sqrt{2}}{Z_i}+\frac{13}{4} & \frac{3\sqrt{2}}{4Z_i}+\frac{69}{16} \\ \frac{15}{8} & \frac{3\sqrt{2}}{4Z_i}+\frac{69}{16} & \frac{45\sqrt{2}}{16Z_i}+\frac{433}{64} \end{bmatrix} \tag{C.67}$$

Using Eq. (C.60), the parallel component of the heat flux with the transport coefficients can be obtained as

$$\begin{bmatrix} u_{e\parallel} - u_{i\parallel} \\ -\frac{2}{5n_eT_e} h_{e\parallel} \\ U_{e2\parallel} \end{bmatrix} = -\frac{1}{n_e m_e \nu_{ei}} \left[\mathcal{L}^e_{ij}\right]^{-1} \begin{bmatrix} \nabla_\parallel P_e - n_e q_e E_\parallel \\ -\frac{5}{2} n_e \nabla_\parallel T_e \\ 0 \end{bmatrix} \tag{C.68}$$

leading

$$h_{e\parallel} = -\frac{5}{2} n_e T_e \frac{\Lambda^e_{10}}{\Lambda^e_{00}} \left(u_{e\parallel} - u_{i\parallel}\right) - \frac{25}{4} Z_i \frac{n_e T_e \tau_{ei}}{m_e} \left(\Lambda^e_{11} - \frac{\left(\Lambda^e_{10}\right)^2}{\Lambda^e_{00}}\right) \nabla_\parallel T_e \tag{C.69}$$

where $\left[\Lambda^e_{ij}\right] = \left[\mathscr{L}^e_{ij}\right]^{-1}$. Crossing Eq. (C.59) with $\vec{B}$,

$$\begin{aligned}\begin{bmatrix}\vec{U}_{e0\perp}\\ \vec{U}_{e1\perp}\\ \vec{U}_{e2\perp}\end{bmatrix} &= \frac{1}{n_e q B^2}\begin{bmatrix}\nabla P_e - n_e q_e \vec{E} - \vec{R}^{(0)}_{ei}\\ -\frac{5}{2} n_e \nabla T_e - \vec{R}^{(1)}_{ei}\\ -\vec{R}^{(2)}_{ei}\end{bmatrix} \times \vec{B}\\ &= \begin{bmatrix}\frac{\vec{E}\times\vec{B}}{B^2}\\ 0\\ 0\end{bmatrix} + \frac{1}{n_e q B}\begin{bmatrix}\hat{b}\times\vec{R}^{(0)}_{ei} - \hat{b}\times\nabla P_e\\ \frac{5}{2} n_e \hat{b}\times\nabla T_e + \hat{b}\times\vec{R}^{(1)}_{ei}\\ \hat{b}\times\vec{R}^{(2)}_{ei}\end{bmatrix}\end{aligned} \tag{C.70}$$

For strongly magnetized plasmas, $\epsilon_B \gg 1$, the linearized distribution $\tilde{f}_{\alpha 1}$ can be expanded in powers of ϵ_B^{-1},

$$\tilde{f}_{\alpha 1} \simeq \tilde{f}^{(0)}_{\alpha 1} + \tilde{f}^{(1)}_{\alpha 1} + \cdots \tag{C.71}$$

that yields

$$\epsilon_B^0 \text{ order:} \qquad \begin{bmatrix}\vec{U}^{(0)}_{e0\perp}\\ \vec{U}^{(0)}_{e1\perp}\\ \vec{U}^{(0)}_{e2\perp}\end{bmatrix} = \begin{bmatrix}\frac{\vec{E}\times\vec{B}}{B^2} - \frac{1}{n_e q B}\hat{b}\times\nabla P_e\\ \frac{1}{qB}\hat{b}\times\nabla T_e\\ 0\end{bmatrix} \tag{C.72}$$

$$\epsilon_B^{-1} \text{ order:} \qquad \begin{bmatrix}\vec{U}^{(1)}_{e0\perp}\\ \vec{U}^{(1)}_{e1\perp}\\ \vec{U}^{(1)}_{e2\perp}\end{bmatrix} = \frac{1}{n_e q B}\begin{bmatrix}\hat{b}\times\vec{R}^{(0)}_{ei}\\ \hat{b}\times\vec{R}^{(1)}_{ei}\\ \hat{b}\times\vec{R}^{(2)}_{ei}\end{bmatrix} \tag{C.73}$$

$$\vdots \qquad\qquad\qquad \vdots$$

While the original expression for the frictional coefficient matrix $\ell^{ij}_{\alpha\beta}$ is developed for the Spitzer problems, which is independent to magnetic fields, it can be generalized by using $\vec{v}$ instead of using $v_\parallel$[90] in Eqs. (C.63) and (C.64) such that

$$\begin{bmatrix}\vec{R}^{(0)}_{ei}\\ \vec{R}^{(1)}_{ei}\\ \vec{R}^{(2)}_{ei}\end{bmatrix} = -n_e m_e \nu_{ei}\left[\mathscr{L}^e_{ij}\right]\begin{bmatrix}\vec{u}_e - \vec{u}_i\\ -\frac{2}{5 n_e T_e}\vec{h}_e\\ \vec{U}_{e2}\end{bmatrix} \tag{C.74}$$

Hence, the perpendicular components of the heat flux become

$$\vec{h}_{e\perp} = -\frac{5}{2}\frac{n_e T_e}{m_e \omega_{ce}}\hat{b}\times\nabla T_e + \frac{3}{2}\frac{n_e T_e}{\omega_{ce}\tau_{ei}}\hat{b}\times\left(\vec{u}_e - \vec{u}_i\right) - \left(\frac{13}{4} + \frac{\sqrt{2}}{Z_i}\right)\frac{n_e T_e \nu_{ei}}{m_e \omega_{ce}^2}\nabla_\perp T_e \tag{C.75}$$

Thus, the heat flux for electrons consists of the advective heat flux part $\vec{h}_u^e$, which is known as Ettingshausen effect, and thermal conductivity part $\vec{h}_T^e$ such that

$$\vec{h}_e = \vec{h}_u^e + \vec{h}_T^e \tag{C.76}$$

$$\vec{h}_u^e = \frac{5}{2} n_e T_e \frac{\mathcal{L}_{10}^e}{\mathcal{L}_{00}^e}\left(u_{e\parallel} - u_{i\parallel}\right)\hat{b} + \frac{3}{2}\frac{n_e T_e}{\omega_{ce}\tau_{ei}}\hat{b}\times\left(\vec{u}_e - \vec{u}_i\right) \tag{C.77}$$

$$\vec{h}_T^e = -\frac{25}{4\mathcal{L}_{11}^e}\frac{n_e T_e}{m_e \nu_{ei}}\nabla_\parallel T_e \hat{b} - \left(\frac{13}{4} + \frac{\sqrt{2}}{Z_i}\right)\frac{n_e T_e \nu_{ei}}{m_e \omega_{ce}^2}\nabla_\perp T_e - \frac{5}{2}\frac{n_e T_e}{m_e \omega_{ce}}\hat{b}\times\nabla T_e \tag{C.78}$$

Similarly, the frictional force $\vec{R}_{ei}$ consists of resistivity $\vec{R}_u^{ei}$ and thermal force $\vec{R}_T^{ei}$, which is known as Nernst effect,

$$\vec{R}_{ei} = \vec{R}_u^{ei} + \vec{R}_T^{ei} \tag{C.79}$$

$$\vec{R}_u^{ei} = n_e q \frac{1}{\Lambda_{00}^e}\frac{m_e \nu_{ei}}{n_e q^2} J_\parallel \hat{b} + \frac{m_e \nu_{ei}}{n_e q^2}\vec{J}_\perp \tag{C.80}$$

$$\vec{R}_T^{ei} = -\frac{5}{2}\frac{\mathcal{L}_{10}^e}{\mathcal{L}_{00}^e}\nabla_\parallel T_e \hat{b} - \frac{3}{2}\frac{n_e}{\omega_{ce}\tau_{ei}}\hat{b}\times\nabla T_e \tag{C.81}$$

The transport coefficients for ion heat flux can be obtained by using the same approach with

$$\begin{bmatrix} \vec{R}_{ie}^{(0)} \\ \vec{R}_{ie}^{(1)} \\ \vec{R}_{ie}^{(2)} \end{bmatrix} = -n_i m_i \nu_{ii}\left[\mathcal{L}_{ij}^i\right]\begin{bmatrix} \vec{u}_i \\ \vec{U}_{i1} \\ \vec{U}_{i2} \end{bmatrix} \tag{C.82}$$

$$\left[\mathcal{L}_{ij}^i\right] = \sqrt{2}\begin{bmatrix} 0 & 0 & 0 \\ 0 & 1 & \frac{3}{4} \\ 0 & \frac{3}{4} & \frac{45}{16} \end{bmatrix} \tag{C.83}$$

$$\vec{R}_{ie} = -\vec{R}_{ei} \tag{C.84}$$

Appendix D

GALILEAN INVARIANCE OF COULOMB COLLISION OPERATOR

Galilean invariant is an unchanged property after Galilean transformation. In the theory of relativity, Galilean transformation can be replaced by the Lorentz transformations. The general form of the collision operator is

$$\left.\frac{\delta f_\alpha}{\delta t}\right|_{coll} = -\sum_\beta \nabla_{\vec{v}} \cdot \vec{J}^{\alpha\backslash\beta} \tag{D.1}$$

where

$$\vec{J}^{\alpha\backslash\beta} = \frac{1}{2} m_\alpha \Gamma_{\alpha\beta} \int \frac{u^2 \overset{\leftrightarrow}{I} - \vec{u}\vec{u}}{u^3} \cdot \left[\frac{f_\alpha(\vec{v})}{m_\beta}\frac{\partial f_\beta(\vec{v}')}{\partial \vec{v}'} - \frac{f_\beta(\vec{v}')}{m_\alpha}\frac{\partial f_\alpha(\vec{v})}{\partial \vec{v}}\right] d^3v' \tag{D.2}$$

$$\Gamma_{\alpha\beta} \equiv \frac{4\pi q_\alpha^2 q_\beta^2 \ln\Lambda}{(4\pi\epsilon_0)^2 m_\alpha^2} \tag{D.3}$$

$$\vec{u} = \vec{v}' - \vec{v} \tag{D.4}$$

Considering $\vec{J}^{\alpha\backslash\beta}$ in the frame moving with velocity $\vec{u}_c$, the velocity components can be transformed as

$$\vec{w} = \vec{v} - \vec{u}_c \tag{D.5}$$

$$\vec{w}' = \vec{v}' - \vec{u}_c \tag{D.6}$$

$$\vec{u} = \vec{v} - \vec{u}_c - (\vec{v}' - \vec{u}_c) = \vec{w} - \vec{w}' \tag{D.7}$$

$$d^3v' = d^3w' \tag{D.8}$$

$$\frac{\partial}{\partial \vec{v}} = \frac{\partial}{\partial \vec{w}} \tag{D.9}$$

$$\frac{\partial}{\partial \vec{v}'} = \frac{\partial}{\partial \vec{w}'} \tag{D.10}$$

which yields

$$\vec{J}^{\alpha\backslash\beta} = \frac{1}{2} m_\alpha \Gamma_{\alpha\beta} \int \frac{u^2 \overset{\leftrightarrow}{I} - \vec{u}\vec{u}}{u^3} \cdot \left[\frac{f_\alpha(\vec{w})}{m_\beta} \frac{\partial f_\beta(\vec{w}')}{\partial \vec{w}'} - \frac{f_\beta(\vec{w}')}{m_\alpha} \frac{\partial f_\alpha(\vec{w})}{\partial \vec{w}} \right] d^3 w' \tag{D.11}$$

and the collision operator can be written as

$$\left. \frac{\delta f_\alpha}{\delta t} \right|_{coll} = -\sum_\beta \frac{\partial}{\partial \vec{v}} \cdot \vec{J}^{\alpha\backslash\beta} = -\sum_\beta \frac{\partial}{\partial \vec{w}} \cdot \vec{J}^{\alpha\backslash\beta} \tag{D.12}$$

Thus, the Coulomb collision operator is Galilean invariant. This Galilean invariance allows to consider the complicated form of the collision operator, for example, in the frame moving with background fluid velocity $\vec{u}_\beta$ that eventually allows to use non-shifted Maxwellian background distributions even if the background is not stationary. Note that the incident particles have a relative fluid velocity $\vec{u}_\alpha - \vec{u}_\beta$ due to the relative frame of reference.

Appendix E

THIRD AND FOURTH ORDER RUNGE-KUTTA METHODS

E.1 Third Order Runge-Kutta Method

The third order discretized equations in the exact form is

$$\begin{aligned}\vec{Q}_l^k(\vec{x}_l^k, t_{n+1}) = \vec{Q}_l^k(\vec{x}_l^k, t_n)\Delta t + \mathscr{L}\Delta t + \frac{1}{2}\left(\frac{\partial \mathscr{L}}{\partial t} + \frac{\partial \mathscr{L}}{\partial \vec{Q}_l^k}\mathscr{L}\right)(\Delta t)^2 \\ + \frac{1}{6}\left(\frac{\partial^2 \mathscr{L}}{\partial t^2} + 2\frac{\partial^2 \mathscr{L}}{\partial t \partial \vec{Q}_l^k}\mathscr{L} + \frac{\partial \mathscr{L}}{\partial \vec{Q}_l^k}\frac{\partial \mathscr{L}}{\partial t} + \frac{\partial^2 \mathscr{L}}{(\partial \vec{Q}_l^k)^2}\mathscr{L}^2 + \left(\frac{\partial \mathscr{L}}{\partial \vec{Q}_l^k}\right)^2 \mathscr{L}\right)(\Delta t)^3 + O\left((\Delta t)^4\right)\end{aligned} \tag{E.1}$$

where

$$\frac{d^3\vec{Q}_l^k}{dt^3} = \frac{\partial^2 \mathscr{L}}{\partial t^2} + \frac{\partial^2 \mathscr{L}}{\partial t \partial \vec{Q}_l^k}\mathscr{L} + \frac{\partial \mathscr{L}}{\partial \vec{Q}_l^k}\frac{\partial \mathscr{L}}{\partial t} + \frac{\partial^2 \mathscr{L}}{\partial \vec{Q}_l^k \partial t}\mathscr{L} + \frac{\partial^2 \mathscr{L}}{(\partial \vec{Q}_l^k)^2}\mathscr{L}^2 + \left(\frac{\partial \mathscr{L}}{\partial \vec{Q}_l^k}\right)^2 \mathscr{L} \tag{E.2}$$

In the third-stage RK method,

$$\vec{Q}_l^k(\vec{x}_l^k, t_{n+1}) = \vec{Q}_l^k(\vec{x}_l^k, t_n) + b_1\mathscr{L}\Delta t + b_2\mathscr{L}(\vec{\mathscr{Q}}_2, t_n + c_2\Delta t)\Delta t + b_3\mathscr{L}(\vec{\mathscr{Q}}_3, t_n + c_3\Delta t)\Delta t \tag{E.3}$$

$\mathscr{L}(\vec{\mathscr{Q}}_2, t_n + c_2\Delta t)$ and $\mathscr{L}(\vec{\mathscr{Q}}_3, t_n + c_3\Delta t)$ can be expanded around $(\vec{Q}_l^k, t_n)$ such that

$$\begin{aligned}\mathscr{L}(\vec{\mathscr{Q}}_2, t_n + c_2\Delta t) &= \mathscr{L}(\vec{Q}_l^k + a_{21}\mathscr{L}(\vec{\mathscr{Q}}_1, t_n)\Delta t, t_n + c_2\Delta t) \\ &= \mathscr{L} + \frac{1}{1!}\left(c_2\Delta t\frac{\partial}{\partial t} + a_{21}\mathscr{L}(\vec{Q}_l^k, t_n)\Delta t\frac{\partial}{\partial \vec{Q}_l^k}\right)\mathscr{L} \\ &\quad + \frac{1}{2!}\left(c_2\Delta t\frac{\partial}{\partial t} + a_{21}\mathscr{L}(\vec{Q}_l^k, t_n)\Delta t\frac{\partial}{\partial \vec{Q}_l^k}\right)^2\mathscr{L} + O\left((\Delta t)^3\right)\end{aligned} \tag{E.4}$$

$$
\begin{aligned}
\mathscr{L}(\vec{\mathscr{Q}}_3, t_n + c_3\Delta t) &= \mathscr{L}(\vec{Q}_l^k + a_{31}\mathscr{L}(\vec{\mathscr{Q}}_1, t_n)\Delta t + a_{32}\mathscr{L}(\vec{\mathscr{Q}}_2, t_n + c_2\Delta t)\Delta t, t_n + c_3\Delta t) \\
&= \mathscr{L} + \frac{1}{1!}\left(c_3\Delta t\frac{\partial}{\partial t} + \Big(a_{31}\mathscr{L} + a_{32}\mathscr{L}(\vec{\mathscr{Q}}_2, t_n + c_2\Delta t)\Big)\Delta t\frac{\partial}{\partial \vec{Q}_l^k}\right)\mathscr{L} \\
&\quad + \frac{1}{2!}\left(c_3\Delta t\frac{\partial}{\partial t} + \Big(a_{31}\mathscr{L} + a_{32}\mathscr{L}(\vec{\mathscr{Q}}_2, t_n + c_2\Delta t)\Big)\Delta t\frac{\partial}{\partial \vec{Q}_l^k}\right)^2\mathscr{L} + O\left((\Delta t)^3\right)
\end{aligned}
\tag{E.5}
$$

where

$$
\vec{\mathscr{Q}}_3 = \vec{Q}_l^k(\vec{x}_l^k, t_n) + a_{31}\mathscr{L}(\vec{\mathscr{Q}}_1, t_n) + a_{32}\mathscr{L}(\vec{\mathscr{Q}}_2, t_n + c_2\Delta t) \tag{E.6}
$$

Collecting terms that involves the same power of Δt,

$$
\begin{aligned}
\mathscr{L}(\vec{\mathscr{Q}}_2, t_n + c_2\Delta t) &= \mathscr{L} + \left(c_2\frac{\partial\mathscr{L}}{\partial t} + a_{21}\mathscr{L}\frac{\partial\mathscr{L}}{\partial\vec{Q}_l^k}\right)\Delta t \\
&\quad + \frac{1}{2}\left(c_2^2\frac{\partial^2\mathscr{L}}{\partial t^2} + 2a_{21}c_2\mathscr{L}\frac{\partial^2\mathscr{L}}{\partial t\partial\vec{Q}_l^k} + a_{21}^2\mathscr{L}^2\frac{\partial^2\mathscr{L}}{\left(\partial\vec{Q}_l^k\right)^2}\right)(\Delta t)^2 + O\left((\Delta t)^3\right)
\end{aligned}
\tag{E.7}
$$

$$
\begin{aligned}
\mathscr{L}(\vec{\mathscr{Q}}_3, t_n + c_3\Delta t) &= \mathscr{L} + \left(c_3\frac{\partial\mathscr{L}}{\partial t} + (a_{31} + a_{32})\mathscr{L}\frac{\partial\mathscr{L}}{\partial\vec{Q}_l^k}\right)\Delta t \\
&+ \frac{1}{2}\left(c_3^2\frac{\partial^2\mathscr{L}}{\partial t^2} + 2a_{32}c_2\frac{\partial\mathscr{L}}{\partial t}\frac{\partial\mathscr{L}}{\partial\vec{Q}_l^k} + 2a_{21}a_{32}\mathscr{L}\left(\frac{\partial\mathscr{L}}{\partial\vec{Q}_l^k}\right)^2 + 2c_3(a_{31} + a_{32})\mathscr{L}\frac{\partial^2\mathscr{L}}{\partial t\partial\vec{Q}_l^k}\right. \\
&\left. + (a_{31} + a_{32})^2\mathscr{L}^2\frac{\partial^2\mathscr{L}}{\left(\partial\vec{Q}_l^k\right)^2}\right)(\Delta t)^2 + O\left((\Delta t)^3\right)
\end{aligned}
\tag{E.8}
$$

Substituting Eqs. (E.29) and (E.30) into Eq. (E.3),

$$\begin{aligned}\vec{Q}_l^k(\vec{x}_l^k, t_{n+1}) = {} & \vec{Q}_l^k(\vec{x}_l^k, t_n) + (b_1 + b_2 + b_3)\mathscr{L}\Delta t \\ & + \left((b_2c_2 + b_3c_3)\frac{\partial \mathscr{L}}{\partial t} + (a_{21}b_2 + (a_{31} + a_{32})b_3)\,\mathscr{L}\frac{\partial \mathscr{L}}{\partial \vec{Q}_l^k}\right)(\Delta t)^2 \\ & + \frac{1}{2}\left((b_2c_2^2 + b_3c_3^2)\frac{\partial^2 \mathscr{L}}{\partial t^2} + 2\,(a_{21}b_2c_2 + (a_{31} + a_{32})b_3c_3)\,\mathscr{L}\frac{\partial^2 \mathscr{L}}{\partial t \partial \vec{Q}_l^k}\right. \\ & \quad + 2a_{32}b_3c_2\frac{\partial \mathscr{L}}{\partial \vec{Q}_l^k}\frac{\partial \mathscr{L}}{\partial t} + \left(a_{21}^2b_2 + (a_{31} + a_{32})^2b_3\right)\mathscr{L}^2\frac{\partial^2 \mathscr{L}}{\left(\partial \vec{Q}_l^k\right)^2} \\ & \quad \left. + 2a_{21}a_{32}b_3\mathscr{L}\left(\frac{\partial \mathscr{L}}{\partial \vec{Q}_l^k}\right)^2\right)(\Delta t)^3 + O\left((\Delta t)^4\right)\end{aligned} \tag{E.9}$$

Comparing Eq. (E.9) with Eq. (E.1),

$$b_1 + b_2 + b_3 = 1 \tag{E.10}$$

$$b_2c_2 + b_3c_3 = \frac{1}{2} \tag{E.11}$$

$$a_{21}b_2 + (a_{31} + a_{32})b_3 = \frac{1}{2} \tag{E.12}$$

$$b_2c_2^2 + b_3c_3^2 = \frac{1}{3} \tag{E.13}$$

$$a_{21}b_2c_2 + (a_{31} + a_{32})b_3c_3 = \frac{1}{3} \tag{E.14}$$

$$a_{32}b_3c_2 = \frac{1}{6} \tag{E.15}$$

$$a_{21}^2b_2 + (a_{31} + a_{32})^2b_3 = \frac{1}{3} \tag{E.16}$$

$$a_{21}a_{32}b_3 = \frac{1}{6} \tag{E.17}$$

While there are eight equations for eight unknowns, the system is not closed because there actually exist only six independent equations. For example, Eqs. (E.15) and (E.17) produce

$$a_{21} = c_2 \tag{E.18}$$

Also, Eqs. (E.11), (E.12) and (E.18 yield

$$a_{31} + a_{32} = c_3 \tag{E.19}$$

Therefore the following six equations are independent

$$b_1 + b_2 + b_3 = 1 \tag{E.20}$$

$$b_2 c_2 + b_3 c_3 = \frac{1}{2} \tag{E.21}$$

$$b_2 c_2^2 + b_3 c_3^2 = \frac{1}{3} \tag{E.22}$$

$$a_{32} b_3 c_2 = \frac{1}{6} \tag{E.23}$$

$$a_{21} = c_2 \tag{E.24}$$

$$a_{31} + a_{32} = c_3 \tag{E.25}$$

E.2 Fourth Order Runge-Kutta Method

The fourth order discretized equations in the exact form is

$$\begin{aligned}
\vec{Q}_l^k(\vec{x}_l^k, t_{n+1}) = {} & \vec{Q}_l^k(\vec{x}_l^k, t_n)\Delta t + \mathscr{L}\Delta t + \frac{1}{2}\left(\frac{\partial \mathscr{L}}{\partial t} + \frac{\partial \mathscr{L}}{\partial \vec{Q}_l^k}\mathscr{L}\right)(\Delta t)^2 \\
& + \frac{1}{6}\left(\frac{\partial^2 \mathscr{L}}{\partial t^2} + 2\frac{\partial^2 \mathscr{L}}{\partial t \partial \vec{Q}_l^k}\mathscr{L} + \frac{\partial \mathscr{L}}{\partial \vec{Q}_l^k}\frac{\partial \mathscr{L}}{\partial t} + \frac{\partial^2 \mathscr{L}}{(\partial \vec{Q}_l^k)^2}\mathscr{L}^2 + \left(\frac{\partial \mathscr{L}}{\partial \vec{Q}_l^k}\right)^2 \mathscr{L}\right)(\Delta t)^3 \\
& + \frac{1}{24}\left(\frac{\partial^3 \mathscr{L}}{\partial t^3} + \frac{\partial^2 \mathscr{L}}{\partial t^2}\frac{\partial \mathscr{L}}{\partial \vec{Q}_l^k} + \frac{\partial \mathscr{L}}{\partial t}\left(\frac{\partial \mathscr{L}}{\partial \vec{Q}_l^k}\right)^2 + 3\frac{\partial \mathscr{L}}{\partial t}\frac{\partial^2 \mathscr{L}}{\partial t \partial \vec{Q}_l^k} + 3\frac{\partial \mathscr{L}}{\partial t}\frac{\partial^2 \mathscr{L}}{\left(\partial \vec{Q}_l^k\right)^2}\mathscr{L}\right. \\
& \quad + \left(\frac{\partial \mathscr{L}}{\partial \vec{Q}_l^k}\right)^3 \mathscr{L} + 3\frac{\partial^3 \mathscr{L}}{\partial t^2 \partial \vec{Q}_l^k}\mathscr{L} + 5\frac{\partial^2 \mathscr{L}}{\partial t \partial \vec{Q}_l^k}\frac{\partial \mathscr{L}}{\partial \vec{Q}_l^k}\mathscr{L} + 4\frac{\partial^2 \mathscr{L}}{\left(\partial \vec{Q}_l^k\right)^2}\frac{\partial \mathscr{L}}{\partial \vec{Q}_l^k}\mathscr{L}^2 \\
& \quad \left. +3\frac{\partial^3 \mathscr{L}}{\partial t\left(\partial \vec{Q}_l^k\right)^2}\mathscr{L}^2 + \frac{\partial^3 \mathscr{L}}{\left(\partial \vec{Q}_l^k\right)^3}\mathscr{L}^3\right)(\Delta t)^4 + O\left((\Delta t)^5\right)
\end{aligned} \tag{E.26}$$

where

$$\begin{aligned}\frac{d^4\vec{Q}_l^k}{dt^4} &= \frac{\partial^3\mathscr{L}}{\partial t^3} + \frac{\partial^2\mathscr{L}}{\partial t^2}\frac{\partial\mathscr{L}}{\partial\vec{Q}_l^k} + \frac{\partial\mathscr{L}}{\partial t}\left(\frac{\partial\mathscr{L}}{\partial\vec{Q}_l^k}\right)^2 + 3\frac{\partial\mathscr{L}}{\partial t}\frac{\partial^2\mathscr{L}}{\partial t\partial\vec{Q}_l^k} + 3\frac{\partial\mathscr{L}}{\partial t}\frac{\partial^2\mathscr{L}}{\left(\partial\vec{Q}_l^k\right)^2}\mathscr{L} \\ &\quad + \left(\frac{\partial\mathscr{L}}{\partial\vec{Q}_l^k}\right)^3\mathscr{L} + 3\frac{\partial^3\mathscr{L}}{\partial t^2\partial\vec{Q}_l^k}\mathscr{L} + 5\frac{\partial^2\mathscr{L}}{\partial t\partial\vec{Q}_l^k}\frac{\partial\mathscr{L}}{\partial\vec{Q}_l^k}\mathscr{L} + 4\frac{\partial^2\mathscr{L}}{\left(\partial\vec{Q}_l^k\right)^2}\frac{\partial\mathscr{L}}{\partial\vec{Q}_l^k}\mathscr{L}^2 \\ &\quad + 3\frac{\partial^3\mathscr{L}}{\partial t\left(\partial\vec{Q}_l^k\right)^2}\mathscr{L} + \frac{\partial^3\mathscr{L}}{\left(\partial\vec{Q}_l^k\right)^3}\mathscr{L}^2\end{aligned} \tag{E.27}$$

In the fourth-stage RK method,

$$\begin{aligned}\vec{Q}_l^k(\vec{x}_l^k, t_{n+1}) &= \vec{Q}_l^k(\vec{x}_l^k, t_n) + b_1\mathscr{L}\Delta t + b_2\mathscr{L}(\vec{\mathscr{Q}}_2, t_n + c_2\Delta t)\Delta t \\ &\quad + b_3\mathscr{L}(\vec{\mathscr{Q}}_3, t_n + c_3\Delta t)\Delta t + b_4\mathscr{L}(\vec{\mathscr{Q}}_4, t_n + c_4\Delta t)\Delta t\end{aligned} \tag{E.28}$$

$\mathscr{L}(\vec{\mathscr{Q}}_2, t_n + c_2\Delta t)$, $\mathscr{L}(\vec{\mathscr{Q}}_3, t_n + c_3\Delta t)$ and $\mathscr{L}(\vec{\mathscr{Q}}_4, t_n + c_4\Delta t)$ can be expanded around $(\vec{Q}_l^k, t_n)$ such that

$$\begin{aligned}\mathscr{L}(\vec{\mathscr{Q}}_2, t_n + c_2\Delta t) &= \mathscr{L}(\vec{Q}_l^k + a_{21}\mathscr{L}(\vec{\mathscr{Q}}_1, t_n)\Delta t, t_n + c_2\Delta t) \\ &= \mathscr{L} + \frac{1}{1!}\left(c_2\Delta t\frac{\partial}{\partial t} + a_{21}\mathscr{L}(\vec{Q}_l^k, t_n)\Delta t\frac{\partial}{\partial\vec{Q}_l^k}\right)\mathscr{L} \\ &\quad + \frac{1}{2!}\left(c_2\Delta t\frac{\partial}{\partial t} + a_{21}\mathscr{L}(\vec{Q}_l^k, t_n)\Delta t\frac{\partial}{\partial\vec{Q}_l^k}\right)^2\mathscr{L} \\ &\quad + \frac{1}{3!}\left(c_2\Delta t\frac{\partial}{\partial t} + a_{21}\mathscr{L}(\vec{Q}_l^k, t_n)\Delta t\frac{\partial}{\partial\vec{Q}_l^k}\right)^3\mathscr{L} + O\left((\Delta t)^4\right)\end{aligned} \tag{E.29}$$

$$\begin{aligned}&\mathscr{L}(\vec{\mathscr{Q}}_3, t_n + c_3\Delta t) = \mathscr{L}(\vec{Q}_l^k + a_{31}\mathscr{L}(\vec{\mathscr{Q}}_1, t_n)\Delta t + a_{32}\mathscr{L}(\vec{\mathscr{Q}}_2, t_n + c_2\Delta t)\Delta t, t_n + c_3\Delta t) \\ &= \mathscr{L} + \frac{1}{1!}\left(c_3\Delta t\frac{\partial}{\partial t} + \left(a_{31}\mathscr{L} + a_{32}\mathscr{L}(\vec{\mathscr{Q}}_2, t_n + c_2\Delta t)\right)\Delta t\frac{\partial}{\partial\vec{Q}_l^k}\right)\mathscr{L} \\ &\quad + \frac{1}{2!}\left(c_3\Delta t\frac{\partial}{\partial t} + \left(a_{31}\mathscr{L} + a_{32}\mathscr{L}(\vec{\mathscr{Q}}_2, t_n + c_2\Delta t)\right)\Delta t\frac{\partial}{\partial\vec{Q}_l^k}\right)^2\mathscr{L} \\ &\quad + \frac{1}{3!}\left(c_3\Delta t\frac{\partial}{\partial t} + \left(a_{31}\mathscr{L} + a_{32}\mathscr{L}(\vec{\mathscr{Q}}_2, t_n + c_2\Delta t)\right)\Delta t\frac{\partial}{\partial\vec{Q}_l^k}\right)^3\mathscr{L} + O\left((\Delta t)^4\right)\end{aligned} \tag{E.30}$$

$$
\begin{aligned}
&\mathscr{L}(\vec{\mathscr{Q}}_4, t_n + c_4\Delta t) \\
&= \mathscr{L} + \frac{1}{1!}\left(c_4\Delta t\frac{\partial}{\partial t} + \Big(a_{41}\mathscr{L} + a_{42}\mathscr{L}(\vec{\mathscr{Q}}_2, t_n + c_2\Delta t) + a_{43}\mathscr{L}(\vec{\mathscr{Q}}_3, t_n + c_3\Delta t)\Big)\Delta t\frac{\partial}{\partial \vec{Q}_l^k}\right)\mathscr{L} \\
&\quad + \frac{1}{2!}\left(c_4\Delta t\frac{\partial}{\partial t} + \Big(a_{41}\mathscr{L} + a_{42}\mathscr{L}(\vec{\mathscr{Q}}_2, t_n + c_2\Delta t) + a_{43}\mathscr{L}(\vec{\mathscr{Q}}_3, t_n + c_3\Delta t)\Big)\Delta t\frac{\partial}{\partial \vec{Q}_l^k}\right)^2\mathscr{L} \\
&\quad + \frac{1}{3!}\left(c_4\Delta t\frac{\partial}{\partial t} + \Big(a_{41}\mathscr{L} + a_{42}\mathscr{L}(\vec{\mathscr{Q}}_2, t_n + c_2\Delta t) + a_{43}\mathscr{L}(\vec{\mathscr{Q}}_3, t_n + c_3\Delta t)\Big)\Delta t\frac{\partial}{\partial \vec{Q}_l^k}\right)^3\mathscr{L} + O\left((\Delta t)^4\right)
\end{aligned}
\tag{E.31}
$$

where

$$
\vec{\mathscr{Q}}_4 = \vec{Q}_l^k(\vec{x}_l^k, t_n) + a_{41}\mathscr{L}(\vec{\mathscr{Q}}_1, t_n) + a_{42}\mathscr{L}(\vec{\mathscr{Q}}_2, t_n + c_2\Delta t) + a_{43}\mathscr{L}(\vec{\mathscr{Q}}_3, t_n + c_3\Delta t) \tag{E.32}
$$

Collecting terms that involves the same power of Δt,

$$
\begin{aligned}
&\mathscr{L}(\vec{\mathscr{Q}}_2, t_n + c_2\Delta t) = \mathscr{L} + \left(c_2\frac{\partial \mathscr{L}}{\partial t} + a_{21}\mathscr{L}\frac{\partial \mathscr{L}}{\partial \vec{Q}_l^k}\right)\Delta t \\
&\quad + \frac{1}{2}\left(c_2^2\frac{\partial^2 \mathscr{L}}{\partial t^2} + 2a_{21}c_2\mathscr{L}\frac{\partial^2 \mathscr{L}}{\partial t\partial \vec{Q}_l^k} + a_{21}^2\mathscr{L}^2\frac{\partial^2 \mathscr{L}}{\left(\partial \vec{Q}_l^k\right)^2}\right)(\Delta t)^2 \\
&\quad + \frac{1}{6}\left(c_2^3\frac{\partial^3 \mathscr{L}}{\partial t^3} + 3a_{21}c_2^2\mathscr{L}\frac{\partial^3 \mathscr{L}}{\partial t^2\partial \vec{Q}_l^k} + 3a_{21}^2c_2\mathscr{L}^2\frac{\partial^3 \mathscr{L}}{\partial t\left(\partial \vec{Q}_l^k\right)^2} + a_{21}^3\mathscr{L}^3\frac{\partial^3 \mathscr{L}}{\left(\partial \vec{Q}_l^k\right)^3}\right)(\Delta t)^3 + O\left((\Delta t)^4\right)
\end{aligned}
\tag{E.33}
$$

$$
\begin{aligned}
&\mathscr{L}(\vec{\mathscr{Q}}_3, t_n + c_3 \Delta t) = \mathscr{L} + \left(c_3 \frac{\partial \mathscr{L}}{\partial t} + (a_{31} + a_{32}) \mathscr{L} \frac{\partial \mathscr{L}}{\partial \vec{Q}_l^k} \right) \Delta t \\
&+ \frac{1}{2} \left(c_3^2 \frac{\partial^2 \mathscr{L}}{\partial t^2} + 2 a_{32} c_2 \frac{\partial \mathscr{L}}{\partial t} \frac{\partial \mathscr{L}}{\partial \vec{Q}_l^k} + 2 a_{21} a_{32} \mathscr{L} \left(\frac{\partial \mathscr{L}}{\partial \vec{Q}_l^k} \right)^2 + 2 c_3 (a_{31} + a_{32}) \mathscr{L} \frac{\partial^2 \mathscr{L}}{\partial t \partial \vec{Q}_l^k} \right. \\
&\qquad \left. + (a_{31} + a_{32})^2 \mathscr{L}^2 \frac{\partial^2 \mathscr{L}}{\left(\partial \vec{Q}_l^k \right)^2} \right) (\Delta t)^2 \\
&+ \frac{1}{6} \left(c_3^3 \frac{\partial^3 \mathscr{L}}{\partial t^3} + 3 a_{32} c_2^2 \frac{\partial^2 \mathscr{L}}{\partial t^2} \frac{\partial \mathscr{L}}{\partial \vec{Q}_l^k} + 6 a_{32} c_2 c_3 \frac{\partial \mathscr{L}}{\partial t} \frac{\partial^2 \mathscr{L}}{\partial t \partial \vec{Q}_l^k} + 6 a_{32} (a_{31} + a_{32}) c_2 \mathscr{L} \frac{\partial \mathscr{L}}{\partial t} \frac{\partial^2 \mathscr{L}}{\left(\partial \vec{Q}_l^k \right)^2} \right. \\
&\qquad + 6 a_{21} a_{32} (c_2 + c_3) \mathscr{L} \frac{\partial \mathscr{L}}{\partial \vec{Q}_l^k} \frac{\partial^2 \mathscr{L}}{\partial t \partial \vec{Q}_l^k} + 3 a_{21} a_{32} (a_{21} + 2(a_{31} + a_{32})) \mathscr{L}^2 \frac{\partial \mathscr{L}}{\partial \vec{Q}_l^k} \frac{\partial^2 \mathscr{L}}{\left(\partial \vec{Q}_l^k \right)^2} \\
&\qquad \left. + 3 (a_{31} + a_{32}) c_3^2 \mathscr{L} \frac{\partial^3 \mathscr{L}}{\partial t^2 \partial \vec{Q}_l^k} + 3 (a_{31} + a_{32})^2 c_3 \mathscr{L}^2 \frac{\partial^3 \mathscr{L}}{\partial t \left(\partial \vec{Q}_l^k \right)^2} + (a_{31} + a_{32})^3 \mathscr{L}^3 \frac{\partial^3 \mathscr{L}}{\left(\partial \vec{Q}_l^k \right)^3} \right) (\Delta t)^3 \\
&+ O\left((\Delta t)^4 \right)
\end{aligned}
\tag{E.34}
$$

$$
\begin{aligned}
\mathscr{L}(\vec{\mathscr{Q}}_4, t_n + c_4\Delta t) = \mathscr{L} &+ \left(c_4 \frac{\partial \mathscr{L}}{\partial t} + (a_{41} + a_{42} + a_{43})\mathscr{L} \frac{\partial \mathscr{L}}{\partial \vec{Q}_l^k} \right) \Delta t \\
&+ \frac{1}{2} \left(c_4^2 \frac{\partial^2 \mathscr{L}}{\partial t^2} + 2(a_{42}c_2 + a_{43}c_3) \frac{\partial \mathscr{L}}{\partial t} \frac{\partial \mathscr{L}}{\partial \vec{Q}_l^k} + 2(a_{21}a_{42} + (a_{31} + a_{32})a_{43})\mathscr{L} \left(\frac{\partial \mathscr{L}}{\partial \vec{Q}_l^k} \right)^2 \right. \\
&\qquad \left. + 2(a_{41} + a_{42} + a_{43})c_4 \mathscr{L} \frac{\partial^2 \mathscr{L}}{\partial t \partial \vec{Q}_l^k} + (a_{41} + a_{42} + a_{43})^2 \mathscr{L} \frac{\partial^2 \mathscr{L}}{\left(\partial \vec{Q}_l^k\right)^2} \right) (\Delta t)^2 \\
&+ \frac{1}{6} \left(c_4^3 \frac{\partial^3 \mathscr{L}}{\partial t^3} + 3(a_{42}c_2^2 + a_{43}c_3^2) \frac{\partial \mathscr{L}}{\partial \vec{Q}_l^k} \frac{\partial^2 \mathscr{L}}{\partial t^2} + 6a_{32}a_{43}c_2 \left(\frac{\partial \mathscr{L}}{\partial \vec{Q}_l^k} \right)^2 \frac{\partial \mathscr{L}}{\partial t} + 6a_{21}a_{32}a_{43}\mathscr{L} \left(\frac{\partial \mathscr{L}}{\partial \vec{Q}_l^k} \right)^3 \right. \\
&\qquad + 6(a_{42}c_2 + a_{43}c_3)c_4 \frac{\partial \mathscr{L}}{\partial t} \frac{\partial^2 \mathscr{L}}{\partial t \partial \vec{Q}_l^k} + 6(a_{42}c_2 + a_{43}c_3)(a_{41} + a_{42} + a_{43})\mathscr{L} \frac{\partial \mathscr{L}}{\partial t} \frac{\partial^2 \mathscr{L}}{\left(\partial \vec{Q}_l^k\right)^2} \\
&\qquad + 6\left(a_{21}a_{42}(c_2 + c_4) + (a_{31} + a_{32})a_{43}(c_3 + c_4)\right) \mathscr{L} \frac{\partial \mathscr{L}}{\partial \vec{Q}_l^k} \frac{\partial^2 \mathscr{L}}{\partial t \partial \vec{Q}_l^k} \\
&\quad + 3\left(a_{21}^2 a_{42} + 2a_{21}a_{42}(a_{41} + a_{42} + a_{43}) + (a_{31} + a_{32})a_{43}\left(a_{31} + a_{32} + 2(a_{41} + a_{42} + a_{43})\right)\right) \mathscr{L}^2 \frac{\partial \mathscr{L}}{\partial \vec{Q}_l^k} \frac{\partial^2 \mathscr{L}}{\left(\partial \vec{Q}_l^k\right)^2} \\
&\qquad + 3(a_{41} + a_{42} + a_{43})c_4^2 \frac{\partial^3 \mathscr{L}}{\partial t^2 \partial \vec{Q}_l^k} + 3(a_{41} + a_{42} + a_{43})^2 c_4 \mathscr{L} \frac{\partial^3 \mathscr{L}}{\partial t \left(\partial \vec{Q}_l^k\right)^2} \\
&\qquad \left. + (a_{41} + a_{42} + a_{43})^3 \mathscr{L}^2 \frac{\partial^3 \mathscr{L}}{\left(\partial \vec{Q}_l^k\right)^3} \right) + O\left((\Delta t)^4\right)
\end{aligned}
\tag{E.35}
$$

Substituting Eqs. (E.33), (E.34) and (E.35) into Eq. (E.28),

$$
\begin{aligned}
&\vec{Q}_l^k(\vec{x}_l^k, t_{n+1}) = \vec{Q}_l^k(\vec{x}_l^k, t_n) + (b_1 + b_2 + b_3 + b_4)\mathcal{L}\Delta t \\
&+ \left((b_2c_2 + b_3c_3 + b_4c_4)\frac{\partial \mathcal{L}}{\partial t} + (a_{21}b_2 + (a_{31} + a_{32})b_3 + (a_{41} + a_{42} + a_{43})b_4)\, \mathcal{L}\frac{\partial \mathcal{L}}{\partial \vec{Q}_l^k} \right) (\Delta t)^2 \\
&+ \frac{1}{2} \Bigg((b_2c_2^2 + b_3c_3^2 + b_4c_4^2)\frac{\partial^2 \mathcal{L}}{\partial t^2} + 2(a_{32}b_3c_2 + a_{42}b_4c_2 + a_{43}b_4c_3)\frac{\partial \mathcal{L}}{\partial \vec{Q}_l^k}\frac{\partial \mathcal{L}}{\partial t} \\
&\qquad +2((a_{31} + a_{32})a_{43}b_4 + a_{21}(a_{32}b_3 + a_{42}b_4))\mathcal{L} \left(\frac{\partial \mathcal{L}}{\partial \vec{Q}_l^k} \right)^2 \\
&\qquad +2\left(a_{21}b_2c_2 + (a_{31} + a_{32})b_3c_3 + (a_{41} + a_{42} + a_{43})b_4c_4\right) \mathcal{L}\frac{\partial^2 \mathcal{L}}{\partial t \partial \vec{Q}_l^k} \\
&\qquad + \left(a_{21}^2 b_2 + (a_{31} + a_{32})^2 b_3 + (a_{41} + a_{42} + a_{43})^2 b_4\right) \mathcal{L}^2 \frac{\partial^2 \mathcal{L}}{\left(\partial \vec{Q}_l^k\right)^2} \Bigg) (\Delta t)^3 \\
&+ \frac{1}{6} \Bigg((b_2c_2^3 + b_3c_3^3 + b_4c_4^3)\frac{\partial^3 \mathcal{L}}{\partial t^3} + 3((a_{32}b_3 + a_{42}b_4)c_2^2 + a_{43}b_4c_3^2)\frac{\partial^2 \mathcal{L}}{\partial t^2}\frac{\partial \mathcal{L}}{\partial \vec{Q}_l^k} \\
&\qquad +6a_{32}a_{43}b_4c_2\frac{\partial \mathcal{L}}{\partial t}\left(\frac{\partial \mathcal{L}}{\partial \vec{Q}_l^k} \right)^2 + 6a_{21}a_{32}a_{43}b_4\mathcal{L}\left(\frac{\partial \mathcal{L}}{\partial \vec{Q}_l^k} \right)^3 \\
&\qquad +6(a_{32}b_3c_2c_3 + b_4(a_{42}c_2 + a_{43}c_3)c_4)\frac{\partial \mathcal{L}}{\partial t}\frac{\partial^2 \mathcal{L}}{\partial t \partial \vec{Q}_l^k} \\
&\qquad +6\left(a_{21}a_{32}b_3(c_2 + c_3) + a_{21}a_{42}b_4(c_2 + c_4) + (a_{31} + a_{32})a_{43}b_4(c_3 + c_4)\right)\mathcal{L}\frac{\partial \mathcal{L}}{\partial \vec{Q}_l^k}\frac{\partial^2 \mathcal{L}}{\partial t \partial \vec{Q}_l^k} \\
&\qquad +3\left(a_{21}b_2c_2^2 + (a_{31} + a_{32})b_3c_3^2 + (a_{41} + a_{42} + a_{43})b_4c_4^2\right)\mathcal{L}\frac{\partial^3 \mathcal{L}}{\partial t^2 \partial \vec{Q}_l^k} \\
&\qquad +6\left(a_{31}a_{32}b_3c_2 + a_{32}^2 b_3c_2 + (a_{41} + a_{42} + a_{43})b_4(a_{42}c_2 + a_{43}c_3)\right)\mathcal{L}\frac{\partial \mathcal{L}}{\partial t}\frac{\partial^2 \mathcal{L}}{\left(\partial \vec{Q}_l^k\right)^2} \\
&\qquad +3\left[a_{21}a_{32}(a_{21} + 2(a_{31} + a_{32}))b_3 + \right. \\
&\left. (a_{21}^2 a_{42} + 2a_{21}a_{42}(a_{41} + a_{42} + a_{43}) + (a_{31} + a_{32})a_{43}(a_{31} + a_{32} + 2(a_{41} + a_{42} + a_{43})))b_4\right]\mathcal{L}^2\frac{\partial \mathcal{L}}{\partial \vec{Q}_l^k}\frac{\partial^2 \mathcal{L}}{\left(\partial \vec{Q}_l^k\right)^2} \\
&\qquad +3\left(a_{21}^2 b_2c_2 + (a_{31} + a_{32})^2 b_3c_3 + (a_{41} + a_{42} + a_{43})^2 b_4c_4\right)\mathcal{L}^2\frac{\partial^3 \mathcal{L}}{\partial t \left(\partial \vec{Q}_l^k\right)^2} \\
&\qquad +(a_{21}^3 b_2 + (a_{31} + a_{32})^3 b_3 + (a_{41} + a_{42} + a_{43})^3 b_4)\mathcal{L}^3\frac{\partial^3 \mathcal{L}}{\left(\partial \vec{Q}_l^k\right)^3} \Bigg) (\Delta t)^4 + O\left((\Delta t)^5\right)
\end{aligned}
\tag{E.36}
$$

Comparing Eq. (E.36) with Eq. (E.26),

$$b_1 + b_2 + b_3 + b_4 = 1 \tag{E.37}$$

$$b_2c_2 + b_3c_3 + b_4c_4 = \frac{1}{2} \tag{E.38}$$

$$a_{21}b_2 + (a_{31} + a_{32})b_3 + (a_{41} + a_{42} + a_{43})b_4 = \frac{1}{2} \tag{E.39}$$

$$b_2c_2^2 + b_3c_3^2 + b_4c_4^2 = \frac{1}{3} \tag{E.40}$$

$$a_{32}b_3c_2 + a_{42}b_4c_2 + a_{43}b_4c_3 = \frac{1}{6} \tag{E.41}$$

$$(a_{31} + a_{32})a_{43}b_4 + a_{21}(a_{32}b_3 + a_{42}b_4) = \frac{1}{6} \tag{E.42}$$

$$a_{21}b_2c_2 + (a_{31} + a_{32})b_3c_3 + (a_{41} + a_{42} + a_{43})b_4c_4 = \frac{1}{3} \tag{E.43}$$

$$a_{21}^2b_2 + (a_{31} + a_{32})^2b_3 + (a_{41} + a_{42} + a_{43})^2b_4 = \frac{1}{3} \tag{E.44}$$

$$b_2c_2^3 + b_3c_3^3 + b_4c_4^3 = \frac{1}{4} \tag{E.45}$$

$$(a_{32}b_3 + a_{42}b_4)c_2^2 + a_{43}b_4c_3^2 = \frac{1}{12} \tag{E.46}$$

$$a_{32}a_{43}b_4c_2 = \frac{1}{24} \tag{E.47}$$

$$a_{21}a_{32}a_{43}b_4 = \frac{1}{24} \tag{E.48}$$

$$a_{32}b_3c_2c_3 + b_4(a_{42}c_2 + a_{43}c_3)c_4 = \frac{1}{8} \tag{E.49}$$

$$a_{21}a_{32}b_3(c_2 + c_3) + a_{21}a_{42}b_4(c_2 + c_4) + (a_{31} + a_{32})a_{43}b_4(c_3 + c_4) = \frac{5}{24} \tag{E.50}$$

$$a_{21}b_2c_2^2 + (a_{31} + a_{32})b_3c_3^2 + (a_{41} + a_{42} + a_{43})b_4c_4^2 = \frac{1}{4} \tag{E.51}$$

$$a_{31}a_{32}b_3c_2 + a_{32}^2b_3c_2 + (a_{41} + a_{42} + a_{43})b_4(a_{42}c_2 + a_{43}c_3) = \frac{1}{8} \tag{E.52}$$

$$\begin{aligned} &a_{21}a_{32}(a_{21} + 2(a_{31} + a_{32}))b_3 \\ &\quad + (a_{21}^2a_{42} + 2a_{21}a_{42}(a_{41} + a_{42} + a_{43}) + (a_{31} + a_{32})a_{43}(a_{31} + a_{32} + 2(a_{41} + a_{42} + a_{43})))b_4 = \frac{1}{3} \end{aligned} \tag{E.53}$$

$$a_{21}^2 b_2 c_2 + (a_{31} + a_{32})^2 b_3 c_3 + (a_{41} + a_{42} + a_{43})^2 b_4 c_4 = \frac{1}{4} \tag{E.54}$$

$$a_{21}^3 b_2 + (a_{31} + a_{32})^3 b_3 + (a_{41} + a_{42} + a_{43})^3 b_4 = \frac{1}{4} \tag{E.55}$$

While there are 19 equations for 13 unknowns, the system is not closed because there actually exist only 10 independent equations such that

$$b_1 + b_2 + b_3 + b_4 = 1 \tag{E.56}$$

$$b_2 c_2 + b_3 c_3 + b_4 c_4 = \frac{1}{2} \tag{E.57}$$

$$b_2 c_2^2 + b_3 c_3^2 + b_4 c_4^2 = \frac{1}{3} \tag{E.58}$$

$$b_2 c_2^3 + b_3 c_3^3 + b_4 c_4^3 = \frac{1}{4} \tag{E.59}$$

$$a_{32} b_3 c_2 + a_{42} b_4 c_2 + a_{43} b_4 c_3 = \frac{1}{6} \tag{E.60}$$

$$a_{32} c_2 b_3 c_3 + a_{42} b_4 c_2 c_4 + a_{43} b_4 c_3 c_4 = \frac{1}{12} \tag{E.61}$$

$$a_{32} a_{43} b_4 c_2 = \frac{1}{24} \tag{E.62}$$

$$a_{21} = c_2 \tag{E.63}$$

$$a_{31} + a_{32} = c_3 \tag{E.64}$$

$$a_{41} + a_{42} + a_{43} = c_4 \tag{E.65}$$

Appendix F

ANALYTICAL SOLUTIONS OF WAVE EQUATIONS IN CYLINDRICAL COORDINATES

The wave equation is

$$\frac{1}{c^2}\frac{\partial^2 u}{\partial t^2} = \nabla^2 u \tag{F.1}$$

where c is the characteristic wave speed. Using the separation of variables, the solution u can be expressed as

$$u(t, r, \theta, z) = T(t)R(r)Q(\theta)Z(z) \tag{F.2}$$

From Eq. F.1,

$$\frac{1}{c^2}RQZ\frac{\partial^2 T}{\partial t^2} = TQZ\frac{1}{r}\frac{\partial}{\partial r}\left(r\frac{\partial R}{\partial r}\right) + TRZ\frac{1}{r^2}\frac{\partial^2 Q}{\partial \theta^2} + TRQ\frac{\partial^2 Z}{\partial z^2} \tag{F.3}$$

For non-trivial solutions such as $T(t) \neq 0$, $R(r) \neq 0$, $Q(\theta) \neq 0$ and $Z(z) \neq 0$, Eq. F.4 can be rewritten as

$$\frac{1}{c^2}\frac{1}{T}\frac{\partial^2 T}{\partial t^2} = \frac{1}{R}\frac{1}{r}\frac{\partial}{\partial r}\left(r\frac{\partial R}{\partial r}\right) + \frac{1}{Q}\frac{1}{r^2}\frac{\partial^2 Q}{\partial \theta^2} + \frac{1}{Z}\frac{\partial^2 Z}{\partial z^2} \tag{F.4}$$

Also the left hand side and the following terms in the right hand side should be constants

$$\frac{1}{c^2}\frac{1}{T}\frac{\partial^2 T}{\partial t^2} = -k_c^2 \tag{F.5}$$

$$\frac{1}{Q}\frac{\partial^2 Q}{\partial \theta^2} = -m^2 \tag{F.6}$$

$$\frac{1}{Z}\frac{\partial^2 Z}{\partial z^2} = -k_z^2 \tag{F.7}$$

which lead

$$\frac{\partial^2 R}{\partial r^2} + \frac{1}{r}\frac{\partial R}{\partial r} + \left[(k_c^2 - k_z^2) - \frac{1}{r^2}m^2\right]R = 0 \tag{F.8}$$

Defining k as

$$k^2 \equiv k_c^2 - k_z^2 \tag{F.9}$$

Eq. F.8 can be simplified as

$$\frac{\partial^2 R}{\partial r^2} + \frac{1}{r}\frac{\partial R}{\partial r} + \left[k^2 - \frac{1}{r^2}m^2\right] R = 0 \tag{F.10}$$

Changing variable by using $x = kr$, Eq. F.10 can be expressed as the Bessel equation

$$\frac{\partial^2 R}{\partial x^2} + \frac{1}{x}\frac{\partial R}{\partial r} + \left[1 - \frac{m^2}{x^2}\right] R = 0 \tag{F.11}$$

The general solutions for the Bessel equation are

$$R(x) = C_1 J_m(x) + C_2 Y_m(x) = R(kr) = C_1 J_m(kr) + C_2 Y_m(kr) \tag{F.12}$$

where C1 and C2 are constants, J_m is the Bessel function of the first kind of order m and Y_m is the Bessel function of the second kind of order m. The general solutions for Eqs. F.5, F.6 and F.7 are as follows

$$T(t) = C_3 e^{\pm i\omega t} \tag{F.13}$$

$$Q(\theta) = C_4 e^{\pm im\theta} \tag{F.14}$$

$$Z(z) = C_5 e^{\pm ik_z\theta} \tag{F.15}$$

where

$$\omega = k_c c \tag{F.16}$$

Note that the constants k_c, m and k_z have the negative in the right hand side of Eqs. F.5, F.6 and F.7 to give the periodic solutions. It is natural to see the periodic solutions in the azimuthal direction to satisfy the boundary conditions. However, it is not necessary to have the negative signs for k_c and k_z. In fact, if they have the positive sign in the right hand side of Eqs. F.5 and F.7,

$$T(t) = C_6 e^{\pm\omega t} \tag{F.17}$$

$$Z(z) = C_7 e^{\pm k_z\theta} \tag{F.18}$$

which yields

$$\frac{\partial^2 R}{\partial x^2} + \frac{1}{x}\frac{\partial R}{\partial r} - \left[1 + \frac{m^2}{x^2}\right] R = 0 \tag{F.19}$$

The general solutions of Eq. F.19 are

$$R(x) = C_8 I_m(x) + C_9 K_m(x) \tag{F.20}$$

where I_m is the modified Bessel function of the first kind of order m and K_m is the modified Bessel function of the second kind of order m.